University of Bath

UNIVERSITY OF BATH

PHD

The impact of natural disasters on the dynamics of infectious diseases

Gaythorpe, Katy

Award date:
2016

Awarding institution:
University of Bath

Link to publication

The impact of natural disasters on the dynamics of infectious diseases

submitted by

Katy Gaythorpe

for the degree of Doctor of Philosophy

of the

University of Bath

Department of Mathematical Sciences

January 2016

Abstract

Over the course of this thesis we will build and develop a model for the dynamics of an environmentally transmitted disease such as cholera. We will also develop methods to analyse and understand that model. The dynamics of a disease in a heterogeneous developing world city have not yet been fully explored, particularly when those dynamics are affected by a natural disaster. Yet, natural disasters such as floods alter infrastructure and population characteristics in a manner that affects disease transmission. Therefore, we shall address this omission from the literature. We will also develop a novel model analysis framework for 'systems epidemiology' where we combine systems biology techniques with epidemiological modelling.

Contents

Chapter 1

Introduction

1.1 The problem

A natural disaster is a disruption of the human ecology which exceeds the community's capacity to adjust so that external help is needed.

Nathalie Floret et al. [45]

Natural disasters can have a number of causes and ramifications. From climatic events to geophysical hazards, natural disasters have drastic impacts on human populations around the world. However, it is not only the event itself which causes devastation but the consequent epidemics that a disaster can facilitate. As we see in figure 1.1, all injuries account for only 9% of deaths globally whereas communicable diseases account for 11% [138]. Of those disease-related deaths, the majority are a result of diarrhoeal diseases, shown in figure 1.2.
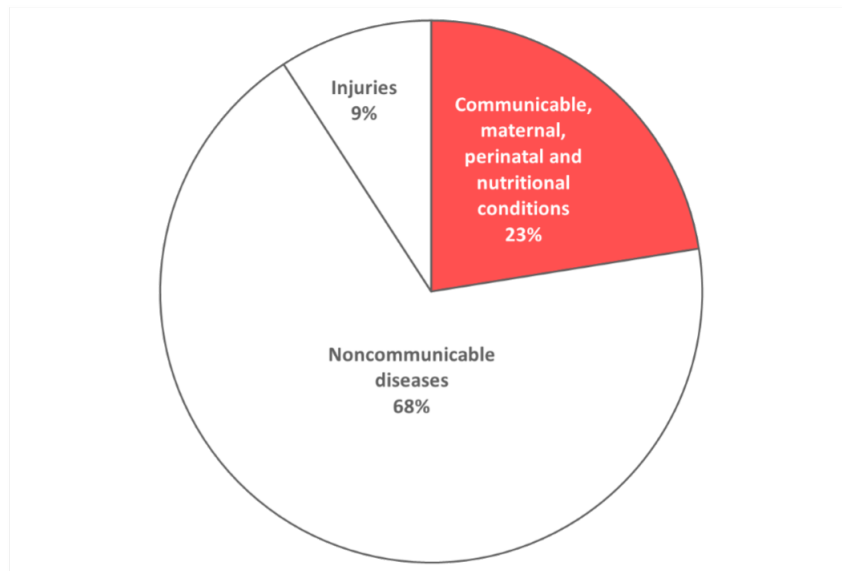
Figure 1.1: The three causes of death in 2015 as projected by the World Health Organisation [138].

Therefore, we will examine the effect of natural disasters on diarrhoeal or environmentally transmitted diseases. Section 1.2 details how natural disasters can facilitate environmental transmission. Section 1.3 describes one of the most prominent environmentally transmitted diseases: cholera. Cholera is responsible for 1.5% to 7.8% of
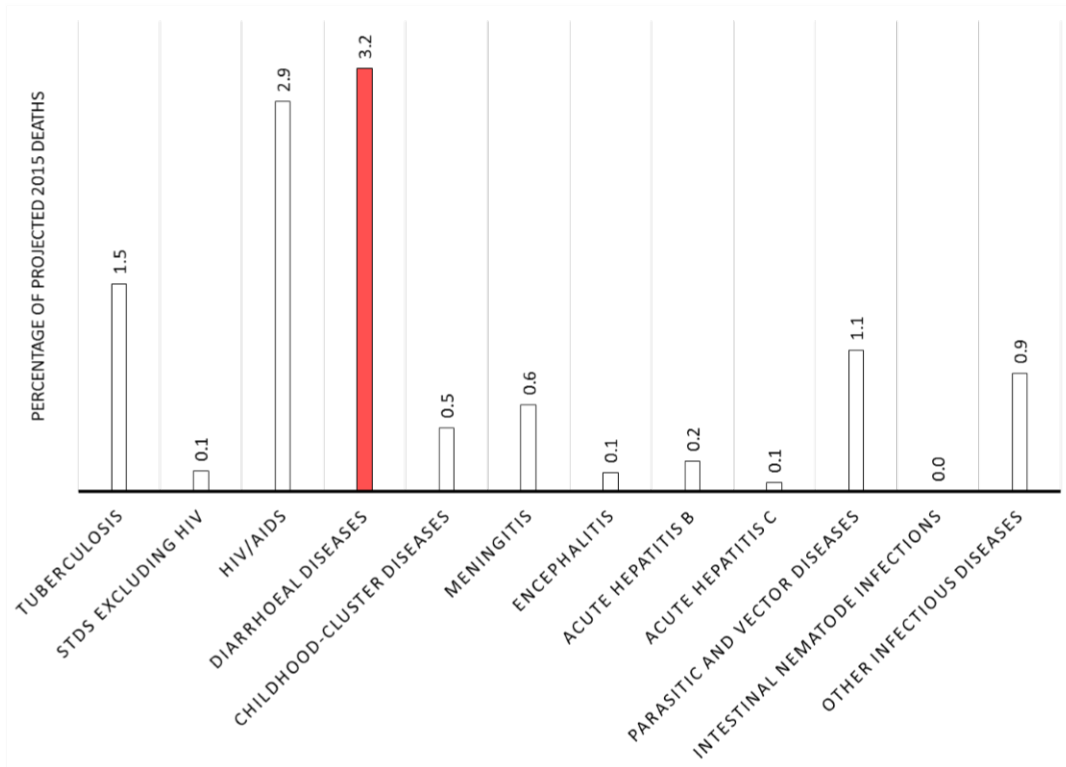
Figure 1.2: The percentages of global deaths due to communicable diseases in 2015 as projected by the World Health Organisation [138].

diarrhoeal-related deaths [140], most recently as a result of the dramatic epidemic in Haiti, which was, in turn, facilitated by the preceding earthquake.

We will now examine natural disasters and their effects.

1.2 Natural disasters and environmentaly transmitted diseases

Environmentally transmitted diseases such as cholera can be strongly affected by the conditions of the habitat and host population. We will mention works where the seasonality is included when modelling the transmission of cholera [30]. This is because factors such as temperature and rainfall are known to affect environmentally transmitted disease spread throughout the year. When the variation in environmental factors is more extreme, we would also expect a greater change in disease transmission. It is for this reason that we examine the effect of natural disasters on environmentally transmitted diseases.

We will focus on climactic natural disasters such as flooding as they have a strong effect on environmental disease transmission. However, they also have consequences in common with other disasters such as population displacement and infrastructure damage. For example, in the two weeks following the Indian Ocean tsunami, 85% of children under five in the Aceh district experienced diarrhoea [23]. Therefore, insight gained into the effect of climactic disasters may be useful for other events.

Floods are the most common type of natural disaster [4, 96]. They account for more than half of natural disasters between 2001 and 2010 [38]. Flooding can increase the risk of environmental transmission [127, 33, 139, 4]. This additional risk is partly as a result of contamination of drinking water and food by flood waters [139, 111].

6

However, population displacement can also contribute to disease transmission when temporary shelters are overcrowded and lack sufficient sanitation or potable water. Indeed, the combined effects of diarrhoeal diseases, malnutrition, measles and acute respiratory infections account for 60-95 % of reported deaths in displaced populations [97]. Flooding may also have secondary effects. In some cases water purification and sewage treatment are disrupted when power supplies are lost due to floods disturbing the infrastructure and utilities of a population [96, 139].

The effects of natural disasters in general are more pronounced in less economically developed countries [4, 136, 123]. For instance, 70% of all flood-related deaths occur in India and Bangladesh [96]. The factors that can contribute to the increased severity of the effects of natural disasters and ensuing epidemics are a higher number of pre-existing diseases, an insufficient level of immunisation in the population, higher population density or less effective utilities and infrastructure [97]. An example of these factors influencing the severity of an epidemic following a natural disaster can be seen in Haiti. The infrastructure was already vulnerable before it was weakened by the violent earthquake [85]. Then, once the population was disrupted and utilities were stretched and damaged, the outbreak of cholera was devastating, claiming 8700 lives by 2014 [85].

In the future, severe weather events are likely to continue and have the potential to worsen with climate change [4, 22]. As a result of this, and for reasons such as changed habitable regions, the impact of water-borne diseases are also likely to be exacerbated. Health developments and mathematical modelling can be used to formulate and assess strategies to cope with diseases in the light of a changing climate. WASH (water, sanitation and hygiene infrastructures) procedures, although controversial, have already benefited many individuals. For instance, in Haiti, cholera incidence in displaced population camps has been surprisingly low due to intervention measures [44]. However, research into optimal control strategies is still needed for diseases influenced by extreme weather events as, for all the success stories such as the camps in Haiti, there are still many situations, including that of the rest of Haiti, that could be improved with better resource management and deployment.

1.3   Cholera

Cholera is a gastrointestinal disease whose etiological agent is *Vibrio cholerae* [30]. The bacteria colonize the small intestine and produce an enterotoxin which stimulates water and electrolyte secretion by intestinal endothelial cells [60]. It leads to fluid loss and profuse diarrhoea which, if left untreated, can be fatal in hours. There are more than 200 serogroups with 01 and 0139 most commonly epidemic. The World Health Organisation (WHO) estimates that there are approximately five million cases of cholera each year, leading to 120,000 deaths [140]. Epidemics of cholera, and other diarrhoeal diseases, often follow flooding and other natural disasters when drinking water is contaminated and sewage management is disrupted. It is mostly developing countries that are affected [22, 71, 132, 136, 139, 33, 4, 96].

Cholera is transmitted environmentally and is commonly water-borne, although it can also be transmitted through contaminated seafood and directly through faecal-oral routes. *V. cholerae* is also a natural part of the aquatic environment and can colonize some shellfish [92]. Susceptible individuals may be infected by ingestion of contaminated food or water. Once infected, they produce bacteria which can be in a short-lived hyper infectious (HI) state and the cycle continues [60].

There are a number of interventions for cholera from preventative measures such as sanitation to reactive controls such as vaccination. In many cases, cholera can be treated

by oral rehydration salts, ORS [44]. These can be rice-based and contain supplements for zinc and vitamin A. There was found to be a 23% fall in mortality due to cholera when zinc supplements were provided and, as vitamin A deficiency is a common result of cholera leading to eye lesions, it is beneficial to combine treatments in this form. However, the storage of ORS can affect its efficacy and needs careful monitoring [44].

When cholera cases are moderate to severe, individuals may need intravenous rehydration fluids, antibiotics or reactive vaccination. Antibiotics such as doxycycline and tetracycline reduce the duration of infection and the amount of bacteria shed [113, 6, 44]. They can, in extreme cases, cut shedding by half. However, there are concerns about antibiotic-resistant strains of cholera. In Haiti, from five commonly used antibiotics: doxycycline, azithromycin, nalixic acid, sulfisoxozole and ciprofoxacin, only two antibiotics are effective, doxycycline and azithromycin. Therefore, there are limitations on antibiotic use. The WHO suggests antibiotics should generally be reserved for severe cases.

The most commonly discussed medical intervention for cholera is vaccination. There are two main types of cholera vaccine, Dukoral and Shanchol [92, 47, 44, 5, 137]. Dukoral was developed in Sweden and licensed for over 60 countries at $6 a dose [44]. It is based on heat killed whole cells of *V.cholerae* 01 and a bacterial toxin subunit. It is administered in two doses, one week apart. The immunity given by Dukoral lasts up to two years and its effectiveness wanes over this period. It works by stimulating the production of antibacterial and antitoxin antibodies in the host. Shanchol works in similar manner to Dukoral but does not include bacterial toxin and retails at less than $2. It allows for a higher retention of immunity over time but is initially less effective than Dukoral. Both vaccines confer herd immunity including the protection of children too young to be vaccinated. As such, the WHO suggests vaccination should be used, in conjunction with other measures, in cholera endemic areas.

Lastly we consider the treatment of the environment to reduce cholera transmission. Cholera is a disease related to poverty and is generally not seen in more economically developed countries [127]. As such, adequate sanitation and water treatment are extremely effective measures against cholera spread. In less economically developed countries, particularly after natural disasters, WASH procedures are the first step in cholera control [47, 127]. These include point-of use water treatment and hygiene promotion. Measures within households can reduce diarrhoeal outbreaks by 30-50% and even just effective hand-washing can reduce risk by up to 47% [22, 44]. Other methods employed within households are those of cloth filtration, solar disinfection and chlorination. Sari cloth filtration was found to reduce cholera incidence by up to 48% [127]. Whereas solar disinfection, where a transparent container is exposed to sunlight in order for the UV to kill unwanted microbes, reduces the odds of cholera infection in children by up to 88%. The chlorination of wells and vessels of water can be problematic. Well chlorination can fail to reduce the contamination to sufficiently safe levels and within vessels there is always the issue of recontamination. The choice of container can reduce this issue with narrow necked containers such as sorai limiting the possibility of recontamination. One study compared just chlorination with use of a sorai initially filled with decontaminated water and found a reduction in cholera incidence of 75 % for the sorai compared to 58% for chlorination [35]. A final consideration for intervention is education. However, this is an ineffective measure if there are not the resources available. For instance, in Haiti there were extreme shortages of soap therefore the promotion of hand-washing was redundant [44].

Several mathematical modelling studies have examined the effects of these control measures on cholera epidemics, we shall examine some of them now.

1.4 Environmental transmission modelling to date, cholera as an example.

We have conducted a literature review for cholera models or maps. The genealogy of the works examined are shown in figure 1.3 and are by no means a complete collection. In order for the review to be tractable we have omitted discrete time models and models of other environmentally transmitted diseases. Some excluded works are those of Pascual, Koelle and Chao [106, 105, 77, 28]. We shall now elaborate on the developments in the works shown in figure 1.3.
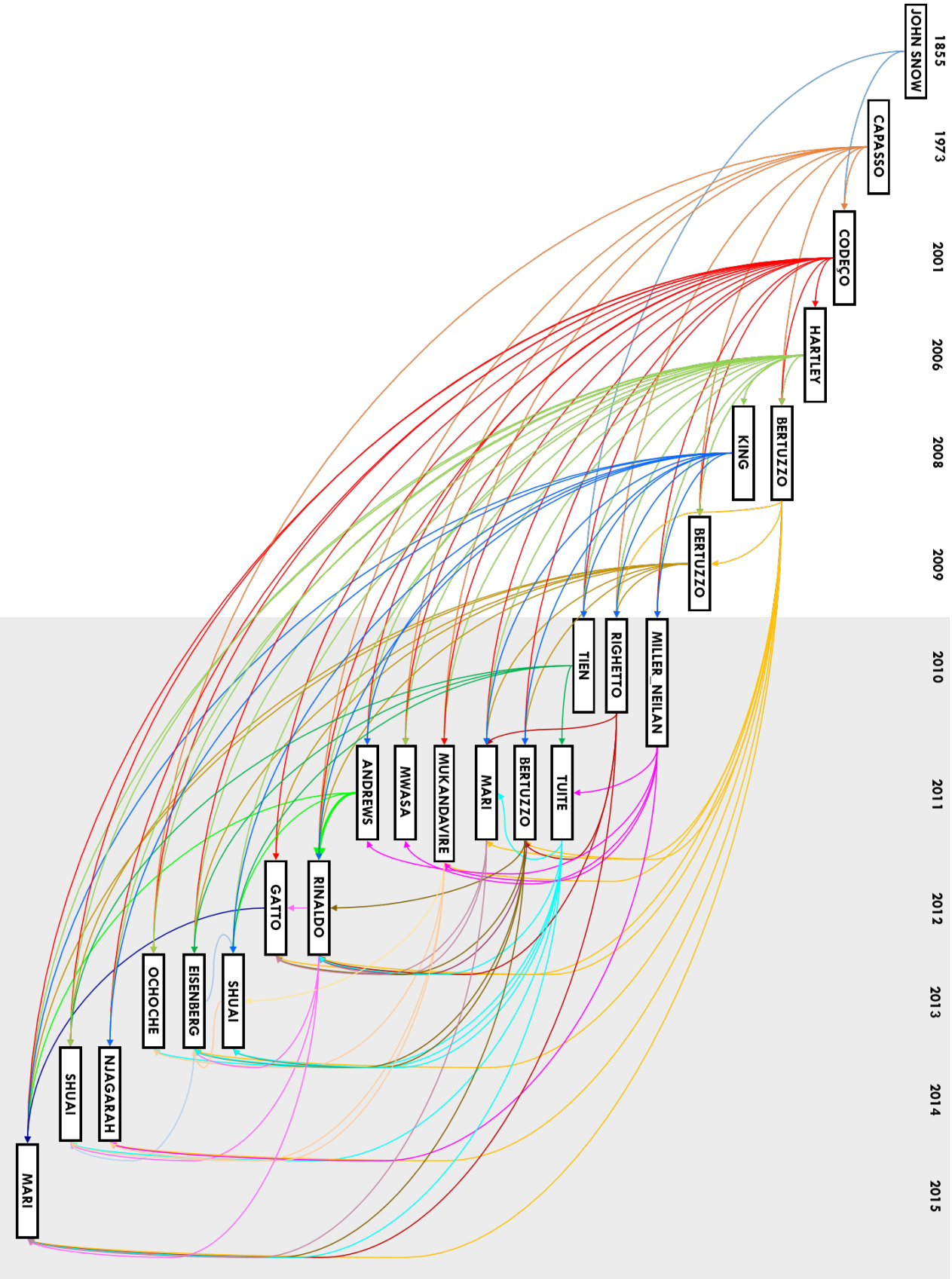
Figure 1.3: The story so far [124, 26, 30, 60, 15, 75, 16, 93, 112, 129, 131, 17, 86, 91, 92, 6, 113, 51, 122, 41, 99, 95, 121, 85]. Arrows denote citation and grey shading denotes the Haiti cholera epidemic duration.

In 1854 there was a dramatic outbreak of cholera in London. The epidemic started in late August and claimed around 600 lives. Dr. John Snow, a medical doctor who was 41 at the time, conjectured that the disease was spread by water. This was a controversial theory as the belief at the time was that cholera was spread by 'bad air' [104]. However, Snow persevered with his theory, using death registry data and personally visiting the homes of 658 cholera victims to build up evidence [1]. He used his collected information to draw the Broad Street map of cholera victims, shown in figure 1.4. This map and Snow's theory were enough to convince the authorities to remove the handle from the Broad Street pump which Snow posited was the source of the epidemic. After this point, the epidemic declined although some argue that the epidemic had already peaked by this point [25, 1].

Snow conjectured that cholera was water-borne and caused by small 'organised matter' [25]. Unfortunately he never heard Fillipo Pacini's description of the *V. cholerae* bacillus in 1854. Nor did he hear of germ theory as he died just five years after the London outbreak. Now, he is hailed as one of the first individuals to suggest cholera is water-borne and to employ spatial mapping to find control strategies.
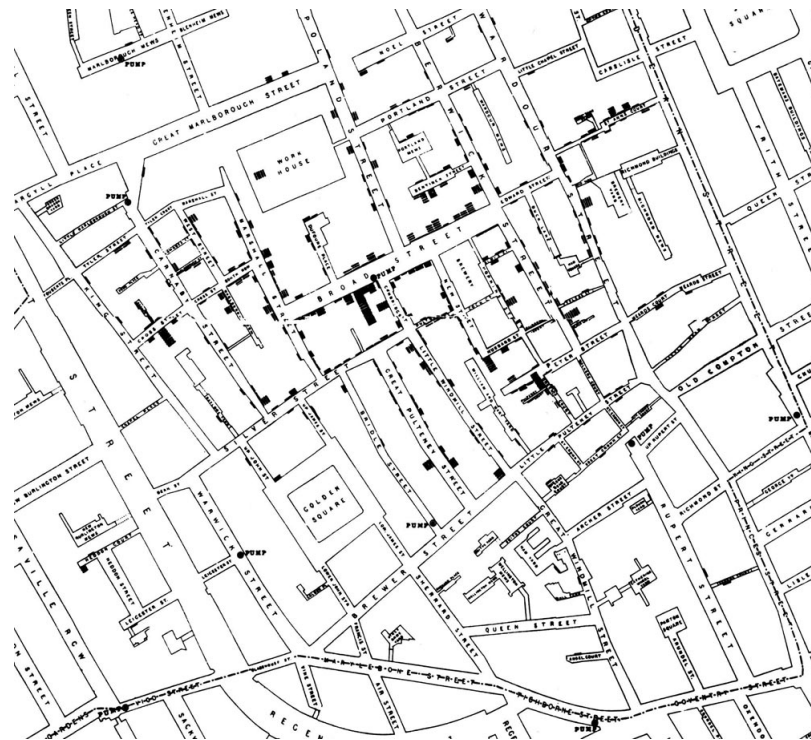
Figure 1.4: John Snow's map of cholera victims in London, 1854 [90]. The black squares indicate numbers of victims at each address.

Possibly, the first use of differential equations to model cholera was by Capasso and Paveri-Fontana [26]. They used two differential equations, one to describe the bacterial population in the sea, x_1, and one to describe the human infected population, x_2. The equations are as shown in (1.1):

$$\frac{d}{dt}x_1 = \left(f - \frac{1}{l_b}\right)x_1 + a_{12}x_2,$$
$$\frac{d}{dt}x_2 = N\beta p f(x_1) - \frac{x_2}{l_h}. \tag{1.1}$$

Here, l_h denotes the duration of infection in the human population, l_b denotes the lifespan of the bacteria in the environment and f denotes the fertility rate of the bacteria. Parameter a_{12} is defined as a growth rate due to the infected hosts, we would now call this a shed rate. The humans are infected through eating contaminated seafood and p denotes the probability that a human will eat a 'raw snack'. The human population size is given by N and parameter β is the probability that an individual is *not* immune to cholera and can therefore be infected with probability $f(x_1)$. In order to characterise $f(x_1)$, Capasso and Paveri-Fontana defined $g(x_1) = N\beta p f(x_1)$ and defined the model as a Cauchy problem. This allowed them to show the model has a unique solution and assign $g(x_1)$ such that the force of infection is an increasing function of x_1 and saturates to $Np\beta$. However, they then redefined the force of infection as $a_{21}x_1$, a linear term with a_{21} a infection rate.

Capasso and Paveri-Fontana defined a parameter, θ, as the transmission terms over the duration of infection. We would now call θ the basic reproduction number, R_0. They used this term to divide their phase space analysis between the disease free and endemic equilibria and found that θ was a threshold for stability of the endemic equilibrium.

Lastly, Capasso and Paveri-Fontana compared their mathematical model with the data from the Bari epidemic of 1973. They did this by assuming that only a fraction of their modelled population exhibited symptoms and defined a hospitalisation rate based on this fraction. They found that their modelled hospitalised numbers reflected those from the epidemic and suggested that the intervention strategies used, sewage chlorination and regulation of mussel consumption, were effective. Finally, they suggested that the construction of the sewage plant could annihilate the disease entirely.

Thus, in 1973, not only did Capasso and Paveri-Fontana design one of the first differential equation models of cholera but they also compared it to data, suggested control strategies, evaluated those controls already implemented and derived a term amounting to the basic reproduction number. Another notable achievement in this paper was the inclusion of asymptomatic infection which we found was not revisited in cholera models until the work of King et. al in 2008 and that of Pascual [105].

The most commonly cited cholera model is the work of Codeço. She extended the model of Capasso and Paveri-Fontana by including the susceptible class in order to study long-term dynamics. She also altered the force of infection term [30]. The model of Codeço was not only a generalisation of the work of Capasso, but also far more accessible and thus more widely cited, see figure 1.3. The model itself is shown in equations (1.2) where S, I and B represent the number of susceptible individuals, infected individuals and concentration of *V. cholerae* in the aquatic reservoir respectively. The infected individuals account for all infections, symptomatic and asymptomatic, although Codeço states that only 1-30% of *V. cholerae* infections become severe.

$$
\begin{aligned}
\frac{dS}{dt} &= n(H - s) - a\lambda(B)S, \\
\frac{dI}{dt} &= -a\lambda(B)S - rI, \\
\frac{dB}{dt} &= B(nb - mb) + eI.
\end{aligned}
\tag{1.2}
$$

The human birth and death rates are denoted by n and the total human population size, H. Susceptible individuals are exposed to the contaminated environment at rate a and are infected with probability $\lambda(B)$, shown in (1.3). Infected individuals recover at rate r and contribute bacteria at rate e. Lastly, $nb - mb$ represents the net growth

of *V. cholerae* in the aquatic environment. The force of infection is represented by a logistic dose response curve:

$$\lambda(B) = \frac{B}{K + B},\tag{1.3}$$

where K is the concentration of *V. cholerae* in the environment that yields a 50% chance of catching cholera. This means that the probability of infection given contact saturates as the concentration of bacteria in the environment becomes very large.

Codeço used this model to examine the conditions for cholera-free populations as well as situations where cholera is epidemic or endemic. In the cholera-free population, all individuals were assumed to be susceptible and there are no bacteria in the environment. She found that the disease, if introduced, would only become an outbreak if the number of susceptible individuals was above a critical threshold. This threshold was proportional to the shed rate, half-saturation constant, recovery rate and net growth rate of the bacteria. This means if the sanitation is good the critical number of susceptible individuals would have to be larger to allow an epidemic. She also derived the critical shed rate for an epidemic to occur which depends on the critical susceptible number. This allowed Codeço to suggest prevention measures for cholera outbreaks. These included: minimising water contamination and consumption of contaminated sources and the dilution of cholera diarrhoea to render the dose ineffective.

In the case of the population with epidemic cholera, the number of susceptible individuals is assumed to be higher than the critical outbreak threshold. Codeço derived an expression for R_0 and simulated an epidemic in this situation. The epidemic declined when the susceptible pool size fell below the critical threshold.

The final case was where cholera was endemic in the population. The size of the susceptible population was once again above the critical threshold but the growth rate was also larger. Therefore, cholera returned successively to the population. Codeço derived terms for the endemic population sizes and the equilibrium number of infected individuals in the population as a fraction of the surplus population. Codeço conducted stability analyses and found the endemic equilibrium to be stable for small perturbations.

Codeço also examined seasonal variation through the contact rate, shed rate and net growth rate of the bacteria. This is because cholera epidemics in endemic regions are often associated with climactic events. She conducted simulations with each rate in turn a sinusoidal function of time. When the contact rate varied, periodic dynamics were seen with an annual peak. When the shed and net bacterial growth rates varied, there also occurred an annual cholera peak.

Codeço's model, whilst simple, was a step forward in understanding outbreak thresholds and the seasonality of cholera. It paved the way for many of the more complicated models to come with its easily adaptable framework.

Following the model of Codeço; Hartley, Morris and Smith used novel laboratory findings to adapt their model by the inclusion of a hyper infectious, HI, state for the bacteria [60]. It was found that passage of *V. cholerae* 01 Inaba El Tor through the human host increases the infectivity of the bacteria. However, this increase in infectivity was short-lived; around five hours after shedding, *V. cholerae* return to their usual state. Hartley et al. used this HI state to explain the quick transmission seen between humans in cholera outbreaks. The model of Hartley et al. was an extension of Codeço's where the bacterial compartment was divided in two to account for the different states of infectivity. This meant that susceptible individuals were either infected as a result of coming into contact with 'normal' bacteria or with those recently shed, in which case the probability of infection was higher. They derived an expression for R_0 and compared the

relative contribution of the two types of bacteria. They found, for their parameter set, that the HI bacteria were around five times more important than the 'normal' bacteria.

Hartley et al. also used simulations initiated from disease-free steady state to examine the effect of HI bacteria. They found the epidemic occurred sooner and had a higher peak when bacteria had a HI state. They also examined the situation where the HI and non-HI bacteria made equal contributions to R_0 i.e. there was proportionally less contact with the HI bacteria than non-HI. They found the epidemic still peaked sooner when bacteria had an HI state and supposed that the HI state drove fast dynamics.

In the model by Hartley et al. the HI state was influential for two reasons: those bacteria recently shed are closer to humans and therefore more influential and the HI state is such a significant competitive advantage over other bacteria that they are more epidemiologically significant. The competitive advantage was a result of adaptation to the host, HI state bacteria were better at surviving within, and being shed by, the host. They do mention the reliance of the model results to the parameter set, particularly the contact rates with HI and non-HI bacteria which are difficult to estimate. However, the inclusion of HI bacteria will still affect dynamics to some extent.

Where Hartley et al. focussed on the bacterial states, Bertuzzo et al. examined the effect of river networks [15]. They included the river networks as they are corridors for bacteria to move between populations of hosts.

Bertuzzo et al. defined an environmental matrix which contained information about a directed graph representing the river network. Nodes on the graph represented human communities and each had a direction based on the flow. They used an adapted form of Codeço's model for each node and included deaths due to cholera. They used the work of Pascual et al., omitted from figure 1.3 as they focused on time-series models, to inform the evolution of the volume of water hosting the bacteria [106]. This scaled the shed rate at each node by the local water volume which was proportional to the node host population size for large populations. For smaller populations, the water volume was kept at a constant value. They modelled the spread of *V. cholerae* as a biased random walk process and derived a term for 'node vulnerability'.

Bertuzzo et al. applied their model to a case-study of the 2000 epidemic in KwaZulu province, South Africa. They used data on the river network and settlements to set-up their model. They found the most affected nodes were those of intermediate size. They theorised that this was because larger settlements are more developed and have better sanitation. Bertuzzo et al. also included seasonality through the net growth of the bacteria in the aquatic environment.

The model developed by Bertuzzo did well at approximating the two outbreaks in KwaZulu province, as well as the spatial spread. However, it may be improved with the inclusion of HI bacteria or seasonality in epidemiological parameters. Yet, it was the first model to accurately examine the effect of spatial factors on cholera spread. This model is used extensively in the works following. Namely those of Bertuzzo et al., Righetto et al., Rinaldo et al., Gatto et al. and Mari et al.. We shall examine these works as they appear chronologically.

Another step forward in cholera modelling was the inclusion of asymptomatic infection by King et al. [75]. They also included the loss of immunity and compared their results to 50 years of mortality data from 26 districts in Bengal. However, they did not include an environmental reservoir explicitly. The inclusion of waning immunity was motivated by the work of Koelle et al. which was omitted from figure 1.3 as they used discrete time models [77]. King et al. fitted their model to data in each of the districts. They found that immunity waned on a scale of weeks to months rather than years and that the

ratio of asymptomatic to symptomatic cases was far higher than previously thought. They also suggested that the reservoir of bacteria was responsible for comparatively few cases. The ramifications of these results are that there may be a higher level of immunity in a population with endemic cholera but that immunity is short-lived and less affected by the bacterial reservoir than previously suggested.

King et al. examined three models. Their inclusion of asymptomatic infection was a new and important step in matching modelling outcomes with reported cases in cholera endemic regions.

From 2009 onwards, we begin seeing the earlier works combined and reused to quantify and qualify intervention strategies and predict future epidemics. Before examining them in more detail, we summarise the similarities and differences between the models in table 1.1.

Table 1.1: Summary of characteristics for models published from 2009 onwards that are featured in figure 1.3.

First author	Year	Model characteristics	Reference
Bertuzzo	2009	Spatial with bacteria movement	[16]
Miller-Neilan	2010	HI bacteria Waning immunity Interventions -Rehydration -Antibiotics -Vaccination -Sanitation	[93]
Righetto	2010	Partial differential equations Spatial with bacteria and human dispersal	[112]
Tien	2010	Direct and environmental transmission	[129]
Tuite	2011	Haiti Direct and environmental transmission Spatial with human movement Interventions -Clean water -Vaccination	[131]
Bertuzzo	2011	Haiti Spatial with bacterial movement Interventions -Clean water -Vaccination -Sanitation	[17]
Mari	2011	Haiti Spatial with bacterial movement and human movement through gravity model Asymptomatic infection	[86]
Mukandavire	2011	Zimbabwe Direct and environmental transmission	[91]
Mwasa	2011	Waning immunity Interventions	[92]

		-Education	
		-Antibiotics	
		-Vaccination	
		-Quarantine	
Andrews	2011	Asymptomatic infection	[6]
		Waning immunity	
		HI bacteria	
		Interventions	
		-Antibiotics	
		-Clean water	
		-Vaccination	
Rinaldo	2012	Spatial with bacteria and human movement	[113]
		Asymptomatic infection	
		Waning immunity	
		Two aquatic reservoirs	
Gatto	2012	Spatial with bacteria and human movement organised by disease state	[51]
		Asymptomatic infection	
		Waning immunity	
Shuai	2013	Star shaped network of patches	[122]
		Bacterial movement	
		Intervention	
		-Vaccination	
Eisenberg	2013	Spatial with human and bacterial movement	[41]
		Waning immunity	
		Direct and environmental transmission	
		Interventions	
		-Vaccination	
		-Clean water	
Ochoche	2013	Intervention	[99]
		-water treatment	
Njagarah	2013	Spatial with human migration	[95]
Shuai	2014	Spatial with shared water source	[121]
		Interventions	
		-Water treatment	
		-Isolation	
		-Vaccination	
		-Clean water	
		-Sanitation	
Mari	2015	Model comparison	[85]

Table 1.1 summarises the model characteristics of the works from 2009 to date shown in figure 1.3. We shall now discuss them in further detail.

Bertuzzo et al. revisited their spatial model in 2009 to examine the effect of network topology on cholera travelling waves. They examined four network types, one and two dimensional lattices, Peano's network and an optimal channel network (OCN). The travelling wave varied across the different network structures. Bertuzzo et al. derived analytical expressions for the wave speed for the two lattices and computed the speed

16

numerically for the more complicated networks. They found that cholera spread more slowly on the more realistic Peano and OC networks. When bias was included, similar to a flow on a river, they found two waves emanating from a single infected node, each with a different velocity. They also noted the necessity to compare local epidemic time-scales for those of spreading to qualify the usefulness of spatial models.

This work was purely an exploration of the network topologies. However it does attempt to quantify the usefulness of spatially structured models.

Miller Neilan et al. used the work of Codeço, Hartley and King to develop a model of cholera including asymptomatic cases and HI bacteria [93]. Their aim was to find optimal intervention strategies including rehydration, antibiotic prescription, vaccination and sanitation. First, they conducted a sensitivity analysis using Latin Hypercube Sampling. They checked the monotonicity of epidemic characteristics such as the epidemic peak, asymptomatic epidemic size and total epidemic size with the model parameters. In all cases they found a monotonic relationship and could therefore use partial rank correlation coefficients (PRCC) to quantify the relationship between input and output, see chapter two for PRCC method. They conducted this analysis before and after the addition of intervention to the model and found that the ratio of symptomatic to asymptomatic cases, contact rates and shed rates were the most influential parameters. When intervention measures were added, they found vaccination was the most influential control.

Miller Neilan et al. applied costs to infection and control with model parameters from Bogra and Calcutta in order to use Pontryagin's Maximum Principle to find the optimal strategies over time. They found that different strategies were required for each of the communities and that a combination of control measures is more successful than just one. Finally they emphasised the importance of combining prevention and treatment to minimise a cholera outbreak.

This paper was an extensive examination of intervention strategies in a homogeneous population. The mechanisms are the focus here and as such we can gain valuable insights into effective methods of control. However, including a spatial aspect would allow more complicated strategies and we could ask about the best strategy over space as well as time.

Righetto et al. focussed their attention on cholera movement down a linear stream through PDEs for which they found travelling wave solutions [112]. They worked with the model used in Bertuzzo et. al 2008 and 2009 and examined how the inclusion of human diffusion changed the model dynamics. They found that if a small number of infected individuals were placed at a node two travelling waves occurred, one forward or progressive, and one backward or regressive. They compared their work directly to that of Bertuzzo et al. in 2008 with the parameters as those from KwaZulu province.

This is a notable addition to the bacterial transport model from Bertuzzo et al. in 2008 where human movement is directly accounted for. However, modelling human movement through diffusion over such a large area cannot be expected to replicate the commuting and gravity-based movement one would expect to find between settlements.

The main development produced by Tien and Earn was the specific inclusion of two transmission routes, direct and environmental [129]. They added a water compartment to a SIR model to model the concentration of bacteria in the environment. However, they did not have a saturating force of infection due to the bacteria, rather they included a mass action term: $b_W W S$ where b_W is the contact rate with the water. They compared the thresholds, R_0, between the SIWR model and that of an SIR model and examined

the stability of the disease free and endemic equilibria. They found that the multiple transmission routes vary in importance as the bacterial lifespan and contact with the environment change. However, they discuss the necessity for the aquatic compartment when modelling water-borne infections.

Tien and Earn do not include the dose-response term for contact with the contaminated environment. Therefore their model implies that the probability of infection given contact with the aquatic reservoir is linear with respect to the bacterial concentration. This serves their purpose of comparison with an SIR model well. However, it may be a simplification that loses some of the interesting dynamics with respect to the bacterial concentration.

In October 2010, cholera was reported in the Artibonite region of Haiti after an absence of 100 years [28, 85, 131]. It came nine months after a catastrophic earthquake which damaged the already poor infrastructures for healthcare, water and sanitation, see section 1.2 for a discussion of disasters and disease spread. As of December 2014, the epidemic had claimed 8700 lives and there have been 72000 cases [85]. It spawned a number of cholera research papers, as did the 2008/09 Zimbabwean cholera outbreak which, by Aug 2008, had 98585 cases and 4287 deaths [91]. The global cholera cases until 2013 are shown in figure 1.5.
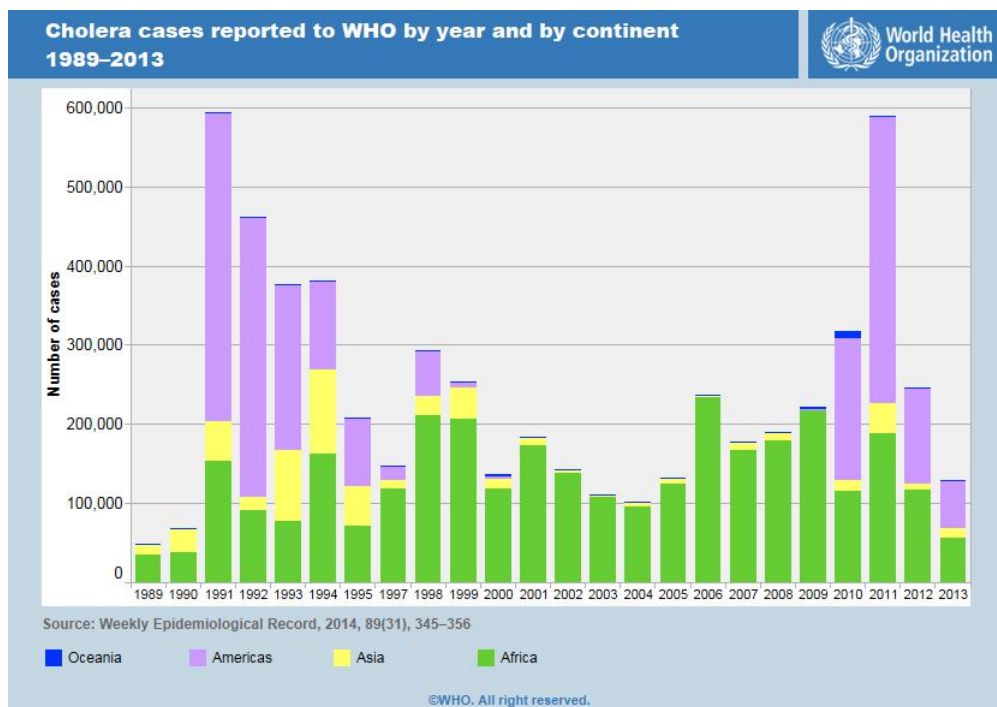
Figure 1.5: WHO graph of cholera cases over time [142].

One of the first papers to focus on Haiti was that of Tuite et al. [131]. Tuite et al. worked with Tien and Earn in extending their model to the 10 Haitian departments through the use of a metapopulation model. Their aim was to assess three vaccination strategies: equal distribution between the departments, distribution proportional to the population size and an 'optimal' simulated distribution. Their model included human movement but no bacterial transport and no dose-response curve for environmental transmission. They found the best strategy was the simulated distribution but, due to the limited number of doses available and the time it takes to distribute vaccine, the benefits of vaccination were modest. However, they also found to arrive at the same

benefit through clean water provision, 1.7 to 2 times as many people would need to receive water than vaccine.

The model in Tuite et al. covers the entirety of Haiti and is divided into ten patches. Yet, there is no examination of the bacterial transport in the water between patches. The only movement is through contact of hosts with the environment of other patches. However there is also no shedding of individuals in other patches despite this contact. Therefore the dynamics of the bacteria in the environment are almost overlooked in this model. This may affect how well the clean water provision is assumed to work and skew the optimal strategy toward vaccination.

Bertuzzo et al. returned to spatial modelling of cholera epidemics in light of the epidemic in Haiti [17]. Their aim was to predict the spatial evolution and effects of intervention on the outbreak. They divided Haiti into more than 500 communities and used the model defined in their previous works on the higher resolution model. Once again, only bacteria moved with a probability based on the distance between nodes and the local community sizes. They compared vaccination and preventative measures such as clean water provision and sanitation. They found all to be very effective at limiting future cholera cases. However, vaccination, if applied early and in large enough doses, could have a more immediate effect on the epidemic.

In a similar manner as with Tuite, we question whether there would be a loss of information when the movement of one of the populations in the model is omitted. Here, Bertuzzo et al. omit all human movement in a model that covers the entirety of Haiti. Whilst the bacterial movements are well defined, it is unclear whether the omission of human movement has affected the optimal strategies.

Mari et al. adapt the model used by Bertuzzo et al. by including human movement. They examine cholera in the KwaZulu province of South Africa and assume humans gravitate towards larger settlements [86]. In this case, infected individuals shed bacteria at home and asymptomatic infected individuals shed at home and at other nodes they visit. They simulated the cholera dynamics in KwaZulu province and found their model predicted the spatial and temporal dynamics well. They also conducted a sensitivity analysis on the model outcomes and found most variance when the parameters quantifying availability of clean water and toilet facilities were altered. Mari et. al considered the model without human movement and found the cholera was then limited to the hydrological catchment it originated from. As such, models with human movement underestimate the spatial spread of cholera. Finally, they included intervention measures such as sanitation and access to clean water. They found that targeting large communities with interventions was not as effective as either a spatially homogeneous approach or focussing on the communities with the worst sanitation. They emphasised the importance of the correlation between population distribution and hygiene conditions when planning optimal control strategies.

The model of Mari et al. accounts for both human and bacterial movement. As such, it predicts the dynamics well in KwaZulu province and gives a good insight into possible intervention benefits.

Mukandavire et al. focussed on the 2008/09 cholera outbreak in Zimbabwe in their work [91]. They incorporated both direct and environmental transmission routes which they termed fast and slow transmission respectively. They fitted their model to each of the ten districts of Zimbabwe separately and estimated the basic reproductive numbers for each population and divided it by direct or environmental transmission. They found R_0 to range between 1.11 and 2.72 for the different districts. In the majority of situations,

most of this value was produced by the direct transmission even without the authors including a HI bacterial state. They used these reproduction numbers to estimate the vaccination coverage threshold for each district.

The work by Mukandavire et al. focussed on each district separately without including interaction or movement between each area. As such, we may consider this a work of ten homogeneous populations. The aim was estimate reproduction numbers and it would be interesting to see if spatial coupling between districts affected those estimates.

The subject of intervention strategies had been discussed by previous works shown in figure 1.3. However, Mwasa and Tchuenche were the first to include education as a control strategy [92]. They added new compartments to the SIRSB model for vaccinated, educated, quarantined and treated individuals in a homogeneous population. The educated individuals were assumed to have better hygiene, report their infection more readily and cooperate with quarantine. The immunity of vaccinated individuals was assumed to wear off over time and they assumed that the system was initially disease free. They examined the stability of the disease free equilibrium and looked at the effect of each intervention on the basic reproduction number. They also conducted sensitivity analyses and simulations including seasonal variation in the contact and shed rates. They found education, vaccination and treatment all reduced R_0 and adopting interventions concurrently significantly affected the effective reproduction number. They emphasised the benefits of good preventative measures and suggested that treatment and education may be most effective in an outbreak.

The work of Mwasa and Tchuenche examines some of the effects of sociological differences in the population as well comparing a range of intervention strategies. It is a very theoretical work which may affect the robustness of the results in prediction. However, it does throw up questions about education which have been otherwise overlooked.

Andrews and Basu used the work of Codeço, King, Hartley and Miller-Neilan to quantify the effect of intervention in Haiti [6]. They simulated the effects of clean water projects, vaccination and expanded antibiotic use on future cholera case numbers. Currently antibiotics are only suggested for severe cases accounting for less than 10% of cases; Andrews and Basu considered extending this to half of the moderate cases. They found provision of clean water to be the most effective measure as it would avert 105000 cases. However, all three interventions used together could avert 170000 cases so a combined strategy is optimal in their case.

Andrews and Basu examined projections of cases for Haiti in the general population. The lack of spatial structure may affect the timespans involved as the whole population is not homogeneously mixed. However, the benefits of extending antibiotic use for moderate cases could be a very important consideration for future policy and intervention strategies.

In the work of Rinaldo et al. they compared four studies of the Haitian cholera epidemic, Bertuzzo, Andrews, Tuite and Chao. They also include waning immunity and the effect of rainfall in their final model [113]. They noted that Andrews and Basu overestimated the cases in the epidemic which Rinaldo at el. attribute to lack of inter-departmental movement in their model. Rinaldo et al. also suppose that Tuite et al. would overestimate the number of cholera cases in the long run as they omit asymptomatic cases in their model. Rinaldo et al. adapt the model from [17] to account for loss of immunity and assume that rainfall may affect contamination rates and/ or washout of defecation sites. They tested four models, two of which divided the environmental reservoir into that for the sewage system and that for drinking water, and fitted those for the data

of Haiti. They found the best ranked model, through AIC, and used that to model the data from Haiti and stress the importance of mathematical modelling in general.

Rinaldo et al. comment on four different cholera models with respect to Haiti. They arrive at the conclusion that spatially structured models such as those developed by Bertuzzo et al. are most effective. However, the explanation behind this could be that they, Rinaldo, Bertuzzo and Mari et al. understand the scope for spatial modelling to a greater extent as it is their chosen method.

Gatto et al. utilise the model of Rinaldo et al. once more to show that local reproduction number thresholds need not be greater than one in order for an outbreak to occur [51]. The aim was to determine onset conditions for a cholera outbreak in Haiti and KwaZulu province, South Africa. They linked outbreak patterns to the dominant eigenvector of a reproduction matrix, the dominant eigenvalue of which was the generalized reproduction number. These patterns were confirmed through an examination of the case-studies of Haiti and KwaZulu province. They found that even if local reproduction numbers were less than one in all communities, the disease may spread and human mobility may favour disease onset.

The model in Gatto et al. was tried and tested in the case studies of Haiti and KwaZulu province. Humans move under a gravity model and bacteria flow along Peano networks. This level of detail pays dividends when compared to outbreak data. However there may be other considerations for disease onset.

In contrast to the previous works, Shuai, Tien and van den Driessche focused on a very specific formation of patches, a star [122]. They included bacterial transport between the central hub and peripheral patches or 'leaves'. They also derived type reproduction numbers which are local reproductive numbers for each patch. Shuai et al. wished to know whether one should vaccinate the hub or the leaf. They found that one should vaccinate the hub if most transmission occured there. However, when most transmission occurs in the leaves, one should vaccinate depending on the amount of bacterial flow between the hub and leaves.

The work of Shuai et. al was a theoretical exercise on the effect of bottlenecks in networks. The omission of human movement is notable here as the settlement is comparatively small which may affect the vaccination strategies.

Eisenberg worked with the authors of the previous paper to look at intervention strategies in a cholera model with direct and indirect transmission, temporary immunity and both water and human movement [41]. The human movement was modelled as migration using a similar format to the bacterial movement. However, infected individuals only shed bacteria in the patch they were currently visiting, they had no 'home' patches. The authors examined the stability of the disease free and endemic equilibria and derived expressions for the type or target reproduction numbers. These could then be used to derive thresholds for vaccination and clean water provision.

This is once again a theoretical work. However, the type and target reproduction numbers are valuable thresholds for control strategies that may be estimated for more complicated models in the manner employed in this work.

Ochoche looked exclusively at the effect of water treatment on the dynamics of the model developed by Codeço [99]. He examined the stability of the disease free and endemic steady states and conducted simulations to view the effect of water treatment.

The main focus of the paper is the stability of the model steady states. The model itself is a simple extension of Codeço's to include water treatment which is measured in

its effectiveness by simulation. The results could perhaps have been predicted by other works mentioned here.

Njagarah and Nyabadza used similar techniques to Ochoche to examine their two patch metapopulation model [95]. However they also conducted a sensitivity analysis and looked at the synchrony between the two populations. They found that if the disease went extinct in one patch, it was reintroduced by contact from the disease endemic patch. They also found the epidemics to be more severe in the patch with worse sanitation.

The work of Njagarah and Nyabadza should be examined as it gives a summary of spatial cholera model behaviour. However the results confirm already held suspicions about the effect of sanitation and coupling.

Shuai and van den Driessche revisited their star model with the assumption that the central hub was only a shared water source and had no residual human population [121]. They assumed the host population was heterogeneous over the various patches and there was no loss of immunity. Shuai and Driessche examined the global stability of the equilibria and derived terms for the target reproduction numbers, the reproduction numbers for each patch in the presence of different control measures. These could then be used as thresholds for disease extinction.

The techniques used here could be extended to find local thresholds for different interventions strategies. However, in its current format, the results are purely theoretical.

The last reference included in figure 1.3 discusses mechanistic models for the Haitian cholera epidemic [85]. They compare a number of models through the AIC and assess their predictive capabilities for the Haitian cholera epidemic. These models included many of the elements we have discussed from previous works such as spatial segregation with human and bacterial moments, asymptomatic infection, temporary immunity and rainfall. They found that all models considered had predictive capabilities. However, when the spatial coupling was omitted, the predictions were less effective. They finish by stressing the importance of mathematical modelling for outbreaks and, in particular, the inclusion of spatial coupling.

1.4.0.1 Summary

Over time there have been a number of additions to the basic cholera model designed by Capasso, shown in figure 1.6. Codeço included the dynamics of the susceptible class. This began the focus on modelling the disease spread in the human population as opposed to two separate populations of bacteria and hosts. The Codeço model was then used as a base for the majority of later work. The newly discovered hyper infectious bacterial state prompted Hartley et al. to adapt the model by dividing the bacterial class by infectivity. This changed the emphasis in the model to controlling the freshly shed bacteria and was included in many of the works later on. Bertuzzo et al. ignored HI bacteria, instead focussing on the role of waterways and pathogen movement. They examined the effect of the waterway topology on the travelling wave of cholera and later included a gravity model for human movement. Lastly, in our figure 1.6, King included asymptomatic infection. It was just becoming apparent that there may be a high ratio of asymptomatic to symptomatic infected which not only affects the case numbers but also the population level immunity.

We stopped our figure 1.6 at King for two reasons. Many of the works that came later included some or all of the elements shown in figure 1.6. Also, many of the works

following included a variety of intervention measures which were difficult to generalise diagrammatically. Interventions examined have been vaccination, antibiotics, clean water provision, sanitation, quarantine and education. There have been differing opinions as to which of these is the most effective. However there is a general consensus that a mix between preventative and reactive strategies are generally better.
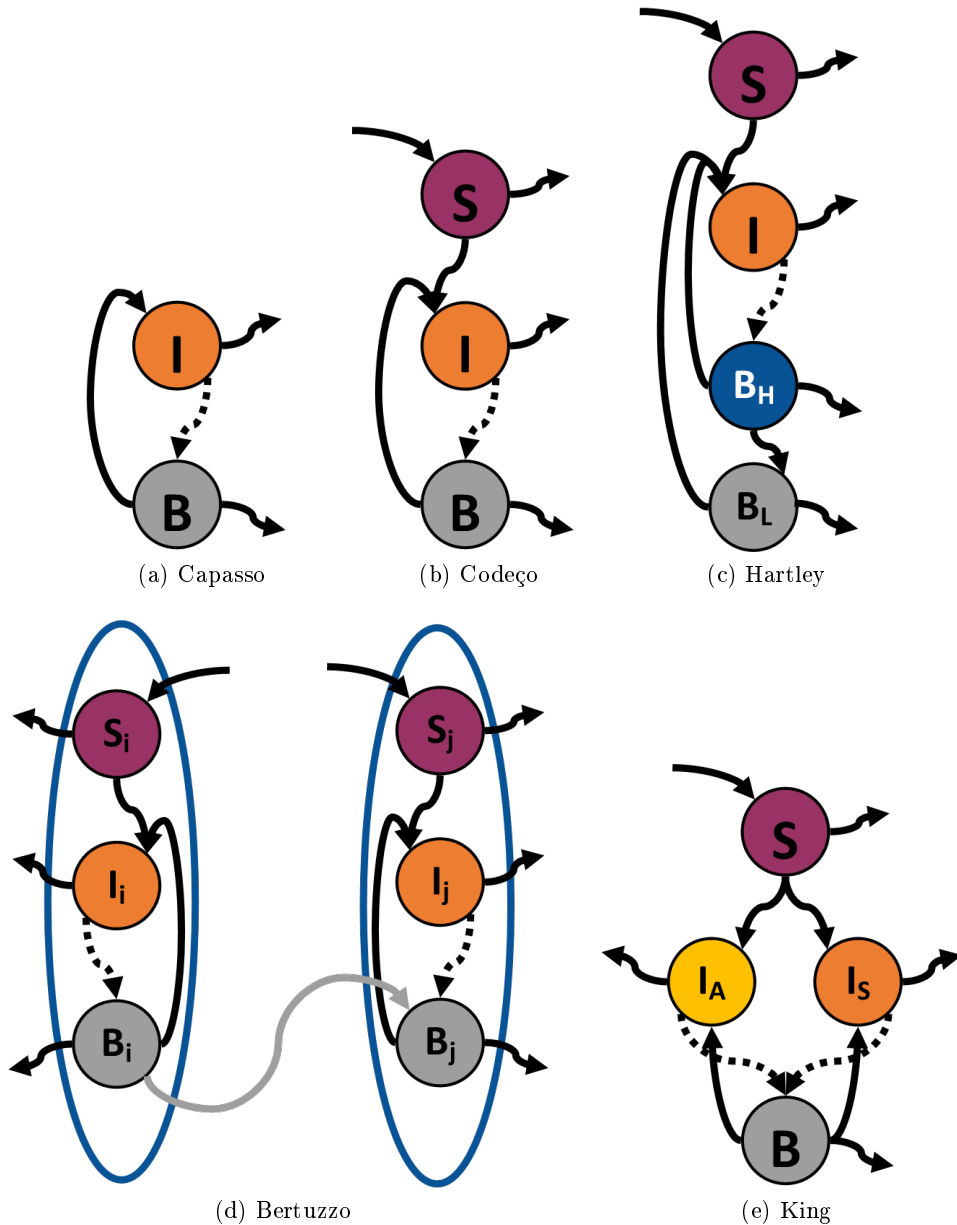
Figure 1.6: Key model diagrams from the works listed in figure 1.3. The variables S, I and B denote the susceptible, infected and bacterial populations respectively. Subscripts H and L denote high and low infectivity, subscripts i and j denote patch numbers and subscripts A and S denote asymptomatic and symptomatic infection.

1.5   Our contribution

There are many aspects of cholera transmission that have been examined in mathematical modelling. However, whilst the effects of the Haitian earthquake have been

mentioned, the effect of natural disasters on cholera epidemics in developing world cities has been overlooked. We shall develop a framework to fill this gap over the course of the thesis.

Figure 1.7 shows diagrams of the model development throughout the thesis. We work towards a complex, heterogeneous model of a developing world city and the cholera dynamics therein when the city is struck by a natural disaster. However, we must first develop the model and understand its baseline behaviour. As such, Chapter Two is an examination of Codeço's model in a homogeneous population. We begin by conducting a sensitivity analysis and simulations of the model in one patch. This will demonstrate the basic disease behaviour. Then, we divide our population in two spatially. We have seen a number of spatial models, most commonly over an entire region or country and the bacterial movement therein. However, we wish to examine a city, therefore the main spreading mechanism spatially is human movement. We will consider separate patches each with their own aquatic reservoir such as a well or borehole. The disease is then moved from one patch to another by human commuter movement. Where migration may be most likely on a country scale, commuting from a home neighbourhood to work and back is more reasonable within a city. Given this movement framework we will conduct further simulations and sensitivity analyses to understand our simple city.

Chapter Three sees us introduce a control measure, treatment of infected individuals. We assume that infected individuals can commute as the majority of cholera cases are not severe [60]. Therefore, the infected individuals may move toward treatment and we assume they do this at an increased rate. We adjust the commuting terms and examine the effects when a treatment facility is only available in one patch. The treatment itself is akin to antibiotics that can be easily transported. Treated individuals have a shorter infectious period and, as a result, shed for a proportionally shorter time. We use a number of classical epidemiological analysis methods at this stage including a bifurcation analysis. This is extended when we add a further condition in Chapter Three B that treatment is limited and the treatment rate falls as the number of infected individuals rises. The new dynamics resulting from this condition prompt a more in-depth bifurcation analysis accompanied by a Poincarè section to classify any oscillatory behaviour.

The eventual aim is to model a heterogeneous population approximating a developing world city. As such, we need to extend our model from two to higher numbers of patches. Chapter Four details this extension in terms of the coupled differential equations, defines three different patch arrangements and examines the difference in disease dynamics for these three arrangements. We examine the three structures through simulation, the basic reproduction number and an ecological concept: the impact. The impact quantifies the effect on each system variable of a perturbation. Therefore, we may use it to measure the effect of a natural disaster on each system element. In this way we may see if the city structure renders the population more resilient to a natural disaster.

In Chapter Five we build on our patch structures with respect to the structure of a developing world city and ask where, in a heterogeneous population, should we place facilities offering treatment and water decontamination. We approach this question initially through simulation and assess distributions of facilities by the allowed epidemic size given a natural disaster. We will find optimal distributions by exhaustive search which is time consuming computationally. However, in Chapter Six, we address the same question of optimal facility deployments with a variety of assessment criteria. These methods are not only less computationally expensive than simulation but may also indicate optimal facility distributions without exhaustive search. These methods will include aspects introduced throughout the thesis and some new such as

(a) Chapter Two

(b) Chapter Three

(c) Chapter Four

(d) Chapter Five
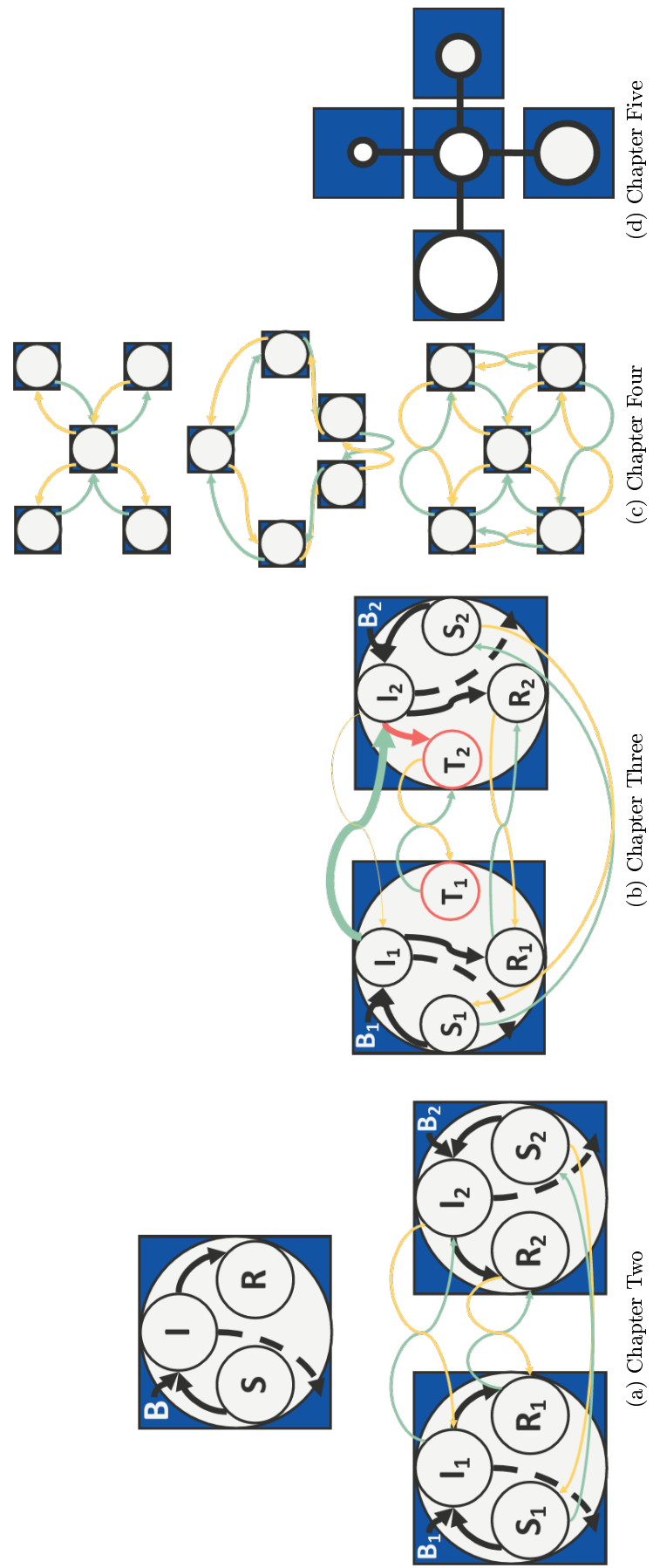
Figure 1.7: Model diagrams for thesis chapters two to five. Arrows denote transitions either in movement, yellow and green, or in disease state, black. The disk represents a population and blue squares represent the bacterial reservoir.

the decomposition of the impact: the sensitivity and influence.

Chapter Six is an assessment of methodologies and we build on this in Chapter Seven. Systems Biology is a growing field and one which we shall borrow techniques from throughout this thesis. In Chapter Seven we investigate its techniques and methods in an in-depth manner to see if Systems Biology could facilitate a new direction for epidemiological modelling. There are many attractive ideas in Systems Biology such as the decomposition of models into nested layers and the examination of steady state reaction pathways through the system. We assess and explain these ideas using a simple epidemiological example. Lastly, we summarise our findings and the manner in which they will advance our knowledge in Chapter Eight.

1.5.1   Summary

Our objective is to understand the effect of natural disasters on environmentally transmitted disease transmission and develop analysis methods to facilitate this objective. Over the course of this thesis we will build and develop our model of an environmentally transmitted disease such as cholera. We will also develop the methods used to analyse and understand that model. The dynamics of a disease in a heterogeneous developing world city have not yet been fully explored, particularly when those dynamics are affected by a natural disaster. Yet, we have seen that natural disasters alter infrastructure and population characteristics in a manner that affects disease transmission. Therefore, we shall address this omission from the literature. We will also develop a novel framework for systems epidemiology- the combination of systems biology techniques and disease modelling.

Chapter 2

Deriving the environmentally transmitted disease model

2.1 Introduction

Diarrhoeal diseases such as cholera are the second largest cause of ill health in children under the age of five years [141]. We will first consider the dynamics of these environmentally transmitted diseases in a population that is homogeneous. We will then examine the disease behaviour in a population that is spatially segregated into two patches. These patches will be linked by the commuter movement of host individuals which we will model in two ways. We examine which model features or parameters are most influential and measure the direction of that influence. This will lay the groundwork for more complicated models later in the thesis.

2.2 Model description

Environmentally transmitted diseases require an external reservoir of bacteria to propagate. This work shall adapt the models for environmentally transmitted diseases used by Codeço [30] for a heterogeneous metapopulation. However, we shall initially consider the host population homogeneous and well mixed.

2.2.1 Homogeneous, one patch model

The simple model we use is adapted from the Susceptible- Infected- Recovered compartmental model mentioned by Keeling and Rohani [74] to include the bacterial reservoir. The disease interactions are shown in figure 2.1.

As shown in figure 2.1, the bacterial class affects the host individual's transition from susceptible to infected. This is because susceptible individuals become infected through contact with the contaminated environmental reservoir. There is a saturating probability that, given contact with the reservoir, infection will occur. This probability is dependant on the concentration of bacteria in the environment. Note also that infected individuals contribute to the bacterial reservoir. This contribution is termed shedding and increases the concentration of bacteria in the environment. This completes the cycle of faecal-oral transmission.

We may formalise the interactions shown in figure 2.1 with ordinary differential equations. Equations (2.1) describe the change over time of the susceptible, infected, recovered and bacterial compartment sizes [30]. We assume the system is at demographic equilibrium and that the population is closed, therefore $\mu N = \mu(S + I + R)$.
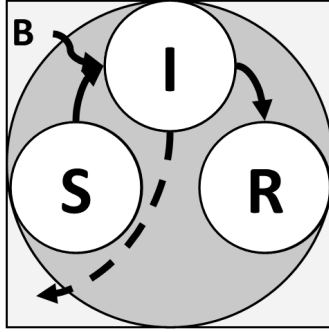
Figure 2.1: Epidemiological interactions in the one patch environmentally transmitted disease model. Disks represent different disease status groups within the patch, S= Susceptible individuals, I=Infected individuals, R=Recovered individuals and B=Concentration of Bacteria.

We also assume that individuals are born susceptible. Infected host individuals may recover at rate γ and contribute bacteria at rate η. The rate they become infected is governed by the force of infection. This depends on the contact rate with the contaminated environment, β, and the probability of infection. This probability is a saturating term dependant on the concentration of bacteria in the environment and half saturation constant, κ such that when $B = \kappa$ the probability of infection given contact is $\frac{1}{2}$. Lastly, the bacteria degrade in the environment at rate θ. All the parameters are explained further in table A.1.

$$
\begin{aligned}
\dot{S} &= \mu N - \beta S \frac{B}{\kappa + B} - \mu S, \\
\dot{I} &= \beta S \frac{B}{\kappa + B} - \gamma I - \mu I, \\
\dot{R} &= \gamma I - \mu R, \\
\dot{B} &= -\theta B + \eta I.
\end{aligned}
\tag{2.1}
$$

2.2.2 Heterogeneous, two patch model

We wish to examine a more realistic population. In a city we would not necessarily expect different areas of population to have the same characteristics. As such, we divide our population spatially into two patches, we choose two to keep the model as simple as possible. The patches are linked by human commuter movement. There is no movement of bacteria in order to focus on the impact of human movement. Also, we assume that the metapopulation forms a city rather than separate settlements. As such, there would be little flow of bacteria. The model is based on the same compartmental system as before with the metapopulation divided by the infectious status of the individuals within it. These disease state compartments are further divided by the current location of the individual, either at home or away. Figure 2.2 shows a summary of these divisions for arbitrary patch p in the metapopulation.

We can express the change in each compartment over time using a system of ordinary differential equations similar to the one patch model. We retain the assumptions from the one patch model and further include the movement and current location of host individuals. Equations (2.2) show that individuals of patch p leave at rate ϕ_p and return at rate τ_p. Therefore, individuals of state X who reside in patch p but are currently visiting patch q are denoted X_{pq}. See table A.1 for further definitions.
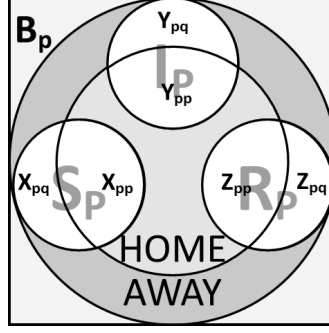
Figure 2.2: Divisions for patch p in a two patch environmentally transmitted disease model. Disks represent different status compartments within the patch e.g. $S_p=$ Susceptible individuals residing in patch p. However, each compartment is divided by current location i.e. $X_{pp}=$Susceptible individuals that reside in patch p currently at home and $X_{pq}=$Susceptible individuals that reside in patch p currently away in patch q.

$$
\text{Susceptible} = \begin{cases} \dot{X}_{pp} = \mu H_{pp} - \beta_p X_{pp} \dfrac{B_p}{\kappa_p + B_p} - \phi_p X_{pp} + \tau_p X_{pq} - \mu X_{pp}, \\[2mm] \dot{X}_{pq} = \mu H_{pq} - \beta_p X_{pq} \dfrac{B_q}{\kappa_q + B_q} + \phi_p X_{pp} - \tau_p X_{pq} - \mu X_{pq}, \end{cases}
$$

$$
\text{Infected} = \begin{cases} \dot{Y}_{pp} = \beta_p X_{pp} \dfrac{B_p}{\kappa_p + B_p} - \gamma_p Y_{pp} - \phi_p Y_{pp} + \tau_p Y_{pq} - \mu Y_{pp}, \\[2mm] \dot{Y}_{pq} = \beta_p X_{pq} \dfrac{B_q}{\kappa_q + B_q} - \gamma_q Y_{pq} + \phi_p Y_{pp} - \tau_p Y_{pq} - \mu Y_{pq}, \end{cases}
$$

(2.2)

$$
\text{Recovered} = \begin{cases} \dot{Z}_{pp} = \gamma_p Y_{pp} - \phi_p Z_{pp} + \tau_p Z_{pq} - \mu Z_{pp}, \\[1mm] \dot{Z}_{pq} = \gamma_q Y_{pq} + \phi_p Z_{pp} - \tau_p Z_{pq} - \mu Z_{pq}, \end{cases}
$$

$$
\text{Total Hosts} = \begin{cases} \dot{H}_{pp} = \mu H_{pp} - \phi_p H_{pp} + \tau_p H_{pq} - \mu H_{pp}, \\[1mm] \dot{H}_{pq} = \mu H_{pq} + \phi_p H_{pp} - \tau_p H_{pq} - \mu H_{pq}, \end{cases}
$$

$$
\text{Bacteria} = \begin{cases} \dot{B}_p = -\theta_p B_p + \eta_p (Y_{pp} + Y_{qp}) \end{cases}
$$

These equations, and the corresponding equations for the other patch, q, describe all the interactions present including the commuter movement. However, using the quasi-equilibrium method described by Keeling, Rohani and Sattenspiel & Dietz we may simplify the above equations with the assumption that commuter movement is fast relative to the disease dynamics and so equilibrates quickly [73, 72, 118]

As the system is at demographic equilibrium, the change in the total number of individuals in each patch is zero i.e. $\dot{N}_p = \dot{H}_{pp} + \dot{H}_{pq} = 0$. Using this and the fast movement assumption we have the following relation for the number of individuals from patch p who are at home:

$$\dot{H}_{pp} = \mu H_{pp} - \phi_p H_{pp} + \tau_p H_{pq} - \mu H_{pp},$$
$$= -\phi_p H_{pp} + \tau_p H_{pq},$$
$$= 0$$
$$\Rightarrow H_{pp} = \frac{\tau_p}{\phi_p} H_{pq}. \tag{2.3}$$

As $N_p = H_{pp} + H_{pq}$ we may use equation (2.3) to express the number of individuals residing in patch p who are currently in patch p in terms of the total population size, N_p, and the movement terms, τ_p and ϕ_p,

$$H_{pp} = N_p - H_{pq} = \frac{\tau_p}{\tau_p + \phi_p} N_p = \sigma_p N_p. \tag{2.4}$$

The parameter σ_p denotes the average proportion of time an individual from patch p spends at home. We may use the above method on each of the disease classes to write the number of individuals in each state in terms of the total number of individuals in that state. For example, $S_p = X_{pp} + X_{pq}$ therefore $X_{pp} = \sigma_p S_p$. Therefore, we may write the equations for the commuter model, given the assumptions above, in terms of the total numbers of individuals in each disease state, shown in equations 2.5.

$$\dot{S}_p = \mu N_p - \beta_p S_p \sigma_p \frac{B_p}{\kappa_p + B_p} - \beta_q S_p (1 - \sigma_p) \frac{B_q}{\kappa_q + B_q} - \mu S_p,$$
$$\dot{I}_p = \beta_p S_p \sigma_p \frac{B_p}{\kappa_p + B_p} + \beta_q S_p (1 - \sigma_p) \frac{B_q}{\kappa_q + B_q} - I_p(\gamma_p + \mu), \tag{2.5}$$
$$\dot{R}_p = \gamma_p I_p - \mu R_p,$$
$$\dot{B}_p = -\theta_p B_p + \eta_p(\sigma_p I_p + (1 - \sigma_q)I_q).$$

Now that we have derived our models, we shall explain the analysis methods employed to understand them.

2.3 Analysis

We wish to understand the dynamics of an environmentally transmitted disease in a population in one and then two patches. We are interested in which parameters are the most influential and the manner in which they affect key system elements such as the growth of an epidemic. The response of the system to a perturbation is also important as we wish to measure the effect of a natural disaster on the disease spread in later chapters. We first define some key system outputs that will be used throughout the thesis. These will be used our measures of system behaviour.

2.3.1 Model outputs

To measure the epidemiological behaviour of our model, we must define some characteristics or outputs that will be informative. We are interested in the growth, duration and severity of an epidemic. Therefore, we must define methods to capture this information. We start with the basic reproduction number which is a measure of the initial epidemic growth.

2.3.1.1 The basic reproduction number and part reproduction numbers

The basic reproductive number, R_0, denotes the expected number of infections caused by one infected individual in a totally susceptible population in one generation [37]. The basic reproductive number can also act as a measure of the risk of an epidemic; if $R_0 < 1$ there can be no epidemic. When $R_0 > 1$ one infected individual may infect more than one susceptible individual and the disease can remain endemic in the population [24].

We may be interested in which infectious class contributes most to the reproductive number and to assess this we must divide R_0 into its constituent parts. R_0 is the lead eigenvalue of the next generation matrix, $\mathcal{NGM}$, linearised about the disease free equilibrium. The method to calculate R_0 is described by Diekmann et al., Heffernan et al. and (more specifically for metapopulations) by Arino and Van den Driessche [9, 10, 36, 37, 62]. The $\mathcal{NGM}$ is found by multiplying the transmission matrix, $\mathcal{T}$, by the inverse of the transition matrix, Σ. These matrices consist of the transmission and transition terms of the system Jacobian at disease free equilibrium. Thus,

$$\mathcal{NGM} = \mathcal{T}\Sigma^{-1}.$$

The ij^{th} element of the $\mathcal{NGM}$ represents the expected number of new infections of type i due to one infection of type j and R_0 can be seen as a weighted average of all the infections caused by each type. We may be interested in the contribution of each infectious class to R_0 and we calculate this contribution through decomposition. We decompose R_0 using the next generation matrix columns and the corresponding lead eigenvector. The linear algebra of this decomposition, for an $n \times n$ matrix $\mathbf{M}$ with lead eigenvalue λ and corresponding eigenvector $\mathbf{v}$, can be explained as follows. We have that,

$$\mathbf{M}\mathbf{v} = \lambda\mathbf{v}, \tag{2.6}$$

and we may consider this equation in terms of its matrix elements as $\mathbf{M} = \left(\begin{smallmatrix} m_{11} & \dots & m_{1n} \\ \dots & \dots & \dots \\ m_{n1} & \dots & m_{nn} \end{smallmatrix}\right)$ and $\mathbf{v} = \left(\begin{smallmatrix} v_1 \\ \dots \\ v_n \end{smallmatrix}\right)$. Then, (2.6) gives,

$$\begin{aligned} m_{11}v_1 + \dots + m_{1n}v_n &= \lambda v_1, \\ m_{21}v_2 + \dots + m_{2n}v_n &= \lambda v_2, \\ &\dots \\ m_{n1}v_1 + \dots + m_{nn}v_n &= \lambda v_n. \end{aligned} \tag{2.7}$$

Equations (2.7) may then be summed to give the following,

$$\sum_i m_{i1}v_1 + \dots + \sum_j m_{jn}v_n = \lambda \sum_k v_k$$

and thus,

$$\frac{\sum_i m_{i1}v_1 + \dots + \sum_j m_{jn}v_n}{\sum_k v_k} = \lambda.$$

In our case, the matrix is the $\mathcal{NGM}$ and the lead eigenvalue is R_0. As such, we may decompose R_0 into components, R_0^i, formed from the sums of the column elements of

the next generation matrix and the eigenvector elements, i.e.

$$R_0 = \sum_i R_0^i,$$

where

$$R_0^i = \frac{\sum_j m_{ji} v_i}{\sum_k v_k}.$$

The interpretation of the part reproduction numbers, R_0^i, is the relative contribution of each type i to the basic reproduction number. That is, the extent to which each class of the system adds to the number of infections caused by one 'typical' individual in one generation.

We now use a simple example, shown in italic, on R_0 to illustrate the algorithm steps.

1. Find the next generation matrix.

   In our one patch model

   $$\mathcal{NGM} = \begin{pmatrix} 0 & \frac{N\beta}{\theta\kappa} \\ \frac{\eta}{\gamma+\mu} & 0 \end{pmatrix}.$$

2. Find the lead eigenvalue, R_0.

   Our one patch model has

   $$R_0 = \sqrt{\frac{\eta\beta N}{\kappa\theta(\gamma+\mu)}}.$$

3. Find the corresponding eigenvector, $\mathbf{v}$.

   In our situation

   $$\underline{v} = (\sqrt{\frac{\beta N}{\theta\kappa}}, \sqrt{\frac{\eta}{\gamma+\mu}})^T$$

4. Find the sum of the elements in each matrix column.

   The part reproduction numbers for the one patch model are then given by the sums of the next generation matrix columns, $\frac{N\beta}{\theta\kappa}$ and $\frac{\eta}{\gamma+\mu}$.

5. Then, the ith part reproduction number, R_0^i, is calculated as the sum of the ith column elements, C_i multiplied by the ith eigenvector element, v_i divided by the sum of the eigenvector elements.

   Thus, we arrive at our part reproduction numbers:

32

$$R_0^1 = \frac{\left(\dfrac{N\beta}{\theta\kappa}\right)^{1.5}}{\left(\dfrac{N\beta}{\theta\kappa}\right)^{0.5} + \left(\dfrac{\eta}{\gamma+\mu}\right)^{0.5}}$$

$$R_0^2 = \frac{\left(\dfrac{\eta}{\gamma+\mu}\right)^{1.5}}{\left(\dfrac{N\beta}{\theta\kappa}\right)^{0.5} + \left(\dfrac{\eta}{\gamma+\mu}\right)^{0.5}}$$

2.3.1.2 Resilience

We wish to measure not only the growth rate of an epidemic but its duration. As such, we examine the resilience at disease free and endemic equilibrium. This measures the time taken for the system to return to a stable equilibrium following a perturbation from that equilibrium [94]. The system is linearised about the disease free or endemic equilibria and the Jacobian matrix for the infectious classes is examined. The resilience is the negated lead eigenvalue of this reduced Jacobian at equilibrium. It is an asymptotic property and thus ignores any transient fluctuations, shown in figure 2.3. A larger resilience means that perturbations decay more quickly.

In the one patch model, the Jacobian for the infectious classes, $\mathcal{J}$, is given by,

$$\mathcal{J} = \begin{pmatrix} -(\gamma+\mu) & \frac{\beta S^* \kappa}{(\kappa+B^*)^2} \\ \eta & -\theta \end{pmatrix},$$

Here S^* and B^* denote the equilibrium values of the susceptible and bacterial populations respectively. The resilience is then given by

$$\text{resilience} = \frac{1}{2}\left((\gamma+\mu+\theta) - \sqrt{(\gamma+\mu+\theta)^2 - 4\left(\theta(\gamma+\mu) - \frac{\eta\beta S^* \kappa}{(\kappa+B^*)^2}\right)} \right).$$

The resilience can also be interpreted as the negative intrinsic growth rate, r. This describes the initial growth of the epidemic over time rather than over each generation like R_0. Therefore, when it is negative, it describes the rate of return to equilibrium.

2.3.1.3 Reactivity

As the resilience is an asymptotic property, we examine the reactivity to capture the transient system behaviour. This can be considered a measure of the severity of an epidemic. The reactivity is the 'maximal instantaneous rate' at which perturbations can be amplified [94]. When the system is perturbed from a stable equilibrium, it may initially move away from the equilibrium. The reactivity measures this movement, shown in figure 2.3. It is calculated as the lead eigenvalue of the Hermitian part of the Jacobian for the infectious classes at equilibrium.

In the one patch model, the Hermitian matrix, $\mathcal{H}$, is given by,

$$\mathcal{H} = \frac{1}{2}\begin{pmatrix} -2(\gamma+\mu) & \frac{\beta S^* \kappa + \eta(\kappa+B^*)^2}{(\kappa+B^*)^2} \\ \frac{\beta S^* \kappa + \eta(\kappa+B^*)^2}{(\kappa+B^*)^2} & -2\theta \end{pmatrix}.$$

The reactivity is then given by,

$$\text{reactivity} = \frac{1}{2}\bigg(-(\gamma + \mu + \theta)$$

$$+ \sqrt{(\gamma + \mu + \theta)^2 - 4\left(\theta(\gamma + \mu) - \left(\frac{\eta(\kappa + B^*)^2 + \beta S^* \kappa}{2(\kappa + B^*)^2}\right)\right)^2} \ \bigg).$$
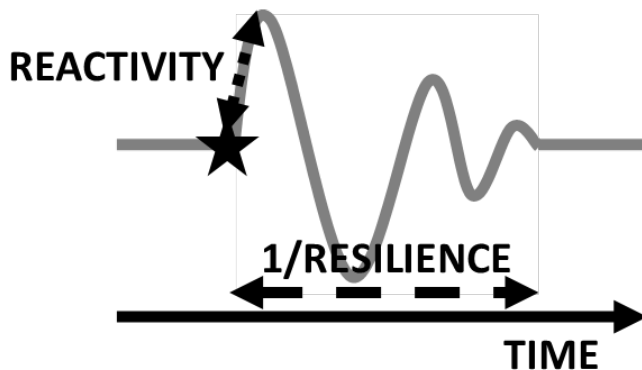
Figure 2.3: The trajectory of a system, grey following a perturbation, star, and the relative measures of the resilience and reactivity.

2.3.2 Analysis Techniques

We have established which outputs of the model we are going to measure and why. Now we describe how we assess and understand these characteristics. One of our foci is how the input parameters affect the behaviour of the system. Therefore we detail an efficient technique for sampling our parameter space which we can use in two sensitivity analyses. These analyses will indicate which parameters are influential. Finally, we outline a method of simulation which will give us insight into the model behaviour over time.

2.3.2.1 Latin hypercube sampling, LHS

The parameters given in table A.1 each take a range of values. As such, we have a large, multi-dimensional parameter space to explore in order to understand the range of system behaviour. This would be impossible to complete fully; therefore, we use an efficient sampling technique to capture many of the possible combinations of parameter values. This is termed Latin Hypercube Sampling or LHS and it allows an unbiased estimate of the average model output [89]. The steps are as follows with a simple example:

1. Define a range and probability distribution for each parameter. In our model, we chose a uniform distribution for each to avoid under sampling.

   In our example, take two parameters, ρ_1 and ρ_2. Let them be uniformly distributed with $\rho_1 \in [0,1]$ and $\rho_2 \in [0,10]$.

2. Calculate the minimum number of samples required, M. In this work we take 5000 samples to thoroughly represent the parameter space.

   For example, let us take three.

34

3. Divide the range of each of the K parameters into M equally probable intervals.

   In our example we assumed the parameters were uniformly distributed. Therefore, we may just divide the range into three equally wide sections. For ρ_1 the sections are [0,0.33], [0.33, 0.66] and [0.66,1] and for ρ_2 the sections are [0,3.33], [3.33,6.66] and [6.66,1].

4. Sample each interval of the parameter space once.

   For instance, for the first parameter, ρ_1, our samples are [0.20, 0.45, 0.97]. For our second parameter, ρ_2 our samples are [0.01,5.50,6.67]

5. Generate the Latin Hypercube Sample table by permuting the sample vectors to give a vector of length M of possible values for each parameter. Use these vectors to form a $K \times M$ matrix where each row is a complete parameter set.

   Our first parameter vector becomes [0.97,0.20,0.45] and our second, [0.01,6.67,5.50]. Therefore, our LHS matrix is
   $$\begin{pmatrix} 0.97 & 0.01 \\ 0.20 & 6.67 \\ 0.45 & 5.50 \end{pmatrix}.$$

2.3.2.2 Partial rank correlation coefficient, PRCC

The partial rank correlation coefficient, or PRCC, uses the parameter sets generated by the Latin Hypercube Sample. It measures the change in a system output, such as R_0, given a change in system input or parameter. This will indicate how the input parameters can change the system behaviour. The PRCC also quantifies the magnitude of influence of an input on output which will give us a clear indication of which parameters are most important. The calculation requires that the relationship between input and output is monotonic. The steps of the calculation and simple example are as follows [21, 53, 58, 66, 67, 87, 117].

1. Calculate the output (e.g. R_0) for each of the M parameter sets generated by the LHS.

   Let us take the parameters as $\rho_1 \in [0,1]$, $\rho_2 \in [0,10]$ and $\rho_3 \in [0,1]$ and the LHS matrix as
   $$LHS = \begin{pmatrix} 0.37 & 1.5 & 0.7 \\ 0.98 & 7.77 & 0.15 \\ 0.55 & 6.24 & 0.32 \\ 0.20 & 4.59 & 0.82 \end{pmatrix}.$$

   If our output, ω, takes the form $\omega = \frac{\rho_1}{(\rho_2+\rho_3)}$ then the output values for each parameter set are
   $[0.1682, 0.1237, 0.0838, 0.0370]^T$.

2. Next, rank each element in the parameter sets and output according to their magnitude starting with the smallest element equal to one. This will give a vector that preserves the relative order of the values. This allows us to compare parameters that span different ranges [66].

   Our new, ranked sample matrix is
   $$LHS^r = \begin{pmatrix} 2 & 1 & 3 \\ 4 & 4 & 1 \\ 3 & 3 & 2 \\ 1 & 2 & 4 \end{pmatrix}.$$

35

Our output, ω has the ranked vector $[4, 3, 2, 1]^T$.

3. Calculate a linear regression model for the inputs and output. This gives an approximate mean value of a variable for a given parameter set. Formally, the regression of output on input is the mean of the output for a given value of the input [31].

   We now focus on one of our example parameters in its ranked form, ρ_2^r and the ranked form of the output, ω^r. We calculate the linear regression model, $\bar{\rho}_2$ using the following equation $\bar{\rho}_2 = X_{\rho_2}((X_{\rho_2}^T X_{\rho_2})^{-1}(X_{\rho_2}^T \rho_2^r))$ where X_{ρ_2} is the LHS^r matrix with ρ_2 column set to ones. This gives us a value of $\bar{\rho}_2$ of $[4, 8, 6, 2]^T$ and a value of $\bar{\omega}$ of $[4, 3, 2, 1]^T$.

4. Calculate the residuals. The residual is the difference between the actual parameter value and the mean or expected value (the linear regression model for that parameter).

   The residual for ρ_2 is $[-3, -4, -3, 0]^T$ and for ω is $[10, 5, 6, 9]^T$.

5. Calculate the PRCC for each parameter using: $PRCC = \dfrac{\text{(input residual)}.\text{(output residual)}}{((\text{input residual})^2(\text{output residual})^2)^{\frac{1}{2}}}$.

   The PRCC for ρ_2 is $\dfrac{[-3, -4, -3, 0].[10, 5, 6, 9]}{(([-3, -4, -3, 0])^2([10, 5, 6, 9])^2)^{\frac{1}{2}}} = -0.66$.

6. Produce a table of the Partial Rank Correlation Coefficients for each parameter. The PRCCs fall between -1 and 1 and coefficients with absolute value greater that 0.5 are considered significant. The magnitude of the PRCC also indicates a stronger correlation.

   Therefore, our value of -0.66 is considered significant and indicates as ρ_2 increases, ω decreases.

2.3.2.3 Elasticity analysis

To complement, and add information to, the PRCC analysis, we will conduct an elasticity analysis of R_0. The elasticity measures the proportional change in the output given a small change in the input at one point in the parameter space. Therefore, whilst the PRCC classifies the relationship between input and output with one number or correlation coefficient, the elasticity classifies it at each point in the parameter space. This can be less clear to interpret. However, the elasticity is a more flexible analysis technique as it does not require monotonicity. We use it here to reinforce our PRCC findings and to show the range of influence that an input has on an output. The elasticity using the following steps [11, 27, 34, 83, 88].

1. Generate a Latin Hypercube Sample.

   We shall use the same sample as with the PRCC.

2. Calculate the output symbolically and find the partial derivative with respect to each parameter, ρ.

   The partial derivative of output, ω, with respect to parameter, ρ_2, is given by $\frac{\partial \omega}{\partial \rho} = \frac{-\rho_1}{(\rho_2 + \rho_3)^2}$.

3. The elasticity for parameter ρ is given by $E_\rho = \frac{\rho}{\text{output}} \frac{\partial \text{output}}{\partial \rho}$. This is evaluated at each parameter set in the sample. The scaling, $\frac{\rho}{\text{output}}$, allows us to compare parameters of different orders of magnitude.

   Thus, for each parameter set in our sample the elasticity of ω with respect to ρ_2 is
   $[-0.6818, -0.9811, -0.9512, -0.8484]$. *This indicates ρ_2 has a strong negative correlation with ω.*

2.3.2.4 Simulation

We use simulation to examine the effect of parameter changes on the size, duration and peak of an epidemic. In the one patch model, we focus on the effect of a perturbation in each parameter value. This will give an insight into the sensitivity of the epidemic characteristics to the system parameters. When we examine the two patch model we focus solely on the effect of the coupling parameters, σ_i. This will suggest how the coupling affects the progress of the epidemic through the segregated population. The simulation will add to our sensitivity analyses by showing the behaviour away from equilibrium over time. The simulations are run as follows:

1. Begin with a disease free system. We shall start with a parameter set, specified in table A.2. In the one patch model, we vary β so we take an initial value in our β range. In the two patch model, we vary σ_1 and so we take an initial value in the σ_1 range. We take 100 equally spaced values for β between 0 and 10 and for σ_1 between 0 and 1.

2. Using MATLAB's ode45 we simulate the epidemic. This is not a stiff solver; however, as we consider the commuter approximation with no fast movement terms, this should be sufficient. We introduce infected individuals in the initial conditions such that there are $N/1000$ such individuals in the population. In the two patch model, $N_1/1000$ infected individuals are introduced into patch one only. The simulation is run for 500 days.

3. We then measure the epidemic characteristics.

   - The peak of the epidemic is defined as the maximum number of infected individuals at any point in time.

   - The duration is defined as the length of time until the number of infected individuals has returned to near equilibrium level i.e. within 1 of the equilibrium value.

   - The size is defined as the total number of infections over the course of the epidemic. This is measured through an extra compartment in the model, similar to the infected class but without loss due to death or recovery.

4. We return to step 2 with the next value of β or σ_1.

5. In the one patch model, we revisit step 2 and use a parameter set with one of the values perturbed to twice their value. We repeat this for each influential parameter.

6. In the one patch model we evaluate R_0 at each value of β and perturbed parameter value. The duration, size and peak of the epidemic over the varying values of β or σ_1 are then plotted against R_0 or σ_1.

We have established the key system elements and the tools that we shall employ to examine them. We will now see the results for the one patch system and discuss the implications.

2.4 Results

Our aim is to find the most influential system parameters and the manner in which they affect the spread of an environmentally transmitted disease through a population. We start with a completely homogeneous host population and one environmental reservoir. This will give us insight into the underlying behaviour of the disease before we examine the effect of spatial segregation through the two patch model.

2.4.1 One patch model results

Here we examine the situation where there is one well mixed host population. We start with the PRCC values for each of the model parameters. These will indicate which parameters most influence the model outputs: R_0, part R_0^i, resilience and reactivity.

2.4.1.1 Partial rank correlation coefficients

We compare the relation between the input parameters and outputs. Recall that a significant coefficient value has magnitude greater than one half.

Output	θ	η	γ	μ	N	β	κ
R_0	-0.5931	0.5978	-0.5997	0.0033	0.6039	0.6020	-0.6073
Part R_0^I	-0.3003	0.8229	-0.8223	0.0080	0.3632	0.3706	-0.2824
Part R_0^B	-0.6619	0.4126	-0.3714	-0.0055	0.6663	0.6689	-0.6562
Resilience (DFE)	0.7845	-0.4686	0.5636	-0.0090	-0.4588	-0.4604	0.2907
Resilience (EE)	0.7875	-0.2611	0.7218	0.0055	-0.2477	-0.2489	0.4871
Reactivity (DFE)	-0.6750	0.3168	-0.5675	-0.0017	0.5690	0.5661	-0.4453
Reactivity (EE)	-0.6428	0.3795	-0.6328	0.0081	0.1191	0.1269	-0.3721

Table 2.1: Partial rank correlation coefficients for one patch model. Parameters take values in the ranges shown in table A.1. The sets are divided into those that give $R_0 < 1$ and those that give $R_0 > 1$ to define the disease free (DFE) and endemic equilibrium (EE) groups. Cell shading indicates a significant PRCC value with grey, positive, and black, negative.

Table 2.1 shows PRCCs describing the level of influence of each parameter on the model outputs. If we first consider the basic reproduction number and part reproduction numbers we notice some important trends. There are three parameters that significantly positively affect R_0 and three that significantly negatively affect R_0. If we increased θ, γ or κ we would expect a notable decrease in R_0. This is because the duration of infection would be diminished if the bacteria degradation rate, θ, or the recovery rate, γ, were increased and the probability of infection given contact with the environment would be reduced if κ was increased. Conversely, we would expect R_0 to increase if η, N or β were increased. This is because more bacteria would enter the environment if the shed rate, η, increased and there would be more individuals to potentially shed if the population size, N, increased. Similarly, an increase in the contact rate, β, leads to increased interaction with the bacteria in the environment.

The part reproduction numbers are cumulatively affected in the same ways as the system R_0. However, the infected class reproduction number is notably related to

38

the shed rate, η, and recovery rate, γ, as these dictate the amount an individual can contribute to the bacteria and for how long. The bacterial class reproduction number is more affected by the bacterial degradation rate, θ, population size, N, contact rate, β and half-saturation constant, κ. This is because these parameters govern how long bacteria can contaminate the environment, how many individuals they can interact with, the amount of interaction and the probability of infection given interaction. This all modifies the contribution of the bacterial class to the system R_0.

The resilience and reactivity are divided in their behaviour by the stability of the equilibria. This was done by testing each parameter set and assigning it as above the epidemic threshold, where $R_0 > 1$ and $r > 0$, or below. There were an equal number of parameter sets either side of the threshold. This calculation method is different to R_0 as the basic reproduction number is calculated assuming the entire population is disease free regardless of whether the disease free equilibrium is stable. We note that the signs of the resilience coefficients are opposite to those for the reactivity. This is because the resilience is an inverse i.e. as it increases the intrinsic growth rate decreases or becomes more negative. Generally, the parameters that raise the resilience and lower the reactivity when increased, also raise R_0. Similarly, those that negatively affect the resilience and positively affect the reactivity positively affect R_0. However, at endemic equilibrium the parameters have less influence on the reactivity in general. This is as there is a reduction in the potential maximal amplification of a perturbation when the susceptible population is depleted. In general, the most important parameters for the resilience and reactivity are the degradation rate, θ, and recovery rate, γ, which govern generation time.

2.4.1.2 Elasticity Analysis

The elasticity results for the basic reproduction number follow. These not only highlight which parameters are influential but also the extent to which they vary in effect.
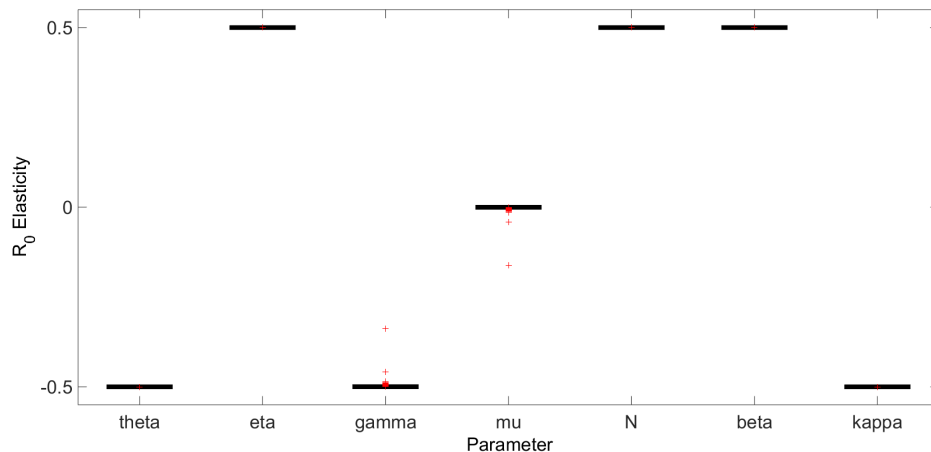
Figure 2.4: Box plot of elasticity values for the one patch model. The output is R_0 and the inputs are the system parameters in the ranges specified in table A.1

Here we see a confirmation of the results of the PRCC analysis. The parameters θ, γ and κ all negatively affect R_0 whereas η, N and β all positively affect it. The death rate μ has little or no effect over its entire range. We see there is little variation in the effect of each parameter over the parameter space. This is unsurprising as R_0 involves a square

root term. Therefore, if $a = \sqrt{b}$ then the elasticity is defined as $\dfrac{b}{a}\dfrac{\partial a}{\partial b} = \dfrac{\partial \log a}{\partial \log b} = 0.5$. Thus, in all cases except μ, where there is no variation as μ is so small, the elasticity should be fairly unvarying.

2.4.1.3   Simulation

Lastly, we examine the disease dynamics away from equilibrium. The system is initially disease free and we introduce $N/1000$ infected individuals. We simulate an epidemic, we repeat for a range of contact values, β, and measure its size, peak and duration. We then repeat the whole procedure with a perturbation to one parameter at a time. As we may see from the elasticity analysis, β and R_0 are proportional. Therefore, we may evaluate R_0 at each value of β, and perturbed parameter value, and plot this as our abscissa. Figure 2.5 shows this information for the epidemic size with respect to R_0 evaluated at each value of β.

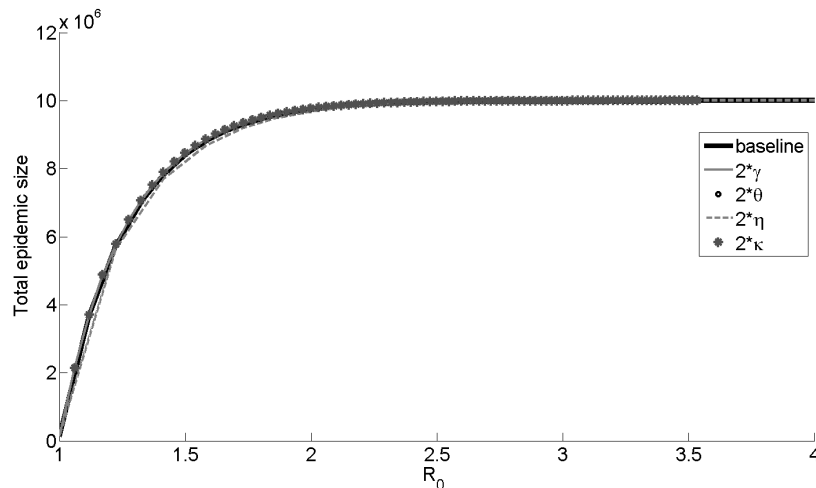Figure 2.5: Relation between R_0 and epidemic size. Contact rate, β, varied between 0 and 10 and all other parameters were held at the values in table A.2 when not perturbed. The system was initially disease free with N/1000 infected individuals introduced.

We start by examining the total epidemic size. The baseline behaviour shows a positive, saturating correlation between the epidemic size and R_0. Therefore, as the basic reproduction number increases, the number of infections over the course of the epidemic also increases. Figure 2.5 shows that the perturbed parameter values do little to alter the relation between R_0 and epidemic size. Therefore, the epidemic size depends on the total R_0 and not the particular parameter values that it consists of. This is because the epidemic size accounts for the duration of infection and the growth rate of the epidemic. The duration categorizes how long an infectious individual remains infectious. Whereas, the growth rate of the epidemic is governed by how quickly infectious individuals may spread that infection. The basic reproduction number also accounts for both of these aspects. It is a *per-generation* growth rate and so is formed from both the force and duration of infection. Therefore, these measures comprise of the same disease characteristics and we may expect them to be strongly correlated.

The relation between epidemic duration and R_0 does alter given perturbations to some of the parameters. In general, the duration is longest when R_0 is near one and decreases as R_0 increases. This is because the force of infection, altered by the contact rate β, becomes stronger and depletes the susceptible population more quickly. Once

Figure 2.6: Relation between R_0 and epidemic duration. Contact rate, β, varied between 0 and 10 and all other parameters were held at the values in table A.2 when not perturbed. The system was initially disease free with N/1000 infected individuals introduced.
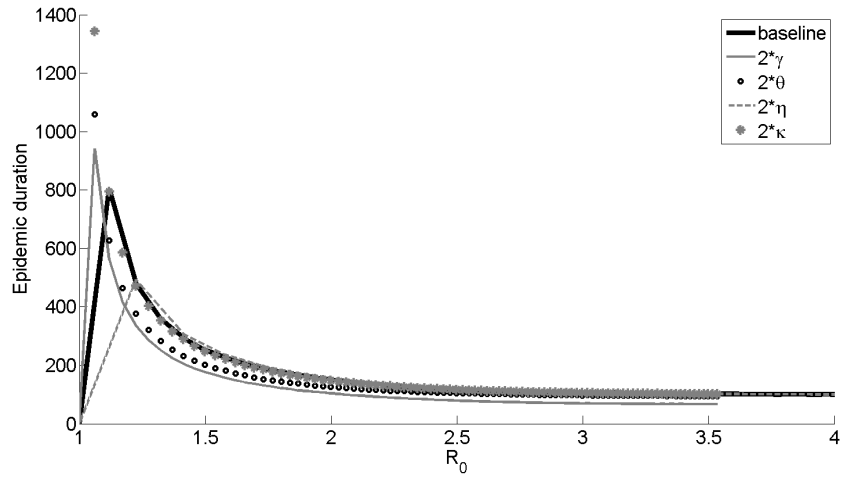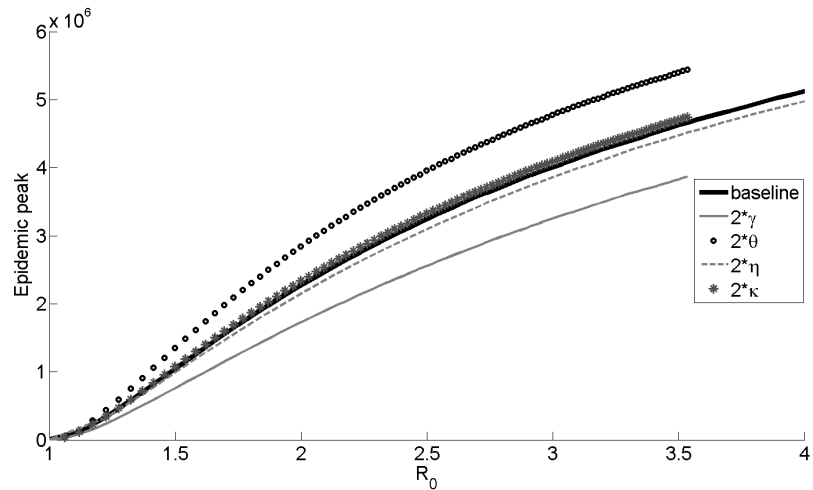

Figure 2.7: Relation between R_0 and epidemic peak. Contact rate, β, varied between 0 and 10 and all other parameters were held at the values in table A.2 when not perturbed. The system was initially disease free with N/1000 infected individuals introduced.

the susceptible population has been sufficiently depleted, the disease begins to die out. As we perturb the parameters we also alter R_0. For instance, when we increase the recovery rate, γ, we will lower R_0. Therefore, for the same R_0 as the unperturbed case, we must have a proportionally higher value of β. This means that the graph of the duration appears to be shifted to the left. In contrast, increasing η increases R_0 and so the graph of the duration is shifted to the right. Thus, the change in the duration graphs is directly related to the change in R_0. The artefact when $R_0 < 1$ is as the duration must be zero when there is no possibility of an epidemic.

Finally, we examine the relation between epidemic peak, R_0 and the key parameters. As R_0 increases, so does the epidemic peak. However, it is higher for the same value of R_0 when θ is doubled and lower for the same R_0 when γ is doubled. When θ increases, R_0 decreases. Thus, to achieve the same R_0 we must have a proportionally higher β value. Therefore, there is a higher number of infections. However, when γ increases, R_0 decreases also. But, γ will check the increase in infected individuals caused by a proportionally higher value of β by their removing them to the recovered class. The net effect of this is that the epidemic peak is lower for the same value of R_0.

2.4.2 Two patch model results

The one patch model results will still be informative when the host population is heterogeneous. However, there is further information we wish to extract now that the population is segregated. Namely, the effect on system outputs such as R_0, of the coupling between the patches. We also measure the effect of the inputs when they can take different values in each patch.

In the following section some of the key parameters, such as β, N and η can take different values in each patch. This is as it is unlikely that both populations will be of equal size or have equal levels of sanitation. We shall keep θ, κ, γ and μ the same for both populations. These are characteristics of the bacteria and hosts themselves and are less likely to vary spatially. This will give us insight into how the variation affects the parameter influence and will lay the foundation for heterogeneities later in the thesis.

2.4.2.1 Partial rank correlation coefficient

We examine the PRCCs for the parameters in the two patch model. As previously mentioned, some parameters will take different values in each patch and some will not. As such, there are 12 parameters to assess. The correlation coefficients for each of these parameters when compared to the R_0, resilience, reactivity and part reproduction numbers are shown in table 2.2.

Let us first discuss the results for the basic reproduction number. Table 2.2 shows that the significant parameters from the one patch model, θ, η, γ, N, β and κ, are still significant here. However, when the parameters take different values in each patch their PRCC appears to be split. For example, the PRCC for each of the population sizes, N_1 and N_2, is around 0.358, not significant in each separate patch, but the combined population size is influential. This is almost as the total range of variation is reduced by the split into the variation of each patch population size.

We now examine the part reproductive numbers. As before, the parameters that most influence R_0 also influence the part R_0. However, the parameters are divided by whether they most affect the infected individuals or bacteria and which patch they apply in. For instance, $R_0^{I_i}$ are most positively affected by the population sizes of patch i. The coupling parameters appear to only affect $R_0^{B_i}$. We see that as individuals of

patch i spend more time at home, and those of patch j spend more time visiting, the contribution of bacterial class of patch i increases. This is a result of a fixed bacterial reservoir. Host individuals must move towards it for it to become influential.

Lastly, we examine the resilience and reactivity. The correlations between the parameters and these outputs remain the same as in the one patch model but vary in magnitude. Generally, there are no 'significant' correlations at endemic equilibrium. This is partly due to the split parameters and partly as a result of the depleted susceptible population which limits the capacity of the system to react.

2.4.2.2   Elasticity of R_0

We now examine the elasticity of R_0 with respect to each of the parameters. We shall see to what extent the parameters vary in their effect and confirm the results of the PRCC.
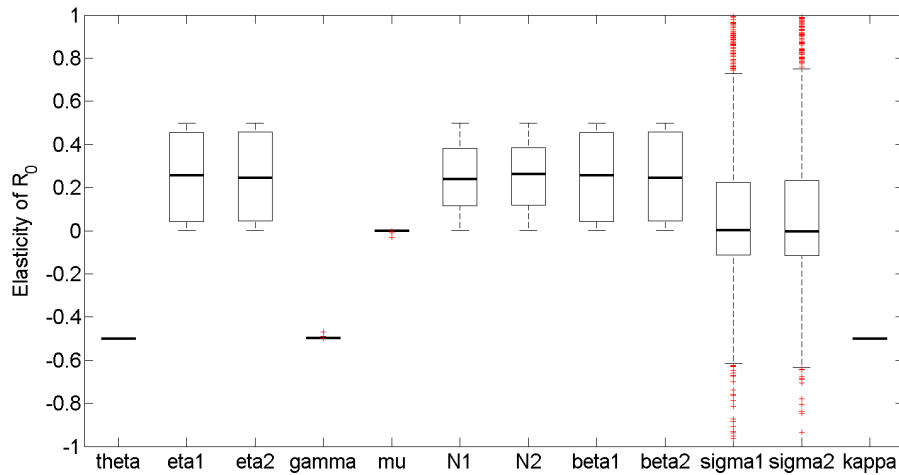
Figure 2.8: Box plot of elasticity values for the two patch model. The output is R_0 and the inputs are the system parameters taking values in the ranges specified in table A.1.

The results of the elasticity analysis confirm those from the PRCC. However, the range of variation can be informative. We see that the parameters that take the same value in both patches do not have varying elasticity values. In contrast, the parameters that take different values in each patch have a variety of elasticity values. The variation is due to the location in the multi-dimensional parameter space. Specifically, the position in the coupling parameter dimensions affects the elasticity of the 'split' parameters. This is because the coupling parameters control the interaction with each patch; if no-one visits a patch, the local parameters will not be significant. The elasticities of the coupling parameters themselves vary widely around zero. Therefore, they can have both negative and positive effects on R_0. This means the relation between the coupling parameters in the range specified in table A.1 and R_0 is not monotonic. Therefore, the PRCC results for these parameters are misleading as a condition for the calculation fails.

2.4.2.3   Simulation

We use simulations to examine the dynamics of the system over time. We have already examined the relationship between R_0, the perturbed parameters and the epidemic

Output	θ	η_1	η_2	γ	μ	N_1	N_2	β_1	β_2	σ_1	σ_2	κ
R_0	-0.6648	0.3610	0.3551	-0.6648	0.0037	0.3589	0.3580	0.3539	0.3601	-0.0504	-0.0487	-0.6668
Part $R_0^{I_1}$	-0.1540	0.4156	0.3961	-0.6847	0.0073	0.6106	-0.4177	0.0894	0.0959	-0.0120	-0.0112	-0.1694
Part $R_0^{I_2}$	-0.1773	0.3822	0.3846	-0.6703	0.0011	-0.4071	0.6044	0.0911	0.0953	0.0033	-0.0039	-0.1602
Part $R_0^{B_1}$	-.4953	0.5396	-0.2667	-0.2587	0.0105	0.2539	0.2589	0.6074	-0.1627	0.5786	-0.5764	-0.5025
Part $R_0^{B_2}$	-.5099	-0.2709	0.5390	-0.2558	-0.0189	0.2464	0.2432	-0.1699	0.6043	-0.5881	0.5785	-0.5051
Resilience (DFE)	0.6908	-0.2739	-0.3201	0.5510	-0.0293	-0.2874	-0.3096	-0.3261	-0.3252	0.0618	0.0442	0.3589
Resilience (EE)	0.4135	0.1443	-0.1645	0.3405	0.2038	-0.1428	-0.1508	-0.1956	-0.2184	0.0011	-0.0037	0.1689
Reactivity (DFE)	-0.6299	0.1432	0.1541	-0.5366	0.0123	0.3905	0.3811	0.3788	0.4173	-0.0182	-0.0233	-0.5488
Reactivity (EE)	-0.3067	0.0646	0.0718	-0.3715	-0.0005	0.1959	0.1936	0.2011	0.2064	-0.0047	-0.0128	-0.4811

Table 2.2: Partial rank correlation coefficients for the two patch model. Parameters take values in the ranges shown in table A.1. The sets are divided into those that give $R_0 < 1$ and those that give $R_0 > 1$ to define the disease free (DFE) and endemic equilibrium (EE) groups. Shading indicates a significant PRCC value with grey, positive and black, negative.

characteristics. We now look at how the coupling between the two patches affects those characteristics. First, we look at the change in the decomposition of R_0 with respect to the proportion of time an individual resident of patch one stays at home, σ_1.
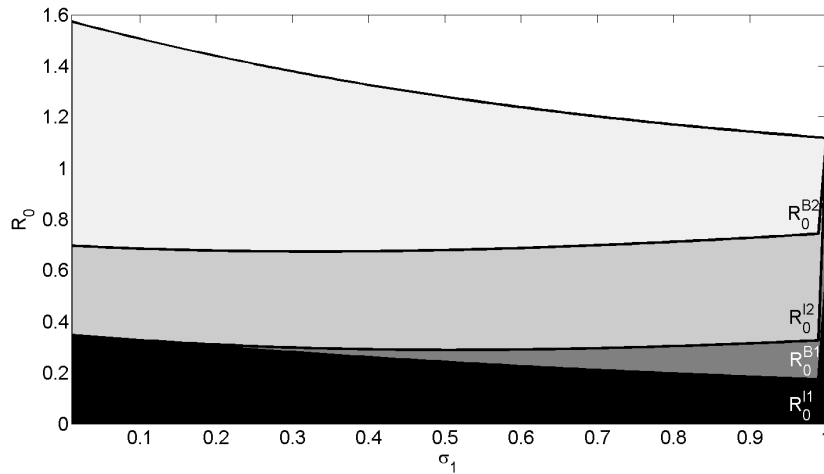

Figure 2.9: Relationship between coupling parameter, σ_1, and R_0. The basic reproduction is decomposed into its constituent parts. The parameters were held at the values shown in table A.2 except for σ_1 which varied between 0 and 1 and σ_2 which was held at 1. Here, the shade indicate the different patch class contributions: from darkest to lightest, I_1, B_1, I_2 and B_2.

The proportion of time that an individual from patch two stays in their home patch is held at 1 which means they do not visit patch one at all. In contrast, we vary the proportion of time an individual from patch one stays at home between 0 and 1. We see that as the individuals from patch one spend more time at home, the bacterial class of patch one becomes more important and the infected class of patch one less so. In contrast, the bacterial class of patch two becomes less important and the infected class of patch two stays approximately the same. Overall, we see a slight decline in the contribution of the patch two classes compared to the classes of patch one. Thus, the component of R_0 in patch two declines compared to patch one as σ_1 approaches one. This leads to a local R_0 in each patch which varies as σ_1 does.

Now that we have established the change in R_0 for this parameter set, we will examine the effect on the epidemic size of the varying coupling.

Figure 2.10 shows that when σ_1 is close to zero, the epidemic size in both patches is the same. This is because all individuals stay in patch two almost all of the time and so the population is essentially homogeneous. When σ_1 is close to one, the epidemic size in patch two falls to zero. This is because all individuals remain in the 'home' patch and there is no transmission between populations. When σ_1 is not close to zero or one, an epidemic occurs in both patches. In this case, the infected individuals of patch one can contaminate the environment of patch two, initialising an epidemic there even without the movement of patch two individuals. The more time that patch one individuals spend at home, the less chance there is of individuals taking disease to the environment of patch two. We see a larger epidemic size in patch two. This is as individuals of patch one are free to travel to, and contaminate the environment of, patch two. However, individuals of patch two are 'trapped' in their home environment. Therefore, residents of patch one are 'exporting' their risk of infection to patch two. This, in turn, lowers the risk in patch one as there is proportionally less contamination there. This is confirmed in the decomposition of R_0. The larger contribution of the bacteria patch two suggests
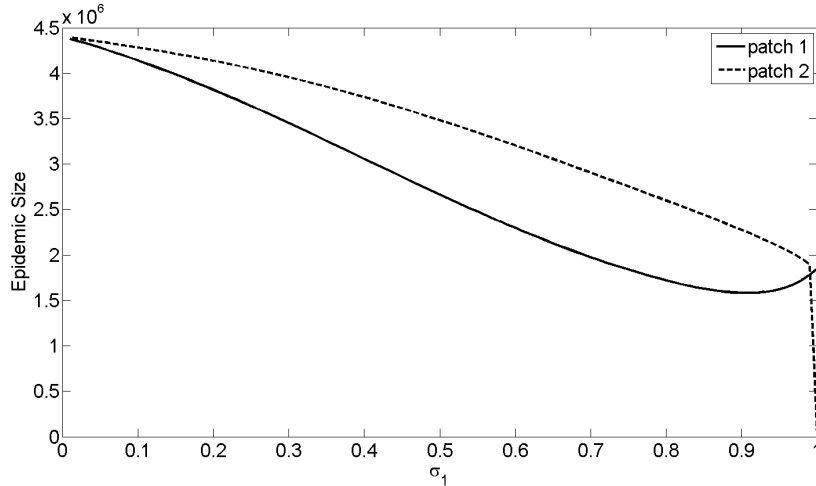
Figure 2.10: Epidemic size over coupling parameter σ_1. The parameters were held at the values shown in table A.2 except for σ_1 which varied between 0 and 1 and σ_2 which was held at 1. The system was initially disease free with $N_1/1000$ infected individuals introduced to patch one only.

the local force of infection is higher. We now examine the epidemic duration.

Figure 2.11: Epidemic duration over coupling parameter σ_1. The parameters were held at the values shown in table A.2 except for σ_1 which varied between 0 and 1 and σ_2 which was held at 1. The system is initially disease free with $N_1/1000$ infected individuals introduced to patch one only.

We look at the relation between epidemic duration and the coupling between the patches and see that as σ_1 increases, so does the duration, until σ_1 is close to 1. The duration and R_0 are negatively correlated and, from figure 2.9 we see that R_0 and σ_1 are positively correlated for this parameter set. Therefore, we may expect an increase in duration as σ_1 increases. We also see that the duration in both patches is the same until σ_1 is close to 1. This is because the coupling allows individuals to reintroduce the disease to the other patch should it die out. As such, with any level of coupling we would not expect the disease to persist in one patch and not the other.

Lastly, we examine how the epidemic peak is affected by σ_1. The relation between epidemic peak and proportion of time spent at home is very similar to that of epidemic

size. It is linked to the reduction in R_0 as σ_1 increases, shown in figure 2.9. We saw from the one patch model simulations that as R_0 increases, so does the epidemic peak. Therefore, as the increase in σ_1 essentially separates the two populations, R_0 decreases and thus the epidemic peak decreases.
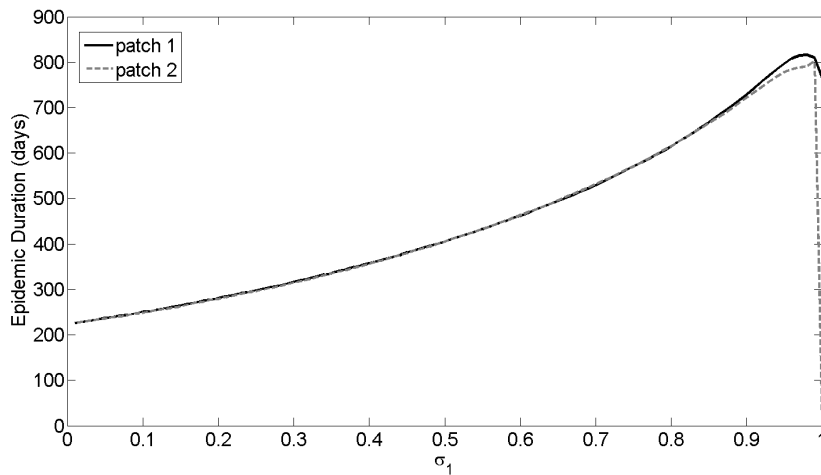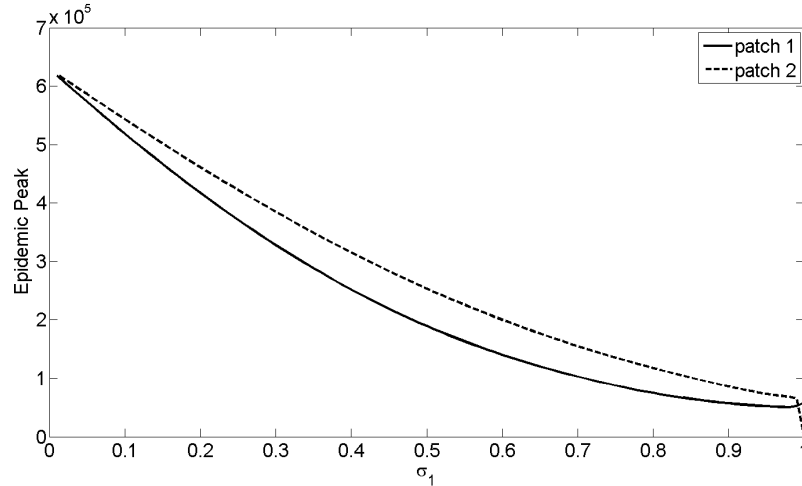

Figure 2.12: Epidemic peak over coupling parameter σ_1. The parameters were held at the values shown in table A.2 except for σ_1 which varied between 0 and 1 and σ_2 which was held at 1. The system is initially disease free with $N_1/1000$ infected individuals introduced to patch one only.

2.5 Conclusion

2.5.1 Summary

Our aim was to develop and examine a model for an environmentally transmitted disease. We started with a homogeneous population of hosts which we then divided spatially. Once the two populations were segregated, we retained coupling through the commuter movement of hosts or individuals. Finally, we simplified this coupling in terms of the average proportion of time an individual from a patch would spend at home over the course of a day. This was made possible by assumptions on the speed of the disease dynamics in comparison to the speed of the host movement.

Once our models were derived we defined some key system outputs to describe the model behaviour. To analyse these outputs, we outlined methods to establish the most influential parameters. These were the elasticity and partial rank correlation coefficients. Both analyses categorized the parameters as influential or not; however, the elasticity denoted the influence of that parameter at each point of the parameter space whereas the PRCC gave the average influence over the parameter space. In order to fully represent the parameter space, we employed an efficient sampling technique called Latin Hypercube Sampling which saved computational time without omitting areas of the parameter space.The sensitivity methods over the parameter samples both gave us insight into the influence of the system parameters; however, the elasticity which does not require monotonic relationships between input and output, was a more accurate tool than the PRCC particularly for the coupling parameters, σ_i. Finally, we fixed most of the parameters at reasonable values in order to simulate the model behaviour away from equilibrium. This afforded a view of the effect of parameter perturbation on the characteristics of an epidemic.

47

2.5.2 Conclusions

We start with the insights gained from the one patch model. We established the key model parameters and the direction of their influence on model characteristics such as R_0. The key parameters were the degradation rate, shed rate, recovery rate, population size, contact rate, and half-saturation constant. These were all highlighted in the R_0 elasticity and PRCC values. However, there were model characteristics that depended differently on the key parameters. The part reproduction numbers split the parameters into those that affected the contribution of the infected and those that affected the bacterial classes. The resilience switched the direction of the influence of the key parameters, as itself acts in a different direction to R_0, and both the resilience and reactivity were less affected by the population size, contact rate or half-saturation constant. Thus, we may say that the bacterial degradation rate and rate of recovery are vital factors in the growth of epidemic, longevity of the epidemic and the way the system responds to a perturbation. This was confirmed through simulation. The perturbations of the degradation and recovery rates caused the largest changes in epidemic peak and duration over R_0. The simulation results with respect to duration also agreed with the PRCC analysis of the resilience which predicted that the degradation and recovery rates are most influential.

The two patch model analysis gives us insight into the effect of spatial segregation. The parameters that take a different value in each patch still affect the model outputs in the same way. However, the magnitude of that effect is divided between the two patches. For instance, the shed rates for each patch positively affect R_0 but to a lesser extent than a shed rate applied to both patches. The sensitivity analyses also indicated the significance of the coupling parameters. The elasticity shows that, whilst they have low PRCCs, the coupling parameters can have dramatic effects. The coupling parameters also affect the influence of the parameters that can take different values in each patch and the epidemic characteristics. Through simulation, we were able to see how the patch coupling can limit the transmission of disease. This is partly as the fixed bacterial reservoirs require individuals to move towards them for them to have an impact on the system dynamics. Thus, whilst the coupling parameters may have a low PRCC value, they 'activate' the effects of the heterogeneous parameters.

Thus, we find the parameters controlling the force of infection can be extremely influential in the model. We also found that the coupling can dominate the effect of localised parameters.

2.5.3 Future considerations

We aimed to develop and understand a basic model of an environmentally transmitted disease. We succeeded in finding key system parameters through a variety of methods. The elasticity, calculated using parameter sets from a Latin Hypercube Sample, portrays the behaviour across the parameter space. However, with so many values to consider, it can be less clear to interpret. The PRCC, in contrast, is very clear to interpret. However, it fails whenever the relation between input and output is not monotonic. This is seen for the coupling parameters, σ_i which have a PRCC near zero as they have both positive and negative influence. A way to avoid this issue is to bound $\sigma_i \in [0.5, 1]$. The simulations were insightful as they showed both the variability in the effect of the coupling parameters and the alteration in disease spread due to the spatial segregation. However, simulation of a larger system may be time consuming for future models and we may need to rely further on the analysis of reproduction numbers, resilience and reactivity of the system.

With the understanding acquired in this chapter, we can now extend the model to examine the effect of control on disease spread. We know that the recovery rate and degradation rate are influential, therefore these may serve as good targets for control measures. These measures would need to limit an epidemic caused by the introduction of infected individuals or a perturbation. Therefore, it may be of interest to examine the endemic equilibrium behaviour as well as that at disease free steady state. Lastly, we are interested in the effect of a natural disaster so we may wish to measure the effect of a perturbation on the system elements. Therefore, we need to introduce new techniques to identify weaknesses in the system to perturbations.

Chapter 3a

Introducing treatment with population response

3a.1 Introduction

The allocation of control facilities can substantially affect the dynamics of an infectious disease. We examine how the tendency of infected individuals to seek treatment alters the spread of an environmentally transmitted disease through a two patch metapopulation. The patches are coupled through the movement of host individuals and there is an environmental reservoir of bacteria in each patch. One patch contains a treatment facility and treatment is through a course of medicine such as antibiotics rather than hospitalisation. As such, once infected individuals collect the medicine, they become 'treated' and are free to continue moving between patches. Until an infected individual has collected their course of medicine, or until they are recovered, they alter their behaviour to seek treatment. Therefore, we must account for two stages of infectiousness: infected and 'treated'.

We adapt the two patch model considered in Chapter Two to accommodate an additional treated class. We reconsider the patch coupling terms in light of the tendency of infected individuals to move toward treatment. Then we define some new outputs and analysis methods, and recap some old, with which we can understand this new model. We start by providing some context for behavioural change in models.

3a.1.1 Literature review: behavioural change in epidemic models

The effect of behavioural change on disease dynamics is a relatively recent consideration in epidemic models [48]. Yet, behavioural change can have various effects on disease spread. From self-isolation to voluntary vaccination, the decisions and actions of people can lead to complicated disease dynamics. One good example of this in effect is the Derbyshire village of Eyam where residents voluntarily quarantined themselves to prevent the spread of bubonic plague [120].

The aim of most behavioural adaptation models has been to include voluntary behaviour change in response to disease prevalence [50]. This change is assumed to affect the disease state, e.g. through vaccination, or the infection and recovery rates, e.g. through seeking treatment earlier. There has also been a focus on game theory to understand individual actions.

Mainly, the focus of these models has been on how the awareness or fear of the disease affects behaviour. Funk, Gilad and Jansen examined the effect of disease awareness on the spread of a SIR disease [49]. They defined two basic reproduction numbers, one for disease awareness and one for the pathogen, both of which were spread through

human-human contact. They found that awareness can affect the disease invasion as the disease is less likely to establish when people become more aware. They also found that awareness, assuming it affects the infectiousness and susceptibility of aware individuals, decelerates the spread of a disease.

Kiss et al. also examined the spread of disease information [76]. They looked at a SIRS model for sexually transmitted infections and incorporated an additional treated class. Individuals were considered to be 'responsive' or 'non-responsive'. The difference was that responsive individuals sought treatment earlier or would reduce their probability of infection. Therefore, there were competing dynamics between the spread of disease and the spread of information causing responsiveness. Kiss et al. focused their analysis on the stability of equilibria for the model and hypothesised a Hopf bifurcation may be found in future work.

Lastly, Epstein et al. examined the effect of fear, rather than awareness, on disease spread [43]. They defined basic reproduction numbers for the disease and for fear. They assumed individuals with fear adapted their behaviour by hiding or fleeing and found that even a small proportion of individuals fleeing exacerbated the epidemic. They also stated the need for behavioural adaptation in disease models.

Therefore, we incorporate a simple form of behavioural adaptation in our model. Like Kiss et al. we assume that individuals seek treatment. However, unlike the works above, we examine an environmentally transmitted disease and only adapt the movement of infected individuals.

3a.2   Model

The following model is an adapted form of Codeço's to include a treatment compartment [30]. It has the same basic form as the two patch model in the previous chapter but with some adjustments. We include an additional compartment for treated individuals and therefore additional interactions, shown in figure 3a.1. There are some further assumptions on the movement on infected individuals which will be examined in detail.
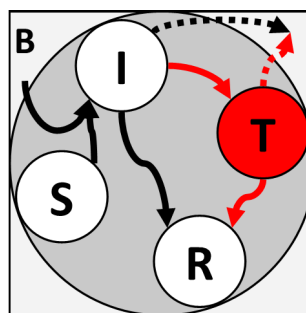
Figure 3a.1: Epidemiological interactions in one patch of the metapopulation. Disks represent different disease status groups within the patch, S= Susceptible individuals, I=Infected individuals, T=Treated individuals, R=Recovered individuals and B=Concentration of Bacteria.

Figure 3a.1 shows that the interactions of the basic model remain from the previous chapter. However, there is an additional compartment and interactions, shown in red. These denote the treated individuals, transition from infected to treated, recovery of treated individuals and shedding by treated individuals into the environment.

3a.2.1 Edge weightings and proportions of exposure

We will define new terms which express a proportion of exposure to the environment of each patch for each individual. We will define the coupling between patches along *edges*. The edges are paths between the two patches and they will have two directions, inward and outward with respect to the patch of interest. The proportion of exposure an individual experiences will depend on these edges and any weightings applied to them. When an individual is infected, the edge weightings will be scaled to reflect the location of a treatment facility. The scaling will increase the weighting on an edge towards a treatment facility and decrease the weighting on the edge away from a treatment facility. In the following equations for patch p, treatment is only available in patch q. As such, an infected individual must first visit patch q in order to become treated. There is the treatment rate denoted by ξ. This it the rate that individuals change from being infected to treated per day, given access to a treatment facility. Once treated, individuals recover at an increased rate, $\alpha\gamma$ where α is larger than one. There are equivalent equations for patch q where an infected individual must stay at home in order to become treated.

$$
\text{Susceptible} = \begin{cases} \dot{X}_{pp} = \mu H_{pp} - \beta_p X_{pp} \dfrac{B_p}{\kappa_p + B_p} - \phi X_{pp} + \tau X_{pq} - \mu X_{pp}, \\[2mm] \dot{X}_{pq} = \mu H_{pq} - \beta_p X_{pq} \dfrac{B_q}{\kappa_q + B_q} + \phi X_{pp} - \tau X_{pq} - \mu X_{pq}, \end{cases}
$$

$$
\text{Infected} = \begin{cases} \dot{Y}_{pp} = \beta_p X_{pp} \dfrac{B_p}{\kappa_p + B_p} - \gamma_p Y_{pp} - \phi \chi_2 Y_{pp} + \tau \chi_1 Y_{pq} - \mu Y_{pp}, \\[2mm] \dot{Y}_{pq} = \beta_p X_{pq} \dfrac{B_q}{\kappa_q + B_q} - \gamma_q Y_{pq} - \xi Y_{pq} + \phi \chi_2 Y_{pp} - \tau \chi_1 Y_{pq} - \mu Y_{pq}, \end{cases}
$$

$$\tag{3a.1}$$

$$
\text{Treated} = \begin{cases} \dot{W}_{pp} = -\alpha\gamma_p W_{pp} - \phi W_{pp} + \tau W_{pq} - \mu W_{pp}, \\[1mm] \dot{W}_{pq} = \xi Y_{pq} - \alpha\gamma_q W_{pq} + \phi W_{pp} - \tau W_{pq} - \mu W_{pq}, \end{cases}
$$

$$
\text{Recovered} = \begin{cases} \dot{Z}_{pp} = \alpha\gamma_p W_{pp} + \gamma_p Y_{pp} - \phi Z_{pp} + \tau Z_{pq} - \mu Z_{pp}, \\[1mm] \dot{Z}_{pq} = \alpha\gamma_q W_{pq} + \gamma_q Y_{pq} + \phi Z_{pp} - \tau Z_{pq} - \mu Z_{pq}, \end{cases}
$$

$$
\text{Bacteria} = \big\{ \dot{B}_p = -\theta_p B_p + \eta_p (Y_{pp} + Y_{qp} + W_{pp} + W_{qp})
$$

We will now define proportions of exposure to the environment in each patch, this follows the method detailed in Chapter Two. To explain the edge weightings and exposure further, let us first calculate the proportion of exposure an *un*infected individual experiences at home. If we consider the susceptible class and assume the system is at demographic equilibrium and the movement is fast enough to reach quasi-equilibrium, we have the following

$$
\dot{X}_{pp} = \mu H_{pp} - \beta_p X_{pp} \frac{B_p}{\kappa + B_p} - \phi X_{pp} + \tau X_{pq} - \mu X_{pp}
$$

$$
= -\beta_p X_{pp} \frac{B_p}{\kappa + B_p} + \mu(H_{pp} - X_{pp}).
$$

This results in the following

$$0 = -\phi X_{pp} + \tau X_{pq}$$

$$X_{pp} = \frac{\tau}{\phi} X_{pq}$$

$$X_{pp} = \sigma N_p$$

Where $\sigma = \dfrac{\tau}{\phi + \tau}$ is the exposure an uninfected individual experiences in their home patch, as in Chapter Two, see table A.3.

Let us now calculate the proportion of exposure an infected individual of patch p experiences at home when the treatment facility is located in patch q. The weighting on the edge towards the treatment facility is scaled up whereas the weighting away from the treatment facility is scaled down. Thus, as we consider an infected individual from patch p, the weighting on the outward edge is $\chi_2 \phi$ and the weighting on the inward edge is $\chi_1 \tau$. Thus,

$$
\begin{aligned}
\dot{Y}_{pp} &= \beta_p X_{pp} \frac{B_p}{\kappa + B_p} - \gamma_p Y_{pp} - \phi \chi_2 Y_{pp} + \tau \chi_1 Y_{pq} - \mu Y_{pp} \\
&= \beta_p X_{pp} \frac{B_p}{\kappa + B_p} - \gamma_p Y_{pp} - \mu Y_{pp} \\
\implies Y_{pp} &= \frac{\tau \chi_1}{\phi \chi_2} Y_{pq} \\
&= \frac{\tau \chi_1}{\tau \chi_1 + \phi \chi_2} I_p
\end{aligned}
$$

i.e. the weighting on the inward edge over the sum of the inward and outward edge weightings. However, we may simplify this in terms of the exposure that an uninfected individual experiences in their home patch,

$$\frac{\chi_1 \sigma}{\chi_1 \sigma + \chi_2 (1 - \sigma)}.$$

Therefore, we may write the equations for the individuals of patches p and q in terms of the exposure they experience in each location. Only individuals that are exposed to the patch with a treatment facility can become treated. As such, the proportion of exposure to the treatment facility is the proportion of exposure in patch q. Further parameter definitions can be found in table A.3.

$$
p\begin{cases}
\dot{S}_p &= \mu N_p - \beta S_p\left(\sigma \dfrac{B_p}{\kappa + B_p} + (1 - \sigma)\dfrac{B_q}{\kappa + B_q}\right) - \mu S_p, \\[2ex]
\dot{I}_p &= \beta S_p\left(\sigma \dfrac{B_p}{\kappa + B_p} + (1 - \sigma)\dfrac{B_q}{\kappa + B_q}\right) - \left(\gamma + \xi\left(\dfrac{\chi_2(1-\sigma)}{\chi_1(1-\sigma) + \chi_2\sigma}\right) + \mu\right)I_p, \\[2ex]
\dot{T}_p &= \xi\left(\dfrac{\chi_2(1-\sigma)}{\chi_1(1-\sigma) + \chi_2\sigma}\right)I_p - (\alpha\gamma + \mu)T_p, \\[2ex]
\dot{R}_p &= \alpha\gamma T_p + \gamma I_p - \mu R_p, \\[2ex]
\dot{B}_p &= -\theta_p B_p + \eta_p\Bigg(\left(\dfrac{\chi_1(1-\sigma)}{\chi_2\sigma + \chi_1(1-\sigma)}\right)I_q + (1-\sigma)T_q + \sigma T_p \\
& \qquad\qquad + \left(\dfrac{\chi_1\sigma}{\chi_1\sigma + \chi_2(1-\sigma)}\right)I_p\Bigg).
\end{cases}
$$

$$q \begin{cases} \dot{S}_q &= \mu N_q - \beta S_q \left(\sigma \dfrac{B_q}{\kappa + B_q} + (1 - \sigma) \dfrac{B_p}{\kappa + B_p} \right) - \mu S_q, \\[2mm] \dot{I}_q &= \beta S_q \left(\sigma \dfrac{B_q}{\kappa + B_q} + (1 - \sigma) \dfrac{B_p}{\kappa + B_p} \right) - \left(\gamma + \xi \left(\dfrac{\chi_2 \sigma}{\chi_2 \sigma + \chi_1 (1 - \sigma)} \right) + \mu \right) I_q, \\[2mm] \dot{T}_q &= \xi \left(\dfrac{\chi_2 \sigma}{\chi_2 \sigma + \chi_1 (1 - \sigma)} \right) I_q - \alpha \gamma T_q - \mu T_q, \\[2mm] \dot{R}_q &= \alpha \gamma T_q + \gamma I_q - \mu R_q, \\[2mm] \dot{B}_q &= -\theta_q B_q + \eta_q \left(\left(\dfrac{\chi_2 \sigma}{\chi_2 \sigma + \chi_1 (1 - \sigma)} \right) I_q + \sigma T_q + (1 - \sigma) T_p \right. \\[2mm] & \qquad\qquad \left. + \left(\dfrac{\chi_2 (1 - \sigma)}{\chi_1 \sigma + \chi_2 (1 - \sigma)} \right) I_p \right). \end{cases}$$

3a.3 Analysis

We have defined the model and new interactions for the treated class. We will now define the model outputs of interest and the methods we shall use to analyse them.

3a.3.1 Model outputs

We describe some model outputs to measure the dynamics of the disease in the population. These outputs measure the initial growth of the epidemic, through R_0 and the intrinsic growth rate; the contributions of each infectious class, through the part reproductive numbers; and the behaviour away from disease free equilibrium, through the endemic equilibrium value. As such, if we understand how they are altered by the system parameters such as the treatment rate, we will have some understanding of the system behaviour in general.

3a.3.1.1 Basic reproduction number, R_0

The basic reproduction number, R_0, is the expected number of secondary infections over one generation arising from one infected individual in an entirely susceptible population. Recall, from Chapter Two, we calculate the value of R_0 using the next generation matrix, $\mathcal{NGM}$. This was found by multiplying the transmission matrix, $\mathcal{T}$, consisting of the new infection terms, by the inverse of the transition matrix, Σ, consisting of the removal terms [8, 10, 37, 36, 62]. However, in this chapter we have a further consideration when calculating the $\mathcal{NGM}$. Treated individuals must first be infected before they can contribute bacteria and propagate the disease. So the treated compartment can be considered a consequence of the infected compartment. Using this assumption, we may transform the next generation matrix over the 'large domain', $\mathcal{NGM}_{LD}$, to that over 'small domain', $\mathcal{NGM}_{SD}$. The small domain consists only of the primary states at infection, therefore the treated compartment does not feature explicitly but rather as a result of the infected class. The method is to take the $\mathcal{NGM}_{LD}$ and pre and post multiply it by a unit vector where the elements corresponding to the treated compartment are set to zero, see below

$$\begin{pmatrix} 1 \\ \vdots \\ 1 \\ 0 \\ \vdots \\ 0 \\ 1 \\ \vdots \\ 1 \end{pmatrix}^{T} \mathcal{NGM}_{LD} \begin{pmatrix} 1 \\ \vdots \\ 1 \\ 0 \\ \vdots \\ 0 \\ 1 \\ \vdots \\ 1 \end{pmatrix} = \mathcal{NGM}_{SD}$$

The $\mathcal{NGM}_{SD}$ has the same spectral radius as the $\mathcal{NGM}_{LD}$ and takes the following form in our model,

$$\mathcal{NGM}_{SD} = \begin{bmatrix} \mathcal{O} & \mathcal{A} \\ \mathcal{B} & \mathcal{O} \end{bmatrix}.$$

Here, the $\mathcal{O}$'s represent 2×2 zero matrices and $\mathcal{A}$ and $\mathcal{B}$ are shown below,

$$\mathcal{A} = \frac{\beta}{\kappa\theta} \begin{bmatrix} \sigma N_p & (1-\sigma)N_p \\ (1-\sigma)N_q & \sigma N_q \end{bmatrix},$$

$$\mathcal{B}_{1,1} = \frac{\eta_p \chi_1 \sigma}{\sigma\chi_1(\gamma+\mu) + (1-\sigma)\chi_2(\gamma+\xi+\mu)}$$
$$+ \frac{\eta_p \xi \chi_2 \sigma(1-\sigma)}{(\sigma\chi_1(\gamma+\mu) + (1-\sigma)\chi_2(\gamma+\xi+\mu))(\alpha\gamma+\mu)},$$

$$\mathcal{B}_{1,2} = \frac{\eta_p \chi_1(1-\sigma)}{\sigma\chi_2(\gamma+\xi+\mu) + (1-\sigma)\chi_1(\gamma+\mu)}$$
$$+ \frac{\eta_p \xi \chi_2 \sigma(1-\sigma)}{(\sigma\chi_2(\gamma+\xi+\mu) + (1-\sigma)\chi_1(\gamma+\mu))(\alpha\gamma+\mu)},$$

$$\mathcal{B}_{2,1} = \frac{\eta_q \chi_2(1-\sigma)}{\sigma\chi_1(\gamma+\mu) + (1-\sigma)\chi_2(\gamma+\xi+\mu)}$$
$$+ \frac{\eta_q \xi \chi_2(1-\sigma)^2}{(\sigma\chi_1(\gamma+\mu) + (1-\sigma)\chi_2(\gamma+\xi+\mu))(\alpha\gamma+\mu)},$$

$$\mathcal{B}_{2,2} = \frac{\eta_q \chi_2 \sigma}{\sigma\chi_2(\gamma+\xi+\mu) + (1-\sigma)\chi_1(\gamma+\mu)}$$
$$+ \frac{\eta_q \xi \chi_2 \sigma^2}{(\sigma\chi_2(\gamma+\xi+\mu) + (1-\sigma)\chi_1(\gamma+\mu))(\alpha\gamma+\mu)}.$$

Thus, we may calculate R_0 from this matrix as it is the lead eigenvalue.

3a.3.1.2 Part reproductive numbers

R_0 as a whole is very informative. However, it can be useful to see where in the population is most influential with respect to the basic reproduction number. We detailed a method to decompose R_0 into its constituent parts in Chapter Two. The $\mathcal{NGM}$ is utilised as well as the lead eigenvector. The ij^{th} element of the $\mathcal{NGM}$ denotes the number of infections of type i produced by an infected individual of type j. As such, the sum of the jth column of the $\mathcal{NGM}$ gives the total infections in all classes caused by

an infected individual of type j. However, as the lead eigenvalue, R_0, gives the number of new infections in the population, the lead eigenvector denotes the stable distribution of infected classes during the exponential growth phase of the epidemic. Therefore, to arrive at the contribution of the jth infectious class to R_0, we must multiply the jth column sum by the jth element of the *normalised* lead eigenvector. In this context, normalisation leads to the eigenvector elements summing to one; the eigenvector thus gives the proportion of infections in each infectious state. The column sums, C_i for our model are as follows:

$$C_{I_p} = \mathcal{B}_{1,1} + \mathcal{B}_{2,1},$$
$$C_{I_q} = \mathcal{B}_{1,2} + \mathcal{B}_{2,2},$$
$$C_{B_p} = \mathcal{A}_{1,1} + \mathcal{A}_{2,1},$$
$$C_{B_q} = \mathcal{A}_{1,2} + \mathcal{A}_{2,2}.$$

The lead eigenvector is omitted due to its length.

3a.3.1.3 Intrinsic growth rate

Whereas R_0 denotes the per generation growth rate, the intrinsic growth rate is the coefficient of epidemic growth over time. It is calculated as the lead eigenvalue of the system Jacobian at equilibrium or the eigenvalue with largest real part. As the intrinsic growth rate, r, can be positive and negative, the largest implies the 'most positive'. In the previous chapter, we discussed the resilience or return time to equilibrium. The resilience is the intrinsic growth rate with inverse sign. Therefore, if the disease free equilibrium is stable, the intrinsic growth rate is negative and the resilience is positive as the system will return to disease free equilibrium once perturbed. The threshold of $r = 0$ corresponds to $R_0 = 1$ and we consider parameter sets producing both positive and negative r. The system Jacobian at disease free equilibrium is shown below.

$$
\begin{bmatrix}
-(\gamma + \xi\left(\frac{\chi_2(1-\sigma)}{\chi_2(1-\sigma)+\chi_1\sigma}\right) + \mu) & 0 & 0 & 0 & \frac{\beta}{\kappa}\sigma N_p & \frac{\beta}{\kappa}(1-\sigma)N_p \\
0 & -(\gamma + \xi\left(\frac{\chi_2\sigma}{\chi_1(1-\sigma)+\chi_2\sigma}\right) + \mu) & 0 & 0 & \frac{\beta}{\kappa}(1-\sigma)N_q & \frac{\beta}{\kappa}\sigma N_q \\
\xi\left(\frac{\chi_2(1-\sigma)}{\chi_2(1-\sigma)+\chi_1\sigma}\right) & 0 & -(\alpha\gamma+\mu) & 0 & 0 & 0 \\
0 & \xi\left(\frac{\chi_2\sigma}{\chi_1(1-\sigma)+\chi_2\sigma}\right) & 0 & -(\alpha\gamma+\mu) & 0 & 0 \\
\eta_p\left(\frac{\chi_1\sigma}{\chi_2(1-\sigma)+\chi_1\sigma}\right) & \eta_p\left(\frac{\chi_1(1-\sigma)}{\chi_1(1-\sigma)+\chi_2\sigma}\right) & \sigma\eta_p & (1-\sigma)\eta_p & -\theta & 0 \\
\eta_q\left(\frac{\chi_2(1-\sigma)}{\chi_2(1-\sigma)+\chi_1\sigma}\right) & \eta_q\left(\frac{\chi_2\sigma}{\chi_1(1-\sigma)+\chi_2\sigma}\right) & (1-\sigma)\eta_q & \sigma\eta_q & 0 & -\theta
\end{bmatrix}
$$

3a.3.1.4 Endemic equilibrium value

Lastly, we examine the size of the infected compartments at endemic equilibrium. This is calculated through simulation. Given a parameter set where $R_0 > 1$ or $r > 0$, the perturbed system will not return to disease free equilibrium. Therefore, we simulate the behaviour of the system over a long time period, 600 years, until it has reached equilibrium. The sizes of the infected compartments are then averaged over a reasonable time span, 10 years, to arrive at the endemic equilibrium value. This is used in the bifurcation analysis.

3a.3.2 Analysis techniques

We recap some of the methods of the previous chapter and explain some new methods. We wish to categorise the sensitivity of the system to parameter change through the

PRCC, Fourier Amplitude Sensitivity Test, elasticities and Multi-Parametric Sensitivity Analysis, and the behaviour away from disease free steady state through the bifurcation analysis.

We examine the parameters over the ranges specified in table A.3 and state the values with the relevant figures when they are fixed. We focus on the proportion of exposure, σ, rather than edge weightings, τ and ϕ. We shall examine R_0 and r both as one entity and split by their behaviour either side of the epidemic threshold. This will be conducted by classifying parameter sets as producing R_0 or r above or below the threshold.

3a.3.2.1 Latin Hypercube Sampling, LHS

We commence with a recap of our parameter sampling technique. Latin Hypercube Sampling is an efficient way of representing the parameter space. In Chapter Two we described the method which we shall briefly restate here. Each parameter is assigned a probability distribution; in our work all parameters are assumed to be uniformly distributed. The parameter range is then split into equally probably intervals which are each sampled once. The vector of samples is then randomly permuted and the matrix of permuted vectors becomes the LHS matrix.

3a.3.2.2 Elasticity and finite difference approximation

The elasticity analysis uses the LHS matrix to quantify the sensitivity of an output across the parameter space. The elasticity of an output, ω, to parameter, ρ, is given by: $E_\rho^\omega = \frac{\rho}{\omega} \frac{\partial \omega}{\partial \rho}$ evaluated at each point in parameter space.

A finite difference approximation facilitates the elasticity calculation. As the model becomes more complex, the symbolic calculation of matrix eigenvalues and partial derivatives becomes prohibitively time-consuming. As such, we approximate the partial derivatives in the following way [148].

$$\frac{\partial \omega}{\partial \rho} \approx \frac{\omega(\rho + \Delta\rho) - \omega(\rho)}{\Delta\rho}$$

Here, $\Delta\rho$ is the small perturbation amount of parameter ρ, $\Delta\rho << 1\%$. This approximation speeds the calculation.

3a.3.2.3 Partial Rank Correlation Coefficient, PRCC

The elasticity is evaluated at each point in the parameter space. However it is useful to understand the relation between input and output throughout. The PRCC denotes the level of association between output and input whilst omitting the effect of other inputs. The steps of the calculation are detailed in full in Chapter Two. We use the parameter sets from the LHS to calculate the output for a range of values. The values of the outputs and inputs are then used to derive expected values of each input and output given a certain parameter set. The expected value is compared to the actual value to give a residual. Finally, the PRCC is found using the following formula,

$$PRCC = \frac{\text{residual in output.residual in input}}{((\text{residual in output})^2 (\text{residual in input})^2)^{0.5}}.$$

The analysis requires a monotonic relationship between output and input. Once calculated, the coefficients fall into the range [-1,1] where a result is considered significant if it has magnitude greater than 0.5. The magnitude itself denotes the degree of association between input and output.

3a.3.2.4 Fourier Amplitude Sensitivity Test, FAST

We examine two sensitivity analyses already, the elasticity and PRCC. However the FAST can produce a slightly different viewpoint. We do not need the monotonicity that PRCC requires yet we arrive at a single value that holds across the parameter space rather than the local result shown by the elasticity. The FAST examines the output uncertainty with relationship to the inputs. A unique frequency is introduced to the inputs and is tested for in the outputs [42, 87, 116, 143, 148]. The method does not require monotonicity in the relationship between input and output which makes it more versatile than the PRCC. The steps are illustrated by a simple example of a an SIR model with equations as (3a.2),

$$
\begin{aligned}
\dot{s} &= \mu N - \beta s i - \mu s, \\
\dot{i} &= \beta s i - \gamma i - \mu i, \\
\dot{r} &= \gamma i - \mu r.
\end{aligned}
\tag{3a.2}
$$

1. The uncertainties for each parameter are defined. This is the range within which the parameter is estimated to fall.

   In our example, the three parameters are

$$
\begin{aligned}
x_1 &= \beta \in [0, 2], \\
x_2 &= \gamma \in [0, 1], \\
x_3 &= \mu \in [0, 0.1].
\end{aligned}
$$

2. The number of samples, M, is decided. This is usually an odd number and follows the formula $M = 2p_{max}\omega_{max} + 1$ where p_{max} is the maximum multiple of the characteristic frequency, ω_i, less than $\frac{M-1}{2}$ or the 'maximum harmonic order'. The parameter ω_{max} is the maximum characteristic frequency for all parameters [116]. In the work by Xu and Gertner, an alternative for the number of samples as $M > 80 \times$ (number of parameters)[143].

   Using the latter and using the nearest odd number, our number of samples is 241.

3. A characteristic frequency must be chosen for each parameter by the user. These are best chosen between 10 and 100 and should not be multiples of one another [143].

   For instance, we choose the frequencies to be $\omega_1 = 13, \ \omega_2 = 17, \ \omega_3 = 23$.

4. The characteristic frequencies allow random samples to be taken for each parameter. These follow the formula of $x_i = F_i^{-1}(\frac{1}{2} + \frac{1}{\pi}\sin^{-1}\sin(\omega_i v))$ [116, 143]. Here, F_i^{-1} is the inverse cumulative frequency distribution for the ith parameter and v is the common variable of the search function.

   As previously stated, all parameters are assumed to be uniformly distributed, therefore $F_i^{-1}(p) = a + p(b-a)$ *where a and b are the lower and upper bounds for the*

range respectively. Thus our parameters are:

$$x_1 = 1 + \frac{2}{\pi} \sin^{-1} \sin(13v),$$

$$x_2 = \frac{1}{2} + \frac{1}{\pi} \sin^{-1} \sin(17v),$$

$$x_3 = \frac{1}{20} + \frac{1}{10\pi} \sin^{-1} \sin(23v).$$

5. Now the output can be calculated as a function of v.

We focus on the basic reproduction number, thus,

$$R_0 = \frac{\beta}{\gamma + \mu},$$

$$= \frac{1 + \frac{2}{\pi} \sin^{-1} \sin(13v)}{\frac{1}{2} + \frac{1}{\pi} \sin^{-1} \sin(17v) + \frac{1}{20} + \frac{1}{10\pi} \sin^{-1} \sin(23v)},$$

$$= \frac{20\pi + 40 \sin^{-1} \sin(13v)}{11\pi + 20 \sin^{-1} \sin(17v) + 2 \sin^{-1} \sin(23v)},$$

$$= f(v).$$

.

6. We then take M samples of our search function variable, v, where the jth sample takes the form $v_j = -\pi + \frac{\pi}{M} + \frac{2\pi}{M}(j-1)$. These samples are then used to decompose the output into a Fourier spectrum which will define the output variance. Thus if a parameter is important to the output, the signal of that parameter will be identified.

In our example, the variance takes the form

$$v\hat{a}r(R_0)^{(i)} = \sum_{k}^{\frac{M-1}{2}} \Omega_k^{(i)},$$

$$= \sum_{k}^{\frac{M-1}{2}} (A_k^{(i)^2} + B_k^{(i)^2}),$$

where the Fourier coefficients along the search curve for x_i are

$$A_k^{(i)^2} = \frac{2}{M} \sum_{j}^{M} f(v_j) \cos(v_j k),$$

$$B_k^{(i)^2} = \frac{2}{M} \sum_{j}^{M} f(v_j) \sin(v_j k).$$

59

7. The variance of a parameter i, W_i, can be singled out as

$$W_i = \sum_{p}^{p_{max}} \Omega_{p\omega}^{(i)}.$$

8. Finally, the individual variance, C_i, is divided by the total variance to define the measure of uncertainty for the ith parameter,

$$C_i = \frac{W_i}{v\hat{a}r(\text{output})}.$$

Thus, the results are as follows:

$$T_\beta = 0.1648,$$
$$T_\gamma = 0.4520,$$
$$T_\mu = 0.0428.$$

Which implies that γ is the most influential parameter. This was implemented using an altered version of the MATLAB program mentioned by Per- Anders Ekström [42].

One issue with the calculation of FAST sensitivities is the computational expense. However, it will not be an issue at this stage.

3a.3.2.5 Multi-Parametric Sensitivity Analysis, MPSA

Whilst we examine the general input-output relationship with the PRCC and FAST, it is insightful to see *where* in the parameter space is most influential. The MPSA gives a value for the sensitivity but also illustrates visually where most change takes place. The method steps are as follows, illustrated by the example from the FAST analysis [29, 107, 148, 149].

1. The LHS is taken and the output is evaluated for each parameter set.

   We will fix $\mu = 0.0005$ and vary β and γ as shown in table 3a.1.

2. The user defines a threshold that splits the output values into 'acceptable' and 'unacceptable' categories.

   We shall use the epidemic threshold, $R_0 = 1$.

3. The corresponding parameter sets are ordered ready to construct frequency graphs.

   Our ordered parameter sets and acceptability are shown in table 3a.1.

4. We construct frequency and cumulative frequency graphs of the acceptable and unacceptable output values for each parameter. These are normalised so we may compare the curves for acceptable and unacceptable frequency.

   Using the table above, we construct the following frequency and cumulative frequency graphs for β and γ.

β	γ	R_0	Acceptable
0.5	0.2	2.49	$\times$
	0.4	1.25	$\times$
	0.6	0.83	$\checkmark$
1	0.2	4.99	$\times$
	0.4	2.50	$\times$
	0.6	1.67	$\times$
1.5	0.2	7.48	$\times$
	0.4	3.75	$\times$
	0.6	2.50	$\times$

Table 3a.1: Table of input parameters, γ and β, and output R_0 with acceptability. Acceptable is defined as being below the threshold $R_0 = 1$.
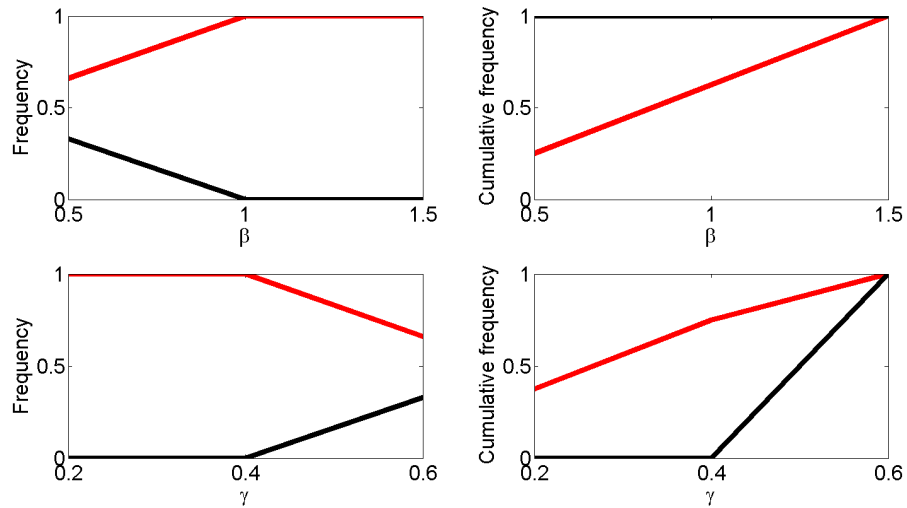

Figure 3a.2: Graphs of frequencies and cumulative frequencies of acceptable, black, and unacceptable, red, outputs. These are normalised, with μ fixed at 0.0005.

5. Finally, the sensitivity is calculated using the Kolmogorov–Smirnov test [148],

$$KS = \sup_x |F_a(x) - F_u(x)|.$$

Here, $F_a(x)$ & $F_u(x)$ denote the normalised cumulative frequency functions for the acceptable and unacceptable outputs respectively. This calculates the maximum vertical distance between the acceptable and unacceptable cumulative frequency curves. The area in the parameter space where the KS statistic is maximised indicates the area of most influence.

Therefore for β the K-S statistic is 0.75 and for γ, 0.66. This suggests that β is more influential for this particular value of μ. The graphs also suggest that β is most influential at the bottom of its range and γ most influential in the middle of its range.

Note that the MPSA does not suggest the direction of influence of an input on an output, only the magnitude. The threshold is also user defined and could affect the results. In our work, the threshold is defined as the mean value of the output.

3a.3.2.6 Bifurcation analysis

We have examined the influence of the parameters in the system in many ways. Now, we wish to understand how the system changes as R_0 crosses the epidemic threshold. Bifurcation analysis is a method for analysing steady states and oscillations and it charts time-varying changes in the state of the system in a multidimensional space [64, 147].

We conduct a bifurcation analysis for the simple example used in the FAST and MPSA. Figure 3a.3 shows an example of a bifurcation diagram over β. The transcritical bifurcation, where stability switches from the disease free to endemic equilibrium, corresponds to $R_0 = 1$ after which the size of the infected population at equilibrium approaches $\frac{\mu N}{\gamma + \mu}$.
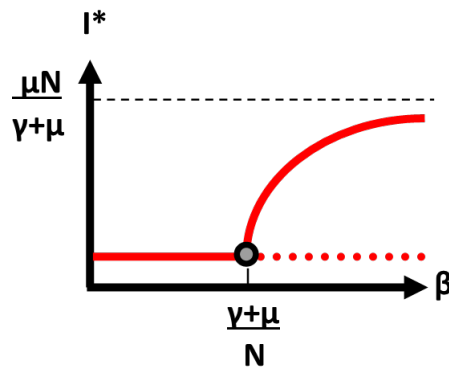

Figure 3a.3: Example bifurcation diagram for simple example. The grey circle represents a transcritical bifurcation.

3a.4 Results

Our aim was to understand the new model, particularly the effect of control on disease dynamics. We start with the sensitivity analyses: the elasticity, PRCC, FAST and MPSA before examining the equilibrium behaviour through the bifurcation analysis.

We sample the parameter space using the Latin Hypercube method to arrive at the following.

3a.4.1 Elasticities

We use the elasticity to examine the relation between input and output at each point in the parameter space. We focus on R_0, the part reproduction numbers and r to understand the disease behaviour in the initial growth phase of the epidemic. In this analysis, we do not split the parameter sets about the epidemic threshold. This is as every elasticity value is displayed individually.

We approximate the partial derivative in the elasticity calculation using the finite difference approximation. This allows a quick computation of the relationship between input and output at each point in the parameter set in the LHS matrix. There are 1000 samples taken in the following analyses and we start with R_0.

3a.4.1.1 Basic reproduction number, R_0

The elasticities for each parameter are shown in figure 3a.4. There were four parameters found to be particularly significant in Chapter Two, θ, β, γ and κ. These are also significant here although the influence of the recovery rate varies based on the value of the treated recovery scaling factor, α. In general, the parameters that vary over the two patches are more influential in the patch with a treatment facility, patch q. This is as infected individuals have proportionately more exposure to the environment of patch q. The exposure an individual experiences in their home patch, σ, has a varying but generally positive influence on R_0. As an individual is exposed more to the environment of their home patch, there is less opportunity for cross contamination of patches. However, for the majority of the range of σ, cross-contamination is possible. The treatment rate, ξ, generally has a negative effect on R_0. This is because, as the treatment rate increases, individuals are more likely to be in the treated class where they recover more quickly. However, there are parameter sets where ξ has a positive influence on R_0. This occurs when the local shed rate in the patch without a treatment facility, η_p, and the weight scaling towards treatment, χ_2, are at the top of their ranges. This scenario is illustrated in figure 3a.5.

The situation is that an infected individual of patch p is strongly attracted to treatment and so the majority of their exposure is to the environment of patch q. Once they become treated, there is no edge scaling and they revert to experiencing most exposure to their home patch environment where the shed rate is high. Thus, increasing the treatment rate means infected residents of patch p return home more quickly and, even though they are treated, cause significant contamination there because the local shed rate is so high.

To confirm this theory, we examine the decomposition of R_0 through the part reproduction numbers. Figure 3a.6a shows a reference parameter set where we see the contribution of the bacteria in patch p is relatively stable over ξ. However, in figure 3a.6b where the scaling towards treatment is higher, as ξ increases, so does the contribution of the bacteria in patch p. Thus, there is a greater effect from the bacteria in the environment of patch p when individuals are 'released' by treatment to face exposure in the patch without a treatment facility.
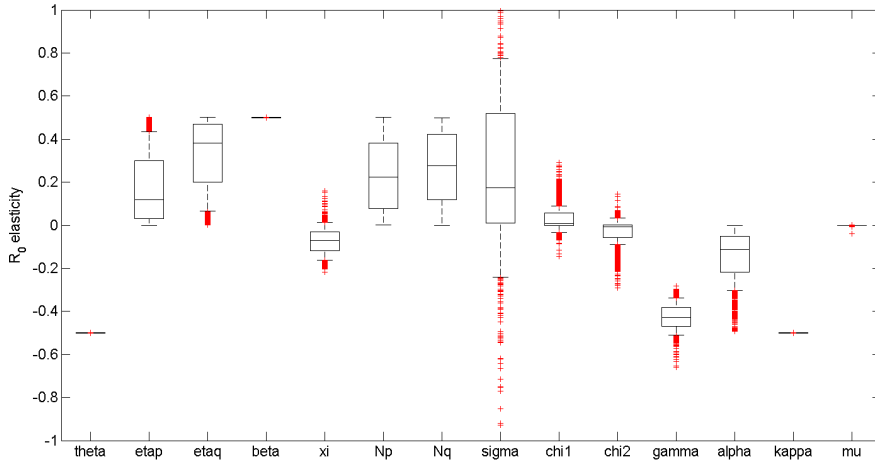
Figure 3a.4: Elasticities of R_0 calculated using the finite difference approximation. Parameters took the values shown in table A.3.
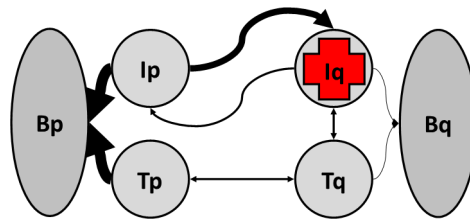

Figure 3a.5: Scenario where treatment rate has a positive influence on R_0. Arrow line width denotes larger rates and the red cross denotes the placement of a treatment facility.

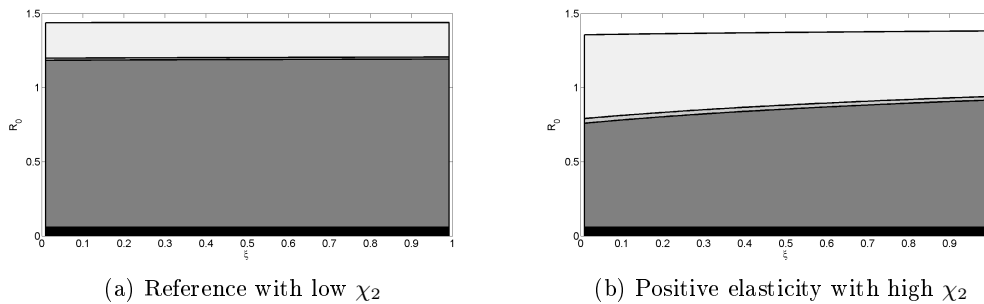(a) Reference with low χ_2 (b) Positive elasticity with high χ_2

Figure 3a.6: Composition of R_0 in terms of the part reproduction numbers over treatment rate ξ. Parameters were chosen in the area of parameter space where the elasticity of R_0 with respect to ξ was positive for figure (b). Part reproduction numbers, from dark to light, are $R_0^{I_p}$, $R_0^{B_p}$, $R_0^{I_q}$ and $R_0^{B_q}$. Parameters were $\theta = 0.2, \eta_p = 0.05, \eta_q = 0.1, \beta = 6, N_p = 4 \times 10^6, N_q = 8 \times 10^5, \tau = 7, \chi_1 = 0.9, \gamma = 0.8, \alpha = 1.01, \kappa = 3 \times 10^6$ and $\mu = 3 \times 10^{-5}$. Weight scaling χ_2 is 1.1 in 3a.6a and 4 in 3a.6b.

64

3a.4.1.2 Part reproduction numbers

The elasticities of the part reproduction numbers, shown in figure 3a.7, see some of the influences that were seen for R_0. The bacteria degradation rate, θ, recovery rate, γ, half-saturation constant, κ, and contact rate, β, all have strong influences. However, we can obtain further information about each patch and each infectious class. The infected class contribution from each patch depends strongly on that patch shed rate and, positively, on that patch population size. The contribution is also strongly *negatively* affected by the population size of the other patch. The direction of this effect is due to the distributions of infections; if proportionately more infections occur in one patch, then there must be proportionately fewer in the other. The bacterial class contributions depend on all parameters of interest to a greater extent than the infected class contributions. Particularly the bacteria degradation rate, θ, contact rate, β, and half-saturation constant, κ.

The difference between the two patches is particularly highlighted by this analysis. Generally, the parameters in patch q have a stronger influence. We also see a change in the direction of influence of the scaling parameters, χ_1 and χ_2, in patch p and q; as χ_2 increases and χ_1 decreases, infected individuals experience more exposure in patch q and less in patch p. This is particularly important for the static bacteria classes. However, there is a further parameter of interest for the bacteria classes. The treatment rate, ξ, has a negative influence on the contribution of bacteria in patch q. However, ξ has a positive influence on the contribution of the bacteria in patch p. This is for the reason mentioned in the previous section. As the treatment rate increases, individuals move from the infected class where edge weightings are scaled, to the treated class where they are not. As such, shedding individuals experience more exposure in patch p, increasing the importance of the bacterial reservoir there. Lastly, there is a large variation in the affect of σ. This is because its effect is directly related to the values of the local parameters. If it is skewed toward a patch where the local parameter values are high, it will have a larger effect.
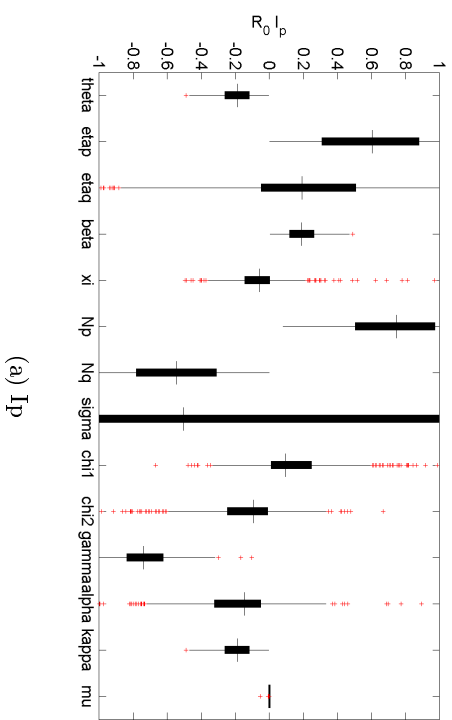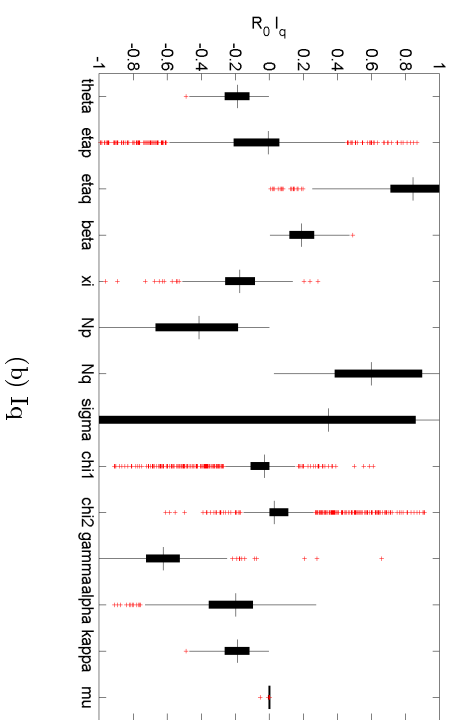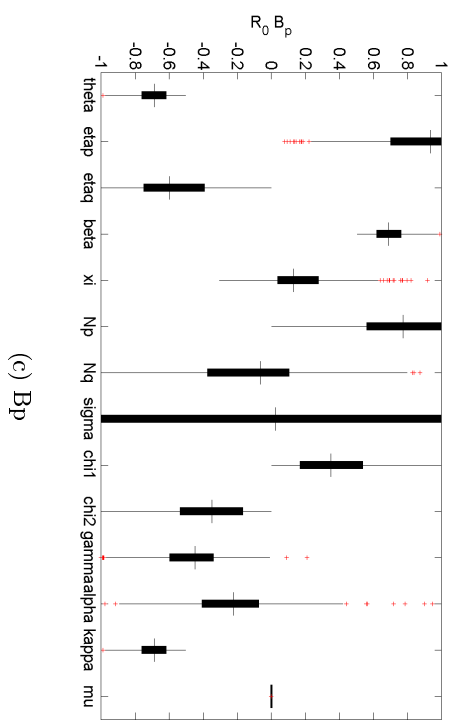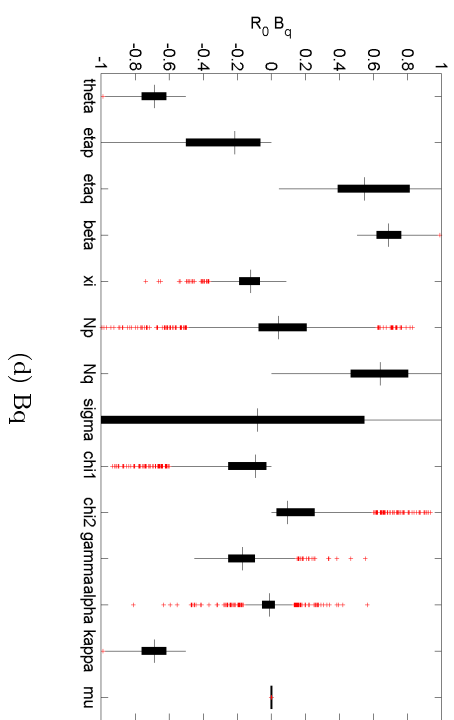
Figure 3a.7: Part reproduction number elasticities. These were calculated in MATLAB using a finite difference approximation. The parameters took values in the ranges shown in table A.3.

3a.4.1.3 Intrinsic growth rate

The R_0 and part reproduction numbers examine the growth rate per generation. We are interested in how that growth rate differs when measured over time. The key influential parameters for intrinsic growth rate, r, are similar to those for R_0, shown in figure 3a.8. The difference is in the variability of their effect. Parameters with only one elasticity value across the sample set with respect to R_0, take a range of elasticity values with respect to r. This is as we are examining and comparing parameters of different scales without the discrete division afforded by a per generation approach.
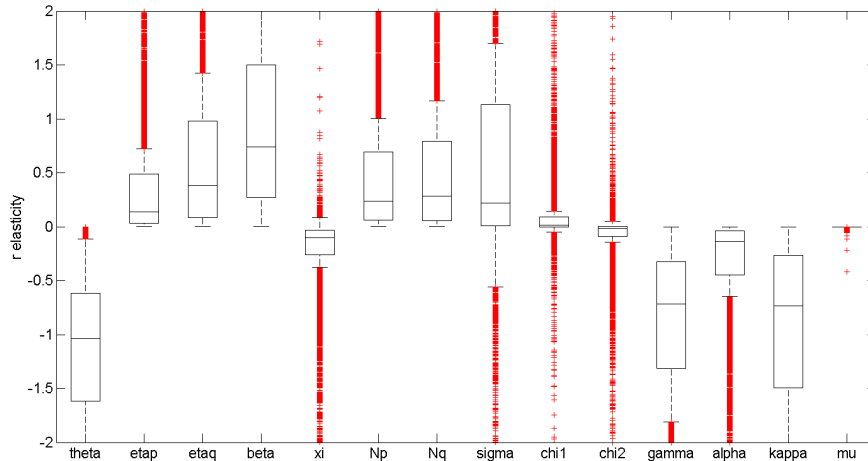

Figure 3a.8: Elasticities of the intrinsic growth rate r calculated using a finite difference approximation. Parameters take values in the ranges specified in table A.3.

3a.4.2 Partial Rank Correlation Coefficient, PRCC

The PRCC generalises the relation between input and output across the parameter space. Therefore, we may not see how different areas within the parameter space change the influence of input on output. As such, we divide our parameter space into sets that give a value of R_0 or r above their epidemic thresholds and sets that produce values below the thresholds. This will allow us to see if there are different correlations either side of $R_0 = 1$ and $r = 0$.

We first examine the basic reproduction number, R_0. Either side of the epidemic threshold θ, γ and κ are significant. This is reminiscent of the elasticity results. However, β, which also had a notable elasticity, is only significant when $R_0 < 1$. This suggests it has a strong influence in that area of parameter space and is a key component in the stability of the disease free equilibrium.

Similarly, the shed rate in the patch containing a treatment facility is significant when $R_0 < 1$. In contrast, the shed rate in patch p, without a treatment facility, is not significant. Thus, the rate of contribution to the bacterial reservoir in the patch with a treatment facility is an important factor in the stability of the disease free steady state. We know that the parameters of patch q are generally more influential as infected individuals are proportionately more exposed to the environment there. Once the disease has established, β and η_q no longer influence to the same extent.

The intrinsic growth rate, r, is also split around the epidemic threshold. When $r > 0$, there are three parameters of interest, β, γ and κ. The contact rate β and

half-saturation constant, κ, dictate the force of infection whereas the recovery rate, γ, influences the duration of infection. The duration appears to be less significant here as the PRCC of θ, the degradation rate, is just below the notable threshold and the PRCC of γ is just above. This is because r is the growth over time rather than per generation. When $r < 0$, only θ and γ are significant. These dictate the duration of infection and as r is the resilience with inverse sign, γ and θ are instrumental in the time taken by the system to return to disease free equilibrium.

Output	θ	η_p	η_q	β	ξ	N_p	N_q	σ	χ_1	χ_2	γ	α	κ	μ
$R_0 > 1$	-0.6770	0.1713	0.2703	0.4153	-0.1069	0.2307	0.2603	0.0993	0.0378	-0.0497	-0.6400	-0.1696	-0.6850	0.0184
$R_0 < 1$	-0.5592	0.2780	0.5106	0.7288	-0.1321	0.3605	0.4168	0.1079	0.0669	-0.0290	-0.5327	0.1401	-0.5695	-0.0225
$r > 0$	-0.4736	0.2236	0.4557	0.5580	-0.0743	0.2901	0.3665	0.1504	0.0305	0.0058	-0.5190	-0.0827	-0.8055	0.0180
$r < 0$	-0.7681	0.1581	0.3119	0.4862	-0.2038	0.2053	0.2583	0.0947	0.0887	-0.0545	-0.6305	-0.1593	-0.3784	-0.0106

Table 3a.2: Partial rank correlation coefficients. Parameters take values in the ranges shown in table A.3. The LHS parameter sets are divided into those that give $R_0 < 1$ and those that give $R_0 > 1$ to define the disease free (DFE) and endemic equilibrium (EE) groups. Shading indicates a significant PRCC value with grey, positive and black, negative.

3a.4.3 Fourier Amplitude Sensitivity Test, FAST

We sample the entire parameter space without dividing it by the epidemic threshold. Thus, as we compare these results to the PRCC and MPSA, we compare the behaviour of the parameters throughout the sample space with that either side of the epidemic threshold.

Output	θ	η_p	η_q	β	ξ	N_p	N_q
R_0	0.0371	0.0013	0.0029	0.0111	0.0014	0.0026	0.0020
r	0.0754	0.0036	0.0216	0.0516	0.0065	0.0075	0.0121
	σ	χ_1	χ_2	γ	α	κ	μ
R_0	0.0015	0.0005	0.0023	0.0238	0.0026	0.0359	0.0006
r	0.0082	0.0025	0.0004	0.0493	0.0014	0.2381	0.0001

Table 3a.3: FAST sensitivities for R_0 and r. Significant values are highlighted in black. Parameters take values in the ranges shown in table A.3.

In both cases of R_0 and r, there are four parameters of interest. The level of uncertainty contributed to R_0 and r, is higher than that of other parameters for θ, β, γ and κ. These have found to be key parameters in other analyses as they influence the force and duration of infection. There are two further parameters of interest for r, N_q and η_q. Thus, the population size and shed rate in the patch with the treatment facility are significant in the growth of the epidemic over time. The parameters in patch q are generally more influential as there is proportionally more exposure experienced there by infected individuals.

3a.4.4 Multi-parametric sensitivity analysis, MPSA

The MPSA allows us to examine not only the parameter influence but *where* in the parameter range is most influential. We start with the basic reproduction number above and below the epidemic threshold, shown in figures 3a.9 and 3a.10.
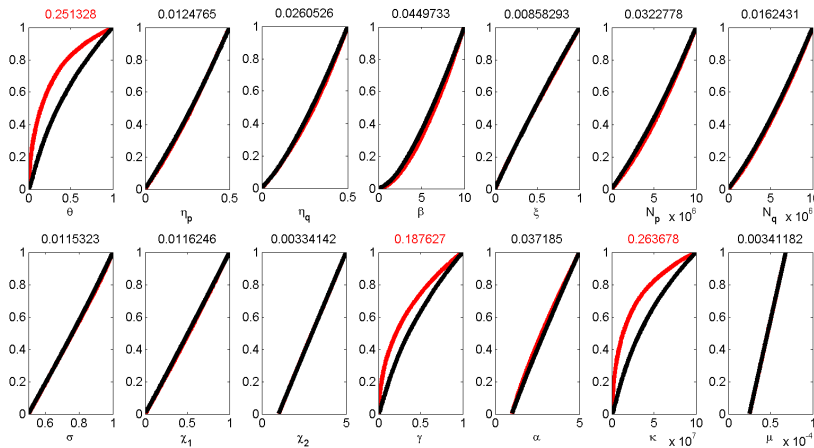

Figure 3a.9: Graphs of MPSA with a threshold of the average value of R_0 over the 1000 parameter samples from table A.3 where $R_0 > 1$. Values in red denote a KS statistic greater than 0.1.

Both sides of the epidemic threshold, θ, γ and κ are influential. The most significant part of the ranges of θ and κ appears to be the middle. This is also the case with β when

$R_0 < 1$ which, like the PRCC results, is the only area where it is significant. Similarly, η_q is significant when $R_0 < 1$ only. However, in contrast to the PRCC results, N_p and N_q are both notable when $R_0 < 1$. However, both have PRCC values just below the threshold of significance but MPSA values just above the corresponding significance threshold. As such, the results from the PRCC and MPSA appear complimentary for R_0.
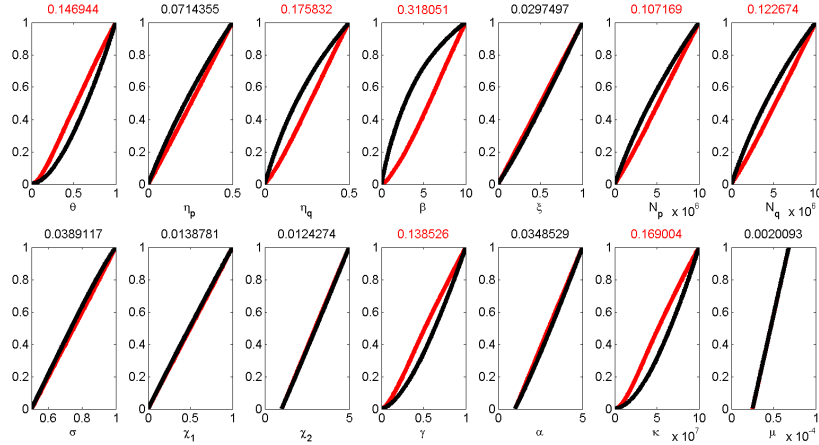

Figure 3a.10: Graphs of MPSA with a threshold of the average value of R_0 over the 1000 parameter samples from table A.3 where $R_0 < 1$. Values in red denote a KS statistic greater than 0.1.

The MPSA results for the intrinsic growth rate appear more interesting. When r is positive, β and κ are significant. Contact rate, β, appears most influential in the middle of its range. However, κ, is far more influential in the lower part of its range. This suggests there is most change in r when $\kappa \in [0, 5e7]$. This is because κ controls the probability of infection given contact with bacteria. Thus, it is most influential when the disease is already established. In contrast to the PRCC results, γ is not significant when $r > 0$. This is not due to the choice of significance threshold as the MPSA value for γ is so low. However, it may be due to the acceptability threshold. A threshold in an area of many small fluctuations will lead to a different MPSA result than if the threshold fell below or above the fluctuations.

When $r < 0$, θ, β and γ are influential. The lower end of the ranges of θ and γ is most influential. Whereas, the effect appears constant over the range of β. We also note that β is significant here which is not the case for the PRCC results. This is due to the threshold of significance. The MPSA value is just 'significant' but the PRCC values is only just 'insignificant'. Therefore, the MPSA compliments the PRCC results once again.
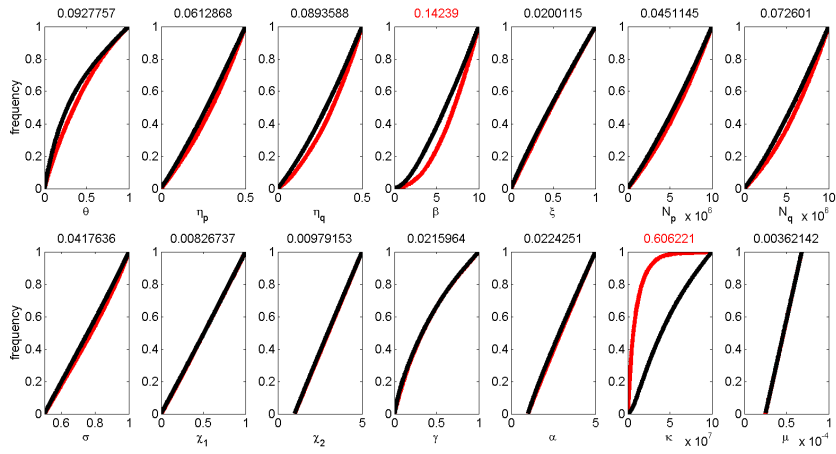
Figure 3a.11: Graphs of MPSA with a threshold of the average value of positive r over the 1000 parameter samples from table A.3. Values in red denote a KS statistic greater than 0.1.
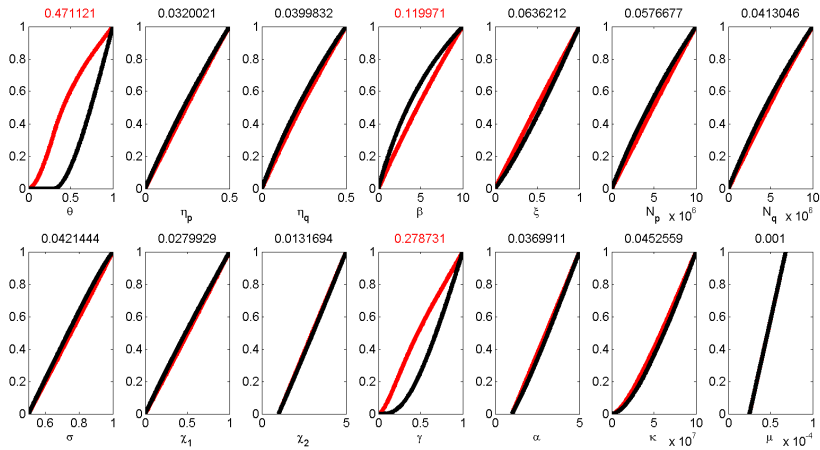

Figure 3a.12: Graphs of MPSA with a threshold of the average value of negative r over the 1000 parameter samples from table A.3. Values in red denote a KS statistic greater than 0.1.

3a.4.5 Bifurcation

We examine the endemic equilibrium values in both patches over the contact rate, β. In figure 3a.13 we chart the stable equilibrium values of the infected classes for each patch.
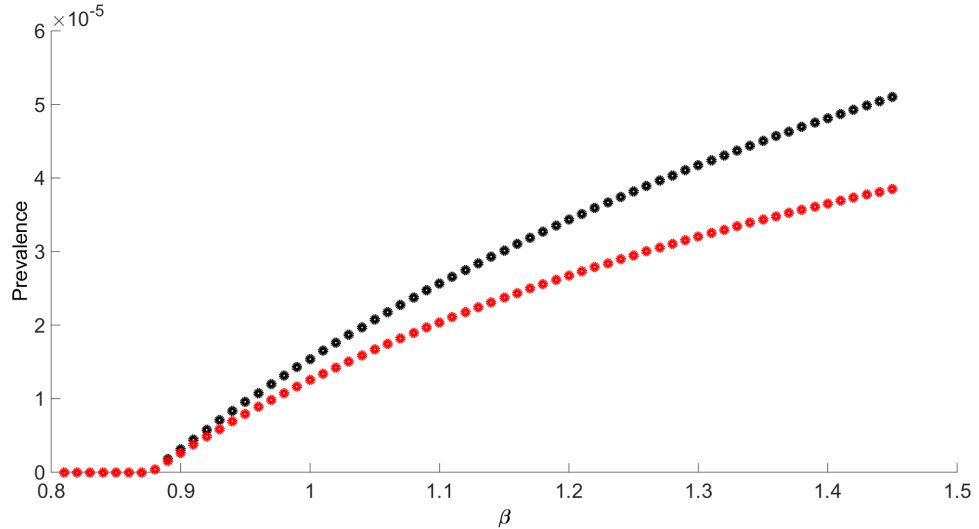

Figure 3a.13: Bifurcation analysis of the infected classes of patch p, black, and q, red over discrete values of β. Other parameters were $\theta = 0.8, \eta_p = 0.4989, \eta_q = 0.3024, \beta = 0.88, \xi = 0.4988, N_p = 1e7, N_q = 1e7, \tau = 6.4982, \chi_1 = 0.6351 \chi_2 = 4.7882, \gamma = 0.2, \alpha = 4.2816, \kappa = 1e7, \mu = 6.27e - 5$.

The bifurcation point corresponds to $R_0 = 1$. Before this point, the disease free equilibrium is stable and the size of the infected compartments are zero. After the transcritical bifurcation, the endemic equilibrium is stable and the infected compartment sizes increase as the contact rate increases. We see that the infected population is generally smaller in the patch with a treatment facility than in the patch without.

3a.5 Conclusion

3a.5.1 Summary

We aimed to find the effect of control on the dynamics of an environmentally transmitted disease through a metapopulation. We first outlined the model with treatment available in one patch. This involved revised exposure weightings for infected individuals as they were assumed to seek treatment. Once the model was derived, the outputs of the model were defined along with some analyses to examine them. These focussed on the sensitivity of the outputs to the model parameters. We used the elasticity and PRCC once more to compare the results of the new model to those of the model in chapter two. Furthermore we utilised the FAST and MPSA to examine the progress of uncertainty from input to output and highlight the areas of the parameter space which were particularly important. Finally, we examined the transition from disease free to endemic equilibrium stability using a bifurcation analysis.

3a.5.2 Findings

We used four methods of measuring the sensitivity of the model outputs to the input parameters. Generally, we found four parameters were influential. The degradation

rate, recovery rate, half-saturation constant and contact rate were all key influencing factors to the disease dynamics. These parameters control the generation time and are fundamental to the force of infection and so we may expect significant change in the disease dynamics given a change in these parameters. However, the analyses highlighted further parameters and behaviours of interest. The parameters from the patch with a treatment facility were generally found to be more influential. This is because infected individuals are proportionally more exposed to the environment surrounding a treatment facility. The variation in exposure experienced by infected individuals also led to some interesting effects of the treatment rate. We saw that in some situations the basic reproduction number actually increased when the treatment rate rose. This was in the situation where the weighting towards a treatment facility was significantly higher than the weighting away and where the shed rate in the patch without a treatment facility was high. As such, infected individuals experience almost all of the exposure to the patch with a treatment facility. However, once they were treated, the exposure to each patch returned to normal and so the exposure in the patch without a treatment facility increased. This also increased the importance of the bacteria in the patch without a treatment facility as individuals were free to contribute bacteria there. Therefore, the behavioural change in response to treatment provision motivates some negative outcomes as well as positive.

We conducted a bifurcation analysis. This allowed us to see how the transition from stable disease free equilibrium to stable endemic equilibrium occurs. We saw that there was a branch-point at $R_0 = 1$. After this point, the disease free equilibrium was no longer stable and the endemic prevalence steadily increased. One key aspect of this was that the endemic prevalence was lower in the patch with a treatment facility. Therefore, even with coupling between patches and proportionally more exposure in the patch with the treatment facility, there is still a marked benefit from the treatment facility to local residents. These dynamics hold for one parameter set. If another parameter set was chosen we would see a different value of the contact rate for the transcritical bifurcation. We would also see differing endemic prevalences. However, the behaviour would remain largely the same.

Our methods were quite different to those used in the works mentioned in the literature review. We also examined a different behavioural adaptation as it was in response to control rather than disease prevalence. We found that the scaling of the edge weightings were not influential for R_0 or r. However, there were situations where the changed behaviour of infected individuals can lead to surprising effects of the treatment rate. We noted that the variation in behaviour of the infected individuals with respect to treatment can mean their exposure is dominated by the environment of patch q. This leads a much higher contribution of bacteria there, until individuals are treated. In comparison with the works reviewed, we found that the behavioural change can both decelerate *and* accelerate disease spread. The deceleration is due to encouraging infected individuals to become treated and recover faster. The acceleration is through the effect of treatment rate in section 3a.4.1.1. However, we did not find a great dependence of the basic reproduction number on behavioural adaptation.

3a.5.3 Assessment of the methods

We used a wide variety of methods- particularly to measure the sensitivity. Each had their benefits and areas of speciality. The elasticity approximated the input/ output relationship at every point in the parameter space. Also, with the finite difference approximation, it was computationally quick. However, the varying values can lead to busy presentation. In contrast, the PRCC gave one value for the relationship between

input and output. This was easy to interpret even when we divided the parameter space around the epidemic threshold. However, the need for monotonicity, especially with the new complicated movement terms, limited the usefulness of PRCC. The FAST is not hampered by the requirement of monotonicity. It measures the spread of uncertainty from input to output and uses that as a measure of the sensitivity. A problem with the FAST is that there can be instances where a parameter, through poor estimation, may contribute a disproportionate amount of uncertainty, leading to a misleading sensitivity result. This is partly because the parameters are assumed to be strictly independent [143]. However, it can also fail when the parameter estimation includes infeasible or extreme values, causing extreme values of the output. For instance, if the order of magnitude was too large, the contribution of uncertainty would be disproportionate compared to the effect. The method also does not indicate the direction of influence of input on output, a valuable piece of information. This is a defect shared by the MPSA. Although the benefit of the MPSA is that it highlights important areas of the parameter space. Thus, we could see that the different intervals of the parameter range were more influential either side of the epidemic threshold. However, it is unclear whether this is a result of the influence of the parameter of whether the epidemic threshold divided the range in this way. Another area of possible error related to the MPSA was the user-defined threshold of acceptability. It may be necessary to check a variety of thresholds to ensure the results are robust.

In conclusion, the elasticity, despite having many values to examine, was computationally quick, did not require monotonicity or a user-defined threshold and would not be unduly affected by uncertainty in parameter estimation. As such, it may be a good method to utilise in further work. However, we have not yet identified methods of analysis with regard to perturbation.

This is not to say that the methods employed in this chapter were not useful. If we wished to build a comprehensive picture of the sensitivity of this model we could gain insight from each analysis method if we asked the right questions. If we wanted to see the range of possible effects of a parameter on an output, we could use the elasticity analysis to see how much the influence varied. In that influence, we could use the MPSA to highlight areas of greatest importance which would be particularly useful if we were unsure whether to examine all of a large range of a parameter. To get an idea of the overall average effect of a parameter on an output we could employ the FAST. However, if we knew the parameters to be correlated and have a monotonic relationship on the output, we could utilise the PRCC instead. Therefore, depending on the relationship between the parameters and the output or the parameters and themselves, we can build a detailed picture of the behaviour.

3a.5.4 Future considerations

We focused once more on highlighting the sensitivity to key system parameters. However, the implementation of treatment here does not take into account the limitations of treatment. In a real situation, there would not be unlimited capacity for treatment and there would be situations where an influx of infected individuals could overwhelm services. We examine this situation in the next part of this chapter.

Chapter 3b

Limiting the treatment capacity

3b.1 Introduction

In Chapter Three part A we examined the effect of one treatment facility in a metapopulation. However, we assumed that the treatment facility had unlimited capacity. In real life, a medical facility would need to cope with changing demand for medicines and supplies which may be overwhelming at times. As such, we now assume that the rate of treatment depends on the number of infected individuals and a fixed capacity.

We wish to understand how this capacity for treatment affects disease dynamics. Therefore, we will see how key system outputs, the epidemic size and endemic equilibrium value, vary with limited treatment provision. We focus on aspects away from disease free steady state as the analysis of the fixed treatment rate model will hold when the number of infected individuals is low. We start with a brief literature review of saturating treatment models.

3b.2 Brief literature review on saturating treatment terms

The idea of varying treatment rates was first addressed by Wang and Ruan in a simple SIR model [135]. In this instance, the treatment term was a step function dependent on the infected class. When there were no infected individuals, the treatment term was zero. Otherwise, there was a constant removal of infected individuals, shown in equation (3b.1).

$$
\begin{aligned}
\dot{S} &= A - dS - \lambda SI \\
\dot{I} &= \lambda SI - (d + \gamma)I - h(I) \\
\dot{R} &= \gamma I + h(I) - dR
\end{aligned}
\tag{3b.1}
$$
$$
h(I) = \begin{cases} r & I > 0 \\ 0 & I = 0 \end{cases}
$$

The model assumed that the population was closed with all individuals born susceptible at constant rate A. Individuals died at rate d and recovered naturally at rate γ. Finally, λ denoted the force of infection and $h(I)$, the number of individuals treated. Wang and Ruan conducted their analysis analytically. They defined R_0 explicitly which gives a threshold for the existence of one endemic equilibrium when $R_0 = 1$ and derived another threshold, $R_0 = (H = \frac{\lambda r}{d(d+\gamma)})$, for the existence of two endemic equilibria. This led to a bifurcation analysis. They found, and derived expressions for, a saddle-node, sub-

critical Hopf and homoclinic bifurcation. Thus, with a simple step function for the removal of infected individuals, a wide array of behaviour was discovered.

The concept of a varying removal rate of infected individuals was revisited by Wang in 2006 [134]. The model in equations (3b.1) was retained. However, the number of individuals treated, $h(I)$, depended linearly on the number of infected individuals until a critical number, I_0, was reached, see equations (3b.2). The aim of the paper was to examine bistability surrounding a backward bifurcation. Analysis was once again conducted analytically to establish thresholds for stability of the disease free equilibrium and no Hopf bifurcation was found.

$$h(I) = \begin{cases} rI & 0 \le I \le I_0 \\ k = rI_0 & I > I_0 \end{cases} \tag{3b.2}$$

In later work, Cui, Mu and Wan examined a SIS model [32]. They defined a treatment rate with nonlinear dependence on the number of infected individuals, shown in equations (3b.3). The treatment rate was zero when there were no infected individuals and approached a maximum, c, as the number of infected individuals increased. When $I = b$, the rate was half its maximum.

$$h(I) = \frac{cI}{(b+I)} \tag{3b.3}$$

They found a backward bifurcation, and an area of bistability, and defined the idea of treatment capacity. However, they found no oscillatory dynamics.

This nonlinear treatment rate was examined repeatedly over the following years. Zhang and Liu found that, as the impact of the treatment rate increased, $R_0 = 1$ was no longer a strict threshold for disease invasion [144]. This is because a backward bifurcation formed and they defined a new threshold for disease persistence, R_c, as the turning point of the backward bifurcation. Zhang and Suo further categorised these thresholds in a SIS model and Wan & Cui examined them in a SIR model to classify the stability and existence of endemic equilibria [133, 145].

Finally, Li and Cui added an additional nonlinear incidence term to their model in 2013 [82]. This, along with a constant removal rate of infected individuals rather than a nonlinear treatment rate, led to complicated dynamics. They derived criteria for the existence of a Hopf bifurcation and analysed the Lyapunov exponents for it. The Lyapunov exponents give the rate of exponential divergence from perturbed initial conditions. When the first Lyapunov exponent is negative, the limit cycles emanating from a Hopf bifurcation are stable and the bifurcation is termed 'supercritical'. Otherwise, and in the case of Li and Cui's work, the limit cycles are unstable and the Hopf bifurcation is termed 'subcritical'.

3b.2.1 Summary

The works mentioned focussed on SIR and SIS models in their simplest forms. In most cases, R_0 and the endemic equilibria could be written explicitly allowing analysis of their existence and stability to be conducted analytically. When the treatment rate saturated, bistability was found in certain situations. This was between $R_0 = 1$, where there was a backwards transcritical bifurcation, and R_c which denoted the turning point of the bifurcation. When there was both a nonlinear incidence rate and step function for the removal of infected individuals, a Hopf bifurcation was found. This meant that the model exhibited oscillatory behaviour as the number of infected individuals fluctuated, affecting both the force of infection and the removal of infected individuals.

In the following model we shall also examine the issue of varying removal of infected individuals through treatment. However, there are some differences with the aforementioned works. We focus on an environmentally transmitted disease. As such, we examine a nonlinear force of infection that is dependent on the bacteria in the environment. We also assume that the treatment rate decreases as the number of infected individuals increases. This is to approximate the demands on a medical facility of an influx of infected individuals. Our treatment rate profile is shown in figure 3b.1. We shall elaborate on the assumptions and form of our treatment rate now.

3b.3 Model

We wish to examine the effect of limited treatment capacity on the dynamics of an environmentally transmitted disease. This limited capacity will affect the rate at which infected individuals enter the treated class. This is defined as the treatment rate whose form is based on the following assumptions.

- The treatment rate is at its potential maximum when there are no infected individuals. Thus, when there is no demand, the facility should operate at its maximum potential.

- There is a capacity that the treatment rate depends on.

- The treatment rate should not immediately fall when the infected population increases, rather there should be a plateau. This is as we assume that the facility can cope with a certain level of demand before it begins to be stretched.

- Similarly, the rate should plateau once more after it has fallen. We assume that even when working at full capacity, the facility is still able to supply some medical aid.

Given these constraints, we choose the following function which contains the preferred characteristics,

$$\xi(I) = \xi^* \left(\frac{1}{1 + (I/\Upsilon)^2} \right). \tag{3b.4}$$

Treatment rate, ξ, is a function of the number of infected individuals with access to treatment. The new parameter, Υ, is related to the capacity of the treatment facility. The capacity can be unlimited which leads to the parameter ξ^* reaching its maximum treatment rate. In Figure 3b.1 the profile of the treatment rate as the number of infected individuals increases is shown.

The model is then as defined in Chapter Three part A including the new saturating treatment term. The treatment facility is placed in patch q. Therefore the proportion of infected individuals exposed to the treatment facility is $I = \left(\dfrac{\chi_2(1-\sigma)}{\chi_1\sigma + \chi_2(1-\sigma)} \right) I_p +$ $\left(\dfrac{\chi_2\sigma}{\chi_2\sigma + \chi_1(1-\sigma)} \right) I_q.$
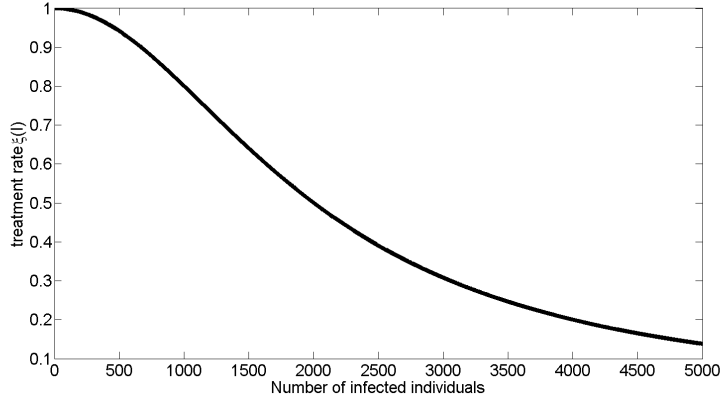
Figure 3b.1: The treatment rate as a function of the number of infected individuals with access to a treatment facility. Here Υ was chosen as 2000 and ξ^* as 1 for illustration.

$$
p\begin{cases}
\dot{S}_p &= \mu N_p - \beta S_p\left(\sigma\frac{B_p}{\kappa + B_p} + (1-\sigma)\frac{B_q}{\kappa + B_q}\right) - \mu S_p, \\[2ex]
\dot{I}_p &= \beta S_p\left(\sigma\frac{B_p}{\kappa + B_p} + (1-\sigma)\frac{B_q}{\kappa + B_q}\right) - \left(\gamma + \xi(I)\left(\frac{\chi_2(1-\sigma)}{\chi_1(1-\sigma) + \chi_2\sigma}\right) + \mu\right)I_p, \\[2ex]
\dot{T}_p &= \xi(I)\left(\frac{\chi_2(1-\sigma)}{\chi_1(1-\sigma) + \chi_2\sigma}\right)I_p - (\alpha\gamma + \mu)T_p, \\[2ex]
\dot{R}_p &= \alpha\gamma T_p + \gamma I_p - \mu R_p, \\[2ex]
\dot{B}_p &= -\theta_p B_p + \eta_p\left(\left(\frac{\chi_1(1-\sigma)}{\chi_2\sigma + \chi_1(1-\sigma)}\right)I_q + (1-\sigma)T_q + \sigma T_p \right. \\[2ex]
&\qquad \left. + \left(\frac{\chi_1\sigma}{\chi_1\sigma + \chi_2(1-\sigma)}\right)I_p\right).
\end{cases}
$$

$$
q\begin{cases}
\dot{S}_q &= \mu N_q - \beta S_q\left(\sigma\frac{B_q}{\kappa + B_q} + (1-\sigma)\frac{B_p}{\kappa + B_p}\right) - \mu S_q, \\[2ex]
\dot{I}_q &= \beta S_q\left(\sigma\frac{B_q}{\kappa + B_q} + (1-\sigma)\frac{B_p}{\kappa + B_p}\right) - \left(\gamma + \xi(I)\left(\frac{\chi_2\sigma}{\chi_2\sigma + \chi_1(1-\sigma)}\right) + \mu\right)I_q, \\[2ex]
\dot{T}_q &= \xi(I)\left(\frac{\chi_2\sigma}{\chi_2\sigma + \chi_1(1-\sigma)}\right)I_q - \alpha\gamma T_q - \mu T_q, \\[2ex]
\dot{R}_q &= \alpha\gamma T_q + \gamma I_q - \mu R_q, \\[2ex]
\dot{B}_q &= -\theta_q B_q + \eta_q\left(\left(\frac{\chi_2\sigma}{\chi_2\sigma + \chi_1(1-\sigma)}\right)I_q + \sigma T_q + (1-\sigma)T_p \right. \\[2ex]
&\qquad \left. + \left(\frac{\chi_2(1-\sigma)}{\chi_1\sigma + \chi_2(1-\sigma)}\right)I_p\right).
\end{cases}
$$

All parameters are as defined in table A.3 except for the saturating treatment terms, shown in table A.5.

3b.4 Analysis

When the system is disease free, the treatment rate is at its maximum and the model is the same as the constant treatment rate case. Therefore, we examine model characteristics or outputs away from disease free equilibrium. We shall define the calculation

to find the epidemic size and endemic equilibrium and then define analysis methods to understand them.

3b.4.1 Model outputs

We focus on the transient behaviour away from disease free equilibrium through the epidemic size, and the long-term behaviour through the endemic equilibrium. The epidemic size is calculated using an additional compartment in the model consisting of the force of infection. This counts the new infections without loss due to recovery or death. We start at disease free equilibrium, introduce a small number of infected individuals, $N/1000$, and count the number of infections over the following 100 days. We choose a fixed time period as the epidemic is likely to have ended in this period and the number of infections over the time period will be proportional or equal to the number over the course of the epidemic. This also circumvents the issue of whether the disease free equilibrium is stable for the parameter set, in which case the epidemic size is zero.

The endemic equilibrium is calculated using simulation as detailed in the previous chapter. However, it is also calculated algebraically in MATLAB and through the program MATCONT, explained in Section 3b.4.3.

3b.4.2 Analysis methods

We conduct an elasticity analysis on the epidemic size to establish the dependence of the short term behaviour on the new saturating treatment term. This is calculated using the finite difference approximation to speed the computation of the partial derivative. It therefore takes the following form,

$$E_{\text{epidemic size}} = \frac{\text{input}}{\text{epidemic size(input)}} \frac{\text{epidemic size(input} + \Delta \text{input})}{\Delta \text{input}}.$$

For a full explanation of elasticity, see Chapter Two, and for a full explanation of the finite difference method see Chapter Three part A.

3b.4.3 Bifurcation analysis

We conducted a simple bifurcation analysis in Chapter Three part A. However, considering the findings of previous works on varying treatment rates, we may expect more complicated dynamics here. Bifurcation analysis examines the value and stability of the system equilibria. We will use MATLAB and MATCONT to plot the disease free and endemic equilibria with respect to the contact rate, β. We shall use the eigenvalues of the system Jacobian linearised about the equilibrium to classify the equilibrium stability [74]. When the eigenvalues have negative real part, the equilibrium is stable. MATCONT works within MATLAB as a continuation and bifurcation toolbox [55]. It can not only examine the stability of equilibria but also classify bifurcations and find limit cycles and periodic behaviour.

As mentioned previously, we may expect some more complicated dynamics in our model. As such we shall employ another tool to analyse the system behaviour. When the system exhibits oscillatory behaviour, a Poincaré section may be used to classify it as periodic, quasi-periodic or chaotic. It is known as the surface of section and is the image of the hyperplane chosen when calculating a Poincaré map [103]. The map replaces a N dimensional autonomous system with a (N-1) dimensional discrete time system [128].

The section is calculated using the following steps:

- A (N-1) dimensional hyperplane transverse to the system flow is chosen. For instance, this can be done by fixing one of the system variables, X, at a constant value, K.

- The system behaviour is simulated and the trajectory is calculated.

- We concentrate on the variable, X. As the system oscillates, X will take a range of values and we note when $X = K$ as this is when the system trajectory intersects the hyperplane. We can consider ourselves sampling the trajectory at this point [103]. Also, as we do not distinguish which direction the trajectory approaches the hyperplane, this is defined as a 'two-sided' Poincaré map.

- If the solutions are periodic, X will return repeatedly to value K after time T in the same position in state space.

- In this situation, T is the minimum period of the limit cycle and our Poincaré section takes the form of figure 3b.2.
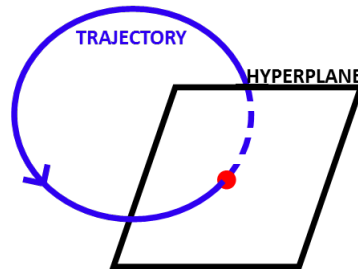

Figure 3b.2: Trajectory and Poincaré map with periodic behaviour.

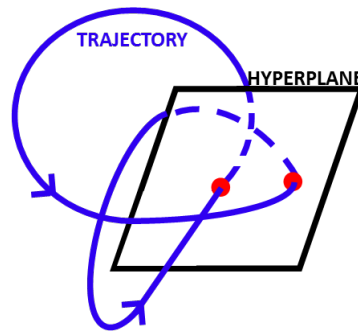It could also take the form in figure 3b.3 for a period-2 orbit.

Figure 3b.3: Trajectory and Poincaré map with period-2 behaviour.

The trajectory in figure 3b.3 has period 2T. The Poincaré section for an N-periodic orbit has N points.

- When the system is quasi-periodic, the position in state space when $X = K$ varies slightly. However, the system is still 'well-behaved' and does repeat to form a fixed shape, a closed curve, shown in figure 3b.4.

- Lastly, there is the situation where the system exhibits chaotic behaviour and what can be seen on the Poincaré section is the 'attractor', a complex and fine-structured pattern.
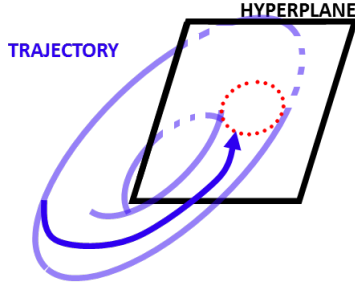
Figure 3b.4: Trajectory and Poincaré map with quasi-periodic behaviour. The trajectories follow the surface of the torus

Given a limit cycle of the underlying flow, different choices of hyperplane can lead to closed orbits of different orders or periods [103]. In our work, we chose our hyperplane as $B_p = mean(B_p)$ where $mean(B_p)$ is calculated as the mean size of the bacterial class in patch p over the timespan. The timespan we used was 3000 years. However, we first simulated the system to equilibrium using a timespan of 300 years, the mean was then calculated after this point. This is as the system acts as a damped oscillator and we wish to ignore the initial fluctuations. We then examined at which points the system trajectory intersected the hyperplane, or when $B_p = mean(B_p)$. These points are plotted on the $S_p - S_q$ plane as this offered the clearest view. We used code adapted from [54] using theory from [103, 126].

3b.5   Results

We start with the short-term effects of limited treatment capacity by examining the epidemic size and its relation to R_0 and the system parameters.

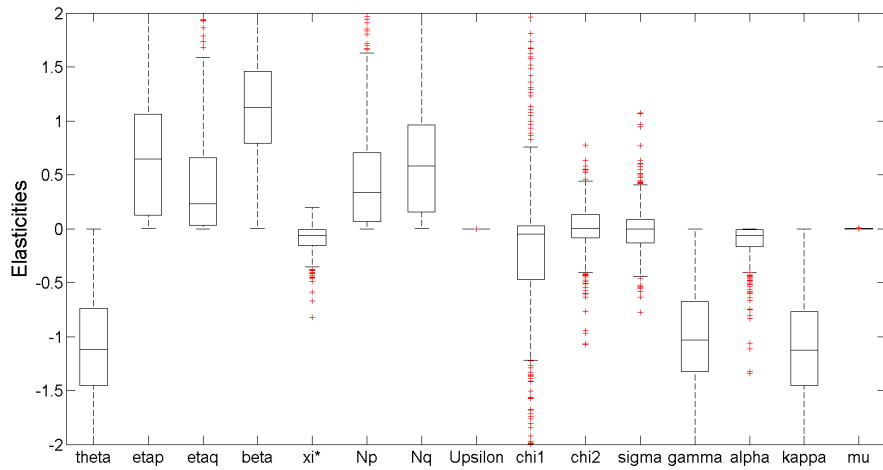### 3b.5.1   Elasticity of the epidemic Size

In figure 3b.5 we examine the relationship between the epidemic size in patches p and q and the system parameters. We see that the capacity does not affect the epidemic size in either patch. This suggests that the short-term behaviour is unaffected by the saturating treatment term. To understand this a little better, we examine the relations between R_0 and the epidemic size in both patches.

As we see from figure 3b.6, R_0 is strongly correlated with the epidemic size. Thus, the epidemic size is almost completely determined by the initial growth rate of the epidemic. Therefore, as the $\xi(I) = \xi^*$ at disease free equilibrium, we see no dependence on the capacity, Υ. However, there is a slight variation in the spread of values when Υ is much smaller, $10^{0.5}$ as opposed to 10^4, but not the relation with R_0.

We will now examine whether the capacity for treatment has any long-term effects through the bifurcation analysis.
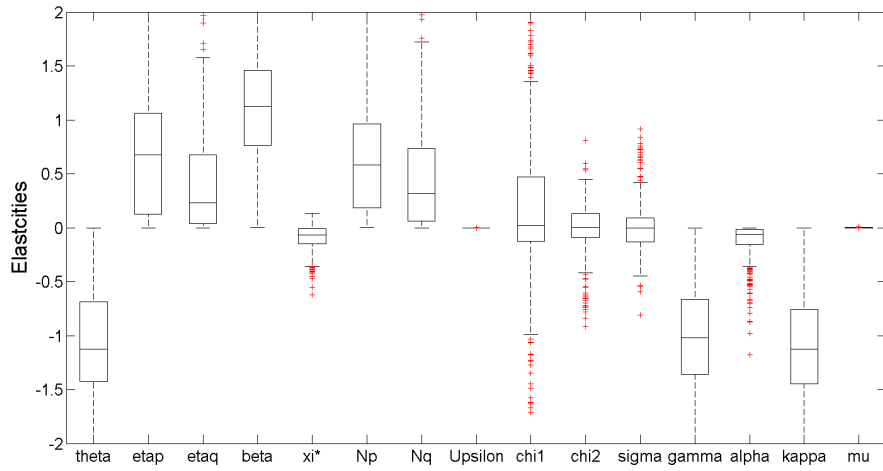
(a) Patch *p*

(b) Patch *q*

Figure 3b.5: Elasticities of the epidemic size in either patch with respect to the system parameters. The parameters took values in ranges specified in tables A.3 and A.5.
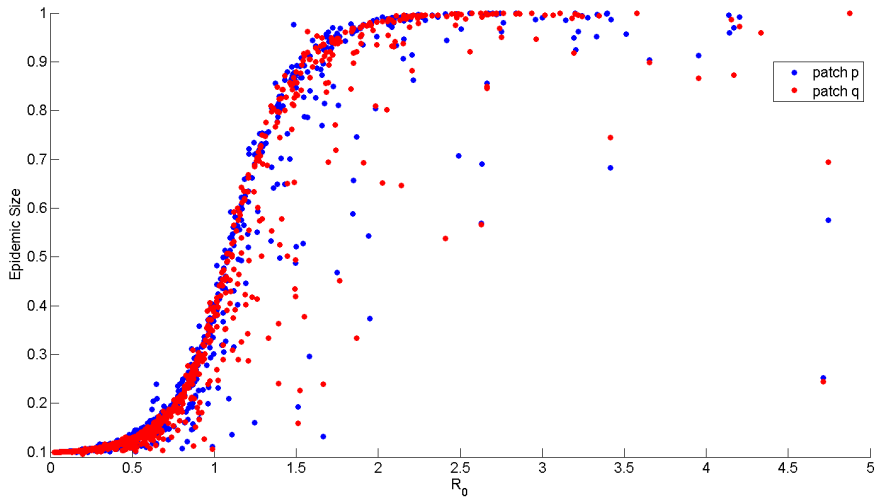
Figure 3b.6: Graph of (normalized) epidemic size for different parameter sets shown in tables A.3 and A.5 over the R_0 with varying treatment.

3b.5.2 Bifurcation Analysis

In the following bifurcation analysis, we choose the parameters to be the same as in chapter 3 part A. The capacity, Υ is set at a value close to the endemic size of the infected population, 10^4, in either patch to test the system under strained conditions.
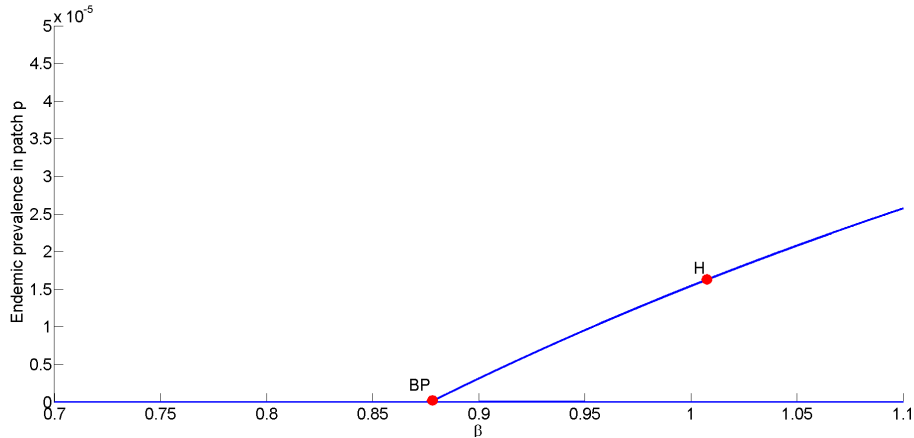

Figure 3b.7: Bifurcation analysis of the infected class of patch p with respect to contact rate, β. We focus on the interval with bifurcation points and the parameters take values shown in table A.4.

In figure 3b.7 we see a transcritical or branch-point bifurcation at $\beta = 0.87$ where the disease free equilibrium loses stability. This is also the case in patch q. After this point, the endemic prevalence increases. However, most interestingly, we see a Hopf bifurcation point when $\beta = 1.007$. This is a point where the behaviour of the system becomes oscillatory. We use MATCONT further to expand the limit cycles emanating from this point, shown in figure 3b.8.

MATCONT suggests the limit cycles are present for $\beta < 1.007$ and then turn [55]. The turn is shown in figure 3b.10. However, for the limit cycles shown in figure 3b.8 we examined the Floquet multipliers to ascertain their stability. Floquet multipliers
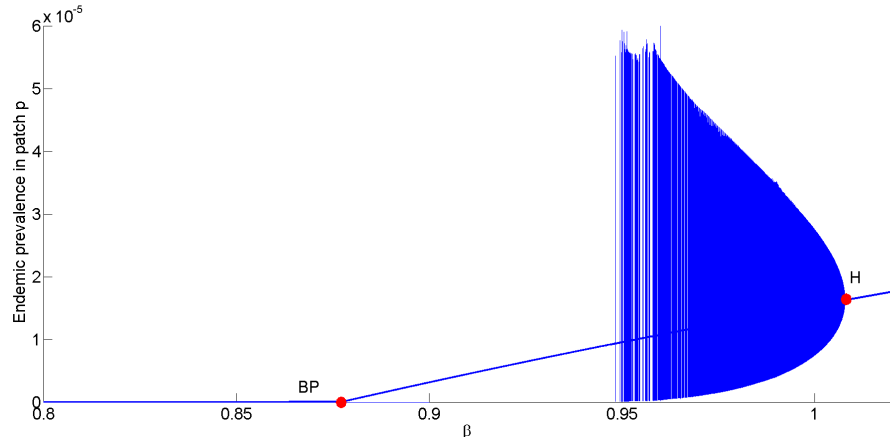
Figure 3b.8: Bifurcation analysis of the infected class of patch p with respect to contact rate, β. We focus on the limit cycles with bifurcation points and the parameters take values shown in table A.4.

are a generalisation of the eigenvalues at an equilibrium point. We linearise the system around a fixed point using the Jacobian to establish the stability of an equilibrium point. When we examine a periodic solution, the system in linearised around a fixed point of the Poincaré map which corresponds to a periodic solution. The 'Jacobian' in this setting yields the Floquet multipliers as eigenvalues. When the multipliers have modulus less than unity, the periodic solution is stable [103]. These can also be calculated in MATCONT and we found the multipliers in this case to be greater than unity, thus the periodic solution shown is unstable.

Also, for the limit cycles shown in figure 3b.8 we may plot how the period of the oscillation changes from the Hopf bifurcation to the turn, shown in figure 3b.9.
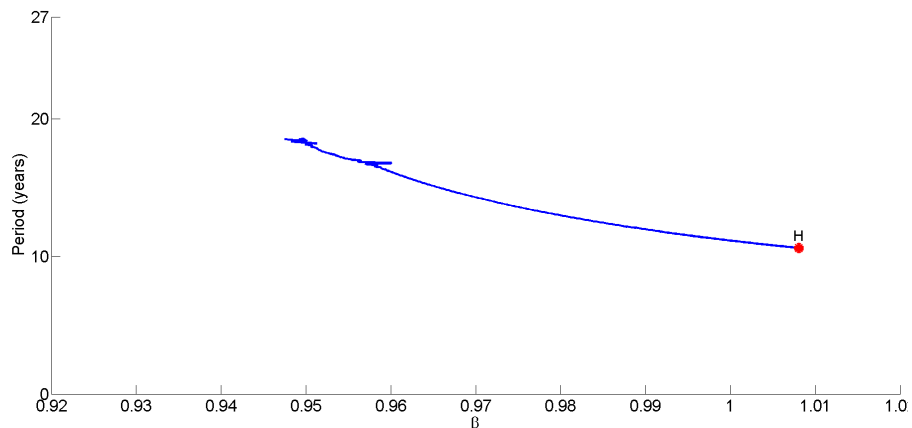

Figure 3b.9: Period of limit cycles from Hopf bifurcation point to turn.

We noted an artefact at the turn of the limit cycles, see figures 3b.9 and 3b.8. At this point, MATCONT fails to find a solution. We therefore use a different method to plot the behaviour of the system. Figure 3b.10 was constructed using a range of methods. The stable and unstable equilibria were calculated by solving the system algebraically in MATLAB. This solution was then substituted into the system Jacobian so that the eigenvalues may be calculated to assess stability. If all the eigenvalues had negative real part, the equilibrium was stable and plotted in black [24]. Otherwise, the solution was plotted in magenta. The system was then simulated over a long timespan to

calculate the extrema of the oscillations. At each value of β, the system was simulated to equilibrium and then simulated for a further 100 years. The maximum and minimum values over this time were then plotted with dotted lines and the method repeated. Finally, the unstable limit cycles were interpreted from the MATCONT plot.
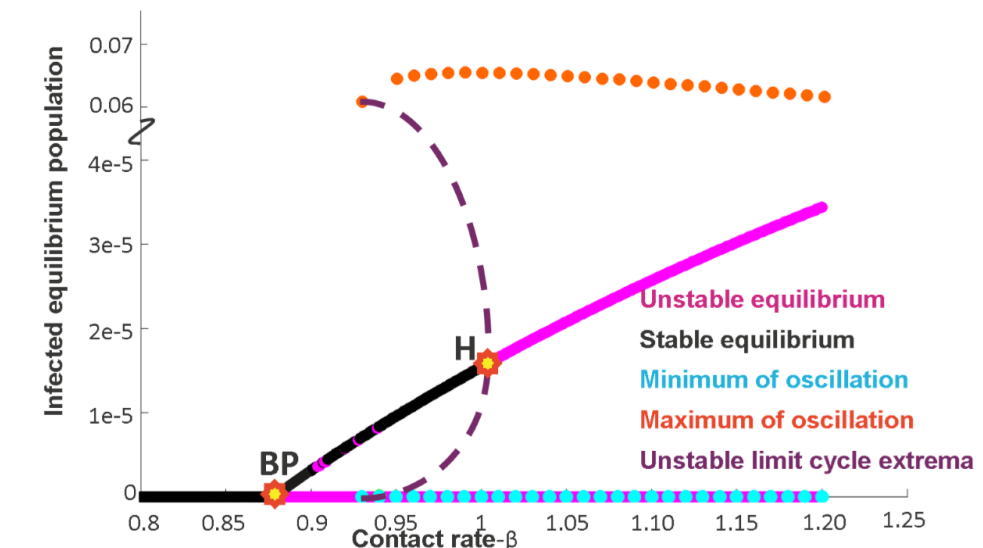

Figure 3b.10: Bifurcation diagram showing transitions in stability and maximum and minimum values of oscillations. The parameters took values in the ranges specified in table A.4.

In figure 3b.10 we see the transition from stable equilibria, black, to unstable, magenta. This occurs, for the disease free equilibrium, at $\beta = 0.8777$. Between $\beta = 0.8777$ and $\beta = 0.92$ we see a stable endemic equilibria only. Then, there is stable oscillatory behaviour from $\beta = 0.92$ with the endemic equilibrium also remaining stable until $\beta = 1.007$ where there is a subcritical Hopf bifurcation. Therefore, the system exhibits a form of bistability.

In figure 3b.11, we compare the time series when the endemic equilibrium and oscillations are stable. The two behaviours are shown for the same value of β but different initial conditions. The question now is whether the oscillations are periodic, quasi-periodic or chaotic. We will now examine the Poincaré section.

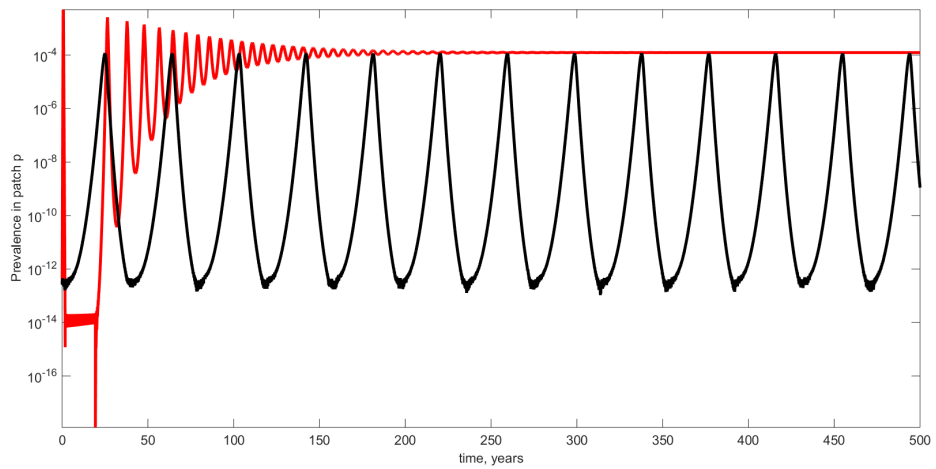### 3b.5.2.1   Poincaré section

We use the Poincaré section to classify the oscillatory behaviour as periodic, quasi-periodic or chaotic.

Figure 3b.12 shows a pair of points for each of the five values of β. This suggests a period-2 system as the trajectory intersects the hyperplane at two distinct points. Thus, it would appear that after the fold, there is a region of periodic oscillation.
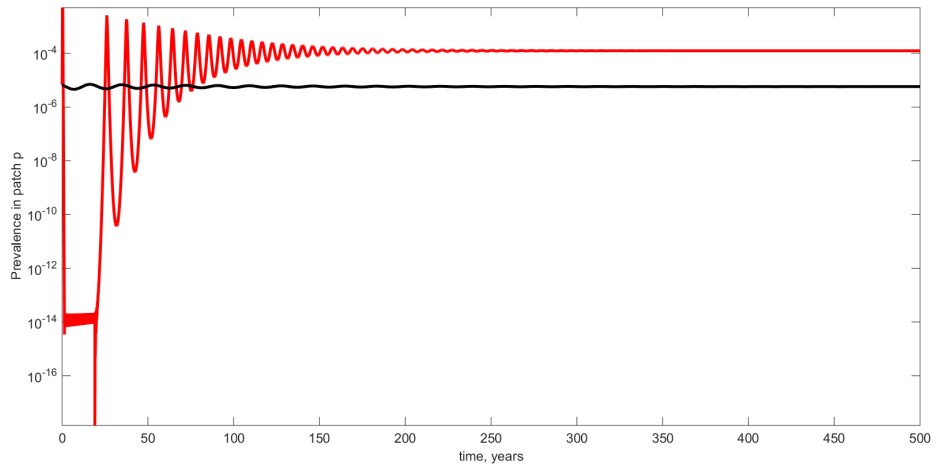
(a) Equilibrium

(b) Oscillation

Figure 3b.11: Time series for the prevalence in patch p. The parameters are set as per table A.4 with $\beta = 0.92$. The system is without treatment, red, and with treatment, black.
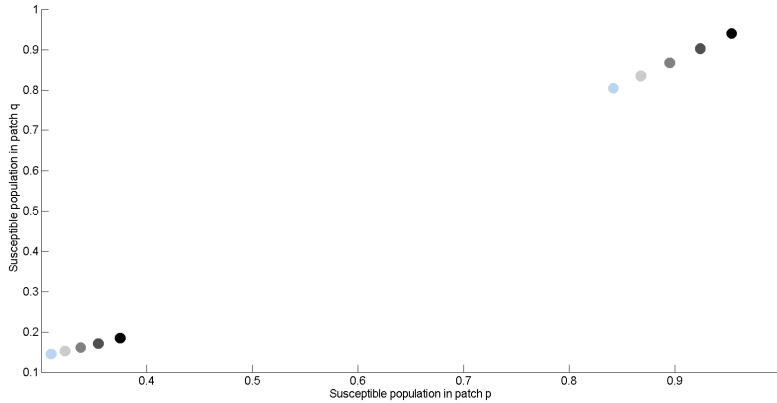
Figure 3b.12: Poincaré section cut about the mean of the bacterial class in patch p with varying values of contact rate, β. This was computed in MATLAB using a program inspired by D. Gonze and using theory from [54, 103, 126]. The parameters are as shown in table A.4 and $\beta = [0.941, 0.981, 1.021, 1.061, 1.101]$ from black to grey.

3b.6 Conclusion

3b.6.1 Summary

Our aim was to examine the effect of a limited capacity for treatment on the dynamics of an environmentally transmitted disease. We first defined the relationship between treatment rate and medical capacity. This was a decreasing function of the number of infected individuals with access to the treatment facility. When there are no infected individuals- the potential rate is at its maximum. This rate remains relatively unchanged for a small number of infected individuals. However, when the number of infected individuals increases, the rate of treatment decreases as the medical facility approaches its capacity.

Once the form of the treatment rate function was established, we detailed some analysis methods. The model is the same as the constant treatment rate case when the system is close to disease free equilibrium. As such, we focused on the model dynamics away from the disease free steady state. We started with the epidemic size and its relation to the capacity for treatment and other system parameters. Then we conducted a bifurcation analysis with respect to the contact rate with the contaminated environment. This included not only the stability of the equilibria of the model but also the oscillatory dynamics. We used MATCONT and MATLAB to examine the extent of the oscillations and a Poincaré section to classify their type.

3b.6.2 Conclusions

The variable treatment rate gave many new dynamics to the system. However, the epidemic size depended only on the basic reproduction number, a property that holds near the disease free equilibrium. As such, the treatment rate is at its maximum and the capacity does not come into effect.

The long-term behaviour was affected by the capacity for treatment. We found a transcritical bifurcation when the contact rate was 0.87 contacts per day that led to the disease free equilibrium losing stability. After this point there was a stable endemic equilibrium until the contact rate was 1.007 contacts per day. At this point, the limited treatment capacity took effect. There was a Hopf bifurcation with unstable limit cycles

emanating backwards until a fold whereupon the oscillatory dynamics became stable. This is consistent with a *subcritical Hopf* bifurcation. Thus, when the contact rate is between 0.92 and 1.007 contacts per day there is a stable endemic equilibrium *and* stable oscillations.

The biological interpretation of these dynamics is that, once the disease is established, there are two ways the system can behave. If there are a small number of infected individuals, the medical facility will have enough capacity and will not be overwhelmed. This means that the system will remain at stable equilibrium and the treatment rate will remain in region 1 in figure 3b.13. However, when there is a larger influx of infected individuals before the treatment has time to to take effect, the treatment facility may be overwhelmed. In this case, the treatment rate moves into region 2 of figure 3b.13 and reduces dramatically. This leads to large epidemics which exhaust themselves. The treatment allows the susceptible population to grow to a larger extent than would otherwise be the case. Therefore, we see larger epidemics than would be the case without any treatment.
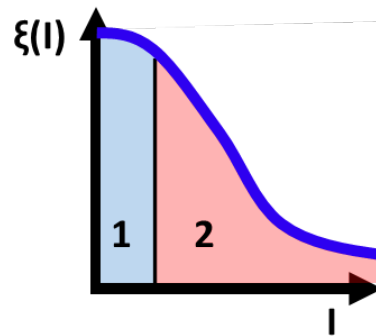

Figure 3b.13: Regions of treatment rate for stable equilibrium and stable oscillatory behaviour.

We conducted a literature review of models involving variable removal rates of infected individuals. We found the works fell into two categories, those with a Hopf bifurcation and oscillatory behaviour and those with a backward bifurcation and bistability. The Hopf bifurcation arose when there was a constant removal of infected individuals and a nonlinear incidence rate. Whereas, the backward bifurcation was a result of a nonlinear or saturating treatment rate. We included a treatment rate of different saturating form to the aforementioned works. However, we found oscillatory behaviour and no backward bifurcation.

3b.6.3   Future considerations

We wished to understand how the limited capacity of a treatment facility affected the disease dynamics. We found oscillatory behaviour symbolising a regime of large epidemics in the long term. In the short term, we found little dependence of the epidemic size on capacity. However, our epidemic was initialised from disease free equilibrium which may affect the behaviour.

We did establish the long-term dynamics in detail for the parameter set of interest through a variety of bifurcation techniques. The bespoke MATLAB program for the oscillation and steady state calculation perhaps yielded the best graphical result. However, the unstable limit cycles and their characteristic or Floquet multipliers were only discovered through the use of the toolbox MATCONT. Finally, the Poincaré section was informative. However, the choice of plane to present the results did affect how

clear they were to interpret. That is, the choice of a different hyperplane affected how dispersed the points were.

We asked how the limited capacity of a treatment facility altered the dynamics of an infectious disease. When considering a larger population, across a city, we may be interested in multiple treatment facilities. Thus the question ceases to involve the effect of internal capacity but rather the *external* capacity for treatment facilities in the patches. We move to ask, given a limited number of control facilities, how is best to deploy them? There are a number of things to establish before we answer this question. Firstly, how would our model extend to a higher number of patches to simulate the real level of diversity you would expect to find in a city? Also, how would those patches be structured within a city? We mentioned epidemic size initiated from endemic equilibrium. This situation would arise from a system perturbation which links back to our thesis-wide question: how would a perturbation such as a natural disease affect disease dynamics? Thus, we need to establish our model over N patches and examine not only the steady state operation but also the perturbed, exceptional behaviour. At this point we will have a more substantial answer to the question of optimal disease control provision in a city affected by a natural disaster.

Chapter 4

Spatially structured populations and the impact of a natural disaster

4.1 Introduction

We have examined the dynamics of an environmentally transmitted disease in a two patch population in the presence of a control measure. Now we wish to investigate the dynamics over an increasingly spatially segregated population. This is in order to model disease spread over a spatially complex population structure. In this chapter we define our model over $M \in \mathbb{N}$ patches. We will also explain the computational tools used when defining higher dimensional models.

Where there are more than two patches present, there is also more than one possible arrangement of patches. As such, we examine how the arrangement affects key system outputs such as R_0. We also investigate the change in these system outputs as the population becomes increasingly spatially segregated. Finally, we introduce a method to quantify the effect of a perturbation to the system. This perturbation will be in the form of a natural disaster at disease free or endemic equilibrium. Specifically, a flood, see the Introduction for a review on natural disaster effects.

4.2 Model formulation

Our model takes the same form in each patch as with the previous chapters. However, we must now accommodate any number of patches and any form of coupling, or link structure, between those patches. Coupled patches are joined by two directed *edges* and if there is an edge from patch i to j there is an edge from patch j to i. We first consider the equations in their most general form, indexed for patch i.

$$
\begin{aligned}
\dot{S}_i &= \mu N_i - \mathcal{F}_i S_i - \mu S_i \\
\dot{I}_i &= \mathcal{F}_i S_i - (\gamma + \mathcal{H}_i + \mu) I_i \\
\dot{T}_i &= \mathcal{H}_i I_i - (\alpha\gamma + \mu) T_i \\
\dot{R}_i &= \alpha\gamma T_i + \gamma I_i - \mu R_i \\
\dot{B}_i &= \mathcal{G}_i - \theta B_i
\end{aligned}
\tag{4.1}
$$

Here we define some terms symbolising the force of infection in patch i, $\mathcal{F}_i$; the treatment rate in patch i, $\mathcal{H}_i$; and the rate of contribution to the bacterial reservoir in patch i, $\mathcal{G}_i$. These will be examined further after we have defined some new parameters to ease notation, table A.6, and clarified the exposure weightings for M patches.

In order to define the force of infection etc., we must define the exposure experienced by an individual of patch i when there are more than two patches in various arrangements. In the previous chapter, we introduced the concept of scaled edge weightings for infected individuals. These were a result of the infected individuals seeking treatment. As such, infected individuals are proportionally more exposed to the environment of a patch with a treatment facility. We retain this assumption and the scaled edge weightings in this chapter. However, the expression for the proportion of exposure experienced by an individual is complicated by the varying number of treatment facilities and altered patch arrangement. For example, in figure 4.1, four patches are connected in a *cycle*. The infected individuals in patch one and three will seek treatment in patches two and four respectively. As such, the edges from one or three to two or four are scaled. However, the edges between one *and* three or two *and* four are not scaled because each patch pair has the same number of treatment facilities. Additionally, there are no edges between patches one and four or two and three and we assume individuals may only travel through one patch. Thus, it is impossible for individuals of patches one or two to be exposed to the environment of patches four or three respectively; and vice versa.
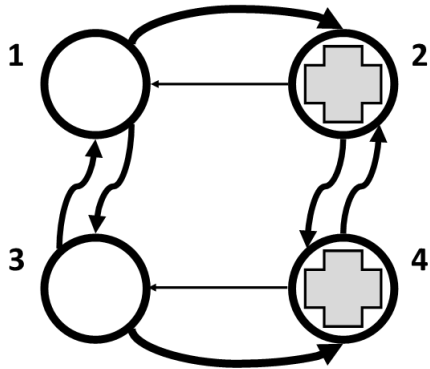

Figure 4.1: Cycle arrangement of four patches with two treatment facilities denoted by a cross. The arrows denote edges with the arrow width proportional to the scaling applied to that edge.

As the exposure experienced by any individual depends on the patch arrangement, we must track which patch is coupled to which and, for the infected individuals, where the treatment facilities are. We introduce the matrix P_{ij} to denote the distribution of exposure experienced by a resident of patch i away from home in patch j. This takes two values; zero when the patches i and j are not connected and $\frac{1}{C^i}$ when patches i and j are connected and patch i is connected to C^i patches in total. As such, the exposure of uninfected individuals is divided equally between all connected patches.

Thus, we may now define the force of infection in patch i,

$$\mathcal{F}_i = \beta_i \sigma \frac{B_i}{\kappa + B_i} + \sum_j \beta_j (1 - \sigma) P_{ij} \frac{B_j}{\kappa + B_j}. \tag{4.2}$$

The distribution of exposure experienced by an infected individual also depends on how many treatment facilities are accessible. We introduce c^i to track the proportion of patches connected to patch i containing treatment facilities. Using this parameter, we may state the proportion of edges that are scaled up, c^i, or down, $1 - c^i$, for patch i. We define X_{ij} as the edge weight scaling between patches i and j. We also define X_{ii} as a weighting for patch i, described in table A.6. Thus, we may define the new proportion of exposure experienced by an infected individual of patch i at home,

$$\sigma_{ii}^I = \frac{X_{ii}\sigma}{X_{ii}\sigma + (1-\sigma)(c^i\chi_2 + (1-c^i)\chi_1)}. \tag{4.3}$$

The proportion of exposure an infected individual of patch i experiences in patch j is given by,

$$\sigma_{ij}^I = \frac{X_{ij}(1-\sigma)P_{ij}}{X_{ii}\sigma + (1-\sigma)(c^i\chi_2 + (1-c^i)\chi_1)}. \tag{4.4}$$

The treatment rate experienced by an infected individual of patch i depends on the location of treatment facilities. This information is contained within the vector, ξ, where the ith element is zero if there is no treatment facility in patch i. We assume that the treatment rate is independent of the number of infected individuals. Therefore we define the rate of treatment experienced by infected individuals of patch i as

$$\mathcal{H}_i = \sigma_{ii}^I \xi_i + \sum_{j \neq i} \sigma_{ij}^I \xi_j. \tag{4.5}$$

Finally, we may define the shedding of bacteria to the environment of patch i as,

$$\mathcal{G}_i = \eta(\sigma_{ii}^I I_i + \sum_{j \neq i} \sigma_{ji}^I I_j + \sigma T_i + (1-\sigma)\sum_j P_{ji}T_j). \tag{4.6}$$

4.2.1 The model in MATLAB

We now have a high-dimensional model with many customization options. As such, we would not wish to write each new arrangement at each step. We define a function to use `MATLAB` to build the equations given a few specifications such as the number of patches, location of treatment facilities etc.. The steps are as follows:

1. We first define a contact matrix. This denotes which patches are connected to which and how many patches there are. For instance, in a five patch system where the patches are in a line or *path*, the contact matrix will take the following form,

$$A = \begin{pmatrix} 0 & 1 & 0 & 0 & 0 \\ 1 & 0 & 1 & 0 & 0 \\ 0 & 1 & 0 & 1 & 0 \\ 0 & 0 & 1 & 0 & 1 \\ 0 & 0 & 0 & 1 & 0 \end{pmatrix}.$$

   Therefore, patch one is connected to patch two only; patch two is connected to patches one and three and so on.

2. Use the contact matrix to define proportion matrix, P_{ij}. For each row i of the contact matrix, A, we count the number of ones to give C^i, the number of patches connected to patch i. Then we assume that the exposure is equally divided between all connected patches. Thus, our proportion matrix when five patches are connected in a path is,

$$P = \begin{pmatrix} 0 & 1 & 0 & 0 & 0 \\ 0.5 & 0 & 0.5 & 0 & 0 \\ 0 & 0.5 & 0 & 0.5 & 0 \\ 0 & 0 & 0.5 & 0 & 0.5 \\ 0 & 0 & 0 & 1 & 0 \end{pmatrix}.$$

3. We decide where the treatment facilities are by defining the vector ξ. For instance, if there is one treatment facility in patch one and the rate of treatment is 1 then, $\xi = [1, 0, 0, 0, 0]$.

4. Once we have the contact matrix and the treatment rate vector, we may calculate our edge scaling matrix, X_{ij}. Therefore, in our example,

$$
X = \begin{pmatrix}
\chi_2 & \chi_1 & 0 & 0 & 0 \\
\chi_2 & \chi_1 & \chi_1 & 0 & 0 \\
0 & \chi_1 & \chi_1 & \chi_1 & 0 \\
0 & 0 & \chi_1 & \chi_1 & \chi_1 \\
0 & 0 & 0 & \chi_1 & \chi_1
\end{pmatrix}.
$$

We do not scale the edges between two patches with the same number of treatment facilities. However, in order for the exposure weighting σ_{ij}^I to take the appropriate form when all or no patches have treatment facilities, we appear to scale edges between two patches without treatment facilities by χ_1 and edges between two patches with treatment facilities by χ_2. For instance, if there are no treatment facilities anywhere, σ_{ij}^I will take the following form,

$$
\begin{aligned}
\sigma_{ij}^I &= \frac{X_{ij}(1-\sigma)P_{ij}}{X_{ii}\sigma + (1-\sigma)(c^i\chi_2 + (1-c^i)\chi_1)}, \\
&= \frac{\chi_1(1-\sigma)P_{ij}}{\chi_1\sigma + (1-\sigma)(0\chi_2 + (1-0)\chi_1)}, \\
&= \frac{\chi_1(1-\sigma)P_{ij}}{\chi_1\sigma + (1-\sigma)\chi_1}, \\
&= (1-\sigma)P_{ij}.
\end{aligned}
$$

Similarly, when we consider the proportion of exposure an infected individual of patch i experiences at home if all patches are without treatment facilities, we have,

$$
\begin{aligned}
\sigma_{ii}^I &= \frac{X_{ii}\sigma}{X_{ii}\sigma + (1-\sigma)(c^i\chi_2 + (1-c^i)\chi_1)}, \\
&= \frac{\chi_1\sigma}{\chi_1\sigma + (1-\sigma)(0\chi_2 + (1-0)\chi_1)}, \\
&= \sigma.
\end{aligned}
$$

5. We may now construct the equations. We define a function with inputs X, P, ξ and our parameter values to build our equations.

We begin by initialising some key parameters C^i, c^i and the number of patches, M. Then we may define the proportion of exposure an infected individual experiences in each patch, σ_{ij}^I. We may now build the equations for each disease class.

Lastly, we define our equation vector as the function output.

6. Once we have a function for constructing the equations we may use the MATLAB command `matlabFunction` to create a file of the equations ready for simulation and other uses.

There are many benefits to this approach. The equations are only written once by hand which leaves less room for error. We also immediately have the equations in a form that can be used in MATLAB. This means we can make the most of other MATLAB commands such as `Jacobian`.

4.3 Analysis

We wish to examine the effect of increasing spatial segregation on disease dynamics. As such, we retain the same total population size, 5×10^7, and increase the number of patches or change the patch arrangement. In effect, we are changing the spatial boundaries for our population. Therefore we will also change the reservoir volume accordingly to preserve the volume of reservoir per person. This will be accounted for in the shed rate which will increase in each patch as the number of patches increases. This does not mean that individuals are contributing more bacteria but rather that the volume of the reservoir to which they contribute is getting smaller. This is in order to examine only the effect of spatial segregation on the disease dynamics. Our total population size is increased from previous chapters as we assume a larger settlement or city, this only scales the results.

We measure the difference that segregation and structure make to key system characteristics. These include R_0, the epidemic size and, a new measure, the impact. The impact quantifies the effect experienced by each system element when perturbed. This will indicate how the system is affected by a natural disaster.

4.3.1 Methods

We will explain the calculation of the system characteristics, R_0, the epidemic size and impact. However, we must first state the arrangements of patches to be examined.

4.3.1.1 Spatial arrangements of patches

We will compare three arrangements of patches. One will be a complete network where every patch is coupled with every other, see figure 4.2 (a). The second arrangement will be a cycle where all patches are coupled with two others, see figure 4.2 (b). Finally, our third arrangement will be a star. In this case, there is always a central patch coupled to all others but there is no coupling between peripheral patches, see figure 4.2 (c).
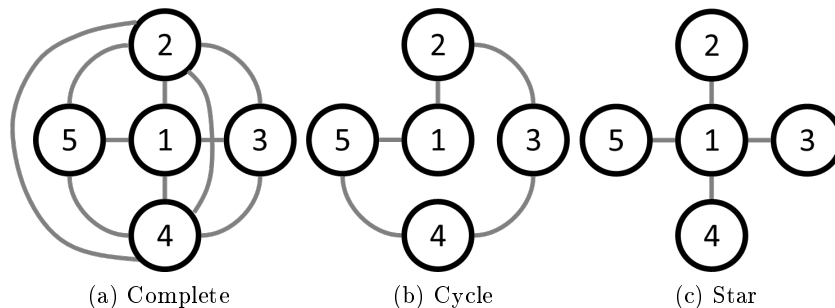

(a) Complete   (b) Cycle   (c) Star

Figure 4.2: Three spatial arrangements of five patches with patch numbering.

These three arrangements differ in the degree or number of connections of the patches within them. They also differ in whether the degree is equal between all patches. However, each arrangement is fairly simple to iteratively add patches to. The patch numbering indicates how this may be done for five patches. We assume that each

patch is homogeneous and only the structure and number of patches change. Finally, we construct contact matrices for the complete, cycle and star arrangements over five patches as the following,

$$A_1 = \begin{pmatrix} 0 & 1 & 1 & 1 & 1 \\ 1 & 0 & 1 & 1 & 1 \\ 1 & 1 & 0 & 1 & 1 \\ 1 & 1 & 1 & 0 & 1 \\ 1 & 1 & 1 & 1 & 0 \end{pmatrix}, A_2 = \begin{pmatrix} 0 & 1 & 0 & 0 & 1 \\ 1 & 0 & 1 & 0 & 0 \\ 0 & 1 & 0 & 1 & 0 \\ 0 & 0 & 1 & 0 & 1 \\ 1 & 0 & 0 & 0 & 1 \end{pmatrix}, A_3 = \begin{pmatrix} 0 & 1 & 1 & 1 & 1 \\ 1 & 0 & 0 & 0 & 0 \\ 1 & 0 & 0 & 0 & 0 \\ 1 & 0 & 0 & 0 & 0 \\ 1 & 0 & 0 & 0 & 0 \end{pmatrix}.$$

4.3.1.2 R_0 calculation

We calculate R_0 using the next generation method from previous chapters. However, we may now automate the process. We do this by exploiting a useful feature of the Jacobian matrices for epidemiological models of this form. Figure 4.3 shows the general structure of the Jacobian for the infectious classes. We can see that there is no element of the Jacobian that contains both a transmission and transition term.
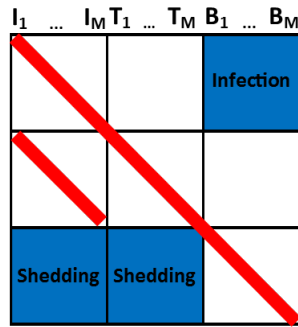

Figure 4.3: Form of Jacobian for infectious classes for an environmentally transmitted disease model with treatment. The red lines denote entries relating to transition terms such as death, treatment and recovery. The blue blocks denote transmission terms such as infection and shedding. The white space represents zeros.

As such, we may construct the transmission and transition matrices by selecting the relevant diagonals and blocks from the Jacobian. The pseudo code for this is as follows:

```
transition=-jacobian;
transition(2*M+1:end,1:2*M)=zeros(M,2*M);
transition(1:M,2*M+1:end)=zeros(M,M);

transmission=zeros(3*M)
transmission(2*M+1:end,1:2*M)=jacobian(2*M+1:end,1:2*M);
transmission(1:M,2*M+1:end)=jacobian(1:NP,2*M+1:end);
```

We may then calculate our next generation matrix of large domain as $\mathcal{T}\Sigma^{-1}$ where transmission is denoted by $\mathcal{T}$ and transition by Σ. Finally, R_0 is given by the largest eigenvalue of this matrix.

4.3.1.3 Epidemic size

We examine the transient system behaviour through the epidemic size. This will give us insight into the progress of the disease through the different patch structures. The calculation steps are as follows:

1. We start in a similar manner as the previous chapters, at disease free equilibrium with N/1000 infected individuals introduced. These introduced individuals are equally distributed across all patches.

2. We simulate the epidemic for one day and then for a further 100 days.

3. In the second time period we monitor the value of each infected class using the event function. If the number of infected individuals reaches the number initially introduced, we stop the simulation, see figure 4.4.

4. Once we have reached the end of the time period, or the end of the epidemic, we count the number of infections. This is done with an extra compartment in the model consisting only of the transmission terms for the infected class.
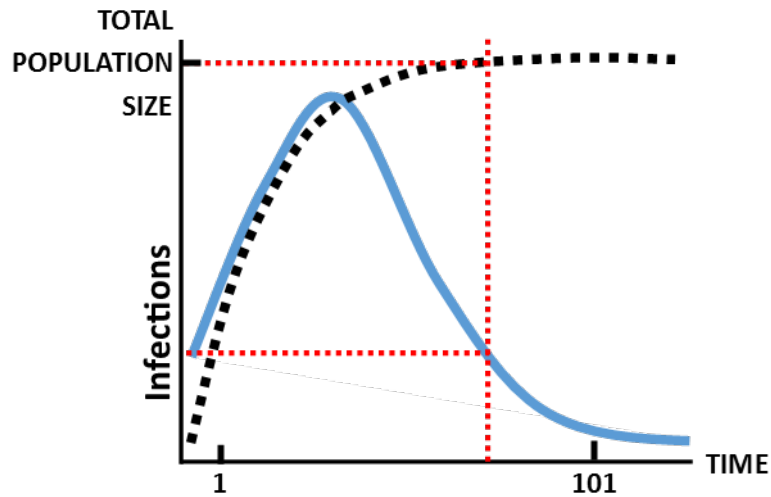

Figure 4.4: Calculation of epidemic size. In blue, the number of infected individuals; in black dashed, the cumulative number of infections and in red dashed, the point at which the number of infected individuals has returned to the initial conditions where we consider the epidemic concluded.

4.3.1.4 Impact

We discussed, in the last chapter, investigating the effect of a perturbation on the disease dynamics. We therefore examine the impact experienced by the infected classes in each patch. The impact assesses the effects of a perturbation on each system component at equilibrium. It is defined as the change in a state variable per unit change in the perturbation [98]. Therefore the impact can be seen as the 'sensitivity' of each state variable to the perturbation.

We detail a method adapted from [12] which is built on the methodologies of [98] using a simple example. This example will be of a directly transmitted disease in a homogeneous population with no recovery i.e. a simple SI model. This has the form of the following non-dimensional equations with S and I as state variables for the susceptible and infected classes. The parameters μ and β represent the death rate and contact rate respectively.

$$\dot{S} = \mu - \beta SI - \mu S$$
$$\dot{I} = \beta SI - \mu I$$

The algorithm to find the impact on each state variable, S and I, is as follows.

1. Find the system Jacobian, $\mathcal{J}$, at equilibrium.

   Our Jacobian is of the following form, $\mathcal{J} = \begin{pmatrix} -\beta I^* - \mu & -\beta S^* \\ \beta I^* & \beta S^* - \mu \end{pmatrix}$. We shall assume the system is at endemic equilibrium thus, $S^* = \frac{\mu}{\beta}$ and $I^* = 1 - \frac{\mu}{\beta}$. Therefore, $\mathcal{J} = \begin{pmatrix} -\beta & -\mu \\ \beta - \mu & 0 \end{pmatrix}$.

2. The perturbation vector, K, is then calculated. This denotes the change in each system state variable when the system is perturbed.

   In our example, we shall examine the effect of a perturbation to the contact rate, β. To calculate K, we must determine the effect of a change in β on each system element. This is done by finding the partial derivative of $\mathcal{J}$ with respect to β, $\frac{\partial \mathcal{J}}{\partial \beta}$. Then, the matrix of partial derivatives is multiplied by $\mathbf{1}$ to arrive at K, where the ith element of K is the cumulative effect of the perturbation on the ith system variable. Thus, as $\frac{\partial \mathcal{J}}{\partial \beta} = \begin{pmatrix} -1 & 0 \\ 1 & 0 \end{pmatrix}$, $K = \begin{pmatrix} -1 \\ 1 \end{pmatrix}$.

3. Find the inverse of the Jacobian, $\mathcal{J}^{-1}$.

   Our example has Jacobian inverse $\begin{pmatrix} 0 & \frac{1}{\beta - \mu} \\ -1/\mu & -\frac{\beta}{\mu(\beta - \mu)} \end{pmatrix}$.

4. Finally, the vector of impacts, where the ith element of the impact is the change in system variable i due to a unit change in the perturbation, is given by $-\mathcal{J}^{-1}K$.

   Therefore, our impact vector is $\begin{pmatrix} \frac{1}{\mu - \beta} \\ \frac{1}{\beta - \mu} \end{pmatrix}$.

In our simple example, the impact on the susceptible class is $\frac{1}{\mu - \beta}$ and the impact on the infected class is $\frac{1}{\beta - \mu}$. This suggests that a positive perturbation to the contact rate always causes a decrease in the number of susceptible and an increase in the number of infected individuals. This is as $I^* = 1 - \frac{\mu}{\beta}$ is only feasible when $\beta > \mu$.

In our model, the flood is calculated as a positive perturbation to two of the system parameters, the contact rate, β, and shed rate η. However, the calculation of K is similar to the simple example above. In our case, we must calculate two matrices of partial derivatives, $\frac{\partial \mathcal{J}}{\partial \beta}$ and $\frac{\partial \mathcal{J}}{\partial \eta}$ which are summed. The steps are then the same as above; the matrix of summed partial derivatives is multiplied by $\mathbf{1}$ to arrive at K, where the ith element of K is the cumulative effect on state variable i due to the flood. Therefore, we may examine the effects of a perturbation to every system variable at both disease free and endemic equilibrium.

4.4 Results

We investigate the difference in the values of R_0, the epidemic size and sum of infectious class impacts for different arrangements of patches. Our parameter values are taken

from a Latin Hypercube with 100 samples, except for the impact and epidemic size, for which we took 1000-5000 samples to ensure we had a sufficient number for each equilibrium. The parameter ranges can be found in tables A.1, A.3 and A.7.

4.4.1   The effect of patch arrangement and number on R_0

We commence with the difference in the range of R_0 for the three arrangements of five patches. In figure 4.5, we can see that R_0 is generally highest when the patches are in a star arrangement. When the patch arrangement is complete or a cycle, R_0 is practically the same. This is due to the number of individuals sharing the same reservoir. When the structure is complete, the proportion of population with access to a reservoir is proportional to the local shed rate. In contrast, all individuals in the star arrangement can access the central reservoir but not the peripheral ones. As such there is a 'hotspot' for bacterial build-up in the centre which is also the patch with most human traffic. The cycle arrangement leads to individuals having access to three patches at any one time. As such, the bacteria may build up but, as the three patches will over lap for an individual of patch i compared to an individual of patch $i+1$ the system is indistinguishable from that of the complete structure.
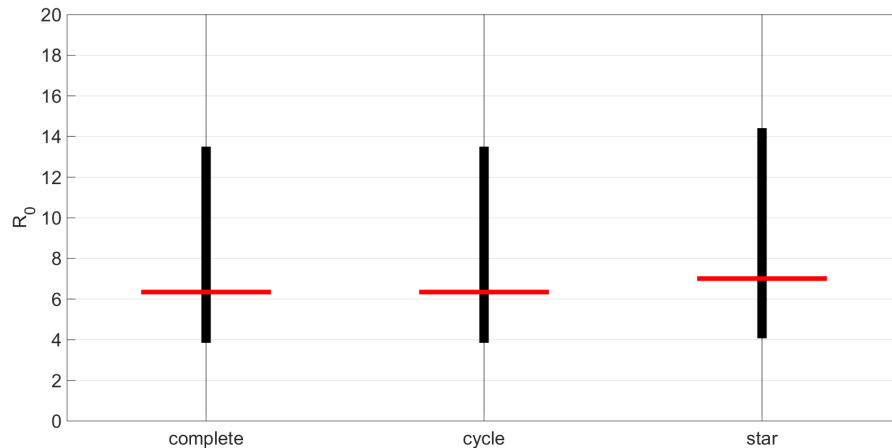

Figure 4.5: R_0 for different arrangements of five patches. There is no treatment and parameters vary over the ranges shown in tables A.6, A.7 and A.3. The horizontal bar denotes the mean value and vertical denotes values between the 25th and 75th quartile.

In figure 4.6 we examine the relationship between R_0 and the number of patches. Recall that as the number of patches is increased, the spatial segregation of the population and reservoir is also increased. As such, the shed rate increases and the relative population size of each patch falls. The net effect of these changes for the complete and cycle arrangements is almost zero; the value of R_0 fractionally increases as the number of patches rises. However, when the patches are arranged in a star, there is a variation. We see that as the number of patches increases, so does R_0. This is because of the central patch and its reservoir. The entire population always has access to the central patch reservoir. However, its volume reduces as the number of patches increases. As such, the shed rate increases as it is related to the reservoir volume. Thus, the number of infections rise in the patch with most human traffic.
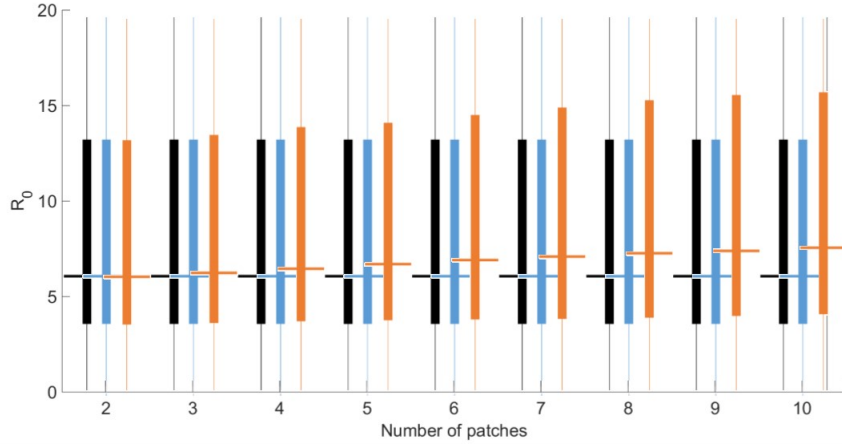
Figure 4.6: R_0 with respect to the number of patches. There is no treatment and parameters vary over the ranges shown in tables A.6, A.7 and A.3. The horizontal bar denotes the mean value and vertical denotes values between the 25th and 75th quartile. The colours denote patch arrangement with black, complete; blue, cycle and orange, star.

4.4.2 The effect of patch arrangement and number on epidemic size

We examine the behaviour away from disease free equilibrium through the epidemic size. We take parameter values from a larger Latin Hypercube Sample, 1000 values, than that used for the R_0 analysis. This is because we remove the results where the epidemic size is very small. Then, the system is simulated from disease free equilibrium as a small number of infected individuals are introduced.
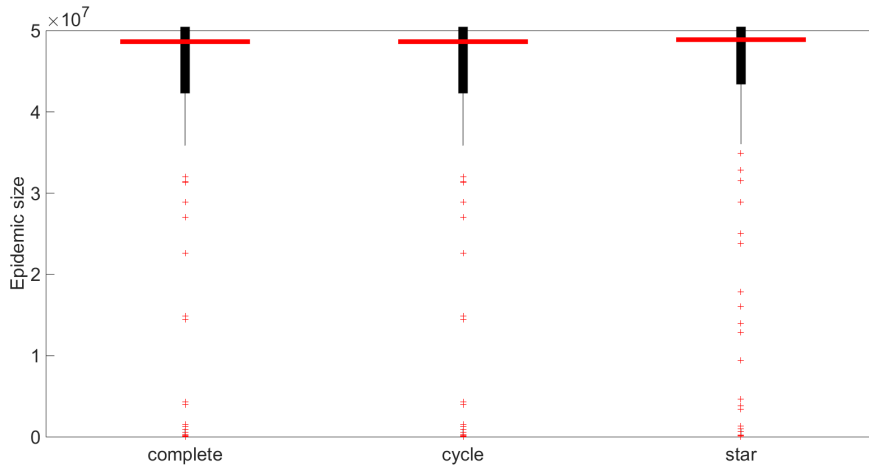

Figure 4.7: Epidemic size for different arrangements of five patches. There is no treatment and parameters vary over the ranges shown in tables A.6, A.7 and A.3. The horizontal bar denotes the mean value and vertical denotes values between the 25th and 75th quartile.

The epidemic size ranges from near zero to the total population size in figure 4.7. Generally, $R_0 > 1$ and could be up to 20 in our parameter space, leading to a large initial growth rate and ensuing epidemic. We see that the epidemic is larger when the patches are in a star arrangement. This is because the entire population may be exposed

100

to the environment of the centre patch, making it a hotspot for infection. In contrast, all patches in the complete or cycle network have the same proportion of individuals exposed to their environment. Therefore, there are no hotspots and the shed rate of each patch is proportional to the number of individuals that have access to it.
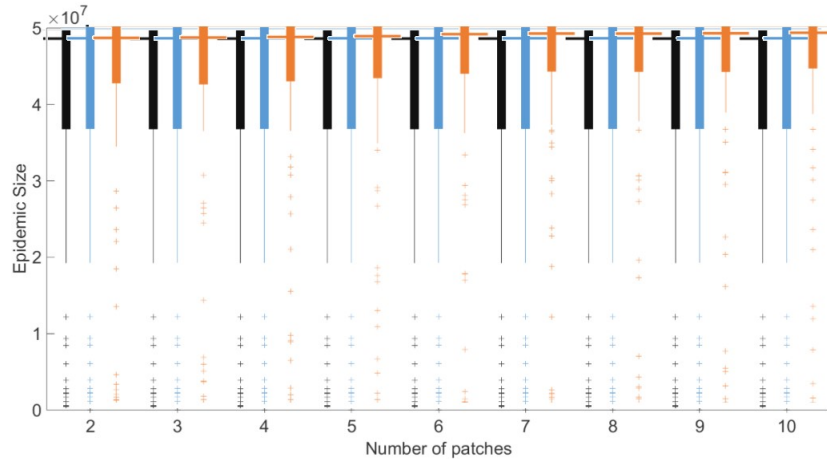

Figure 4.8: Epidemic size with respect to the number of patches. There is no treatment and parameters vary over the ranges shown in tables A.6, A.7 and A.3. The horizontal bar denotes the mean value and vertical denotes values between the 25th and 75th quartile. The colours denote patch arrangement with black, complete; blue, cycle and orange, star.

In figure 4.8, the epidemic size once again follows the trends seen for R_0 with little change when the patches are in a cycle or complete network. However, when the patches are in a star arrangement, the size of the epidemic increases as the number of patches increases. This is because epidemic size, when measured from the disease free equilibrium, is correlated with R_0.

We now examine the impact at endemic and disease free equilibrium.

### 4.4.3 The effect of patch arrangement and number on impact

In the impact analysis we examine the system at disease free and endemic equilibrium. Therefore, we investigate the sensitivity of the infected classes to a perturbation when the disease is endemic or the system is disease free. This will give us insight into which arrangements are most vulnerable to a perturbation and when. We shall also see whether a segregated population is more or less resilient to a perturbation. To conduct the following analyses, we increased the number of parameter samples to 5000 to ensure there are a sufficient number of samples rendering the disease free equilibrium stable.

We see in figure 4.9 that the sum of the infected class impacts varies between equilibria, but the impact is always positive. Therefore as the contact and shed rates are perturbed, the infected classes increase in size. This is most notable at disease free equilibrium when the five patches are in a star arrangement. This is because the perturbation can be amplified most effectively when there is a central hub. That is, the perturbation in shed and contact rates facilitates an increase in the number of infected individuals which is aided by a central bacterial reservoir. The entire population may come into contact with the environment of the centre patch which acts as a conduit for disease transmission, this is particularly the case when the main transmission parameters are perturbed.
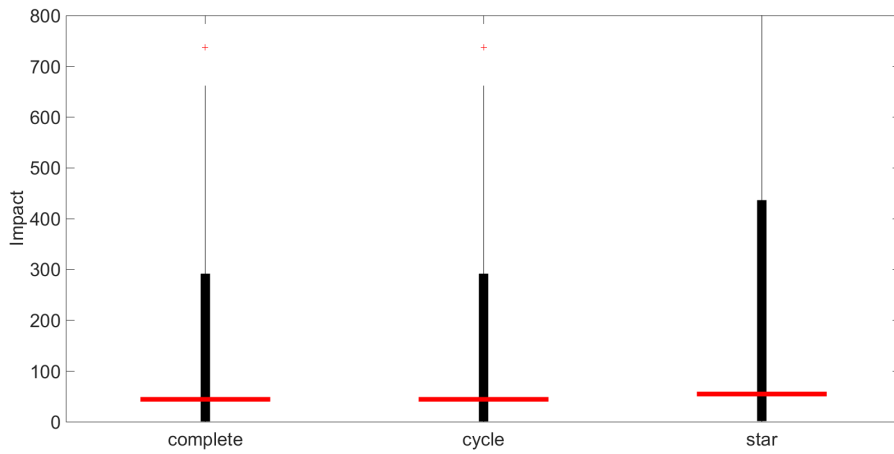
(a) DFE
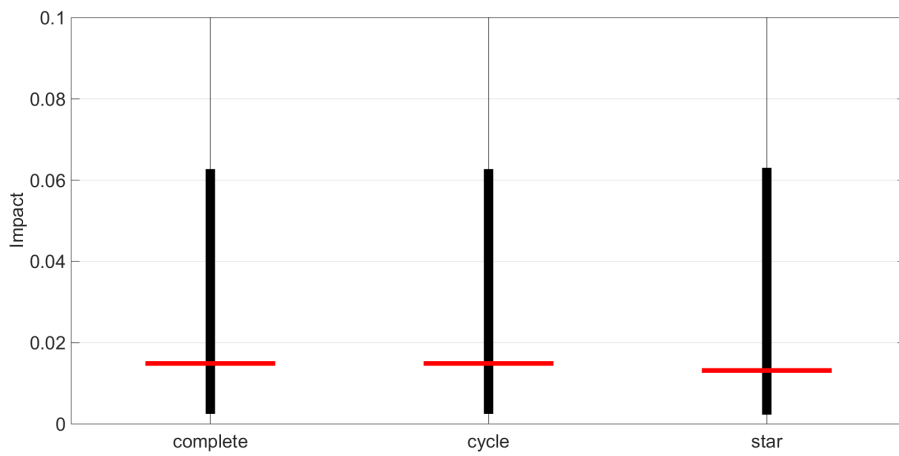
(b) EE

Figure 4.9: Impact at disease free equilibrium (a) and endemic equilibrium (b) for different arrangements of five patches. There is no treatment and parameters vary over the ranges shown in tables A.6, A.7 and A.3. The horizontal bar denotes the mean value and vertical denotes values between the 25th and 75th quartile.

When the endemic equilibrium is stable, the impact has smaller magnitude. This is because the capacity of the system, related to the size of the susceptible class, is reduced. Therefore, it is not possible to have a large increase in the number of infected individuals as there are fewer susceptible individuals to be infected. Between the three arrangements, we see that the magnitude of the impact in the star arrangement is the smallest on average. This is because the endemic proportion of the population which is susceptible is smallest in this arrangement and therefore it has the smallest capacity to react to a perturbation, see figure 4.10.
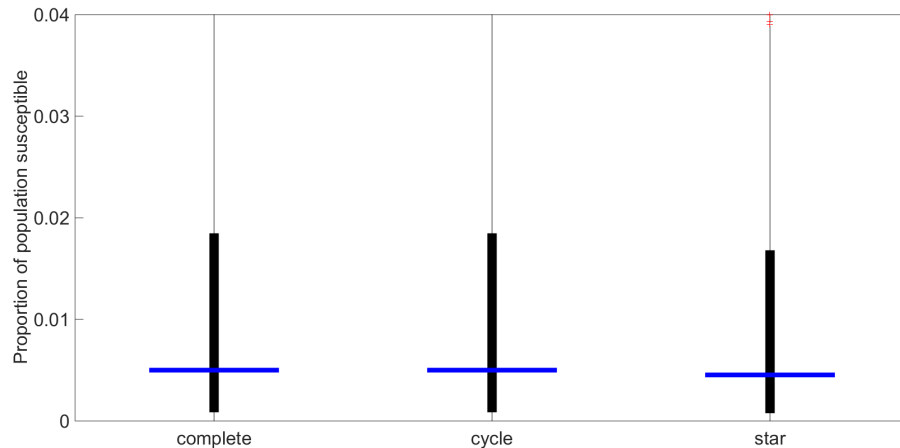

Figure 4.10: Proportion of population over five patches that is susceptible at endemic equilibrium. There is no treatment and parameters vary over the ranges shown in tables A.6, A.7 and A.1. The horizontal bar denotes the mean value and vertical denotes values between the 25th and 75th quartile.

We now examine the impact as the number of patches increases, see figures 4.11 and 4.12. There are different trends seen at each equilibrium. When the disease free equilibrium is stable the impact increases as the number of patches rises. This is seen for all arrangements because the shed rate into each patch reservoir increases. Therefore, whilst the number of individuals living in each patch falls, the production of bacteria can be amplified to a greater extent. The amplification is a result of the proportional perturbation of the shed rate; a larger initial shed rate leads to a larger *actual* difference when perturbed. This is particularly the case when the patches are in a star arrangement because of the central reservoir.

When the endemic equilibrium is stable the impact decreases as the number of patches increases. This is because the proportion of the population that is susceptible falls as the number of patches increases. As such, there is less capacity for the infected population to respond to a perturbation because the resource of infection, the susceptible individuals, is depleted. This is shown in figure 4.13, as the number of patches increases there is a small rise in R_0 leading to a smaller proportion of the population left susceptible at endemic equilibrium.
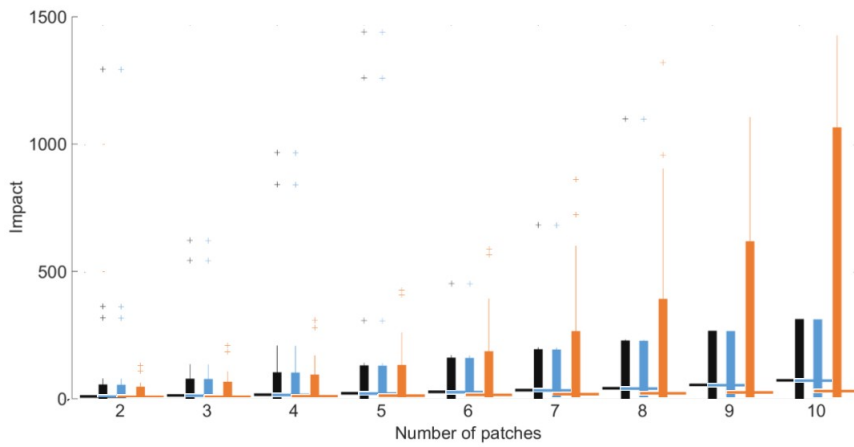
Figure 4.11: Impact at disease free equilibrium with respect to the number of patches. There is no treatment and parameters vary over the ranges shown in tables A.6, A.7 and A.3. The horizontal bar denotes the mean value and vertical denotes values between the 25th and 75th quartile. The colours denote patch arrangement with black, complete; blue, cycle and orange, star.
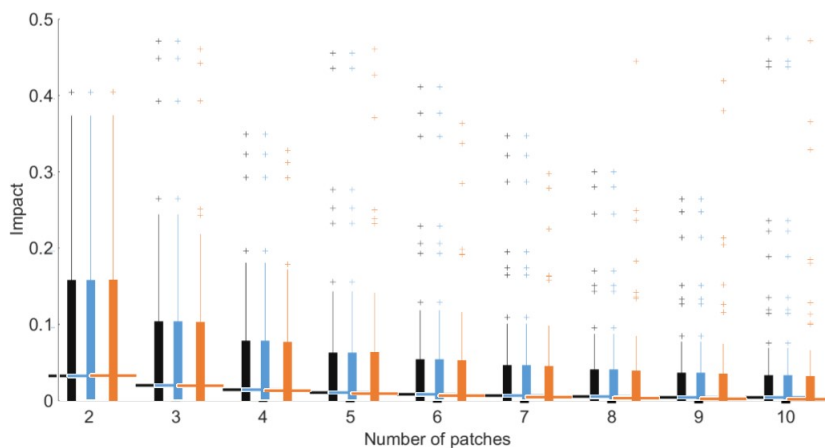

Figure 4.12: Impact at endemic equilibrium, right, with respect to the number of patches. There is no treatment and parameters vary over the ranges shown in tables A.6, A.7 and A.3. The horizontal bar denotes the mean value and vertical denotes values between the 25th and 75th quartile.The colours denote patch arrangement with black, complete; blue, cycle and orange, star.
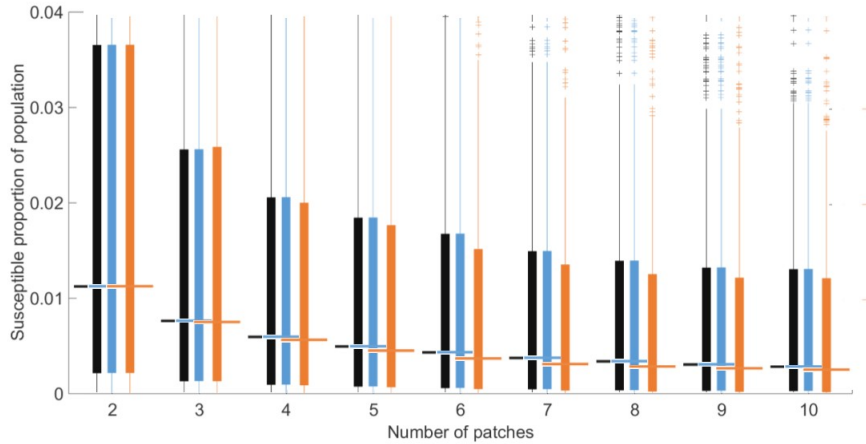
104

Figure 4.13: Size of susceptible population at endemic equilibrium with respect to the number of patches. There is no treatment and parameters vary over the ranges shown in tables A.6, A.7 and A.3. The horizontal bar denotes the mean value and vertical denotes values between the 25th and 75th quartile. The colours denote patch arrangement with black, complete; blue, cycle and orange, star.

4.5 Conclusion

4.5.1 Summary

We wished to understand how increasing the segregation and arrangement of our population affected the disease dynamics. We examined how the effect of a natural disaster was altered by these aspects. The first thing to establish was how our model worked over M patches in different arrangements. To do this, we introduced some additional parameters to ease notation and defined the exposure weightings in the new, higher-dimensional case. We then detailed a method of equation generation in `MATLAB` that simplified the process and left less room for error. Finally, we defined our methods for calculating R_0, the epidemic size and the impact of a perturbation or natural disaster for different numbers of patches and arrangements.

4.5.2 Findings

There was minimal correlation between each of R_0 and the epidemic size with the number of patches when the patches are in the complete or cycle arrangement. This is because the proportion of the population with access to a patch reservoir is always proportional to the shed rate. In the complete arrangement, N/M individuals have access to a patch reservoir at any point. The local shed rate in this case is $M\times$ the shed rate in an unsegregated population. As such, when a new patch is added, the population 'attention' is further divided but the local shed rate is increased proportionally in every patch. This is also the case in the cycle arrangement. When a new patch is added, the number of individuals with access to a particular reservoir reduces but the shed rate to that reservoir increases as its volume decreases. In contrast, when the patches are arranged in a star, there is a correlation between R_0 and epidemic size and the number of patches. We noted that as the number of patches rises, the R_0 and epidemic size also increased for the star arrangement. This is because of the degree of the central patch. The entire population may be exposed to the environment of the central

105

patch; therefore, as the reservoir there reduces in size, increasing the shed rate, the concentration of the bacteria in the patch with the most human exposure increases. This causes more infections, increasing R_0 and the epidemic size.

Finally we considered the effect of a natural disaster through the impact. This was a new analysis method which identified the infected classes that would be most affected in the event of a perturbation. The results depended strongly on which equilibrium is stable. The capacity of the infected class to react to a perturbation is partly dictated by the size of the susceptible class. As such, the magnitude of the impact at disease free equilibrium is far larger than that at endemic equilibrium. We see that, at disease free equilibrium, the largest impact is experienced by the infected classes when the patches are in a star arrangement. The magnitude also increases as the number of patches increases. This is because the increasing shed rate may amplify the contribution of bacteria, causing more infections. For example, the proportional change in shed rate may be 1%; however, if the unperturbed shed rate is twice as large, the actual change is also twice as large. As such, when we scale the shed rate as the number of patches increases, we alter the actual size of the perturbation. However, we may consider the size of a perturbation caused by a flood to be proportional to the conditions of the unperturbed system.

When the endemic equilibrium is stable, the impact is proportional to the susceptible proportion of the population. This is lowest when the patches are in a star arrangement, therefore the capacity to react is lowest when the patches are arranged in a star. The capacity also falls as the number of patches increases leading to a more resilient system as it is segregated. Therefore, the capacity and ability for the system to react to a perturbation are intrinsically linked.

Therefore, we see that the arrangement of patches can strongly affect the disease dynamics. This is particularly the case when the patch degree is heterogeneous, i.e. there are patches with more connections than others. In our examination we considered three arrangements, one of which had a central patch with far more connections than the other patches. This central patch was a conduit for disease transmission allowing individuals to shed into, and be exposed to, a central bacterial reservoir. This not only led to increased infections but also amplified the effect of a perturbation when the system was disease free. We also learnt that the division of the reservoirs, and the ensuing effect on the shed rate, was instrumental in amplifying the effect of a natural disaster. We see a larger effect of a perturbation when a reservoir has a smaller volume and the system is initially disease free. Therefore the spatial segregation of the bacterial reservoir is as important as the segregation of the human population. However, the state of the system at the point of perturbation is also extremely important as the size of the susceptible population can influence the effect of a natural disaster.

4.5.3 Future considerations

We found some interesting effects of the spatial segregation of a population. However, we have not examined which arrangement of patches most resembles the structure of a city. To approximate the dynamics of an environmentally transmitted disease within a population we must consider the average or most likely arrangement of sub-populations We may also consider those sub-populations to be heterogeneous as well as the overall structure. Our parameters in this chapter cover a large sample space. This led to range of R_0 values some of which were very large and could be considered extreme. In the above work, we simply compare the output values over the whole space. However, when we examine a arrangement that resembles the structure of a city we should consider a narrowed parameter space or more reasonable set. This will allow us to start examining

optimal control strategies and facility placements.

Chapter 5

Optimal resource deployment in the wake of a natural disaster

5.1   The Problem

So far we have developed a environmentally transmitted disease model in a spatially structured population. We have examined the effect of treatment both when it is dependant and independent of demand and seen that the behavioural change of infected individuals can have varying effects on the efficacy of that treatment. In the preceding chapter we extended our model to higher numbers of patches and investigated the effect of different patch arrangements on key model aspects such as the basic reproduction number, epidemic size and impact. We will now build on the insights gained previously in order to approximate the disease dynamics in a developing world city and to find an optimal control strategy.

We consider how best to use limited resources to control an environmentally transmitted disease outbreak in a heterogeneous developing world city. The control measures to be examined are no longer limited to treatment of humans, but will also include treatment of the environmental reservoir. The outbreak will be instigated by a natural disaster such as a flood and we ask where, in a spatially structured population, is it best to locate control facilities. We assess the placements through the benefits to the community, namely the reduction in epidemic size and duration.

Our work begins with an examination of city structure. From there, we define the flood in model terms and detail the method of simulation. Finally, the optimal arrangements of control facilities in the presence of one or two control facility types are discussed.

5.2   The structure of a developing world city in model terms

To determine the optimum control facility placement, we must assess the population structure before the disease dynamics can be examined. We first discuss the pertinence of a developing world city. Then we define the characteristics of such a city.

Conditions related to poverty, such as poor sanitation, are considered a 'pre-requisite' for cholera spread. Also, diarrhoeal disease epidemics following natural disasters are more common in the developing world than the developed [22, 71, 123, 132, 136]. The developing world cities of interest are those that have, or could potentially have epidemic or endemic cholera. These are mainly African and Asian cities as they have had cholera epidemics most recently [140]. However, the Latin American city structure will also be considered as it is generally taken as a model for all developing world cities.

Furthermore, there is a possibility that the cholera outbreak in Haiti could lead to new epidemics in South America.

City structures vary depending on the level of social development and location. The pre-industrial city was hypothesised by Sjoberg to have concentric rings dictated by social status (1960 mentioned in [110]). The elite classes are found at the centre and there is a social gradient toward the edge. The population density follows a similar gradient, from low density, high-cost housing in the centre to high-density, low-cost housing on the periphery.

It was hypothesised by the UN in 1973 that cities in Africa follow the pattern of the pre-industrial city with a few variations (mentioned in [110]). The model they developed is shown in figure 5.1 and is usually representative of cities with one to two million residents. There is an indigenous core which is high density and external, low-density areas where the elite classes reside. There are transitional areas with medium density residences and areas of shanty towns. However, the shanty towns are a result of large influxes of individuals hoping to find work in the industrial areas.
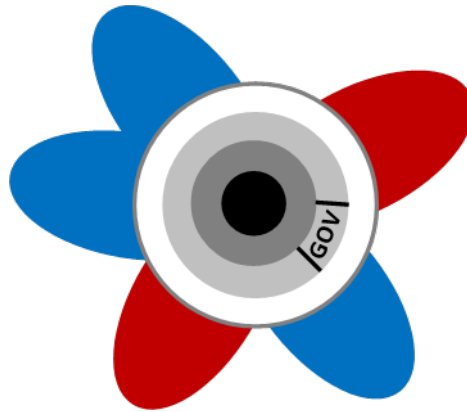

Figure 5.1: Diagram of African city (UN 1973 mentioned in [110] page 120 onwards). Black: core commercial or residential; dark grey: indigenous or high-density residential; light grey: elite or low density residential; white: medium density residential; blue: high density shanty towns and villages; red: industrial.

This structure still has the concentric rings found in the pre-industrial model but with a different gradient, additional shanty towns and areas of industry. It should also be noted that the population density is high in the centre and periphery with a band of low density in between. However the centre, whilst having a high amount of human traffic, has few residents as it is a commercial area.

In the case of the Asian cities, there is usually an original port as the source of the city. Generally, there is a port extension and the whole city has a colonial influence which affects the structure. A model put forward by Brunn and Williams is shown in figure 5.2 [110]. The structure is partly determined by spatial heterogeneity, in particular the presence of the sea. In contrast, the pre-industrial and African cities, shown in figure 5.1, were assumed to lie in a flat, featureless plain. There is an emphasis on the purpose, rather than the population density, of each area. However, we re-interpret the models in terms of population density to allow comparison with the African city model.

The port and port extension are areas of commercial activity and have a high amount of traffic but few residents. This is similar to the core commercial area in the African city. The native town is a high density residential area with limited services such as sanitation and water supply. European and mixed residential sectors are intermediate
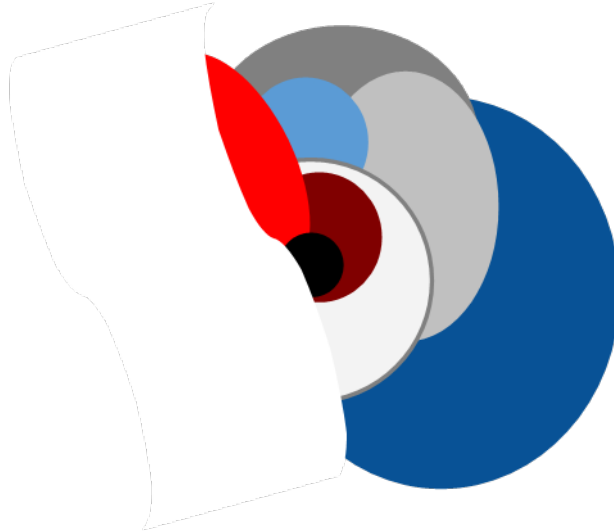
Figure 5.2: Diagram of Asian city (Brunn and Williams 1983 mentioned in [110] page 120 onwards). Black: original port; red: port extension; dark grey: native town; light grey: European town; white: open space; dark red: fort; light blue: mixed residence; dark blue: new wealthy residences.

density areas with an intermediate level of services. The wealthy residential area is equivalent to the elite residential area in the African city model. It has a low density and is well-serviced. The port and green space have few or no residents.

We mentioned earlier that the Asian city model lies in a heterogeneous landscape. However, the areas of low-density and high-density, with their attached levels of services, are represented in the other city structure models. The link between population density and services will therefore be incorporated in the final model choice in Section 5.2.1.

The Latin American city structure is most commonly used to represent the 'typical' developing world city, shown in figure 5.3. The model was developed by Griffin and Ford (1980, mentioned by [110] page 120 onwards) and has many similarities with the previous three structures, figures 5.2 and 5.1 and the pre-industrial city. There is a central core (central business district (CBD)), which is desirable and well-serviced. This has the same high level of traffic as in the structures mentioned previously in the previous structures. Around the centre there is a middle income sector surrounded by a transition area which leads to lower class, higher-density housing at the edge of the city with few or no services. These high-density areas are shanty towns or squatter settlements linked to rapid expansion of the city, similar to that seen in the African city model. Disrupting the concentric ring structure is a road or spine from the CBD to the edge. This is flanked by elite housing placed close to the transport links and improved services that the road development brings.

The models shown all have a central hub from which the other sections are grown. This is referred to as mono-centric. Not all cities have this form. As the city grows, new areas of importance develop, such as a university district or retail park, and most settlements progress toward being poly-centric.

The concept of mono centricity was examined by Alain Bertaud. Adapted diagrams of a mono-centric and poly-centric city are shown in figure 5.4 [14]. These illustrate the differences produced in the human movement throughout a city due to its mono or poly-centricity.

We now formulate the model for a city in terms of epidemiological characteristics. This model is based on the population density structures described above and the idea

Figure 5.3: Diagram of Latin American city (Griffin and Ford 1980 mentioned in [110] page 120 onwards). Black: CBD and spine; light grey: elite residential; dark grey: middle income area with medium density residential; blue: transition area from medium to high density residential; red: squatter settlements of high density housing and very few services.
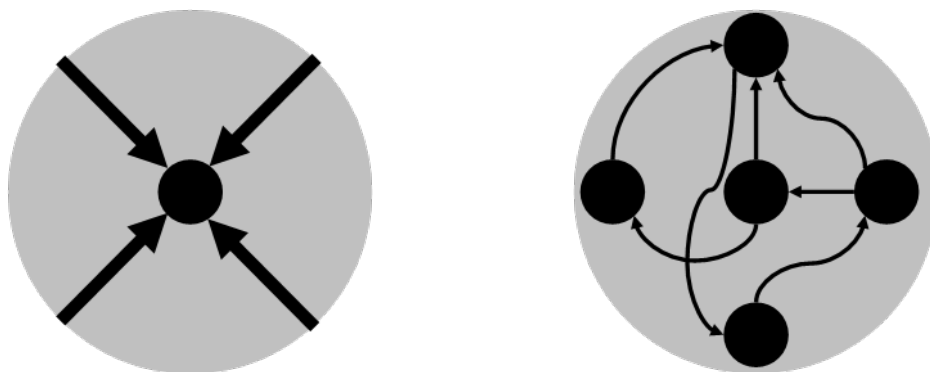

Figure 5.4: Diagrams of mono-centric (left) and poly-centric (right) cities adapted from the work of Alain Bertaud [14]. Black: attractive centres such as the CBD; grey: general residential areas; arrows: possible population movements.

of mono and poly-centric settlements explained by Bertaud.

5.2.1 Model population structure

We will focus on the epidemiological dynamics in the population of a mono-centric city. In abstract terms, this means there is a central patch with other, peripheral, patches connected by human movement (shown in figure 5.5). The central patch is attractive to the surrounding patches. Therefore, we may consider additional weighting terms for the human movement from the peripheral patches towards the centre patch. The peripheral patches have varying degrees of services provided, with population density and services correlated in all patches.

This structure is linked to the structures seen in figure 5.1 and 5.3. Both are mono-centric structures which capture the behaviour in a developing city. The evolution to poly-centric comes as a result of redevelopment of areas of the city rather than virgin city growth. Therefore a mono-centric structure is representative of the cities we wish to model. The areas of our mono-centric city have the characteristics of sectors of the African and Latin-American city models. There will be patches with high population density and limited services such as sanitation and more elite areas that are well serviced and sparsely populated. The centre will be reasonably well-serviced in line with the CBD of the Latin American city model. It will also see a high amount of traffic but not sustain a high number of residents.

There are of course shortcomings of this mono-centric structure. It can be argued that every settlement has multiple areas of interest and so would be more accurately portrayed by a poly-centric structure. The lack of interaction between the peripheral patches in the following model, shown in figure 5.5, is also an exaggeration of the human movements likely to occur in real life.
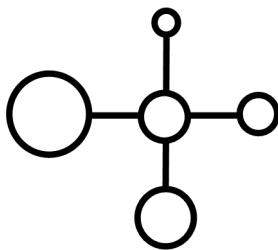

Figure 5.5: Diagram of a developing world city structured into patches. The outer patches are the periphery. These represent the residential areas away from the CBD that vary in population density. There is one central patch which represents the CBD or commercial hub of the city. There are five patches in total. The links between patches indicate human movement routes.

We examine the disease dynamics through the population structure shown in figure 5.5. The figure shows all patches have differing characteristics. In sections 5.2.2 and 5.2.3 heterogeneities such as variation in population density and the rate of contact with the environmental reservoir will be investigated.

5.2.2 Heterogeneous population densities

We wish to examine how variation in population density within the city structure affects the disease dynamics. The aim is to approximate the distributions of population density seen in the city structure models in figure 5.1 and 5.3. These distributions included sectors of high and low population density with large areas of transitional or

medium density. We seek a distribution in our model that retains the high level of mean population densities but includes some extreme values. However we also wish to keep the heterogeneity as general as possible so that any trends found as a result of the variation in population densities are applicable for other, similar distributions. For example, suppose it is found that high density patches are important when the patch densities are linearly decreasing. Then this is likely to be the case when there is one high-density patch and a number of equally low density patches as the relative densities determine priority. Therefore we need a set of densities where the values are clustered around a mean value but there are also patches with higher and lower densities to drive interesting behaviour at the extrema. Thus a set of population densities that are normally distributed seems appropriate.

The algorithm to calculate the individual patch densities in `MATLAB` is as follows. This will be accompanied by a simple example for four patches. Our algorithm aims to create a list of population densities that are all equally likely and whose values are normally distributed. The central patch is always patch one.

1. Define the number of patches (M) and total population size, N.

   We commence with, $M = 4$ and $N = 5 \times 10^7$. However, the population size is directly linked to the reservoir volume, if we scaled the population size and reservoir volume accordingly there would be little or no difference in the model behaviour and results.

2. Calculate the mean population density as the total size divided by the number of patches.

   For our example, the mean is $\bar{N} = 5 \times 10^7/4 = 1.25 \times 10^7$.

3. Choose the standard deviation of the population densities, *sd*. This will dictate how much the densities vary over the peripheral patches. It will also define the proportion of the normal distribution that will be lost with truncation.

   The distribution is truncated at zero and $2\bar{N}$. Thus, the variance gives the proportion of values in the distribution that lie between zero and $2\bar{N}$. For instance, as 99.8% of values lie within three standard deviations of the mean we may choose a standard deviation equal to $\bar{N}/3$. The truncation, as it is symmetric, does not affect the mean [78].

   The value for sd we shall use is 4.1667×10^6 which is approximately $\bar{N}/3$.

4. The number of peripheral patches is always $M - 1$ therefore divide the truncated distribution into $M - 1$ equally likely intervals.

   The interval endpoints are calculated using `MATLAB`'s `normcdf` function, $F(:,:)$, which gives the probability of sampling a point less than or equal to the value of interest i.e. $F(x|\mu, sd) = \frac{1}{sd\sqrt{2\pi}} \int_{-\infty}^{x} \exp(\frac{-(t-\mu)^2}{2sd^2})dt$ where μ is the mean, *sd* the standard deviation and x, the value of interest. Here, the probabilities will lie between $F(0|\bar{N}, sd)$ and $F(2\bar{N}|\bar{N}, sd)$ as the distribution is truncated.

   Our example intervals will each have cumulative probabilities given by:

   $(normcdf(2 \times \bar{N}, \bar{N}, sd) - normcdf(0, \bar{N}, sd))/(M - 1) = (0.9986 - 0.0014)/3 = 0.3324.$

   Therefore our interval bounds are the following,

   `normcdf`$(0, \bar{N}, sd), interval\ probabilities \times [1 : (M - 1)],$`normcdf`$(2 \times \bar{N}, \bar{N}, sd)]$

   $= [0.0014, 0.3338, 0.6662, 0.9986].$

5. Next, average over the probability intervals to find an appropriate mean point on the population density distribution. It is necessary to average the probabilities rather than the densities themselves to preserve the normally distributed values over each interval.

   In our simple case, the midpoints of the probability intervals are as follows:

   $midpoints = [0.1676, 0.5, 0.8324].$

6. Finally, use the midpoints of the probability intervals to find the equally likely points in the normal distribution. These points will become the population densities in the periphery. We invert the probabilities using MATLAB's `norminv` which finds the corresponding value of the normal cumulative density function for each probability, see figure 5.6.

   Thus, $N(i) =$`norminv`$(midpoints(i), \bar{N}, sd)$ and $N = [8.4846e6, 1.25e7, 1.6515e7]$ on the periphery. The centre is kept at the mean population density, $\bar{N}$.
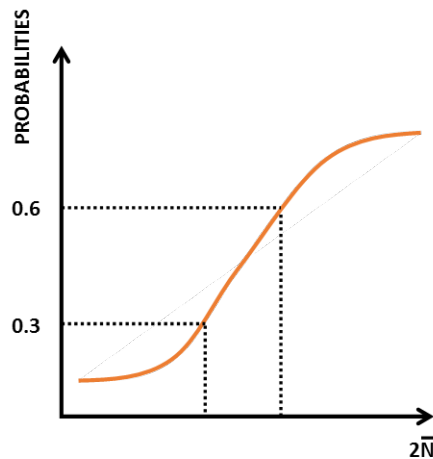

Figure 5.6: Diagram of normal cumulative density function. MATLAB's norminv takes a probability value and finds the corresponding population density.

The above algorithm generalises to any number of peripheral patches. It also produces a distribution of population densities for four peripheral patches as shown in figure 5.7. Population density and size are interchangeable here as the spatial area and reservoir volume are kept fixed between patches to allow the effect of different population sizes to be studied independently of reservoir volume.

The change in standard deviation shown in figure 5.7 moves the distribution from an uniform distribution to an increasing set of values. Unless otherwise stated, we will keep the standard deviation as one third of the mean population density, shown in blue in figure 5.7. This will truncate the normal distribution to 99.8 % of its original size. This choice of *sd* will also preserve the shape of the distribution, as shown for a higher number of patches in figure 5.8. However, the truncation may omit the most extreme density values for a small number of patches.

In addition to population density, we also consider heterogeneity in the rate of contact with the contaminated environment.
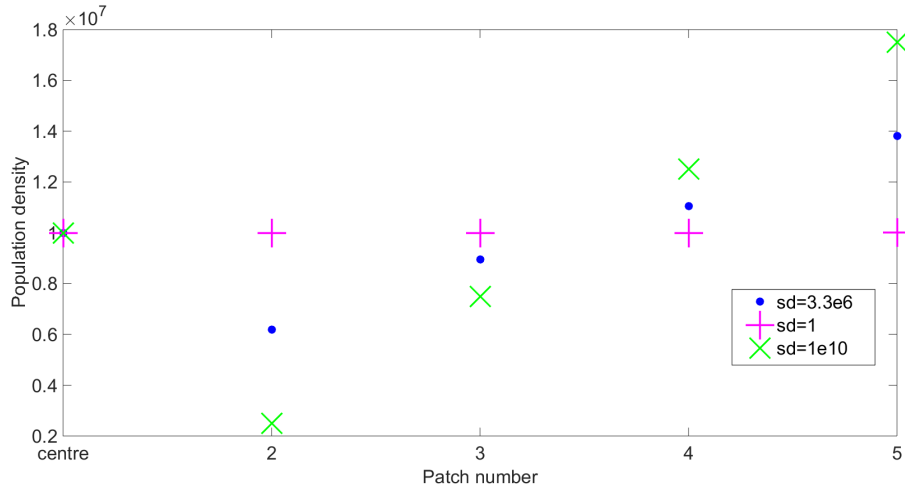
Figure 5.7: Population densities in the centre and four peripheral patches for different standard deviation values. The total population size here is 5×10^7.
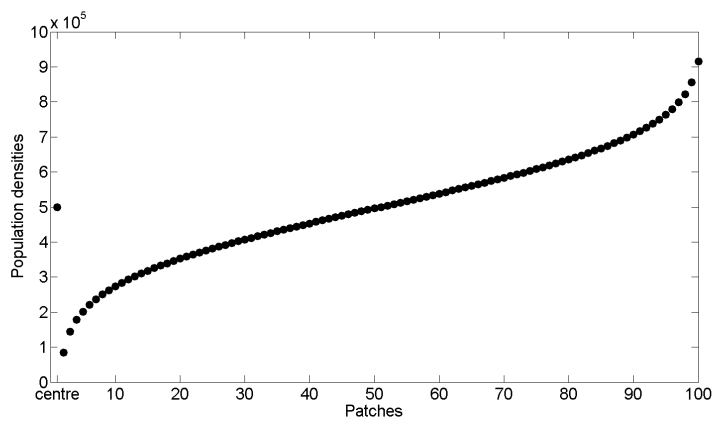

Figure 5.8: Population densities in the centre and 99 peripheral patches. The total population size here is 5e7 and *sd* is one third of the mean population density.

5.2.3 Heterogeneous contact with the contaminated reservoir

There may be considerable variation in access to clean water throughout a developing world city. We can model this through the contact rate parameter β_i. The contact rate is defined as the number of contacts with the contaminated environmental reservoir per day. Therefore, if there is clean water freely available, the contact rate will be almost zero.

In terms of the disease spread, the higher the contact rate with the contaminated reservoir, the higher the chance of infection. The question will be the same as before, when the structure and contact rates are heterogeneous, which is the optimum patch to place control measures such as a treatment facility?

As before, we assume that the contact rate is normally distributed around the periphery and keep the contact rate in the central patch at the mean value for the system. The total population size was fixed in the previously considered. We fix the 'total' contact rate in a similar way i.e. to be $M\times$ (average contact rate).

When both heterogeneities are present, they are proportional. The population structure models for developing world cities suggest that areas with high-density housing are generally less well serviced. The low-density areas are high cost and most recently updated and therefore have access to the best services such as clean water and sanitation. This correlation is seen in all the models of developing world city structure. Thus, the heterogeneities for contact rate and population density are proportional without intervention measures.

5.2.4 Control methods

In previous chapters we examined the treatment of infected individuals alone. Now, we introduce a control measure with the environmental bacteria in mind. This control will aim to account for water decontamination in the city and each facility will affect the environmental reservoir in the patch where it is located. The control will increase the rate at which bacteria degrade in the environment and will be included as an extra term in the equations shown in sections 5.6 and 5.7. This term is $\zeta_i B_i$ where ζ_i is the rate at which the bacteria degrade due to water decontamination in patch i. We also assume that the degradation due to decontamination is greater than that occurring naturally.

Therefore we examine two controls in a heterogeneous population. The manner in which we combine heterogeneities is now discussed.

5.2.5 Summary of city structure and heterogeneities

A developing world city can be approximated in structure by concentric rings of different housing patches with additional peripheral heterogeneities. This can be represented by a star of patches with a central patch that is linked to every other patch. The centre is a well-serviced, mean density patch surrounded by peripheral patches with varying densities. These peripheral patches have services which are proportional to their density as some patches are in poverty and others are wealthier. The service is clean water provision, which reduces people's contact with the contaminated environment.

5.3 Epidemiological dynamics

We consider the epidemiology of an environmentally transmitted disease following a flood. In this section, we explain the disease dynamics and parameters. The derivation of the proportions of exposure to the environment of each patch can be found in previous chapters as well as the model equations for a fully connected M patch system.

Recall that there is a weighting attached to the outward and return edges between two patches. These are scaled when considering the infected individuals where edges towards a treatment facility are scaled **up** and edges away from treatment facilities are scaled **down**. We use these weightings to define the proportions of exposure experienced by uninfected or infected individuals residing in the centre or peripheral patches.

For uninfected individuals, the proportions of exposure are the following:

$$\sigma_{ii} = \sigma = \frac{\tau}{\phi + \tau}, \qquad\qquad \sigma_{ic} = 1 - \sigma = \frac{\phi}{\phi + \tau},$$

$$\sigma_{cc} = \sigma \quad , \qquad\qquad \sigma_{ci} = \frac{1 - \sigma}{M - 1}.$$

The proportions of exposure for infected individuals have the additional inertia weight χ_1 and animation weight χ_2. For peripheral patch i they are as follows:

$$\sigma_{ii}^I = \begin{cases} \dfrac{\chi_2 \sigma}{\chi_2 \sigma + \chi_1(1 - \sigma)} & \text{treatment facility in peripheral patch } i \text{ but not in centre,} \\ \dfrac{\chi_1 \sigma}{\chi_1 \sigma + \chi_2(1 - \sigma)} & \text{treatment facility in centre patch but not in peripheral patch } i, \\ \sigma & \text{else,} \end{cases}$$

$$\sigma_{ic}^I = 1 - \sigma_{ii}^I.$$

The proportions of exposure for infected individuals residing in the centre patch have a larger number of forms as there could be a treatment facilities in proportion n of the $M - 1$ peripheral patches. The proportions are given by the following,

$$\sigma_{cc}^I = \begin{cases} \dfrac{\chi_1 \sigma}{\chi_1 \sigma + (1 - \sigma)(n\chi_2 + (1 - n)\chi_1)} & \text{treatment facility not in centre,} \\ \dfrac{\chi_2 \sigma}{\chi_2 \sigma + (1 - \sigma)(n\chi_2 + (1 - n)\chi_1)} & \text{treatment facility in centre,} \end{cases}$$

$$\sigma_{ci}^I = \begin{cases} \dfrac{\chi_2 (1 - \sigma)}{\chi_1 \sigma + (1 - \sigma)(n\chi_2 + (1 - n)\chi_1)} & \text{treatment in peripheral patch } i \text{ but not centre,} \\ \dfrac{\chi_1 (1 - \sigma)}{\chi_1 \sigma + (1 - \sigma)(n\chi_2 + (1 - n)\chi_1)} & \text{treatment not in peripheral patch } i \text{ or centre,} \\ \dfrac{\chi_2 (1 - \sigma)}{\chi_2 \sigma + (1 - \sigma)(n\chi_2 + (1 - n)\chi_1)} & \text{treatment in peripheral patch } i \text{ and in centre,} \\ \dfrac{\chi_1 (1 - \sigma)}{\chi_2 \sigma + (1 - \sigma)(n\chi_2 + (1 - n)\chi_1)} & \text{treatment not in peripheral patch } i \text{ but in centre,} \end{cases}$$

These are a special case of the general equations seen in Chapter Four. The force of infection experienced by residents of the central patch $\mathcal{F}_c$ is composed of terms representing exposure in patch c, and exposure in each peripheral patch i,

$$\mathcal{F}_c = \beta_c \frac{B_c}{\kappa + B_c} \sigma + \sum_i \beta_i \frac{B_i}{\kappa + B_i} \left(\frac{1 - \sigma}{P} \right). \tag{5.1}$$

Similarly, the force of infection experienced by residents of peripheral patch i, $\mathcal{F}_i$ is composed of terms representing exposure in patch c, and exposure in patch i:

$$\mathcal{F}_i = \beta_c \frac{B_c}{\kappa + B_c} (1 - \sigma) + \beta_i \frac{B_i}{\kappa + B_i} \sigma. \tag{5.2}$$

Infected residents of the central patch are treated at rate $\mathcal{H}_c$, and residents of peripheral patch i are treated at rate $\mathcal{H}_i$ where

$$\mathcal{H}_c = \sigma_{cc}^I \xi_c + \sum_i \sigma_{ci}^I \xi_i,$$
$$\mathcal{H}_i = \sigma_{ic}^I \xi_c + \sigma_{ii}^I \xi_i, \tag{5.3}$$

and

$$\xi_j = \begin{cases} \xi & \text{if patch } j \text{ has a treatment facility,} \\ 0 & \text{if patch } j \text{ does not have a treatment facility.} \end{cases} \tag{5.4}$$

The total rates at which bacteria are shed into the central patch, $\mathcal{G}_c$, and into peripheral patch i, $\mathcal{G}_i$, are composed of terms representing the contributions of residents and contributions of visitors

$$\mathcal{G}_c = (\sigma_{cc}^I I_c + \sum_i \sigma_{ic}^I I_i + \sigma T_c + \sum_i (1 - \sigma) T_i) \eta,$$
$$\mathcal{G}_i = (\sigma_{ci}^I I_c + \sigma_{ii}^I I_i + \left(\frac{1 - \sigma}{P} \right) T_c + \sigma T_i) \eta. \tag{5.5}$$

A flow diagram for the system is shown in figure 5.5. Parameter values are given in table A.8. The complete epidemiological dynamics for residents of the central patch are given by

$$\dot{S}_c = \mu N_c - \mathcal{F}_c S_c - \mu S_c,$$
$$\dot{I}_c = \mathcal{F}_c S_c - (\gamma + \mathcal{H}_c + \mu) I_c,$$
$$\dot{T}_c = \mathcal{H}_c I_c - (\alpha \gamma + \mu) T_c, \tag{5.6}$$
$$\dot{R}_c = \alpha \gamma T_c + \gamma I_c - \mu R_c,$$
$$\dot{B}_c = \mathcal{G}_c - (\zeta + \theta) B_c.$$

The epidemiological dynamics for residents of any peripheral patch i are given by

$$\dot{S}_i = \mu N_i - \mathcal{F}_i S_i - \mu S_i,$$
$$\dot{I}_i = \mathcal{F}_i S_i - (\gamma + \mathcal{H}_i + \mu) I_i,$$
$$\dot{T}_i = \mathcal{H}_i I_i - (\alpha \gamma + \mu) T_i, \tag{5.7}$$
$$\dot{R}_i = \alpha \gamma T_i + \gamma I_i - \mu R_i,$$
$$\dot{B}_i = \mathcal{G}_i - (\zeta + \theta) B_i.$$

The parameter definitions for these equations are shown in table A.8 and three important assumptions in equations (5.6) and (5.7) are

- A patch with a treatment facility is more attractive to infected individuals. Thus edges toward treatment facilities are scaled up by an animation weight and edges away are scaled down by an inertia weight for infected individuals.

- The decontamination facilities do not alter the movement rates.

- Treated individuals continue to contribute bacteria to the contaminated reservoir at the same rate as untreated individuals.

We fix the parameters given in table A.8 at the values shown in table A.8. There are two parameter sets corresponding to stable equilibria in which the disease is absent or

endemic. When the system is disease free, the value of β is altered to give $R_0 < 1$. This was chosen as it has a large impact on R_0 and is significant in the model. When the disease is endemic, $R_0 > 1$.

We gave a background in Chapter One about natural disasters and the effect of floods. We now describe the simulation of the flood.

5.3.1 Simulating a flood perturbation

Recall, flooding can contaminate drinking water and hinder sanitation. We model a flood using a step change in the relevant parameter values; the shed and contact rates. The flood is modelled as a step up to a perturbed value of the parameter, β and η, and a step down to the normal value at the end of the a fixed time span. This profile is shown in figure 5.9.
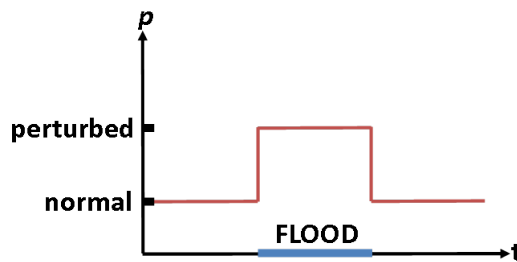

Figure 5.9: Profile of binary flood in terms of parameter p.

The perturbed parameter values are proportional to the normal values. We consider a 100% change i.e. perturbed value $= 2\times$(normal value). This will be large enough to show trends that represent the large effect that a natural disaster would produce.

5.4 The Solution: using simulation

In this chapter we have been considering the problem of deciding where, in a population structured by one or more heterogeneous characteristics, a treatment or decontamination facility should be located in order to minimise the impact of environmentally transmitted disease following a natural disaster. One way to find a solution to this problem is by simulation.

We seek a definitive solution by exhaustive search. This approach examines every possible option for locating a treatment or decontamination facility and finds the 'best'. We consider a population structured into five patches. An environmentally transmitted disease is either endemic in the population or introduced through the initial conditions. At the beginning of each simulation, a flood is modelled by parameter perturbation as described in section 5.3.1. The number of infections above those expected in normal endemic circumstances is recorded.

The steps of the algorithm are shown below. We add all the treatment and/or decontamination facilities at the same time before the flood. However, adding the facilities following the flood perturbation is also considered.

1. Choose initial distribution of treatment and/or decontamination facilities, for instance, if there is one treatment facility, start by trying it in patch one, the centre, then try patch two, three and so on in turn. If there are several facilities, generate the full list of possible arrangements using MATLAB's `nchoosek` function. Then,

examine each distribution scenario in turn before finally simulating the flood perturbation.

2. Solve the system until it is at equilibrium. For endemic equilibrium use parameter set 1 in table A.8. For disease free equilibrium use parameter set 2 in table A.8. It should be noted that there may occur a point at endemic steady state where the number of control facilities brings R_0 below one.

3. Simulate the flood, this is detailed in section 5.3.1. If the initial equilibrium is disease free, introduce a small number of infected individuals into each patch (set $I_i^0 = (10^{-4}) * N_i$).

4. Record the total number of new infections over the course of the flood. This is done using an additional model compartment which describes the dynamics of the infected class without recovery, treatment or death. This 'collects' infections over the time specified.

5. If the initial equilibrium is not disease free, find the total number of new infections over the course of the flood due to endemic turnover with unperturbed parameters. Remove these from the total number of infections recorded for the flood simulation. The result is the number of excess infections attributed to the flood.

6. Repeat step 1-5 with the next arrangement of facilities until all possibilities have been exhausted.

7. Compare the numbers of excess infections attributed to the flood for each arrangement of treatment and/or decontamination facilities. The optimum arrangement is the one that minimises the number of infections.

The above algorithm leads to the optimal, pre-emptively placed control facility distributions to minimise the epidemic size. However, we also consider those distributions that are placed at the beginning of the perturbation to minimise the infections over the flood. These are termed reactively placed control facility distributions and do not affect the equilibrium properties prior to the flood. Therefore, the optimal distributions of control facilities placed reactively or pre-emptively only differ at endemic equilibrium.

We also consider how long the system takes to return to equilibrium. To calculate the return time, we follow the algorithm to step 5 and then continue to simulate until the system is sufficiently close to the equilibrium value. This is measured through the infected individuals in the centre patch as they are most sensitive to changes in the system. However, we have also used different infected classes as the measure to arrive at the same results.

These algorithms lead to the results shown in the following Sections. They will first be discussed when one control facility is available. Then, once the optimum treatment or decontamination facility distributions have been understood, we may examine the distributions of both control facility types.

5.5 Results

5.5.1 Distributions with a single control measure

We first examine the results when there is only one type of control measure available, either treatment **or** decontamination. The aim is to discover which optimal distributions are common to both control types and which only apply with one type.
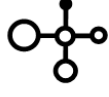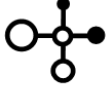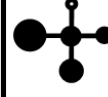
5.5.1.1 Summary of results
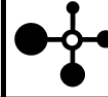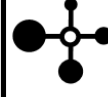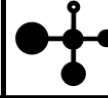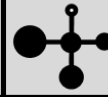
Table 5.1: Optimal distributions of between one and four control facilities in a city structured by a heterogeneity. Optimisation minimises the size of the epidemic associated with a flood in a system that is initially at endemic equilibrium (top rows) or disease free equilibrium (bottom row). The heterogeneity may be in the contact rate, population density or both. Larger circles indicate higher contact rates/ densities. Control facilities may provide treatment or decontamination. Shaded circles denote control facility locations. The unmarked distributions shown are optimal for all combinations of heterogeneity, control measure and placement time mentioned in table B.1 of the appendix. Distributions marked with (*) are not optimal for all heterogeneities but are not significantly worse that the alternative distributions which are shown in table B.2.

We start with the distributions that minimise epidemic size. Table 5.1 shows that, when the system is at endemic equilibrium, and the facilities are placed pre-emptively, treatment and decontamination facilities are optimally placed in the peripheral patches with lowest contact rate/density. In the final instance, when four facilities are to be placed, treatment facilities are optimally positioned in the centre and peripheral patches with highest contact rate and/or density whereas decontamination facilities are placed in the peripheral patches only. Pre-emptively placed facilities are placed before the system is simulated to its equilibrium state. Therefore, their placement may affect the equilibrium population characteristics. In contrast, when facilities are placed reactively, at the beginning of the perturbation, the centre patch is included in many of the optimal distributions. The optimal, reactively placed distributions of treatment facilities include the centre and peripheral patches with lowest contact rate and/or density for one to three facilities. Then four treatment facilities are placed in the peripheral patches only. The optimal, reactively placed distributions of decontamination facilities include the centre patch and peripheral patches with highest contact rate/density.

Table 5.2: Optimal distributions of between one and four control facilities in a city structured by a heterogeneity. Optimisation minimises the time to return to equilibrium after an epidemic associated with a flood in a system that is initially at endemic equilibrium or disease free equilibrium. Larger circles indicate higher contact rates/ densities. Shaded circles denote control facility locations. The distributions shown are optimal for all combinations of heterogeneity, control measure and placement time mentioned in table B.1 except for a few specific cases detailed in table B.3 denoted with an (*) .

When the system is initially at disease free equilibrium the decontamination facilities are once again placed in the centre and peripheral patches with highest contact rate/density. The optimal distributions of treatment facilities are more varied. The optimal distribution of one treatment facility at disease free equilibrium is in the centre. The optimal distribution of two facilities includes the centre and peripheral patch with lowest contact rate/density. However, when three facilities are available, it is best to place them in the peripheral patches with highest contact rate and/or density only. This distribution is retained when four facilities are placed as they are positioned in the peripheral patches. The changing distributions of treatment facilities will be discussed in Section 5.5.1.2.

We now consider the distributions that optimise, i.e. minimise, the return time. Table 5.2 shows that, when the system is at endemic equilibrium and the facilities are placed pre-emptively, treatment facilities are optimally positioned in the centre patch and peripheral patches with lowest contact rate/density. Pre-emptively placed decontamination facilities are optimally distributed if positioned in the highest contact rate/density peripheral patches. When the facilities are placed reactively, decontamination facilities are optimally placed in the lowest contact rate and/or density peripheral patches. Treatment facilities are best placed in the centre patch and peripheral patches with highest contact rate and/or density. When the system is initially at disease free equilibrium, the optimal distributions of one to three treatment facilities include the centre patch and the peripheral patches three and two i.e. the peripheral patches with second highest and second lowest contact rate/density respectively. The optimal distribution of four treatment facilities omits the centre. The decontamination facilities are optimally positioned in the centre and highest density/contact rate peripheral patches. There are some exceptions where another distribution is slightly better, denoted with an asterisk. These are discussed in Section 5.5.1.4 and the alternative distributions can be found in table B.3.

5.5.1.2 The effect of weighting on optimal distributions of treatment facilities

We found that the optimal configurations of treatment facilities varied with the number of facilities to be placed and the state of the system. This is related to the weight scaling of infected individuals towards treatment. When the scaling is weak or absent, the optimal configurations of treatment facilities are similar to those for decontamination facilities. Locating treatment facilities in the centre benefits the most people because it is accessible from all peripheral patches and infected people are drawn in when weights are scaled. However, as the scaling towards a treatment facility increases and scaling away from a treatment facility decreases, a number of transitions occur. A higher ratio of scaling towards treatment facilities to scaling away from treatment facilities, or bias, means that infected individuals have proportionally more exposure to the environment of the patch with the treatment facility. This leads to increased contamination of the environment around a treatment facility. Figure 5.10 shows how the bias can alter the optimal distributions of treatment facilities. As the bias increases, we see a transition from the optimal configurations including the centre and *high* density or contact rate peripheral patches, region (A) in figure 5.10, to including the centre and *low* density or contact rate peripheral patches, region (B). This is because the increased contamination raises the force of infection in the patches with treatment facilities. As such, it can increase the number of infections. This is particularly the case when the density or contact rate is high. Thus, the peripheral patches with lower density or contact rate become more viable options for treatment facility placement.

Figure 5.10: Epidemic size over weighting towards treatment facilities when densities are heterogeneous for different placements of two treatment facilities. As the inertia weight decreases and the animation weight increases, infected individuals are proportionally more exposed to the environment surrounding a treatment facility. Line style denotes where the treatment facilities are placed; in the centre and peripheral patches (dashed with a darker shade indicating a higher density) or the periphery (solid with a darker shade indicating a higher density). Regions A, B and C are divided by which distributions are optimal. Parameters as shown in table A.8 and the system is initially at disease free equilibrium.

As the bias increases further, the centre patch is omitted from the optimum distribution, region (C) in figure 5.10. At this point the negative effect of increased contamination of the centre patch outweighs the benefit of having a treatment facility in such an accessible position. This is because locating treatment facilities in the periphery has an 'auto-quarantine' effect; infected individuals move towards a treatment facility if they have access to it. Consequently, treatment facilities on the periphery tend to keep residents at home, providing them with quicker treatment and preventing contamination of the centre patch. Therefore, when three or four treatment facilities are placed at disease free equilibrium it is optimal to omit the centre. At endemic equilibrium the regime does not reach the point at which it is optimal to omit the centre until four facilities are placed. This is because the susceptible population is depleted and the auto-quarantine effect produces only a marginally smaller epidemic size than distributions including the centre patch.

There is another consideration, the waiting time until treatment. This depends on the treatment rate as well as the number of facilities an infected individual has access to. Figure 5.11 shows that as the waiting time increases it is no longer optimal to place a treatment facility in the centre patch. This is because infected individuals are biased towards the patch with the treatment facility. A longer waiting time means a longer infectious period. Therefore, there is an extended period of shedding in the patch with the treatment facility.
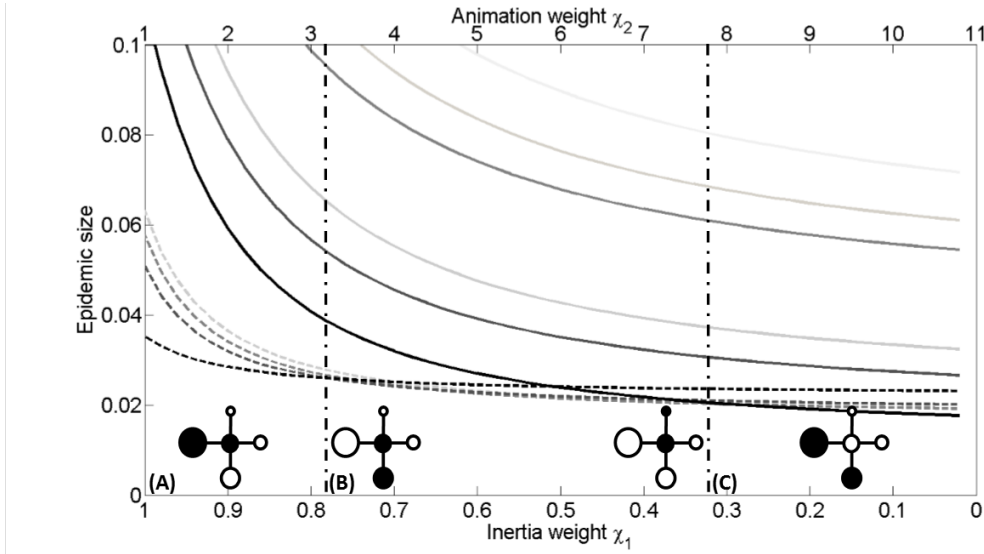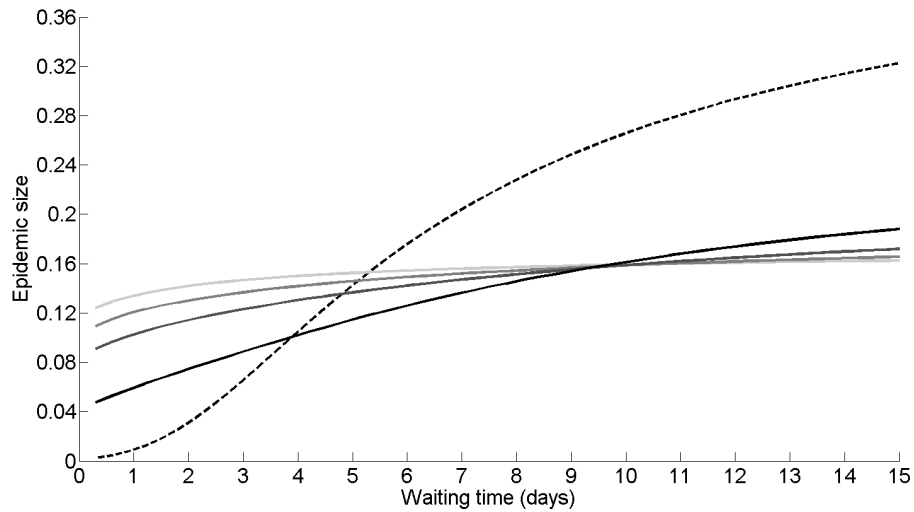
Figure 5.11: Epidemic size over treatment rate when densities are heterogeneous for different placements of one treatment facility. Line style denotes where the treatment facility is placed; in the centre (dashed) or the periphery (solid with a darker shade indicating a higher density). Parameters as shown in table A.8 and the system is initially at disease free equilibrium.

5.5.1.3 The difference between pre-emptive and reactive placement of control facilities

Pre-emptive deployment added control facilities to the system with endemic disease and allowed it to move to the new endemic equilibrium before any transmission perturbation occurred. Thus pre-emptively deployed facilities affect the epidemic associated with the perturbation directly, and indirectly through their effect on the equilibrium state before the perturbation. Consequently, the optimal pre-emptive configurations of control facilities to minimise the size of an epidemic associated with a transmission perturbation are not optimal when minimising the infection risk during endemic circulation, see table 5.3.

Table 5.3: Optimal configurations of control facilities to minimise the lifetime infection probability at endemic equilibrium. Population densities (N) or environmental contact rates (β) or both may be heterogeneous. Larger circles indicate patches with higher densities and/or contact rates. Shaded circles indicate control facility locations. In the lower two rows grey indicates decontamination, black treatment. Configurations marked (*) are optimal but only marginally better then the configurations suggested by applying the general rule.

In all of the cases we have examined, for pre-emptive deployment, the configurations that minimise epidemic size are also the configurations that minimise the size of the total susceptible population at endemic equilibrium. The susceptible population is the fundamental resource for an epidemic, and depletion of this resource has a direct impact on the epidemic size. All configurations also reduce the endemic infection risk. However, since the endemic infection risk is proportional to the size of the susceptible population, it follows that the optimal configuration for minimising epidemic size is always the least beneficial configuration for reducing the endemic infection risk. Therefore, when deciding on an appropriate configuration for the pre-emptive deployment of control facilities we would have to weight the frequency with which perturbation are expected to occur against the impact of endemic circulation.

5.5.1.4 Notable differences in the optimal control facility distributions

The distributions in 5.1 and 5.2 were optimal in many situations but there were some exceptions, shown in tables B.2 and B.3 in the appendix. When the system is initially at endemic equilibrium there is one alternative to the distributions shown. This occurs when two decontamination facilities are placed reactively and contact rates are heterogeneous. In this situation the optimal distribution includes the centre patch and peripheral patch with second lowest contact rate/density. However, the difference between this distribution and the one optimal in most cases is 0.88%, see table C.3, which is not considered significantly different when compared to the greatest possible difference between distributions. The same applies for many of the alternative distributions that are optimal at disease free equilibrium, see table C.1. However, when three and four treatment facilities are placed, there are alternative distributions that are significantly different to the configuration that is optimal in most cases. These occur when both contact rates and densities are heterogeneous as facilities are optimally placed in the centre and lowest contact rate/density peripheral patches, rather than just in the peripheral patches. To explain this we refer to figure 5.10. When both contact rates and densities are heterogeneous, the omission of the centre comes at a higher price than when only one heterogeneity is present. This is because the force of infection is higher in a high density and high contact rate patch. As such, the transition to omitting the centre from optimal distributions occurs at a higher bias or waiting time than the one employed here.

We now examine the alternative distributions that minimise return time. When the system is initially at endemic equilibrium and the facilities are placed reactively, there is one exception, when two treatment facilities are positioned and densities are heterogeneous. In this situation the optimal distribution includes the centre patch and peripheral patches with highest density. However, the difference in return time allowed by this distribution and the most commonly optimal one is 28 minutes, see table C.4. Therefore, this is an insignificant difference when compared to the maximum possible difference of 6 days. When the system is initially at disease free equilibrium, there are only two significantly different alternative control facility distributions. These occur when four treatment facilities or two decontamination facilities are placed when both contact rates and densities are heterogeneous. In the case of treatment, the alternative optimal distribution includes the centre patch and peripheral patches with lowest contact rate and density. This distribution reduces the return time to equilibrium as it reduces the epidemic size, see table B.2. However, for decontamination, the alternative distribution is optimal for a different reason. When the number of available decontamination facilities is low, the optimal distributions allow large epidemics that exhaust themselves quickly, minimising return time. However, as the number increases,

it becomes viable to minimise the return time through limiting the epidemic size. The point at which it becomes viable to limit return time through limiting epidemic size when contact rates and densities are heterogeneous comes at a higher number of decontamination facilities than when only one heterogeneity is present. Therefore, there is a significant alternative optimal distribution of two decontamination facilities when contact rates and densities are heterogeneous.

5.5.2 Distributions with two control measures

We now examine the situation where treatment and decontamination facilities can both be placed. The optimal distributions of these facilities will indicate whether one control measure should be prioritised in certain situations than the other. They will also show whether the placement of one control measure affects the placement of the other.

5.5.2.1 Summary of results

We separate the distributions by equilibrium and assessment criteria, as before. We start with the distributions that minimise epidemic size. Table 5.4 shows that when the system is initially at endemic equilibrium and facilities are placed pre-emptively, it is optimal to place one to four decontamination facilities in the lowest contact rate/density peripheral patches. When five facilities are available it is optimal to place three decontamination and two treatment facilitates in the peripheral patches with lowest contact rate and/or density. However, when six or more facilities are available, a treatment facility is placed in every patch and decontamination facilities are positioned in the peripheral patches with lowest contact rate/density. When the system is initially at endemic equilibrium and facilities are placed reactively, the results are the same as when the system is initially at disease free equilibrium. It is optimal to place a treatment facility in the centre then both decontamination and treatment facilities in the centre. This distribution is retained as decontamination facilities are placed in the peripheral patches with highest contact rate/density until all patches contain a decontamination facility. When decontamination facilities are placed in all patches, treatment facilities are placed in the peripheral patches with lowest contact rate/density until the final instance, where they are placed in the peripheral patches only. There are exceptions to these optimal distributions, shown in table B.4 and discussed in section 5.5.2.2.

We now examine the distributions that minimise the return time. Table 5.5 shows that when the system is initially at endemic equilibrium and the facilities are placed either reactively or pre-emptively it is optimal to place one treatment facility in the centre. This placement is retained and two decontamination facilities are placed in the peripheral patches with highest contact rate/density. When four to six facilities are available, both treatment and decontamination facilities are placed in the centre with decontamination facilities in the high contact rate/density peripheral patches. Then when seven and eight facilities are available, decontamination facilities are placed in all patches with treatment facilities placed in the centre and peripheral patches with lowest contact rate/density. Finally, when nine facilities are placed pre-emptively it is optimal to position decontamination facilities in all patches and treatment facilities in the centre and lowest contact rate/density peripheral patches. However, when facilities are placed reactively the treatment facilities should be positioned in the peripheral patches only. It should be noted that the final three distributions of reactively placed control facilities are assessed on their return time to disease free equilibrium as these distributions bring $R_0 < 1$.

Table 5.4: Optimal distributions of between one and nine control facilities placed in a city structured by a heterogeneity. Optimisation minimises the size of an epidemic associated with a flood in a system that is initially at endemic or disease free equilibrium. Larger circles denote higher contact rates/ densities. Shaded circles denote control facility locations with grey representing decontamination and black, treatment. The distributions shown are optimal for all combinations of heterogeneity mentioned in table B.1 except for particular cases, denoted (*), mentioned in table B.4.

Table 5.5: Optimal distributions of between one and nine control facilities pre-emptively placed in a city structured by a heterogeneity. Optimisation minimises the return time to equilibrium for an epidemic associated with a flood in a system that is initially at endemic or disease free equilibrium. Larger circles denote higher contact rates/ densities. Shaded circles denote control facility locations with grey representing decontamination and black, treatment. The distributions shown are optimal for all combinations of heterogeneity mentioned in table B.1 except for particular cases, denoted (*), mentioned in table B.5.

5.5.2.2 Notable differences in the optimal control facility distributions

The general rules shown when placing control facility types to minimise epidemic size have a few exceptions. However, these exceptions can not be considered significantly different to the general rule, see tables C.1 and C.3. As such, we may consider the general rules as representative up to parametrization.

5.6 Conclusion

We separate our conclusion into three areas; a summary of our methods and results, a commentary on the effectiveness of our analysis and finally a review of our progress towards answering our main question.

5.6.1 Summary

We aimed to find the optimum distribution of one to nine control facilities of two types in a heterogeneous city with an environmentally transmitted disease. This disease was either endemic or introduced and an epidemic occurred as a result of a natural disaster in the form of a flood. We determined these distributions when the facilities were placed pre-emptively or reactively through simulation. The simulations calculated the number of new infections over the course of an epidemic, excluding endemic turnover where appropriate, and the return time to equilibrium. The steps of the simulation are shown in figure 5.12. The number of infections or duration was saved as the control facility distribution 'score'. The distribution with the minimum score was declared the optimum.
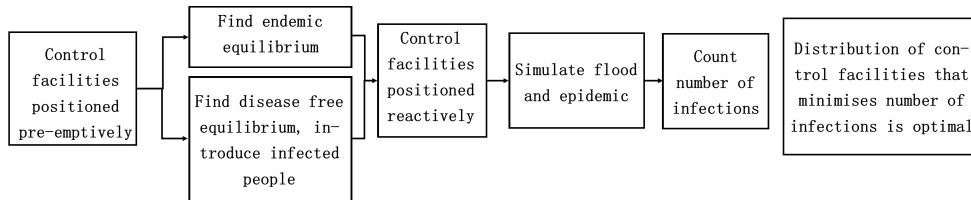
Figure 5.12: Flowchart depicting simulation steps.

The optimum distributions of one control type were generally indicative of the optimum distributions of two types of control facility. When the system was initially at disease free equilibrium or the facilities were placed reactively at endemic equilibrium, the centre and peripheral patches with highest contact rate/density were prioritised for decontamination and the centre and lowest contact rate/density peripheral patches were prioritised for treatment.

A notable feature of the results is the variability of the optimal distributions of treatment facilities. This is due to the bias in the exposure weightings for infected individuals. As the bias increases the infected individuals can be increasingly exposed to areas with high force of infection or high susceptible traffic. Consequently, a compromise must be reached between areas that allow access to the greatest number of individuals and areas that may be more negatively affected by any increased shedding of bacteria.

5.6.2 Assessing the assessments

Generally, the epidemic size is the most intuitive measure of an epidemic. It gives the excess number of individuals who are infected over the course of the flood for each distribution of control facilities. The optimum distributions which minimise epidemic size

are fairly consistent. They are also clear to interpret. Although, there are issues with placement time. The pre-emptive placement of control facilities can affect the equilibrium characteristics of the population. Namely, it can reduce the number of susceptible individuals prior to the perturbation. This effectively maximises the lifetime probability of infection which is the least desirable situation when managing an endemic disease. Therefore, there are conflicts between those strategies that minimise the new infections over a perturbation and those that minimise the lifetime probability of infection. This placement time issue is partly resolved using reactive placement. The reactive placement time in this situation is unrealistic but it does give insight into those distributions of control facilities that minimise the infections over the perturbation only.

The return time may not be as good an assessment of the optimum distribution of control facilities. To a certain extent, there is a correlation between epidemic size and duration. A very small epidemic will have few infections and die out quickly. However, the rate at which an epidemic declines is not necessarily related to the rate at which it grows or its peak value. Therefore, there are situations where a smaller epidemic will have a longer duration than a larger one. This means that the optimum distributions found using return time as an assessment may allow epidemics with undesirable attributes such as a high growth rate and large peak value. This issue is illustrated in figure 5.13. The figure shows the number of infected individuals over time for three epidemics. The reference epidemic, in black, has fewest infections; however the epidemic of shortest duration is the orange, due to a larger growth rate and steeper decline. Therefore, in this case, the optimum distribution of control facilities to minimise return time would allow a more sudden and extreme epidemic.
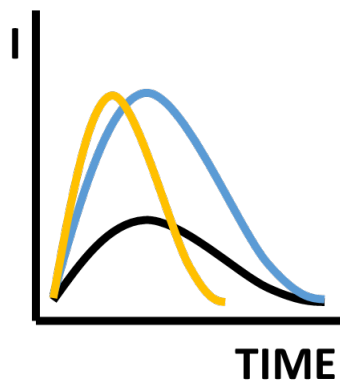
Figure 5.13: Graph of infections over time for three epidemics. The black represents the reference time series of smallest epidemic size. The orange and blue both have greater epidemic size but the orange epidemic is of shorter duration due to faster growth and decline rates.

5.6.3   The solution

There are a few things to consider when determining the optimum distribution of control facilities. One of the most important factors is the population response to the control measure. We have seen that the bias in exposure weighting for infected individuals towards treatment facilities, as well as the treatment waiting time, strongly influence the optimal distributions of control facilities. In a situation where bias is high, it may be beneficial to avoid placing treatment facilities in areas such as the centre. This is because the high bias increases shedding around a treatment facility. As such, it

is optimal to place treatment facilities in patches with low force of infection or low susceptible traffic.

Other considerations are the number, placement time and state of the system prior to the flood. The number of facilities to be placed also affects the optimum distributions. We assumed that all facilities were placed at the same time rather than iteratively. As such, there are situations where the optimum distribution of '$(n-1)$' facilities bears little resemblance to that for '(n)'. For example, the optimum distributions of eight and nine facilities placed reactively to minimise epidemic size vary substantially when the unperturbed system is at endemic equilibrium.

In summary, city authorities wishing to minimise an epidemic caused by a flood would need to consider the following questions before deciding on a course of action.

1. **How will the population respond to the control measures?**

   There may be negative outcomes of the control measures which need to be balanced against their potential benefit.

2. **What is the state of the city before the flood?**

   If the disease is endemic and facilities are placed pre-emptively a very different distribution of control facilities is optimal compared to when the disease is newly introduced.

3. **How many facilities are to be placed?**

   The number of facilities to be placed and whether those facilities are to be placed at the same time affects which patches should be prioritised for control measures. As such, it may be necessary to choose between a distribution that is optimal now or one that will be optimal if further facilities are added in future.

4. **Which control facility type is to be used?**

   Treatment and decontamination are both optimal measures but in different situations.

Once these three questions have been answered, the different areas or patches of the city may be prioritised for control facilities by their population density, contact rate with the environment and whether the patch lies in the centre or on the periphery.

5.6.4 Further work

So, is the problem solved? We would say that it is but with some codicils. The question appears to be a simple one: when should we deploy limited resources to minimise infections given a perturbation in transmission rates. However, the pre-emptive deployment results demonstrate that there is more to consider than just the number of infections. The pre-emptively placed distributions of control facilities limit an epidemic by minimising the susceptible population. Conversely, protecting the population by limiting endemic prevalence can make it more vulnerable to epidemics given a transmission perturbation. These two strategies are clearly at odds. Therefore, in future it may be beneficial to conduct a cost-benefit analysis of endemic prevalence management against epidemic control given different frequencies of transmission perturbations.

Another consideration is that the simulations we used are not quick or computationally cheap. Every possible arrangement of control facilities must be checked and when there are two available controls, the list of possible arrangements is extensive. If we wished to examine a higher number of patches or even an additional control measure,

simulations would soon become prohibitively expensive. Therefore, whilst we have a solution for five patches and two control measures, we can not extend this solution easily. Thus, a proviso for our current solution is that the number of patches is low.

To extend this work to a higher number of patches, we will need a faster method for identifying optimum distributions. We can test the new method or methods using the results shown in this chapter. Then, we can confidently use the new method to find optimum distributions of control facilities for higher numbers of patches. The criteria for the new methods are:

- To indicate the results shown in this chapter for the five patch model.

- Be computationally inexpensive.

- Make biological sense.

The last item is pertinent as we need a method that has an interpretation which agrees with the meaning of the simulation to ensure any predictions are useful.

A place to start the search for the new methods is the equilibria properties such as R_0 and the value of the endemic equilibrium. These may be useful as our results indicate a clear dependence on the equilibrium value. We may also explore features such as the resilience and reactivity which relate to the speed at which the system returns to equilibrium once perturbed and the route that it returns via. Finally, we can examine how the flood affects the system and where the damage is felt most. These methods should build a picture of the system behaviour that not only predicts the results of the simulations but explains the system response to perturbation more thoroughly.

Chapter 6

Alternative indicators of optimal resource deployments

6.1 The problem

In the previous chapter we found the optimal distributions of treatment and decontamination facilities to minimise the size of a disease epidemic. The disease was transmitted environmentally and was either introduced or endemic in the system. The epidemic was initiated by a flood and the size of epidemic was calculated over the course of the flood. We assessed possible control facility distributions using simulation to find those that allowed the smallest epidemic. We now seek alternative methods to find these optimal distributions. These methods will be required to have a biologically realistic interpretation and be computationally less expensive.

We start by introducing our alternative methods and their capabilities. We will then use them both as an assessment in an exhaustive search for optimal control facility distributions and as a way of prioritising patches for control. Lastly, we discuss their agreement with the simulation results of the previous chapter.

6.2 Alternative methodologies

Our objective in this chapter is to predict and understand the optimum distributions of pre-emptively and reactively placed control facilities, shown in the previous chapter, using more efficient and informative methods. We wish to use procedures that have biologically meaningful interpretations. Therefore we will use a variety of analyses that apply at different points in time with respect to a flood. These are placed in three categories: equilibrium properties, the response to the flood and the recovery of the system. These apply before the flood occurs, at the start of the flood and when the epidemic starts to decline, shown in figure 6.1.

We shall use our assessments in two ways. Firstly we shall prioritise patches for treatment and/or decontamination facilities based on their local assessment value. An example of this prioritisation is shown in the section of part reproductive numbers. The second way we shall use our assessments is through exhaustive search. We shall test every possible distribution of control facilities by their effect on the global assessment criteria. Finally, we compare the prioritisation and optimal distribution found through exhaustive search to those distributions deemed optimal by simulation.

The aim of this section is to explain the methodology of each of the analyses. We shall also state the results we would expect from each analysis if they are effective at predicting the optimum distributions of control facilities found through simulation.
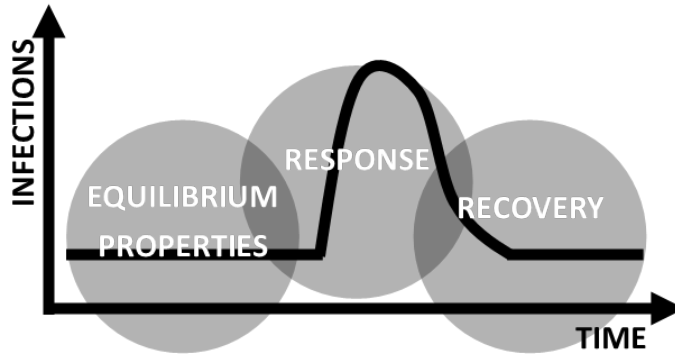
Figure 6.1: Analysis areas of an epidemic associated with a flood. The black line denotes the change in the number of infected individuals over time.

6.2.1 Equilibrium Properties

The first aspects of the system we can examine are the equilibrium properties in the absence of the flood. The state before the flood, disease free or endemic, affects the optimal distribution of control facilities. We aim to examine these states or equilibria through different, but related, quantities. At disease free equilibrium we examine the basic reproductive number and part reproductive numbers. At endemic equilibrium, we focus on the endemic prevalence, the proportions of susceptible individuals in each patch and the effective reproductive number.

6.2.1.1 R_0, R_E and the part reproduction numbers

We detail the method for finding and decomposing the basic reproductive number, R_0, in Chapter Two. We now additionally consider the effective reproduction number, R_E, which applies when the entire population is not susceptible. It is calculated in the same manner as R_0 and we expect $R_E = 1$ when the system is at endemic equilibrium.

We may be interested in which infected class contributes most to the reproduction numbers and to assess this we must divide R_0 or R_E into their constituent parts. R_0 is the lead eigenvalue of the next generation matrix, $\mathcal{NGM}$, linearised about the disease free equilibrium whereas R_E is the lead eigenvalue of the next generation matrix linearised about the endemic equilibrium. The $\mathcal{NGM}$ is found by multiplying the transmission matrix, $\mathcal{T}$, by the inverse of the transition matrix, Σ. These matrices consist of the transmission and transition terms of the system Jacobian at equilibrium. We detailed the full steps of the decomposition in Chapter Two and the computing method for these matrices in Chapter Four. The interpretation of the part reproduction numbers, R_0^i or R_E^i, is the absolute contribution of each type i to the basic or effective reproduction number. That is, the extent each class of the system adds to the number of infections caused by one individual in one generation.

We will examine whether the part reproduction numbers may be used to predict the results of the simulations by prioritising the patches for treatment facilities using the infected class R_0^i, and for the decontamination facilities using the bacterial R_0^i. The patch with the highest R_0^i for the infected class is prioritised for a treatment facility. The patch with the highest R_0^i for the bacterial class is prioritised for a decontamination facility. In figure 6.2 an example of the ordering is shown where the prioritisation is given in white numbers.

In section 6.3.2.1 we shall also examine the distributions of control facilities found by exhaustive search that minimise the reproduction numbers or sum of infected class part
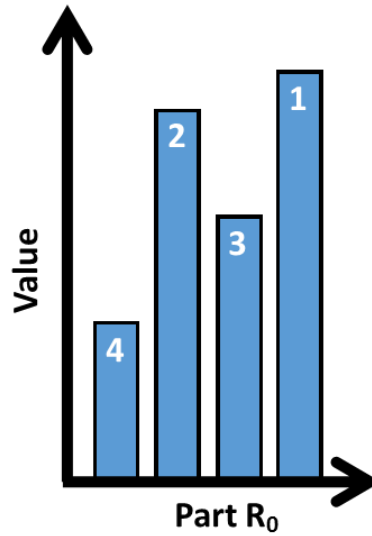
134

Figure 6.2: An example of the prioritisation of patches for control facilities based on their part R_0 value for the infected or bacterial class. Bar height is part R_0^i magnitude, white number is ordering.

reproduction numbers. This will indicate which distributions limit the initial growth of the epidemic to the greatest extent.

6.2.1.2 The endemic prevalence and proportion of susceptible individuals

We also consider the composition of the population at endemic equilibrium. The endemic prevalence and proportion of susceptible individuals are calculated by algebraically solving the system of ordinary differential equations assuming that they are at equilibrium. The equilibrium values can also be calculated by simulation as with the previous chapter. The endemic prevalence is a quantity of interest as it can affect the number of infections due to a perturbation. For instance, a higher number of infected individuals can infect a larger number of individuals if transmission is perturbed. However, there can only be new infections if there are available susceptible individuals. Therefore, we also measure the proportion of the population in each patch that is susceptible to evaluate the *capacity* of the population for new infections. The susceptible proportion of the population is also related to R_E and is a measure of the lifetime probability of infection given by $1 - \frac{S^*}{N}$ at endemic equilibrium.

We use the endemic prevalence and susceptible population size to prioritise patches for treatment facilities in section 6.3.2.2. We prioritise patches in ascending order with respect to the size of the susceptible population at endemic equilibrium and in descending order with respect to the patch prevalence at endemic equilibrium. We also examine the distributions of control facilities found by exhaustive search that minimise the proportion of the population that is infected and maximise the proportion of the population that is susceptible. This will indicate which distributions allow the lowest number of infections at endemic equilibrium and which protect the susceptible individuals to the greatest extent. Finally, we consider the optimal pre-emptively placed distributions by examining those distributions that *minimise* the size of the susceptible population at endemic equilibrium.

6.2.2 Response to flood

Whilst the state of the system prior to the flood may be informative, we also wish to examine the system reaction to the perturbation. As such, we need a measure of the change in each system aspect due to the perturbation. We consider three such measures in this section: the impact, sensitivity and influence.

6.2.2.1 Impact

We introduced the impact in Chapter Four. It is a measure of the reaction of each system element to a perturbation. We examined the effect of a perturbation approximating a natural disaster on different patch arrangements and levels of spatial segregation. We will now order the infected classes by their impact and prioritise treatment facilities to the patches for which the infected class impact is highest. We will order the bacterial classes by their impact and prioritise decontamination facilities to the patches for which the bacterial class impact is highest. This will be based on the impact experienced by each class in the absence of any control. We will assess whether this can be used instead of an exhaustive search to predict optimal control facility distributions. Then we shall find distributions by exhaustive search that minimise the sum of the infected and bacterial class impacts and compare those to the distributions that minimise epidemic size.

6.2.2.2 Sensitivity and Influence

The sensitivity and influence explain some elements of the reaction to a perturbation that the impact misses. They utilise the system Jacobian once again to find which state variables are most susceptible to a perturbation, and which are most able to amplify a perturbation. There is a key difference between the sensitivity and influence compared to the impact: the perturbation that is used. The perturbation in this case is a press perturbation which means it affects all classes and patches equally. Therefore, the perturbation is not specifically representative of a flood.

The sensitivity and influence were explained in [12] from the work in [98]. They both use the eigenvalues and eigenvectors of the Jacobian, the sensitivity using the right eigenvectors and the influence the left. The eigenvalues represent the magnitude of the effect of the perturbation and the eigenvectors represent the distribution of that effect at steady state. The right eigenvector dictates where the perturbation is most felt i.e. which class has the largest change due to the perturbation. The left eigenvector dictates which classes are most effective at spreading the perturbation. The magnitude and distribution is summed for each class. This is because, although the lead eigenvalue dominates the system behaviour, there are other behaviours that need to be accounted for through the other eigenvalues. The final mathematical formula is then as follows.

$$\text{sensitivity}(i) = -\sum_k |v_i^{(k)}|/Re(\lambda_k),$$
$$\text{influence}(i) = -\sum_k |w_i^{(k)}|/Re(\lambda_k).$$

Here, $v_i^{(k)}$ represents the ith element of the kth right eigenvector, arranged in columns; $w_i^{(k)}$ represents the ith element of the kth left eigenvector, arranged in rows, and λ_k represents the kth eigenvalue of the Jacobian at equilibrium.

To explain this calculation, we refer back to the simple example in Chapter Four. This example was of a one patch direct transmission disease with no recovery, i.e. a simple SI model. This had the form of the following non-dimensional equations with S and I as state variables for the susceptible and infected classes. The parameters μ and β represent the death rate and contact rate respectively.

$$\dot{S} = \mu - \beta SI - \mu S$$
$$\dot{I} = \beta SI - \mu I$$

Therefore the Jacobian at endemic equilibrium, its eigenvalues and eigenvectors, are

$$\mathcal{J} = \begin{pmatrix} -\beta & -\mu \\ \beta - \mu & 0 \end{pmatrix}, \quad \lambda_1 = -\mu, \quad \lambda_2 = (\mu - \beta), \quad \mathbf{v} = \begin{pmatrix} \frac{\mu}{\mu-\beta} & 1 \\ 1 & -1 \end{pmatrix}, \quad \mathbf{w} = \begin{pmatrix} 1 & 1 \\ \frac{\beta-\mu}{\mu} & 1 \end{pmatrix}.$$

Thus, the sensitivity and influence are:

$$\text{Sensitivity}(1) = -\left(\frac{|\frac{\mu}{\mu-\beta}|}{-\mu} + \frac{|1|}{\mu-\beta} \right) = \frac{2}{\beta - \mu},$$

$$\text{Sensitivity}(2) = -\left(\frac{|1|}{-\mu} + \frac{|-1|}{\mu-\beta} \right) = \frac{\beta}{\mu(\beta - \mu)},$$

$$\text{Influence}(1) = -\left(\frac{|1|}{-\mu} + \frac{|\frac{\beta+\mu}{\mu}|}{\mu-\beta} \right) = \frac{2}{\mu},$$

$$\text{Influence}(2) = -\left(\frac{|1|}{-\mu} + \frac{|1|}{\mu-\beta} \right) = \frac{\beta}{\mu(\beta - \mu)}.$$

If we let $\beta = 2$ and $\mu = 0.5$, the infected class, class two, has a greater reaction to a perturbation as its sensitivity value is $2.\dot{6}$ compared with $1.\dot{3}$ for the susceptible class. However, the susceptible class has an influence value of 4 as opposed to $2.\dot{6}$ for the infected class. This means that a perturbation to the susceptible class has a greater overall effect than one to the infected class.

The sensitivity and influence are decompositions of the impact assuming a press perturbation. They function as a measure of excitability in each class [12]. We may expect those patches with high influence values for their infected classes to feature in the optimal distributions of control facilities. This is in order to minimise the effect that infected individuals have in the population. We may also expect the patches with the most sensitive infected classes to feature in the optimal distributions of control facilities. This is in order to protect vulnerable individuals. Therefore we use the influence and sensitivity to prioritise patches for treatment and decontamination facilities in the same manner as the impact.

In section 6.3.3.2 we shall also examine those distributions found by exhaustive search that minimise the sum of the infected and bacterial class influences and the sum of the infected and bacterial class sensitivities. The distributions that minimise infected class influence limit the ability of the infected classes to affect other classes such as the susceptible class. This may indicate which distributions limit new infections the most. The distributions that minimise the infected sensitivity allow the smallest reaction of the infected classes to the perturbation. As such, this may indicate which distributions

limit the growth of the epidemic due to a perturbation.

6.2.3 Recovery

Finally, we wish to examine how the system recovers after an epidemic associated with a flood. The recovery denotes the return of the system to the initial equilibrium state. Therefore, we may study how quickly the system returns to equilibrium and whether it moves further away from the equilibrium initially.

6.2.3.1 Resilience

We introduced the resilience in Chapter Two as a decay rate for the perturbations. We may decompose it in the same manner as described for R_0 in section 6.2.1.1. The resilience is the negative of the lead eigenvalue of the Jacobian at equilibrium. So it may be decomposed into part resiliences using the columns and lead eigenvector of the Jacobian at equilibrium. The interpretation of these part resiliences is that they measure the contribution of each class to the system resilience. A larger, more positive part resilience increases the system resilience which means that the rate of decay of perturbations is higher. Whereas, a negative part resilience decreases the system resilience, slowing the rate of decay of perturbations.

In section 6.3.4.1 we examine the part resiliences for each infected class at the endemic and disease free equilibria to prioritise patches for treatment facilities, using the infected classes, and decontamination, using the bacterial classes. Those patches with a smaller, more negative part resilience are prioritised for control facility placement. We also discuss the distributions of control facilities found by exhaustive search that maximise the system resilience and sum of infected class part resiliences to speed the decay of perturbations to the system.

6.2.3.2 Reactivity

The reactivity gives the maximal rate that perturbations can be amplified initially. We introduced it in Chapter Two as the lead eigenvalue of Hermitian part of the Jacobian at equilibrium. Therefore it may be decomposed in a similar way to the resilience and reproduction numbers. The part reactivities for each class, found using this decomposition, can be interpreted as the contribution of that class to the system reactivity. A larger part reactivity increases the system reactivity and thus increases the rate that perturbations can be amplified. A positive reactivity means that the system is reactive and any perturbation applied to the system will be initially amplified. We use the part reactivities for the infected and bacterial classes to prioritise patches; a higher part reactivity for a patch will lead to a higher priority. In section 6.3.4.2 we shall also inspect the distributions of control facilities found by exhaustive search that minimise the system reactivity and sum of infected class part reactivities. These distributions will limit the rate at which perturbations are amplified initially, reducing the initial epidemic.

6.3 Alternate methods results

We shall now use our defined assessments to predict and understand the optimal distributions of control facilities found through simulation. We shall do this in two ways. Firstly, we prioritise patches for facility deployment based on the local patch assessment value. Secondly, we shall use exhaustive search to test each possible control

facility distribution by the global assessment value. If the distribution that optimises the assessment also minimises the epidemic size in simulation then that assessment is effective. We consider the distributions to agree if they exactly match or match the general rule.

6.3.1 Summary of results

The aim was to find the optimum distributions of control facilities to minimise epidemic size using more efficient methods than simulation. We have outlined the methods to be examined and how to interpret them. We will now show an overview of how well the distributions that optimise these new assessments, found by exhaustive search, agree with those that minimise epidemic size. Figures 6.3 and 6.4 show the proportion of situations in which the optimal facility distribution is correctly found by the given method. A situation accounts for one possible number of facilities with one possible heterogeneity. For instance, at disease free equilibrium, there are 20 situations where one control facility type minimises both R_0 and the epidemic size, see figure 6.3. There are 24 situations with one control facility type at each equilibrium as one to four facilities providing either treatment or decontamination can be placed across three heterogeneities. There are 27 situations with two control facility types at each equilibrium as one to nine facilities may be placed across three heterogeneities.

We notice that there are a higher proportion of situations where assessments agree at disease free equilibrium and when facilities are placed reactively at endemic equilibrium. We also see more agreement for the equilibrium properties. To examine why this is the case we will now look at the distributions that optimise each assessment. We shall particularly focus on why some analyses are optimised by the same distributions that minimise epidemic size and why some are not.

Figure 6.3: Proportion of situations of one control type that both minimise the epidemic size and optimise the given analyses. Part R_0 denoted by P. R_0, part R_E denoted by P. R_E, part reactivity denoted by P. Rea and part resilience denoted by P. res. The different colours denote the equilibria, DFE= disease free equilibrium, EE=endemic equilibrium with facilities either pre-emptively or reactively placed. The distributions apply for one to four facilities providing either treatment or decontamination when densities and/or contact rates are heterogeneous.
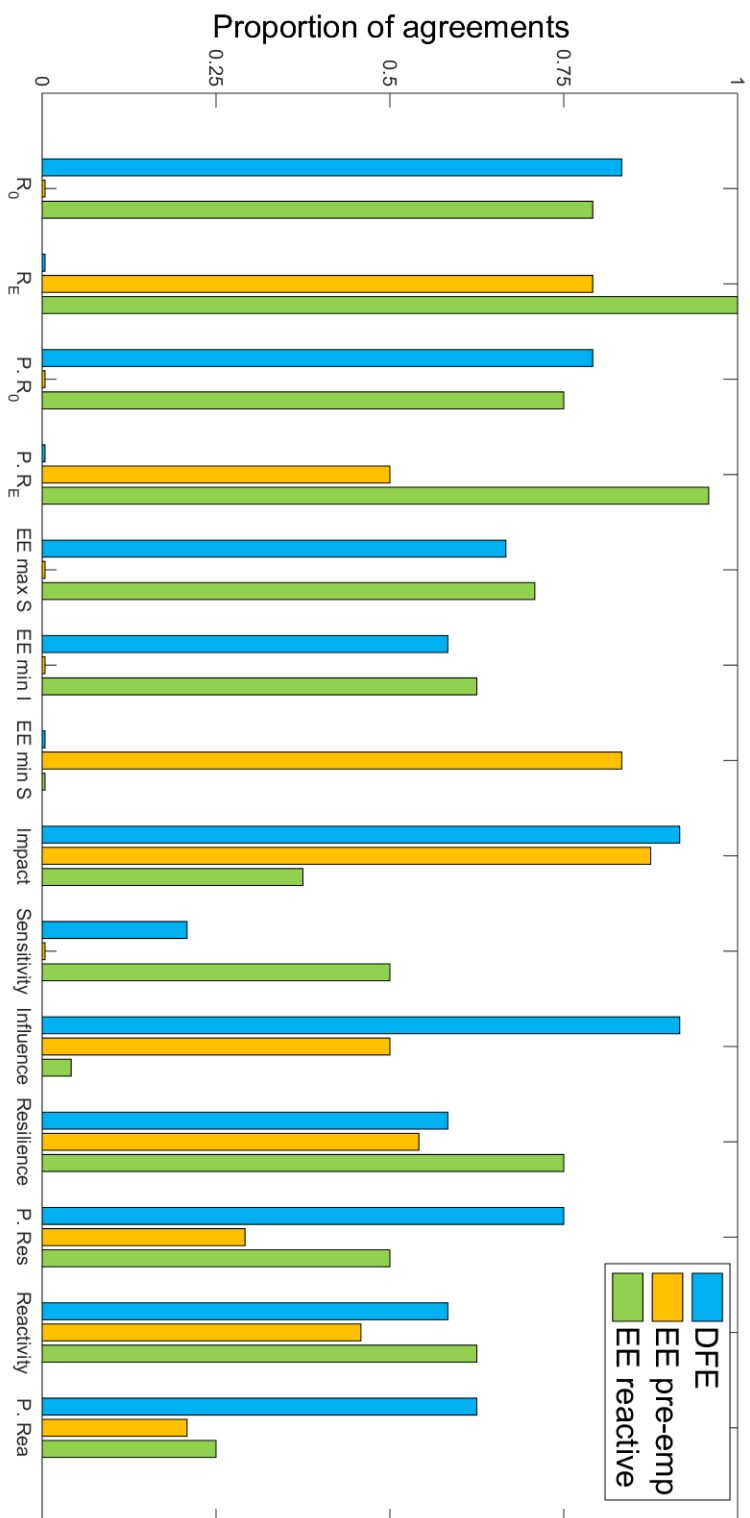
Figure 6.4: Proportion of cases of two control types that both minimise the epidemic size and optimise the given analyses. Part R_0 denoted by P. R_0, part R_E denoted by P. R_E, part reactivity denoted by P. Rea and part resilience denoted by P. res. The different colours denote the equilibria, DFE= disease free equilibrium, EE=endemic equilibrium with facilities either pre-emptively or reactively placed. The distributions apply for one to nine facilities providing either treatment or decontamination when densities and/or contact rates are heterogeneous.
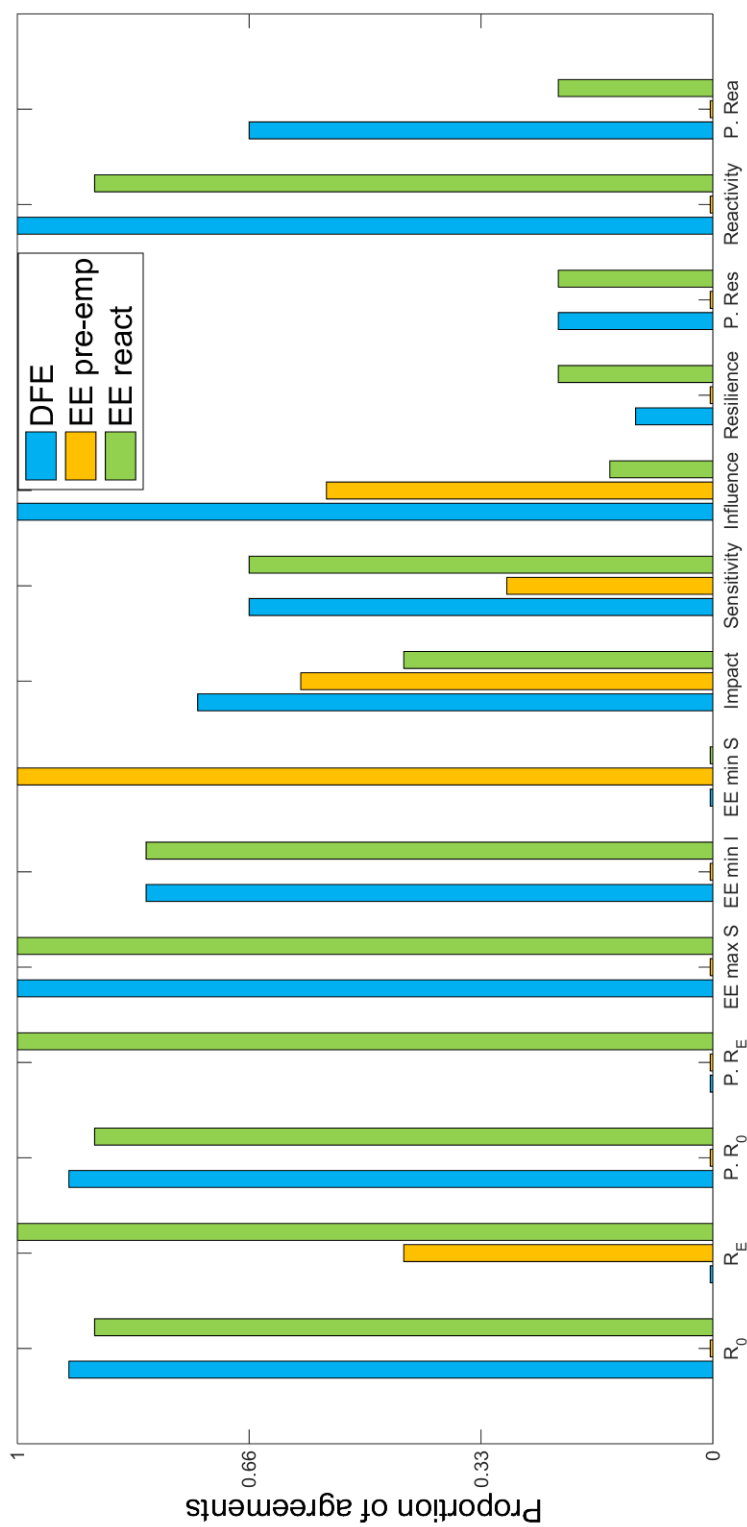
6.3.2 Equilibrium Properties

In this section, we examine the effectiveness of R_0, R_E, part reproduction numbers and endemic population characteristics as assessments of distributions of control facilities. If they are successful, the distributions that optimise the assessments will also minimise the epidemic size.

6.3.2.1 R_0, R_E and the part reproduction numbers

We first prioritise patches for control facilities based on the part reproduction numbers R_0^i and R_E^i in the absence of control. We order the patches for placement of treatment facilities by the part reproductive numbers for the infected classes. We order the patches for decontamination facility placement by the part reproductive numbers for the bacterial classes.

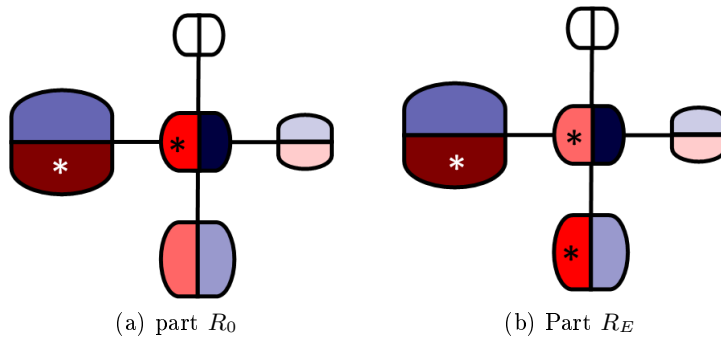(a) part R_0 (b) Part R_E

Figure 6.5: Prioritisation order for treatment, in red, and decontamination, blue, where a darker shade indicates a higher priority. Patches are prioritised by R_0^i at disease free equilibrium (6.5a) and R_E^i at endemic equilibrium (6.5b) in each patch of a city structured by a heterogeneity. The order holds across all heterogeneities except when marked with an asterisk. The parameters used are those found in table A.8.

We may see in figure 6.5 at disease free equilibrium, the centre and high density patches should be prioritised for the placement of control facilities. This is the case for all heterogeneities; however, when contact rates are heterogeneous, the order of the centre and highest contact rate peripheral patch is reversed for the placement of treatment facilities. If we compare this prioritisation with the simulation results, we see general agreement for the decontamination facilities. However, the part R_0 only effectively predict the placement of one to two treatment facilities as the optimal distributions found by simulation then omit the centre patch.

When we prioritise patches for control facilities by the effective part reproduction numbers, we see good agreement for the reactive placement of decontamination facilities. However, the simulation results suggest that the centre and low density/ contact rate patches should be prioritised for the placement of treatment facilities which is not seen here.

We now examine the optimal distributions of control facilities found through exhaustive search to minimise the R_0 and the sum of the infected class part R_0. Note, we examine only the infected class contribution to R_0 rather than infected and bacterial. This is because if we were to consider both classes it would almost amount to the system R_0 which we already consider. Table 6.1 shows the optimal distributions of one control facility type.

As seen from the summary bar graphs in figures 6.3 and 6.4, the distributions that minimise the reproduction numbers at disease free equilibrium and endemic equilibrium,

(a) R_0 (b) Part R_0

Table 6.1: Optimum distributions of one control facility type in a city structured by a heterogeneity. The optimisation minimises R_0 (6.1a) or the sum of R_0^i for the infected classes (6.1b). The parameters used are those found in table A.8 at both DFE and EE. Larger circles denote higher contact rates/ densities. The shaded cells indicate those distributions also minimise epidemic size at DFE (blue) or when placed reactively at EE (green).

when placed reactively, also generally minimise the epidemic size. There are some exceptions to this. The blue denotes distributions optimal at disease free equilibrium. There are three situations where the distributions that minimise R_0 do not minimise the epidemic size. This is the same for R_0^i. The green denotes distributions optimal when placed reactively at endemic equilibrium. We see four situations where the distributions that minimise R_0 do not minimise epidemic size when placed reactively at endemic equilibrium. However, there are six such situations for the part R_0.

Table 6.2: Optimum distributions of two control facility types in a city structured by a heterogeneity. The optimisation minimises R_0 or the sum of the part R_0^i for the infected classes. The parameters used are those found in table A.8 at both DFE and EE. Larger circles denote higher contact rates/ densities. The shaded cells indicate those distributions also minimise epidemic size at DFE (blue) or when placed reactively at EE (green).

Table 6.2 shows the optimal distributions of two types of control facilities to minimise R_0 or the sum of R_0^i for the infected classes. The results were the same for R_0 and the part R_0 using the parameters at disease free and endemic equilibria. Only a few distributions that minimise R_0 do not also minimise epidemic size: namely, four situations at disease free equilibrium and three situations at endemic equilibrium. In table 6.2, R_0 and the sum of R_0^i for the infected classes are equally effective as analyses of the optimal distributions of control facilities. They are both quite efficient as methods, requiring only the next generation matrix, its eigenvalues and eigenvectors.

We will now examine the reproduction numbers, R_E, with parameters as in the flood at endemic equilibrium.

The effective reproduction numbers and part reproduction numbers are calculated with the Jacobian linearised about the endemic equilibrium before the flood using the parameters during the flood i.e. using the perturbed values of β and η. This measures the growth of the epidemic at the beginning of the flood assuming the system is at endemic equilibrium. It also allows us to place facilities reactively or pre-emptively. Table 6.3 shows that the R_E and part R_E for the infected classes are very effective identifiers of the optimal distributions of control facilities. There are only a few distributions that minimise R_E but not epidemic size, namely five when they are placed pre-emptively and none when they are placed reactively. There is one reactively placed distribution and 12 pre-emptively distributions that minimise the sum of the part R_E but not epidemic size.

The effective reproduction number continues to be a good predictor of the optimal control facility distributions when two control facility types are placed reactively. Table 6.4 shows that this is particularly the case when facilities are placed reactively as every distribution minimises both R_E and the epidemic size. When the facilities are placed pre-emptively 15 distributions minimise R_E for the flood but not the epidemic size.

144

(a) R_E (b) Part R_E

Table 6.3: Optimum distributions of one control facility type in a city structured by a heterogeneity. The optimisation minimises the R_E for the flood (a) or sum of R_E^i for the infected classes in the flood (b). The parameters used are those found in table A.8 at EE. Larger circles denote higher contact rates/ densities. The shaded cells indicate those distributions also minimise epidemic size when placed pre-emptively (yellow) or when placed reactively (green).

Table 6.4: Optimum distributions of two control facility types in a city structured by a heterogeneity. The optimisation minimises the R_E for the flood. The parameters used are those found in table A.8 at EE. Larger circles denote higher contact rates/ densities. The shaded cells indicate those distributions also minimise epidemic size when placed pre-emptively (yellow) or when placed reactively (green).

Table 6.5: Optimum distributions of two control facility types in a city structured by a heterogeneity. The optimisation minimises the sum of the part R_E for the infected and bacterial classes. The parameters used are those found in table A.8 at EE. Larger circles denote higher contact rates/ densities. The shaded cells indicate those distributions also minimise epidemic size when placed pre-emptively (yellow) or when placed reactively (green).

The part reproduction numbers are less successful as an indicator than R_E, see table 6.5. They only predict the optimal reactively placed distributions of control facilities.

The reproductive numbers describe the risk of an epidemic and the number of new infections per generation. As such, a distribution of control facilities that minimises these quantities, minimises the initial growth of an epidemic. This can, in turn, limit the epidemic size. The optimal pre-emptively placed distributions to minimise epidemic size are not always well predicted here. This may be as the limiting nature of the size of the susceptible pool is not fully incorporated into the calculation of the part R_E in the flood. We now investigate the size of the susceptible population directly as an indicator.

6.3.2.2 The endemic prevalence and proportion of susceptible individuals

We examine the endemic equilibrium by the proportions of infected and susceptible individuals in each patch. Figure 6.6 shows the results if we use these quantities to prioritise patches for treatment facilities. We focus only on the human population and so do not order the patches for decontamination facilities.
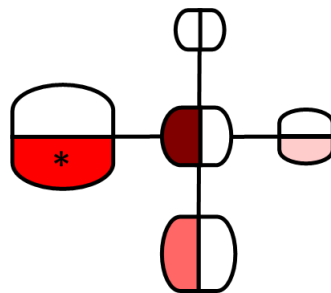
Figure 6.6: Prioritisation order for treatment in red where a darker shade indicates a higher priority. Patches are prioritised by endemic prevalence and the size of the susceptible population at endemic equilibrium in each patch of a city structured by a heterogeneity. The order holds across all heterogeneities except when marked with an asterisk. The parameters used are those found in table A.8.

Figure 6.6 shows that whether we use the endemic prevalence or proportion of susceptible individuals to prioritise the patches, the results are the same. Treatment facilities should be placed in the centre first and then patches with high density and/or contact rate. This does not agree fully with the simulation results as the treatment facilities were placed in the patches with lowest density/ contact rate as well as the

centre patch.

We now examine the optimal distributions of control facilities found by exhaustive search to minimise the size of the infected population, maximise the size of the susceptible population or minimise the size of the susceptible population at endemic equilibrium, table 6.6. These have a slightly different aims. We compare the optimal distributions here to those that minimise epidemic size in a system initially at disease free equilibrium and in systems initially at endemic equilibrium. Whilst we compare the distributions that maximise the susceptible population at endemic equilibrium etc. with those that minimise the epidemic at disease free equilibrium, we use a slightly different parameter set. The reason for this comparison is the population composition at endemic equilibrium gives information about the historical behaviour of the system. For example, if there have been many infections in the system, the susceptible population will be smaller at endemic equilibrium. Therefore, we may infer information about the system behaviour before reaching equilibrium by examining the population composition at equilibrium.
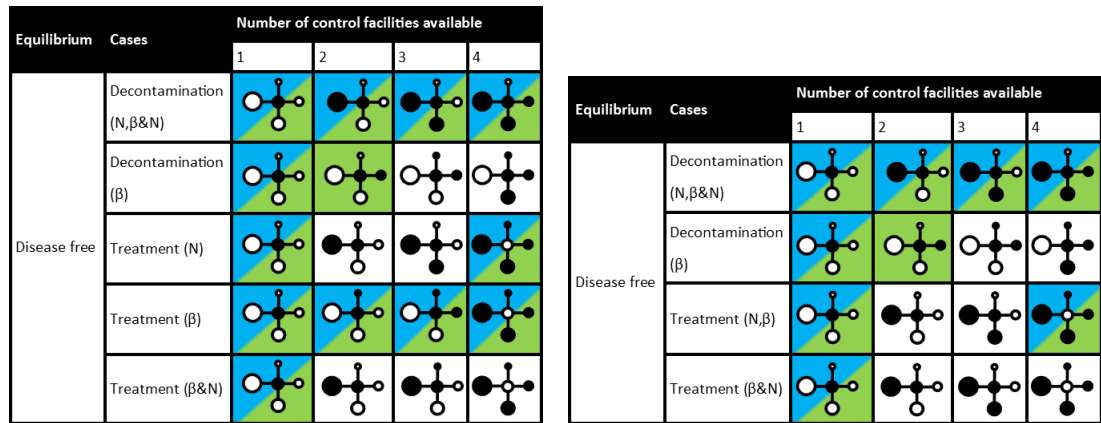
(a) maximises the size of the susceptible population

(b) minimises the size of the infected population
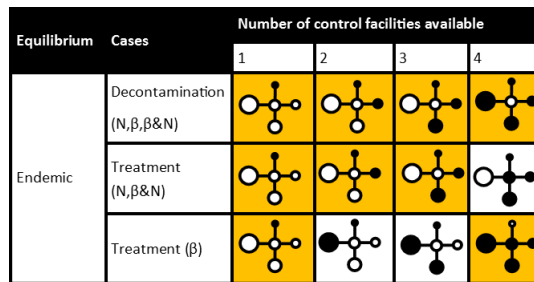
(c) minimises the size of the susceptible population

Table 6.6: Optimum distributions of one control facility type in a city structured by a heterogeneity. The optimisation maximises the susceptible population (6.6a), minimises the infected population (6.6b) and minimises the susceptible population (6.6c) at endemic equilibrium. The parameters used are those found in table A.8 at DFE and EE. Larger circles denote higher contact rates/ densities. The shaded cells indicate that those distributions also minimise epidemic size at disease free equilibrium (blue) and at endemic equilibrium when placed pre-emptively (yellow) or when placed reactively (green).

Table 6.6a shows the distributions that maximise the susceptible population at endemic equilibrium also, often, minimise the epidemic size at disease free equilibrium

and at endemic equilibrium when placed reactively. There are eight exceptions to this agreement at disease free equilibrium. There are seven distributions of control facilities that maximise the susceptible population but do not minimise the epidemic size when placed reactively.

The distributions that minimise the infected population are less successful at minimising the epidemic size, see table 6.6b. At disease free equilibrium there are ten distributions that minimise the infected population but not epidemic size; at endemic equilibrium there are nine such reactively placed distributions.

Lastly, we compare those distributions that minimise the susceptible population with those that minimise epidemic size when placed pre-emptively at endemic equilibrium, table 6.6c. These agree in all but four situations.

Table 6.7: Optimum distributions of two control facility types in a city structured by a heterogeneity. The optimisation maximises the size of the susceptible population at endemic equilibrium. The parameters used are those found in table A.8 at DFE and EE. Larger circles denote higher contact rates/ densities. The shaded cells indicate those distributions also minimise epidemic size at disease free equilibrium (blue) and at endemic equilibrium when placed pre-emptively (yellow) or when placed reactively (green).

Table 6.8: Optimum distributions of two control facility types in a city structured by a heterogeneity. The optimisation minimises the size of the infected population at endemic equilibrium. The parameters used are those found in table A.8 at DFE and EE. Larger circles denote higher contact rates/ densities. The shaded cells indicate those distributions also minimise epidemic size at disease free equilibrium (blue) and at endemic equilibrium when placed pre-emptively (yellow) or when placed reactively (green).

The optimal distributions of two control facility types to maximise the susceptible population or minimise the infected population generally minimise the epidemic size

at disease free equilibrium or at endemic equilibrium when placed reactively, table 6.7. This is particularly the case when maximising the endemic susceptible population size which is a 100% effective indicator of the optimal distributions to minimise epidemic size. There are five distributions that minimise the infected population but not the epidemic size, shown in table 6.8.

We have linked epidemic size and prevalence. However the prevalence may not be the clearest predictor of epidemic size. If a greater number of individuals are infected they may infect a larger number of susceptible individuals. However, a small infected population does not necessarily mean a smaller epidemic, it could mean a large epidemic with swift recovery. In contrast, a large susceptible population at endemic equilibrium can only mean that there have been few infections as there is no re-entry to the susceptible class once infected and the birth rate is kept fixed. Thus, the susceptible population at endemic equilibrium, more so than the infected, is an effective indicator of epidemic size. There appears to be more agreement when two control facility types are placed; however, we have allowed agreement where the difference between the optimal distribution of control facilities is only negligibly different from the most commonly optimal distribution, see Appendix C for differences.
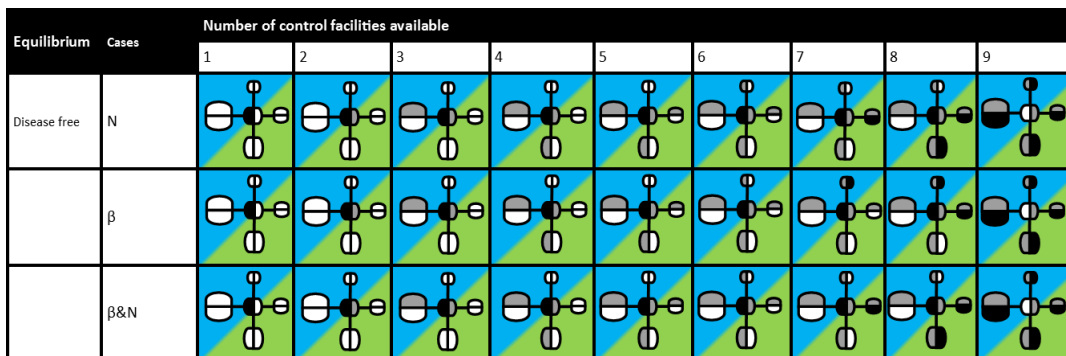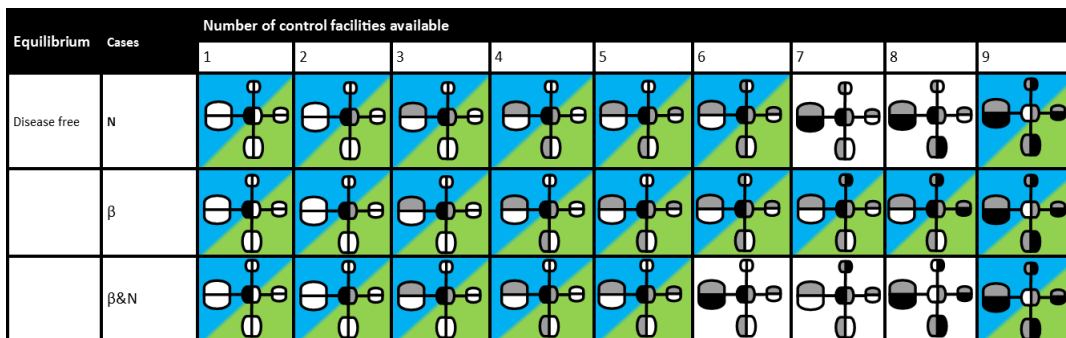

Table 6.9: Optimum distributions of two control facility types in a city structure by a heterogeneity. The optimisation minimises the size of the susceptible population at endemic equilibrium. The parameters used are those found in table A.8 at EE. Larger circles denote higher contact rates/ densities. The shaded cells indicate those distributions also minimise epidemic size at endemic equilibrium when placed pre-emptively (yellow).

We also compared those distributions that minimise the susceptible population with those that minimise the epidemic size at endemic equilibrium when placed pre-emptively. Table 6.9 shows 100% agreement. This is because those distributions that remove the resource of the an epidemic, the susceptible individuals, reduce the epidemic over the course of the flood. This is not an optimal control strategy, as discussed in the previous chapter, but it does illustrate the use of examining the endemic population proportion of susceptible individuals.

We have examined the properties of both equilibria without factoring in the effect of the flood. We will now address this with the impact, sensitivity and influence analyses which take into account the perturbation.

6.3.3 Response to flood

In this section, we examine the effectiveness of the impact, sensitivity and influence as indicators of optimal distributions of control facilities. If they are successful, the distributions that optimise the assessments will also minimise the epidemic size. These analyses take into account the effect of perturbations on every system element.

6.3.3.1   Impact

The impact measures the propensity of each infected and bacterial class in each patch to react to a flood. A class with a high impact value will vary to a greater extent when perturbed by the flood and may be a good focus for control. Similarly, the control facility distribution that minimises the sum of the infected and bacterial class impacts limits the variation in the infected and bacterial classes due to the flood. Less variation in these classes can mean a smaller epidemic when perturbed. We first prioritise the patches for treatment facilities, based on the infected class impacts, and for decontamination facilities, based on the bacterial class impacts.

(a) DFE   (b) EE
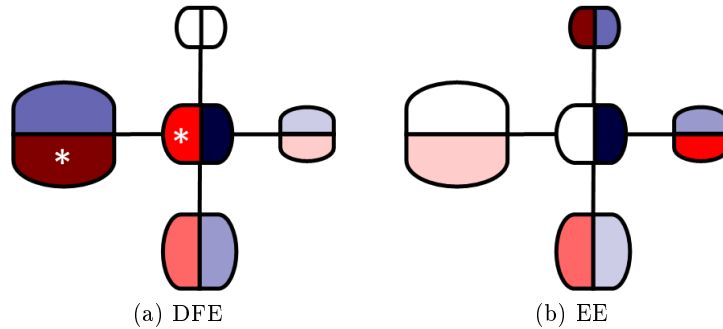
Figure 6.7: Prioritisation order for treatment, in red, and decontamination, blue, where a darker shade indicates a higher priority. Patches are prioritised by the impact at disease free equilibrium (6.7a) and at endemic equilibrium (6.7b) in each patch of a city structured by a heterogeneity. The order holds across all heterogeneities except when marked with an asterisk. The parameters used are those found in table A.8.

We see a different ordering at each equilibrium in figure 6.7. At disease free equilibrium, the centre and highest density/ contact rate peripheral patches are prioritised for treatment and decontamination facilities. There is one exception, when contact rates are heterogeneous, the ordering of the centre and highest contact rate peripheral rate patch is reversed for treatment facilities. These generally agree with the ordering seen in the simulation results.

When the endemic equilibrium is stable, a different ordering is seen. The bacterial class impacts indicate decontamination facilities should be placed in the centre and then lowest contact rate/density peripheral patches. Whereas the treatment facilities should be placed in the lowest contact rate/density peripheral patches only. These both agree well with the simulation results for pre-emptively placed facilities. We now examine the full optimal distributions found by exhaustive search to minimise the impact.

The Jacobian is linearised around the disease free equilibrium or endemic equilibrium in the impact calculation. When at endemic equilibrium, control facilities are either placed before or after the equilibrium is calculated and input into the Jacobian to take account of pre-emptive or reactive control facility placement. This leads to the results shown in table 6.10.

In table 6.10 we compare the distributions that minimise the impact when control facilities are placed reactively or pre-emptively at endemic equilibrium and placed at disease free equilibrium. These distributions also minimise epidemic size in many cases, particularly at disease free equilibrium and endemic equilibrium when placed pre-emptively. There are two exceptions to this at disease free equilibrium. At endemic equilibrium, when facilities are placed pre-emptively, there are three that minimise the impact but do not minimise the epidemic size. There are 15 exceptions when facilities are placed reactively.

Table 6.10: Optimum distributions of one control facility type in a city structured by a heterogeneity. The optimisation minimises impacts of both infectious and bacterial classes. The parameters used are those found in table A.8 at DFE and EE. Larger circles denote higher contact rates/ densities. The shaded cells indicate those distributions also minimise epidemic size at disease free equilibrium (blue) and at endemic equilibrium when placed pre-emptively (yellow) or when placed reactively (green).

Table 6.11: Optimum distributions of two control facility types in a city structure by a heterogeneity. The optimisation minimises the sum of the impacts of the infected and bacterial classes. The parameters used are those found in table A.8 at DFE and EE. Larger circles denote higher contact rates/ densities. The shaded cells indicate those distributions also minimise epidemic size at disease free equilibrium (blue) and at endemic equilibrium when placed pre-emptively (yellow) or when placed reactively (green).

When two control facility types are placed the level of agreement between distributions that minimise the sum of the infected and bacterial class impacts and those that minimise epidemic size is similar to when one control facility type was placed, see table 6.11. There are seven exceptions at disease free equilibrium. At endemic equilibrium, when facilities are placed pre-emptively, there are 11 exceptions. When facilities are placed reactively, there are 15 distributions minimising the impact but not epidemic size.

The impact assesses the change in a state variable per unit change in the perturbed parameter. In the above, we see a good level of agreement between those distributions that minimise the sum of the impacts for the infected and bacterial classes except when facilities are placed reactively. This is as the method breaks down in this situation. As shown previously, we calculate the equilibrium and then the perturbation and impact. However, with reactive placement, we calculate the the equilibrium and then change the system so that, arguably, the equilibrium values used in the following calculations are no longer valid.

6.3.3.2 Sensitivity and influence

The sensitivity and influence are related to the impact in that they measure the response of the system elements to a perturbation. A highly sensitive variable reacts to a greater extent to a perturbation; an influential state variable affects other state variables to a greater extent.

(a) Influence DFE   (b) Sensitivity DFE

(c) Influence EE   (d) Sensitivity EE
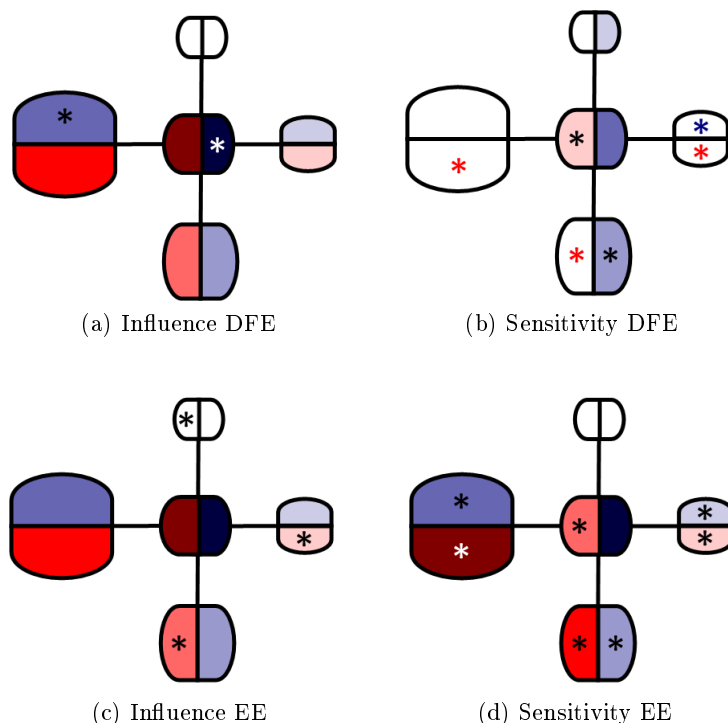
Figure 6.8: Prioritisation order for treatment, in red, and decontamination, blue, where a darker shade indicates a higher priority. Patches are prioritised by influence at disease free equilibrium (6.8a) and at endemic equilibrium (6.8c) or ordered by sensitivity at disease free equilibrium (6.8b) and at endemic equilibrium (6.8d) in each patch of a city structured by a heterogeneity. The order holds across all heterogeneities except when marked with an asterisk. The parameters used are those found in table A.8.

Figure 6.8 shows the prioritisation of patches based on their infected or bacterial

class sensitivity and influence. We start with the influence, which has the same patch ordering at both equilibria. It suggests we should prioritise the centre and high density/ contact rate patches for treatment and decontamination facilities. This agrees with the simulation results well for decontamination facilities with a few exceptions where the order of the patches has been reversed when densities and contact rates are heterogeneous.

The sensitivity has a number of patch orderings which do not agree over any heterogeneity, particularly at disease free equilibrium. When the disease free equilibrium is stable, treatment facilities should be placed in the lowest density/ contact rate patch for all heterogeneities. However, there is no other prioritisation consistent across all heterogeneities although patches are generally ordered by density for the placement of treatment facilities. There is no such trend for decontamination facilities. The ordering at endemic equilibrium is more consistent with the centre and high density/ contact rate patches generally chosen first for control facilities except when contact rates are heterogeneous where is no discernible trend. The ordering when densities are heterogeneous agrees with the simulation results for reactive placement of control facilities.

We now examine the optimal distributions found by exhaustive search to minimise the sum of the infected and bacterial class sensitivities or influences.

(a) Influence   (b) Sensitivity

Table 6.12: Optimum distributions of one control facility type in a city structured by a heterogeneity. The optimisation minimises influence (6.12a) and sensitivity (6.12b) of the infected and bacterial classes. The parameters used are those found in table A.8 at DFE and EE. Larger circles denote higher contact rates/ densities. The shaded cells indicate those distributions also minimise epidemic size at disease free equilibrium (blue) and at endemic equilibrium when placed pre-emptively (yellow) or when placed reactively (green).

The optimal distributions of control facilities to minimise the sum of the infected and bacterial class influences often minimise epidemic size when placed at disease free equilibrium or pre-emptively at endemic equilibrium, see table 6.12. There are three distributions that minimise the influence at disease free equilibrium but not the epidemic size. There are eight distributions that minimise the influence, but not epidemic size, at endemic equilibrium when placed pre-emptively. The distributions for the influence are unsuccessful at minimising epidemic size at endemic equilibrium when placed

reactively, see table D.1. In this situation only one distribution minimises the influence and epidemic size.

The sensitivity is less effective as a measure of the optimal distributions of control facility distributions at disease free equilibrium and pre-emptively at endemic equilibrium, see table D.2. There are 19 distributions at disease free equilibrium that minimise the sum of the infected and bacterial class sensitivities but not epidemic size. There are no distributions of control facilities that minimise both the sensitivity and epidemic size when placed pre-emptively at endemic equilibrium. There are 12 distributions placed reactively at endemic equilibrium that minimise the sensitivity but not epidemic size. This leads to the optimal distributions of two control facility types to minimise the sum of the influence or sensitivity for the infected and bacterial classes.

Table 6.13: Optimum distributions of two control facility types in a city structured by a heterogeneity. The optimisation minimises influence of the infected and bacterial classes. The parameters used are those found in table A.8 at DFE and EE. Larger circles denote higher contact rates/ densities. The shaded cells indicate those distributions also minimise epidemic size at disease free equilibrium (blue) and at endemic equilibrium when placed pre-emptively (yellow) or when placed reactively (green).

The distributions of control facilities that minimise the sum of the infected and bacterial class influences at disease equilibrium, and some pre-emptively placed at endemic equilibrium also minimise the epidemic size, see table 6.13. There are 12 pre-emptively placed distributions and 23 reactively placed distributions that minimise the influences but not epidemic size. Once again, the influence is not an effective measure of the distributions that minimise the epidemic size when placed reactively at endemic equilibrium.

When we compare those distributions that minimise the sum of the sensitivities for the infected and bacterial classes with those that minimise epidemic size we see more agreement when facilities are placed reactively. At disease free equilibrium and endemic equilibrium when facilities are placed reactively, only 9 distributions of facilities do not minimise both sensitivity and epidemic size. However, when facilities are placed pre-emptively at endemic equilibrium, 19 distributions minimise sensitivity but not epidemic size.

Table 6.14: Optimum distributions of two control facility types in a city structured by a heterogeneity. The optimisation minimises sensitivity of the infectious classes. The parameters used are those found in table A.8 at DFE and EE. Larger circles denote higher contact rates/ densities. The shaded cells indicate those distributions also minimise epidemic size at disease free equilibrium (blue) and at endemic equilibrium when placed pre-emptively (yellow) or when placed reactively (green).

The influence and sensitivity do not use the same perturbation in their calculation as the impact. However, they still capture some of the optimal distributions of control facilities at disease free equilibrium, see table 6.14. At endemic equilibrium, neither analysis is fully successful at predicting the optimal distributions to minimise the epidemic size. The distributions that minimise the influence often minimise the epidemic size when placed pre-emptively but seldom when placed reactively. The converse is true for the sensitivity although it is a less successful predictor overall. Thus, whilst both analyses capture some of the dynamics at each equilibrium there are issues brought by the unrealistic press perturbation and invalid equilibrium when facilities are placed reactively.

6.3.4 Recovery

In this section we examine the last area of interest in figure 6.1, the way the system recovers from the perturbation. We will scrutinise the resilience and reactivity as assessments of distributions of control facilities. In previous sections, we inspected the state of the system before the flood and its reaction to a perturbation. We now examine the behaviour after the perturbation. This will complete our view of the dynamics of an epidemic caused by a flood.

6.3.4.1 Resilience

The resilience is a measure of the decay rate of a perturbation to the system. A larger resilience means that perturbations decay more quickly and the system returns to equilibrium faster. Therefore, the distribution of control facilities that maximises the resilience speeds the decay of perturbations and will limit their ongoing effects. However, first we shall examine the prioritisation of patches based on their part resilience.

We aim to maximise the resilience to reduce the return time to equilibrium. Therefore, we are interested in those classes that negatively contribute to the system resilience

(a) DFE   (b) EE
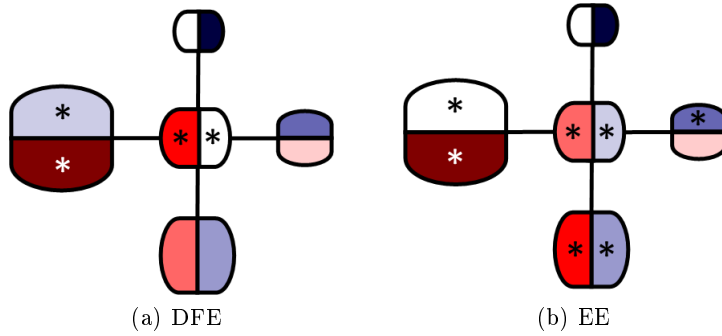
Figure 6.9: Prioritisation order for treatment, in red, and decontamination, blue, where a darker shade indicates a higher priority. Patches are prioritised by the part resiliences at disease free equilibrium (6.9a) and at endemic equilibrium (6.9b) in each patch of a city structured by a heterogeneity. The order holds across all heterogeneities except when marked with an asterisk. The parameters used are those found in table A.8.

as they may be good foci for control measures. As such, figure 6.9 shows the prioritisation of patches for treatment facilities, based on their infected class part resilience, or decontamination facilities, based on their bacterial class part resilience. We see that, at both equilibria, treatment facilities should be placed in the highest contact rate/density peripheral patches and centre whereas decontamination facilities should be placed in the lowest contact rate/density peripheral patches. Therefore, the agreement with the simulation results is only in the case when decontamination facilities are placed pre-emptively at endemic equilibrium and treatment facilities are placed at disease free equilibrium. The exceptions in the ordering occur for the treatment and decontamination facilities at endemic equilibrium when contact rates are heterogeneous and for the decontamination facilities at disease free equilibrium when contact rates and densities are heterogeneous.

Table 6.15 shows the optimal distributions of control facilities to maximise the system resilience or sum of part resiliences for the infected classes. There are ten distributions that maximise the system resilience but do not minimise the epidemic size at disease free equilibrium. At endemic equilibrium six reactively placed distributions and 11 pre-emptively placed distributions maximise the resilience but do not minimise epidemic size. There are six distributions that maximise the sum of the part resiliences for the infected classes but do not minimise epidemic size. The distributions that minimise the system resilience and epidemic size also minimise the part resiliences except for nine reactively placed distributions at endemic equilibrium. There are 17 distributions that maximise the sum of the part resiliences but do not minimise epidemic size.

These results suggest that asymptotic nature of the resilience limits its effectiveness as a measure. There are very few distributions of two control facility types that maximise both the resilience or part resiliences and minimise the epidemic size, see tables D.6 and D.5 in the appendix. These distributions may speed the return to equilibrium but the analysis fails to take into account the intermediate infections. This leads to it failing to predict the optimal distributions of treatment facilities which have complex effects due to the weighting bias. The weighting bias plays a role as the resilience is a more effective indicator of optimal distributions of decontamination facilities, which do not have any weight scaling attached to them. We examine the reactivity to account for these transient dynamics.

156

(a) Resilience

(b) Part resilience

Table 6.15: Optimum distributions of one control facility type in a city structured by a heterogeneity. The optimisation maximises the resilience (6.15a) and the sum of the infected class part resiliences (6.15b). The parameters used are those found in table A.8 at DFE and EE. Larger circles denote higher contact rates/ densities. The shaded cells indicate those distributions also minimise epidemic size at disease free equilibrium (blue) and at endemic equilibrium when placed pre-emptively (yellow) or when placed reactively (green).

6.3.4.2 Reactivity

The reactivity measures the maximum possible initial amplification of a perturbation to the system. A positive reactivity suggests that if the system is perturbed at equilibrium it will initially move further away even if that equilibrium is stable. Therefore, the distribution of control facilities that minimises the reactivity limits the growth of any perturbation to the system. We first examine the contribution of each infected class to the reactivity in the absence of control.
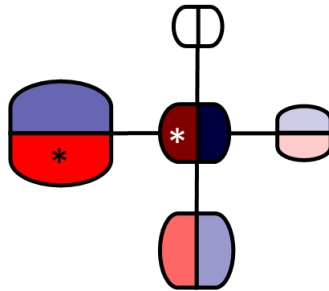
Figure 6.10: Prioritisation order for treatment, in red, and decontamination, blue, where a darker shade indicates a higher priority. Patches are prioritised by part reactivity at disease free and endemic equilibrium in each patch of a city structured by a heterogeneity. The order holds across all heterogeneities except when marked with an asterisk. The parameters used are those found in table A.8.

In figure 6.10, we examine the ordering of patches based on their part reactivities for the infected and bacterial classes. We see the same prioritisation at both disease free and endemic equilibrium. That is, facilities should be placed in the centre patch and then the highest density/contact rate peripheral patches. This agrees with the simulation results perfectly for the decontamination facilities placed at disease free equilibrium and reactively at endemic equilibrium. However, the simulations suggested the treatment facilities should be placed in the centre and then lowest density/contact rate peripheral patches. Thus, the part reactivities are less good as indicators of the optimal placement of treatment facilities.

We now examine the optimal distributions found by exhaustive search to minimise the system reactivity and the sum of the infected class part reactivities and their agreement with the distributions that minimise epidemic size in table 6.16.

Firstly, there are a number of situations where the distributions that minimise the reactivity do not minimise the epidemic size; namely ten at disease free equilibrium, 15 at endemic equilibrium when placed pre-emptively and nine when placed reactively at endemic equilibrium. Similarly, there are distributions that minimise the sum of the part reactivities but not epidemic size; specifically nine at disease free equilibrium, 19 pre-emptively placed and 18 reactively placed at endemic equilibrium.

This leads us to the distributions of two control facility types that minimise the reactivity or sum of part reactivities and epidemic size.

In some situations, we see more agreement between those distributions that minimise the system reactivity and epidemic size when two control facility types are placed, see table 6.17. There are only three distributions that do not minimise both reactivity and epidemic size at disease free equilibrium or when placed reactively at endemic equilibrium. However, no distributions minimise reactivity and the sum of the part reactivities when placed pre-emptively at endemic equilibrium, see table D.3 in the appendix. The distributions that minimise the sum of the part reactivities also do not minimise epidemic size when placed pre-emptively, see table D.4. However, at

(a) Reactivity   (b) Part reactivity

Table 6.16: Optimum distributions of one control facility type in a city structured by a heterogeneity. The optimisation minimises the reactivity (6.16a) and the sum of the infected class part reactivities (6.16b). The parameters used are those found in table A.8 at DFE and EE. Larger circles denote higher contact rates/ densities. The shaded cells indicate those distributions also minimise epidemic size at disease free equilibrium (blue) and at endemic equilibrium when placed pre-emptively (yellow) or when placed reactively (green).

Table 6.17: Optimum distributions of two control facility types in a city structured by a heterogeneity. The optimisation minimises the system reactivity. The parameters used are those found in table A.8 at DFE and EE. Larger circles denote higher contact rates/ densities. The shaded cells indicate those distributions also minimise epidemic size at disease free equilibrium (blue) and at endemic equilibrium when placed pre-emptively (yellow) or when placed reactively (green).

disease free equilibrium, there are 18 situations and at endemic equilibrium there are six situations when reactively placed distributions minimise both the epidemic size and the sum of the part reactivities, see table 6.18.

Table 6.18: Optimum distributions of two control facility types in a city structured by a heterogeneity. The optimisation minimises the infectious class part reactivities. The parameters used are those found in table A.8 at DFE and EE. Larger circles denote higher contact rates/ densities. The shaded cells indicate those distributions also minimise epidemic size at disease free equilibrium (blue) and at endemic equilibrium when placed pre-emptively (yellow) or when placed reactively (green).

The reactivity is a successful measure when predicting the optimal distributions of control facilities at disease free equilibrium and at endemic equilibrium when facilities are placed reactively. This is particularly the case when two control facility types are placed. However, the analysis is not effective when considering pre-emptively placed control facilities. This is as the reactivity examines the maximum possible spontaneous amplification of perturbations to the system. It does not measure the return to equilibrium after this amplification. Therefore, the distributions we see are best at minimising this initial *potential* growth of the perturbation but do not take into account limitations imposed by the size of the susceptible population for example. The reactivity is also not a good indicator of the optimal distributions of treatment facilities. This is because it only partly takes the edge weight scaling into account. The distributions will reduce the initial growth of a perturbation. However, they will not safeguard against a rise in secondary infections. It is also worth noting that the part reactivities for the infected classes are less effective at predicting optimal distributions of control facilities. Therefore, we may consider the system reactivity a better measure of the instantaneous dynamics at the beginning of the epidemic than its decomposition.

6.4 Discussion

We sought alternative methods to find optimal distributions of control facilities to minimise epidemic size. We described a number of analyses that gave information on the state of the system before the flood; the response of the system to the flood and the way the system returns to steady state following the flood. Together, these analyses should outline all disease dynamics of the system relating to the flood.

The analyses that examined the state of the system before the flood were the reproduction numbers, endemic prevalence and population proportion of susceptible individuals at endemic equilibrium. The reproduction numbers, R_0 and R_E, were particularly effective when used with exhaustive search as the distributions of control facilities that minimised them also minimised epidemic size in almost every case. They are also effective when prioritising the patches for decontamination facilities but not treatment facilities. The part reproduction numbers for the infected classes were similarly effective as measures of the optimal distributions of control facilities. The reproduction numbers

describe the risk of an epidemic and the growth of one should it occur. Therefore, they are directly related to the initial number of infections which can dictate the final epidemic size.

We assessed the endemic prevalence and population proportion of susceptible individuals at endemic equilibrium through the agreement between the distributions that optimise them and the distributions that minimise the epidemic size. We compared those distributions that minimise the endemic prevalence and maximise the proportion of susceptible individuals at endemic equilibrium with distributions that minimise the epidemic size at disease free equilibrium and when placed reactively at endemic equilibrium. We also compared those distributions that minimised the proportion of susceptible individuals with those that minimised the epidemic size when placed pre-emptively at endemic equilibrium. The proportion of susceptible individuals was the most effective indicator in all cases as a high proportion can only mean few infections have occurred and a low proportion means a low capacity for further infections. The proportion of infected individuals was slightly less informative as a low prevalence can either mean few infections or many recoveries. We also prioritised patches for treatment facilities. However, this was only optimal when one treatment facility was placed.

To take into account the effect of a perturbation on the system at equilibrium, we examined the response to the flood. This was assessed through the impact, sensitivity and influence. All three analyses captured aspects of the dynamics of the system, particularly at disease free equilibrium. There may be issues using the impact and influence away from equilibrium as the method breaks down. However, we may still consider them effective measures of optimal control facility distributions placed at equilibrium. This is also reflected in the prioritisation which was very successful for the impact and influence when decontamination facilities were placed, but was not successful when we used the sensitivity.

Lastly, we examined the system recovery. This was measured through the resilience and reactivity. The resilience is an asymptotic property inversely related to the return time to equilibrium following a perturbation. The ordering indicated by the part resiliences only agreed with the simulation results when decontamination facilities were placed pre-emptively at endemic equilibrium. The distributions that maximise the system resilience or sum of part resiliences for the infected classes minimise the epidemic size in only some situations. Therefore, we consider the resilience an ineffective measure of the optimal distributions of the control facilities to minimise epidemic size. The reason that the resilience does not reliably predict these optimum distributions is that it is an asymptotic property that ignores transient behaviour [94]. Thus, the epidemic, which can be entirely classed as transient behaviour, is not adequately measured by the resilience.

The reactivity, in contrast to the resilience, only measures transient behaviour. Specifically, the reactivity gives the maximum possible instantaneous rate of amplification of perturbations to the system [94]. Therefore, it can describe, at the instance of perturbation onset, whether the system strays further from equilibrium or starts to return to it. Generally, it was a more effective measure of optimal control facility distributions than the resilience. For instance, it accurately indicates the optimal patch ordering for decontamination facilities. However, neither reactivity nor part reactivities were 100% efficient measures, particularly when control facilities were distributed pre-emptively. The reason for this is that the reactivity is a measure of possibility; given all possible initial perturbations, what is the *maximum possible* amplification. Therefore, there may be initial conditions where the perturbation is not amplified to the same extent and the reactivity is not a true representation of the behaviour. It is for this reason that the reactivity is not the best measure of control facility distributions to

minimise epidemic size.

6.5 Conclusion

We set out to find alternative methods to assess distributions of control facilities to minimise epidemic size. In many ways, we were successful. The distributions that minimise the reproduction numbers which describe the rate of growth of an epidemic, match those that minimise the epidemic size. Therefore the traditional indicators of epidemic severity are still valid here. However, we have also had some success with measures not traditionally used in epidemiological models. The impact is a concept borrowed from ecology; but it was an effective indicator of the optimal distributions of control facilities to minimise the epidemic size at disease free equilibrium and, when placed pre-emptively, at endemic equilibrium. It also gave a good indication of which patches should be prioritised for control facility placement, particularly when the control was decontamination. In a similar manner, the influence gave a good prediction of which patches should be prioritised and which distributions of control facilities were optimal to minimise epidemic size. The sensitivity was less successful in this respect. However, recall that we only seek distributions that minimise epidemic size, not any other beneficial information. Thus, even though the sensitivity does not indicate these optimal distributions it can still give us vital information about the system. Namely, the 'weak links' in our perturbed epidemiological chain. These could then be isolated by reducing patch coupling. This could lead to an interesting exercise in optimising the patch arrangement to reduce sensitivity in 'hot spots'.

The last indicators we examined were the resilience and reactivity. Of the two, the reactivity was the more successful predictor of optimal control facility distributions to minimise epidemic size. However, the resilience may be informative when we examine the long-term dynamics rather than a brief epidemic.

There were no 100% effective measures of the optimal control facility distributions to minimise epidemic size. Of the indicators we examined, the reproduction numbers were the closest to accurate and we could confidently use them to predict 'near' optimal distributions. Similarly, with the susceptible population size at endemic equilibrium. Other indicators such as the impact would need corroboration before we could be certain of their accuracy and some methods, such as the resilience, may be best avoided in this setting.

Therefore we finish with our decision. In a situation where the model is more complex, spatially segregated and intractable for simulation, which of our alternative methods should we employ to find optimal control strategies? We found that the basic reproduction numbers to be most consistent with their agreement with simulation and so we would conclude they should be used in exhaustive search algorithms for more complicated models. The prioritisation of patches in the absence of control may be used with caution. This is as the method breaks down when the optimal distribution of $n + 1$ facilities does not incorporate that of n facilities. However, the particular requirements of the output would need to be considered as other methods such as the impact could come into their own.

Chapter 7

Systems epidemiology

7.1   Introduction

We have focused on the epidemiological characteristics of systems and effective methods for finding optimal control strategies. However, many of the methods we have adapted are primarily used in systems biology. Here, we consider using the complete systems biology mentality for complex epidemiological models.

Analysis and construction of complex epidemiological models can be disjointed. We consider whether the system-wide approach of systems biology might offer a standardised framework for model development and analysis of complex epidemiological and ecological systems.

The structure of this chapter revolves around figure 7.1. We start by explaining the subject of systems biology and its key methods. Then, we put those methods to the test on a simple epidemiological model. Finally, we compare the new methods with classical techniques to find the scope for 'systems epidemiology'.

7.2   Systems and Synthetic Biology

The fields of systems and synthetic biology are growing at a ferocious rate. Systems biology has been defined as the the study of biological systems before and after genetic or chemical perturbation [3]. It aims to establish computational models that predict the behaviour of a system. Systems biology has also been hailed as an 'emerging field of biological research that aims at systems- level understanding of genetic or metabolic pathways' [100]. There are four properties of particular interest in systems biology: system structures, system dynamics, control methods and design methods [64]. These describe the topology of the systems, interactions and inter-relationships of this topology and the implementation of control strategies to improve the system. Synthetic biology has a less theoretical objective. It applies engineering principles to biology in order to rationally construct complex systems [84]. In other words, it is a method of engineering cellular systems to perform specific functions [102]. Therefore, synthetic biology is the application of systems biology to build systems with preferable qualities.

The stages shown in figure 7.1 show how the different analyses and strategies relate to one another in systems and synthetic biology. We focus on the mathematical modelling area which encompasses parameter estimation and optimisation and we will detail some methods for both.

One of the key approaches of systems biology is the generalisation of a complex system into layers of components each with their own functionality and role. We define this concept now with some examples.
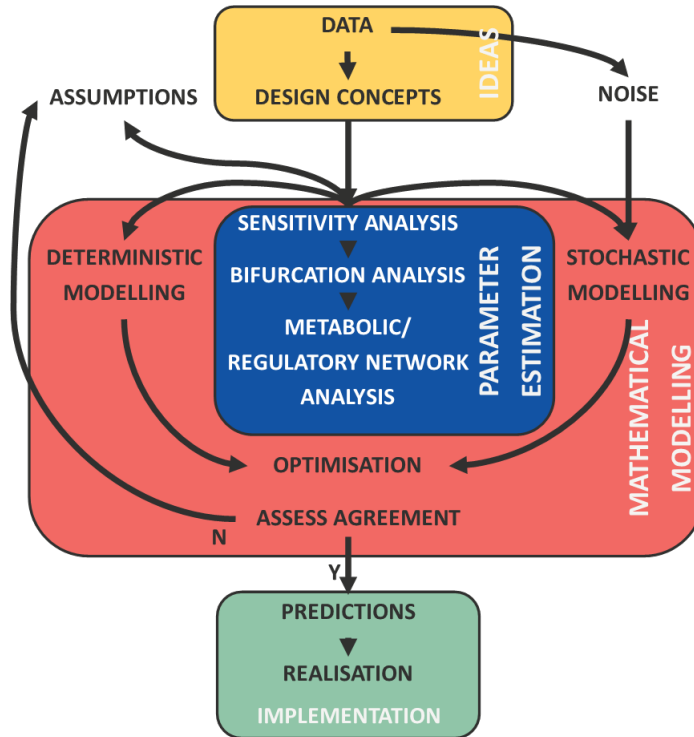
Figure 7.1: Diagram of the role of mathematical modelling and analysis in synthetic biology [147].

7.2.1 Abstraction Hierarchies

A valuable procedure in systems biology is the deconstruction of the model into layers. This leads to an abstraction hierarchy. We can define abstraction hierarchies as 'an assembly of complex systems from orthogonal sub-systems' [20]. They separate a complicated problem and the aim is to have a more manageable system where each layer can be examined independently. Endy stated that the hierarchies should allow individuals to ignore complexities of all levels except the one under examination and allow limited information exchange across levels [39]. This idea is shown in figure 7.2 where the levels are separate except for a small information exchange. The higher levels should hide unnecessary information from lower levels through abstraction [20].

7.2.1.1 Hierarchical levels

The most commonly used level names in abstraction hierarchies are shown in figure 7.2. The layers represent sub-systems with the levels below functioning as part of the levels above. There is a limited exchange of information between layers denoted by the arrows. We conducted a literature review shown in table 7.1 to further define or categorize these levels. Generally, the DNA is just that, the most basic unit of genetic building material. If we use the analogy of a computer chip, the DNA would be the wire. This component forms 'parts' which have a very simple purpose. They are similar to a resistor or bulb in an electrical circuit and can be combined to form 'devices'. Devices are a slightly more complicated functional unit which are akin to a electric circuit. The devices then work together, rather than being actually combined, as a unit with a more complicated function. This is analogous to circuits in a memory chip where the system encompasses the whole chip. Finally, we have a chassis which holds the components. This is the environment in which they work and is akin the actual board that a circuit

is printed on.
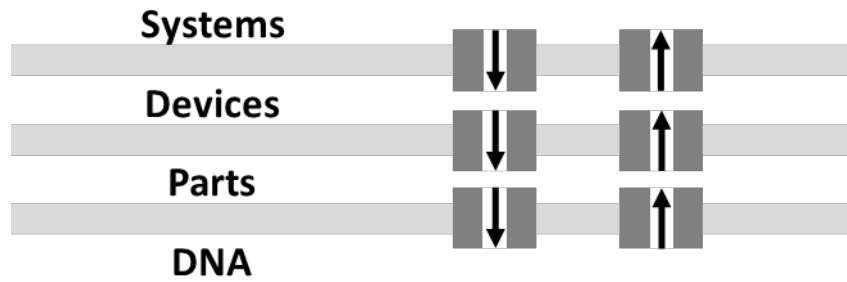
Figure 7.2: Abstraction Hierarchy Diagram for Genetic Systems adapted from the work of Endy [39].

We compare the layers to electrical components as circuits partly inspired systems biology techniques. The final row in table 7.1 is one of engineering definitions and in figure 7.3 we directly compare computing and biology layers.

(a) Computing
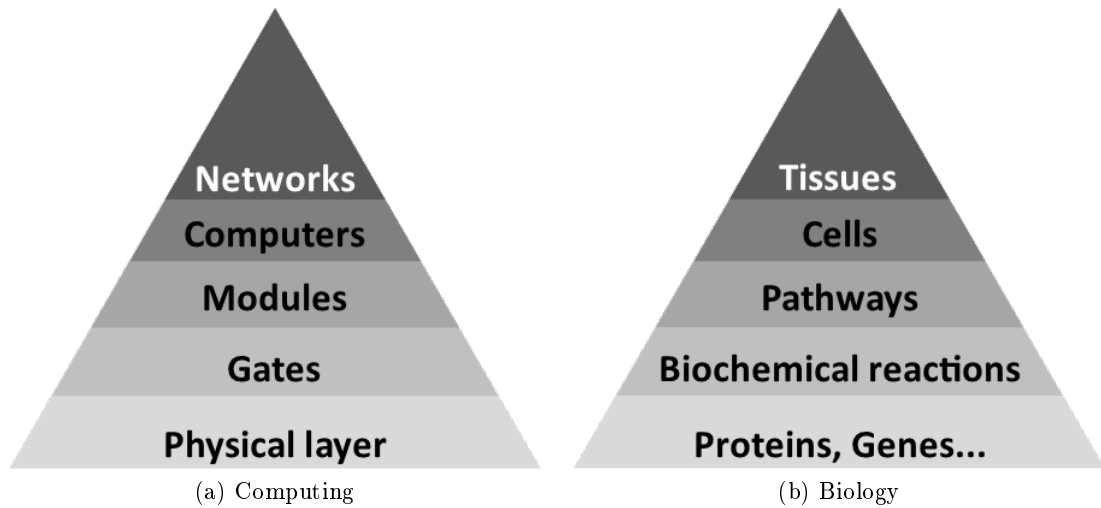
(b) Biology

Figure 7.3: Comparison between computing and biological abstraction hierarchies. [7]

Citation	Definition				
	DNA	Parts	Devices	Systems	Chassis
[39]	Genetic material	Basic biological functions.	Any combination of 'parts' to perform a human-defined function.	Combination of devices.	
[7]	RNA, DNA analogous to transistors, capacitors and resistors.	Biochemical reactions that regulate the flow of information and manipulate physical processes.	Library of biological parts to assemble complex pathways that function like circuits.	Populations of communicating cells or tissues.	
[81]		A single basic biological function e.g. a ribosome binding site.	Parts combined to achieve a single human-defined function.	Combination of various devices to execute a specific task.	A host cell where systems reside which supplies necessary resources.
[56]			Component of some functional interest (physical unit).	Collection parts that operate together and expose a defined functional interface (functional units).	Combinations of devices that realise a final application.
[57]	*Physical layer.*	*Basic components.*	*Basic operations.*	*Protocol units.*	*Lab-on-chip.*

Table 7.1: Table of abstraction hierarchy level definitions The final row corresponds to electrical engineering definitions.

We have examined the various definitions for the levels of an abstraction hierarchy in detail. We now formalise this definition into the following example, shown in figure 7.4:

- DNA: The first level is the smallest unit of construction- the bricks of the system. These should be units of a very basic nature with many possible purposes when combined but almost none individually.

- Part: The next level should have a simple unit purpose, these could be the walls and floors constructed from the bricks. Their purpose should be singular and basic and they should be 'combinable' with each other.

- Device: The walls and floors will now be combined into a house. This is multipurpose unit that works independently, it cannot be functionally combined with other components of the same level but they can work together.

- System: Finally these devices lie in a system, which in the analogy could be a town. The components of this level function together but are independent units.
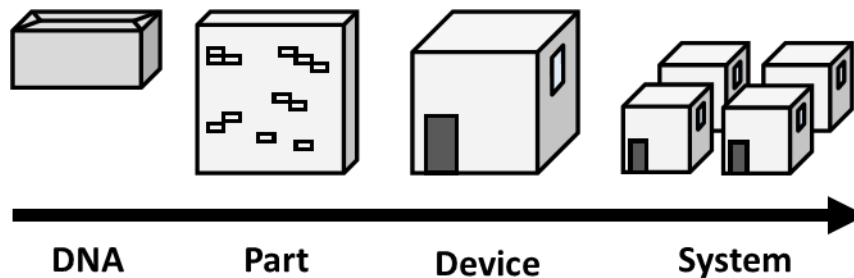
Figure 7.4: Brick abstraction hierarchy example.

7.2.1.2 Biobricks

The best example of abstraction hierarchies in systems biology is shown in BioBricks. BioBricks is a standardised database of biological components. The components in the BioBrick database cover a range of levels in the hierarchy of systems biology (Parts, Devices, Chassis). The parts and devices are ordered by type, function and chassis (although most parts in the database work in E.Coli). All are constructed from the components detailed in table 7.2. A summary of some of these components is shown in table 7.3. Thus, the components in the BioBrick database can be used to build systems such as those in figure 7.5.

Table 7.2: Key for BioBrick components [65].

Component	Meaning	Layer
Terminators	Stops transcription	Part
Protein coding	Alters direction of RNA polymerase coding	Device
Cell strain	Type of cell	Chassis
Reporter	Express proteins, often florescent	Part
Signalling	Allows cells to communicate with other cells	Device
Primer	Directs DNA polymerase where to direct DNA replication	Part
Tag	Forms part of protein coding	Part
Protein generator	Protein coding to enable MRNA expression	Device
Inverter	Outputs repressor concentration	Device
Regulatory / Promoters	Provide RNA polymerase binding regions	Device
Plasmid backbone	Holds components within cell	Chassis

Table 7.3: BioBrick definitions [65].
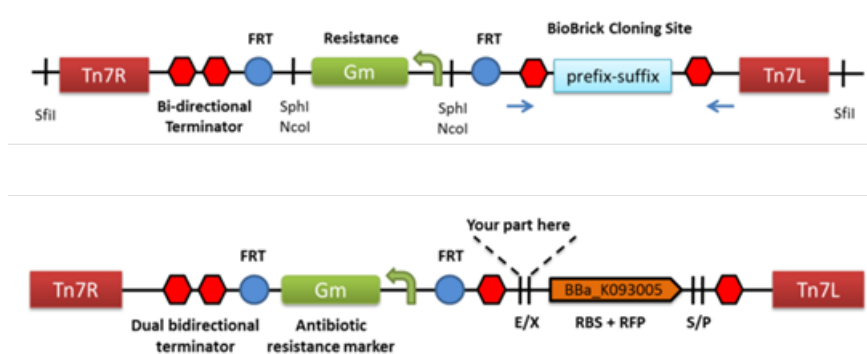
Figure 7.5: Two of examples of BioBrick components [65]. The first is a plasmid BBa_K510000 and the second a composite BBa_K510037.

168

7.2.2 Sensitivity Analyses

One of the key methods of parameter estimation and model analysis is examining the sensitivity of an output to a change in an input, see figure 7.1. We have already used a range of sensitivity analyses to find the important input parameters for our epidemiological model. We divide the analyses into two types of sensitivity: local and global. Local sensitivity is the change in an output given a change in an input at one point in the parameter space. Global sensitivity is a form of average change in output given a change in the input which holds across the parameter space. We shall explain a few of each sensitivity analysis type and, where appropriate, signpost the relevant chapter where we introduced the concept.

7.2.2.1 Local Sensitivity

We examine analyses that may be conducted at specific points in the parameter space. As such, they lead to insights into the input- output relationship which may not hold for all parameter sets. First, we describe two numerical methods commonly used to facilitate sensitivity analyses.

Finite difference approximation We used the finite difference approximation as a method for approximating a derivative in Chapter Three. To calculate a derivative of $f(x)$ from first principles we take the limit of the following $\frac{f(x+h)-f(x)}{h}$ as $h \to 0$. The finite difference approximation assumes $h > 0$ and takes the value of this function rather than its limit to describe the change in output, $f(x)$, given a change in input, x.

Direct differential method The direct differential method is a differential computation method which solves the system equations for the sensitivity coefficients [148]. In this case, it is possible to write a differential equation for the sensitivities, $\mathbf{T}$, in matrix form with respect to the system Jacobian, $\mathbf{J}$, and vector $\mathbf{f}_p$, consisting of $\frac{\partial f_i}{\partial p}$, the derivative of the ODEs with respect to parameter, p.

$$\dot{\mathbf{T}} = \mathbf{f}_p + \mathbf{J} \wedge \mathbf{T}.$$

We may solve the sensitivities of all variables with respect to a parameter simultaneously using this method. It can be improved by a Green's kernel and function, termed an 'adjoint sensitivity analysis'.

Metabolic Control Analysis, MCA MCA is a standard mathematical framework for quantifying the dependence of the network properties on parameters [148]. The general form is the control coefficient defined:

$$C_x^{f(x)} = \frac{x}{f(x)} \times \frac{\partial f(x)}{\partial x}.$$

This class of coefficients includes the elasticity which we used from Chapter Two onwards. However, there are many different control coefficients using the outputs and inputs, detailed in table 7.4. Some of these values hold globally, such as the concentration control coefficients, and some only hold locally, such as the elasticity.

Symbols	Explanation
n	Number of steps (enzymes) in network
J	Flux
M_j	Concentration of metabolite j
v_i	Activity of enzyme i
p	Parameter
$C_{v_i}^x$	Control coefficient of v_i on x
$\epsilon_{M_j}^{v_i}$	Elasticity coefficient of v_i toward M_j
R_p^x	Response coefficient- the relative change in x with p
Definitions	
$C_{v_i}^J = \left(\dfrac{dJ/J}{dv_i/v_i} \right)_{\text{steady state}}$	Flux Control Coefficients (global)
$C_{v_i}^{M_j} = \left(\dfrac{dM_j/M_j}{dv_i/v_i} \right)_{\text{steady state}}$	Concentration Control Coefficients (global)
$\epsilon_{M_j}^{v_i} = \left(\dfrac{\partial v_i/v_i}{\partial M_j/M_j} \right)_{\text{steady state}}$	Elasticity Coefficients (local)
$R_p^J = \left(\dfrac{dJ/J}{dp/p} \right) = \sum C_{v_i}^J \epsilon_p^{v_i}$	Response Coefficients

Table 7.4: Table of control coefficients for Metabolic Control Analysis [63, 70, 115, 148].

7.2.2.2 Global Sensitivity

Table 7.4 demonstrates that MCA can hold globally and locally as a sensitivity analysis. Yet, there are some specifically global sensitivity analyses. These generally begin with a parameter space sampling technique such as Latin Hypercube Sampling, LHS, which we used from Chapter Two onwards.

Weighted Average of Local Sensitivities, WALS WALS is a simple extension of local analyses to the whole parameter space. Local sensitivities are measured at random locations in the parameter space and then weighted using a Boltzman distribution, $\exp(\frac{-E}{k_bT})$ [146, 148]. Here E is the weighted least squares error between the perturbed model and a reference model and k_b is a customisable scaling factor for the sensitivity, **T**. The weight factor for the parameter p in set x_k is as follows:

$$w_p^k = \exp \left(\frac{-E(x_k)}{\min\{E(x_i)\}} \right).$$

Therefore the global sensitivity coefficient of parameter p is defined as:

$$WALS_p = \sum_{k=1}^N T_p^k w_p^k.$$

Where T_p^k is the local sensitivity of the output with respect to parameter p in set k.

Multi-Parametric Sensitivity Analysis, MPSA We introduced the MPSA in Chapter Three to establish which, and for what values, parameters were most influential. The parameter space is sampled and these values are used to calculate the output. The output values for each parameter set are then categorised as 'acceptable' or 'unacceptable' in relation to a user-defined threshold. The frequency of acceptable to unacceptable values is calculated over the range of the input parameter and used to

draw a normalised cumulative frequency graph. The maximum distance between the normalised cumulative frequency graphs for the acceptable and unacceptable values is used as the sensitivity. This is termed a Kolmogorov- Smirnoff statistic.

Partial Rank Correlation Coefficient, PRCC We introduced the PRCC in Chapter Two and used it extensively to find the relationship between inputs and outputs in our model. It holds only when the relationship between input and output is monotonic. We start with a parameter sample and calculate the output for each parameter set. These output values are then ranked by magnitude and the same is done for the input values. The expected values for the ranked inputs and outputs are calculated for each parameter set using a linear regression. This is used to calculate the residuals which are the differences between expected and actual values. Finally, the PRCC is calculated from these residuals and takes values in the range $[-1, 1]$ where a value outside $[-0.5, 0.5]$ is considered significant. The sign of the PRCC indicates the direction of influence.

Fourier Amplitude Sensitivity Test, FAST We examined the FAST in Chapter Three. It is calculated by introducing a frequency into the input and searching for that frequency in the output. The final sensitivity is calculated by dividing the variance of the parameter by the variance of the output. We calculated the FAST using a an adapted version of the program written by Per- Anders Ekström [42].

7.2.3   Bifurcation Analysis

We introduced bifurcation analysis in Chapter Three and used it extensively when the treatment rate of infected individuals was a function of the size of the infected population. We used `MATLAB` and `MATCONT` to chart changes in equilibrium stability to find bifurcation points. These are parameter values where a change of stable state is seen.

7.2.4   Metabolic/ Regulatory Network Analysis

A key method in figure 7.1 is metabolic and regulatory network analysis which examines the topology of the system in order to find pathways and key nodes. We start with a technique for examining metabolite flows through the system at steady state.

7.2.4.1   Flux Balance Analysis, FBA

FBA is a mathematical tool for analysing the flow of metabolites through system networks. Metabolites are the intermediates and products of metabolism. They are a result of enzyme catalysed reactions that occur with the cell [59]. FBA charts metabolite movement at steady state and has the benefit of being computationally inexpensive. It requires only the stoichiometry of the system and demands of the network [101]. The stoichiometry of a reaction details the relative numbers of reactants and products required. It should be noted that the FBA cannot be used to predict specific concentrations of metabolites as it defines the 'best' a system can do [40]. It is also only applicable to the system at steady state [101]. FBA is based on the law of mass conservation and application of optimisation principles. It predicts the optimal distribution of metabolic resources within a metabolic network [119]. The mass conservation equation for a metabolic network is as follows:

$$\frac{d}{dt}\mathbf{X} = \mathcal{S}.\mathbf{v} - \mu.\mathbf{X}.$$

Here, $\mathbf{X}$ is the concentration of internal metabolites and $\mathcal{S}$ is the stoichiometry matrix where s_{ij} is the stoichiometry coefficient of element i involved in reaction j. We also include the vector of reaction rates or fluxes, $\mathbf{v}$, and dilution rate, μ, related to the change in volume in the system [40, 130].

The system is assumed to be at steady state where fluxes for each reaction are maximal and positive and the dilution rate is assumed to be slow with respect to the reaction rates. Thus:

$$\mathcal{S}.\mathbf{v} = 0 \tag{7.1}$$

$$\mathbf{v} \geq \mathbf{0} \tag{7.2}$$

Equations 7.1 and 7.2 give an under-determined system which can be solved by three techniques:

1. Metabolic Flux Analysis

   Here, the equations are divided into measurable, subscript m, and unmeasurable, subscript u, coefficients or fluxes. The non-singular nature of $\mathcal{S}$ is utilised in order to solve the equation for the unmeasured fluxes like so:

   $$\mathbf{r}_u = -\mathcal{S}_u^{-1}\mathcal{S}_m.\mathbf{r}_m.$$

2. Flux Balance Analysis

   FBA examines the intersection of the nullspace of $\mathcal{S}$ and the area defined by the inequalities, the *feasible set*, using linear programming. This is done by first defining an objective function, $\mathbf{Z}$, to show how much each reaction contributes to the overall behaviour of the system [101]. It is defined as follows:

   $$\mathbf{Z} = \mathbf{c}.\mathbf{v}. \tag{7.3}$$

   Here, $\mathbf{c}$ is the vector of weights for the linear combination of fluxes. For example, if the aim was to target reaction one, the vector of weights would be a unit vector with first element equal to one.

   The linear programming problem in canonical form is as follows:

   $$\begin{aligned}
   \text{maximise} \quad & c^T\mathbf{v}, \\
   \text{subject to} \quad & \mathcal{S}\mathbf{v} = 0, \\
   \text{and} \quad & \text{lower bound} \leq \mathbf{v} \leq \text{upper bound.}
   \end{aligned}$$

   Where the upper and lower bounds are determined by the minimal and maximal fluxes for each reaction in the system.

   Once this problem has been formulated and the feasible set defined in flux space, the system can be solved using linear programming software such as LINDO [40].

The solution of the FBA is an optimal solution for the system. However, it is not unique. Thus, for a complete set of solutions in the feasible set, Metabolic Pathway or Elementary Mode analyses are required as well.

3. Metabolic Pathway Analysis

   One such metabolic pathway analysis is elementary mode analysis explained in the next section.

7.2.4.2 Elementary Mode Analysis, EMA

EMA is a form of metabolic pathway analysis that identifies structure in a metabolic network. The analysis begins with the problem formulated in equations 7.1 and 7.2. This identifies all metabolic flux vectors in the admissible flux space. The admissible space (also know as the feasible set) is a convex polyhedral cone and each solution contained in the cone is an *Elementary Mode*. Each mode is a unique and minimal set of enzymes that support steady state operation [130]. However, there is a subset of this defined as *Extreme Pathways*. Extreme pathways are the set of independent elementary modes that span the polyhedral cone and can be used to define the admissible flux space. We can consider the extreme pathways as the basis for the admissible flux space.

This analysis technique has been used to engineer a strain of E. coli to simultaneously utilize xylose and glucose to produce ethanol. EMA has also been used to identify a minimum set of metabolic pathways that support growth and ethanol production by reaction deletion in E. coli [80].

7.2.4.3 Combining Pathway and Flux Balance Analyses

The equations 7.1 and 7.2 lead to the definition of a flux space within the context of convex analysis. As previously mentioned, this admissible flux space is a polyhedral cone spanned by the extreme pathways of the system; they form the edges of the cone [119]. Thus, one approach for identification and analysis of the system is to use convex analysis tools such as elementary modes and extreme pathways to define limitations and production capabilities. The theory starts similarly to before. The system is described by a series of ordinary differential equations representing the dynamic mass balances for each metabolite. Once this is complete, the system is assumed to be at steady state and equation 7.1 is arrived at. Then the constraints are added as before in equation 7.2 where any reversible reaction is decomposed into two reactions to retain positive rates for all reactions. Next, the admissible flux space cone $\mathbf{A}$ is defined:

$$\mathbf{A} = \{\mathbf{v} : \mathbf{v} = \sum_{i=1}^{k} w_i \mathbf{p}_i, w_i \geq 0 \quad \forall i\}. \tag{7.4}$$

In equation 7.4, w_i are coefficients for each of the convex spanning vectors $\mathbf{p}_i$, the extreme pathways. As the admissible flux space is defined in this way, any flux distribution will be a linear combination of the extreme pathways.

The next stage is to assess the system performance to demands. This leads to the addition of an exchange flux and corresponding constraints to the system of equations. In doing so, the same or increased number of extreme pathways is arrived at for the new balanced set of demands. These new pathways form a higher dimensional cone that can be projected onto the original one. In this case the new extreme pathways can be written in terms of a linear combination of the old which is termed an equivalency. Equivalencies allow flux distributions to be written in terms of pathways that produce a distribution pattern.

Now that the flux cone is fully defined, the area within must be assessed. This leads to the use of flux balance analysis on the (now bounded) cone. The problem is formulated as before and solved through linear optimization to give a distribution that is a linear combination of the extreme pathways. More specifically, the flux distribution lies on the extreme edges of the cone (a simple example is shown by Schilling et al. [119]). This means that changing demands on the system lead to movement of a flux distribution across the faces of the flux cone and optimal solutions will be found on the vertices.

We have considered the analysis techniques. Now, we examine methods for improving the system.

7.2.5 Optimisation

We focus on evolutionary algorithms as an efficient way of improving a system with respect to a specific objective. Initially, the system has an arbitrary set of characteristics and is developed step by step until it has certain desirable properties. The steps of one such an algorithm are as follows, we use a similar algorithm later, [46, 125]:

1. **Initial network set** A set of independent systems are generated.

2. **Growth Phase** The set grows in size as each system in the original set is altered at random following one or two simple rules. These rules could be one of the following:

   (a) Modified degradation rate (there may be several and one will be chosen at random).
   (b) Modified kinetic constant.
   (c) New gene created.
   (d) New interaction between gene and promoter.
   (e) Post-transcriptional reaction added.

   These are specific to designing genetic networks but it is possible to generalise them.

3. **Selection Phase** The assessment of each network takes place based on a specific fitness function. Once each network has been assessed, the 'worst' proportion of the set will be deleted and the algorithm repeats.

There are a number of ways of expediting this process. Haseltine and Arnold suggest using the sensitivity and bifurcation analyses to find targets for improvement [61]. Thus, influential parameters or structures can be prioritised for mutation. Batt et al. advocate discretisation of the system [13]. This is similar to examining a continuously heterogeneous population as a number of separate sub populations with different characteristics. It allows a greater flexibility when conducting robustness analyses whilst relating to characteristics of the original system.

There are a variety of computing programs designed with optimal regulatory networks in mind. `MATLAB` has a genetic programming toolbox and can be used with RoVerGeNe (Robust Verification of Gene Networks) to model genetic systems [46]. Genetdes works in C as a simulated annealing algorithm to find specific behaviour in a genetic system [114]. There is also BioJade, a graphical design algorithm in JAVA specifically for synthetic biology use [52]. This simulates designs based on a library of parts. However, the modification of systems in these methods can come with its issues.

There is always the possibility of creating physically impossible arrangements and so rigorous checks must be carried out [79].

7.3 Systems epidemiology

We have detailed the key systems biology methods. Now, we use an example of a simple epidemiological model to examine how the system epidemiology could work [19, 18]. Recall, we wish to see how the systems biology framework could facilitate epidemiological model construction and analysis. Therefore we investigate the new insights brought by these methods. The differential equations for the example model are as follows:

$$\dot{s} = \mu N - \beta si - \mu s,$$
$$\dot{i} = \beta si - \gamma i - \mu i,$$
$$\dot{r} = \gamma i - \mu r.$$

The variables s, i and r correspond to the susceptible, infected and recovered populations respectively. The parameters μ, N, β and γ represent the death/ birth rate, total population size, contact rate and recovery rate. We assume the population size is constant with $N = s + i + r$. We now consider the reactions or transitions in the system to formulate this in a metabolic or regulatory network form. These reactions as follows:

$$r_1 : \rightarrow S,$$
$$r_2 : S + I \rightarrow I + I,$$
$$r_3 : S \rightarrow,$$
$$r_4 : I \rightarrow R,$$
$$r_5 : I \rightarrow,$$
$$r_6 : R \rightarrow .$$
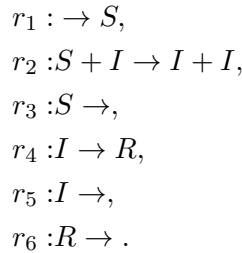
These reactions allow us to reformulate the differential equations as metabolic equations. In this setting we focus on the concentration of our 'metabolites', S, I and R, denoted by $\|S\|, \|I\|$ and $\|R\|$. Coefficient, k_{r_i}, is the reactivity the reaction i or the rate at which reaction i occurs. The metabolic equations are:

$$\Delta\|S\| = k_{r_1} - k_{r_2}\|SI\| - k_{r_3}\|S\|,$$
$$\Delta\|I\| = k_{r_2}\|SI\| - k_{r_4}\|I\| - k_{r_5}\|I\|,$$
$$\Delta\|R\| = k_{r_4}\|I\| - k_{r_6}\|R\|.$$

We start with the abstraction hierarchy.

7.3.1 Abstraction hierarchy

This model represents one device layer of the hierarchy. We could consider the individuals as the layer below which we have averaged to form our device layer. The layer above could be a composite population, a metapopulation. The real benefits of abstraction hierarchies would come when the model becomes increasingly complex and we may use many modules of the form of our simple example model to build a composite system.

175

Next, we examine the sensitivity analyses applied to the differential equations. We shall also examine R_0 and r for this model, given by $R_0 = \frac{\beta N}{\gamma + \mu}$ and $r = \beta N - (\gamma + \mu)$.

7.3.2 Sensitivity

7.3.2.1 Local Analyses

We examine the sensitivities that apply at one point in the parameter space. We begin with most basic measure of sensitivity, the partial derivative.

Partial Derivative The sensitivity of an output to an input at one point is traditionally the partial derivative at that point. We utilised this method as part of the elasticity which is scaled. As such, we have not used the sensitivity as it does not allow parameters with different scales to be compared. However, for completeness, the sensitivities, T, of R_0 with respect to each parameter are:

$$T_N = \frac{\partial R_0}{\partial N} = \frac{\beta}{\gamma + \mu},$$
$$T_\beta = \frac{\partial R_0}{\partial \beta} = \frac{N}{\gamma + \mu},$$
$$T_\gamma = \frac{\partial R_0}{\partial \gamma} = \frac{-\beta N}{(\gamma + \mu)^2},$$
$$T_\mu = \frac{\partial R_0}{\partial \mu} = \frac{-\beta N}{(\gamma + \mu)^2}.$$

Therefore, if the parameters take the following values, $N = 1$, $\beta = 1$, $\gamma = 0.8$ and $\mu = 0.0001$, the local sensitivities are as follows:

$$\frac{\partial R_0}{\partial N} = 1.25,$$
$$\frac{\partial R_0}{\partial \beta} = 1.25,$$
$$\frac{\partial R_0}{\partial \gamma} = -1.6,$$
$$\frac{\partial R_0}{\partial \mu} = -1.6.$$

Thus, we see at this point that γ and μ have a negative effect on R_0 with the same magnitude and β and N a positive impact. If we calculated the elasticities for these parameters we would have the following values for each parameter: N, 1; β, 1; γ, -1 and for μ, -1×10^{-4}. The elasticities are far more comparable and representative of the influence of each parameter. We also consider related quantities in the metabolic control analysis.

Direct Differential Method The direct differential method formulates the calculation of the sensitivities as a matrix equation. Once again, T represents the sensitivity, p is an arbitrary parameter and f is defined as the function satisfying $R_0 = f(N, \beta, \gamma, \mu)$. Thus the matrix equation becomes:

$$\dot{T} = f_p$$

Therefore, in this simple case, the sensitivities are the same as the partial derivatives.

Metabolic Control Analysis, MCA   The advantage of all MCA is that the sensitivities are non-dimensionalised. As such, we may compare the effect of inputs on an output even if those inputs are on different scales.

We consider the response coefficients, defined in table 7.4, for our simple model. These coefficients find the elasticity of the flux with respect to the system parameters. We must define the flux for our epidemiological system. The flux represents a flow and as we are interested in the number of infections, we define the flux as a flow of infected individuals; this is the intrinsic growth rate of the epidemic. We examined the elasticity of the intrinsic growth rate with respect to the system parameters in Chapter Two and Three. In the SIR case, the response coefficients are:

$$r = \beta N - (\gamma + \mu)$$
$$R_r^N = \frac{\beta N}{\beta N - (\gamma + \mu)},$$
$$R_r^\beta = \frac{\beta N}{\beta N - (\gamma + \mu)},$$
$$R_r^\gamma = \frac{-\gamma}{\beta N - (\gamma + \mu)},$$
$$R_r^\mu = \frac{-\mu}{\beta N - (\gamma + \mu)}.$$

Thus, if the values of the inputs are taken as before ($N = 1, \beta = 1$, $\gamma = 0.8$ and $\mu = 0.0001$) the response coefficients are:

$$R_r^N = 5,$$
$$R_r^\beta = 5,$$
$$R_r^\gamma = 4,$$
$$R_r^\mu = -5 \times 10^{-4}.$$

Therefore, the intrinsic growth rate depends most on the total population size and contact rate at this point in parameter space.

There are many other coefficients in metabolic control analysis. In order to use these, we first define the activity of an enzyme in terms of an epidemiological system. This is discussed further in the Comparison.

7.3.2.2   Global Analyses

We now look at analyses that hold across the parameter space. As such, we start by sampling the parameter space using Latin Hypercube Sampling. For the following analyses, we hold the population size at 1. The chosen ranges for the other parameters

are $\beta \in [0, 2]$, $\gamma \in [0, 1]$ and $\mu \in [0, 0.1]$ and the distributions are assumed to be uniform so as not to under-sample any part of the parameter space. These ranges are sampled five times and permuted to form the matrix L below (the rows correspond to the parameters in the order β, γ, μ).

$$L = \begin{bmatrix} 0.0135 & 1.1613 & 1.1585 & 1.1855 & 1.1208 \\ 0.5204 & 0.8638 & 0.1324 & 0.2942 & 0.1919 \\ 0.0094 & 0.0014 & 0.0076 & 0.0090 & 0.0083 \end{bmatrix}$$

Weighted Average of Local Sensitivities, WALS WALS uses the local sensitivities at points throughout the parameter space and weights them using the Boltzman distribution. We shall use the partial derivatives of R_0 as our sensitivities. The Botzman distribution depends on the weighted least squares error, E. In the following, with no experimental data, E will be assumed the same for all parameter sets. The weight factor follows the form mentioned in section 7.2.2.2. In this case, the weight factor is e^{-1} for all sets and so the WALS for R_0 with respect to β, γ and μ are as follows,

$$WALS_p = \sum_{k=1}^{N} T_p^k e^{-1},$$
$$WALS_\beta = 0.4598,$$
$$WALS_\gamma = -0.5886,$$
$$WALS_\mu = -0.5886.$$

In this case, the analysis suggests that γ and μ are more influential than β. However, the assumption of equal weighting for each set is not realistic. To improve this, one could weight the sets depending on whether $R_0 > 1$ or $R_0 < 1$ for example.

7.3.3 Metabolic/ Regulatory Network Analyses

We defined the model in terms of concentrations of our 'metabolites' or reactants, S, I and R. We will now state the stoichiometric matrix in order to conduct the flux and elementary mode analyses.

7.3.3.1 Flux Balance Analysis

The first stage with this methodology is to define the stoichiometric matrix, $\mathcal{S}$. In the case of the epidemiological model, there are three 'reactants' and six reactions. The stoichiometric matrix takes the following form with the columns as reactions and the rows as reactants [68].

$$\mathcal{S} = \begin{bmatrix} 1 & -1 & -1 & 0 & 0 & 0 \\ 0 & 1 & 0 & -1 & -1 & 0 \\ 0 & 0 & 0 & 1 & 0 & -1 \end{bmatrix}$$

Now $\mathcal{S}$ is defined, we may formulate the problem in the format of equations 7.1 and 7.2. We consider how to optimise the recovery rate. Thus, we define an objective function with weight vector, c, as a unit vector in the direction of interest, the recovery transition,

$$\mathbf{c} = \begin{bmatrix} 0 \\ 0 \\ 0 \\ 1 \\ 0 \\ 0 \end{bmatrix}.$$

Thus, the problem is:

$$
\begin{array}{ll}
\text{Maximise} & v_4, \\
\text{subject to} & \mathcal{S}.\mathbf{v} = 0, \\
\text{and} & \mathbf{0} \le \mathbf{v} \le \mathbf{1}.
\end{array}
$$

We solve this problem using linear programming in LINDO. The solution is reaction rates 1,2,4 and 6 equal to 1 and all others zero. Therefore, the objective function is equal to one. The interpretation is that the birth rate, rate of infection, recovery rate and recovered individual death rate are all maximised. As such, to maximise the recovery of individuals, we must maximise the production of infected individuals. Whilst this is not an 'optimal' solution in terms of controlling an epidemic, it does demonstrate how we can define an aim and use FBA to show us the pathway to that aim. However, we must carefully specify the problem.

7.3.3.2   Elementary Mode Analysis

We use the software `METATOOL` to calculate the elementary modes. This works within `MATLAB` and is freely available [2, 108]. The inputs used for the computation of the elementary modes are the stoichiometric matrix and a row vector denoting the reversibility of each reaction. However, it is possible to create a `METATOOL` file with the full network details or a SBML model. The elementary mode matrix for the system is,

$$\begin{bmatrix} 1 & 1 & 1 \\ 1 & 1 & 0 \\ 0 & 0 & 1 \\ 0 & 1 & 0 \\ 1 & 0 & 0 \\ 0 & 1 & 0 \end{bmatrix}.$$

Recall, an elementary mode is a minimal set of reactions that allow steady state operation. Therefore, the following elementary modes contain the possible reaction combinations occurring at steady state:

$$
\begin{aligned}
& \rightarrow S \rightarrow I \rightarrow, \\
& \rightarrow S \rightarrow I \rightarrow R \rightarrow, \\
& \rightarrow S \rightarrow .
\end{aligned}
$$
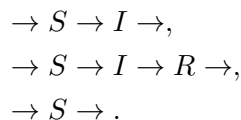
The first two pathways correspond to endemic steady state where an individual is born, infected and dies or they are born, infected, recover and then die. The third pathway corresponds to disease free steady state where an individual is born and then dies naturally.
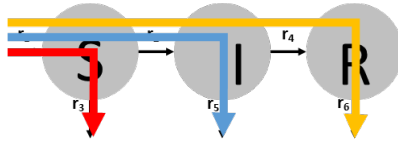
Figure 7.6: Elementary pathways for SIR model. Pathway 1: red, 2: blue and 3: yellow.

7.3.3.3 Combining Pathway and Flux Balance Analyses

We have examined the elementary modes and the fluxes that maximise the recovery reaction and keep the system balanced. However, we can relate the two. The FBA suggested we should maximise the reactions in $\to S \to I \to R \to$ to maximise recovery rates. Thus, the optimal pathway distribution is $0 \times p_1 + 1 \times p_2 + 0 \times p_3$. However, if we wanted to answer a slightly more complicated question on more complicated network, the optimal combination of pathways would be altered. Schilling et al. examined how the distribution of fluxes and pathways through the system are altered by different constraints and structures [119].

7.3.4 Optimisation

We used a very simple evolutionary algorithm on our SIR model to find the optimal parameter combination when there was a fixed population size. We follow the algorithm explained by Spears et al. [125].

1. Initialising

   The set of initial networks is specified by the user or randomly generated.

   In our `MATLAB` code, the parameters for the SIR model were randomly generated. The parameters of interest are γ, β and μ and the values were generated in a Latin Hypercube with ten samples.

2. Evaluation of Population

   We use a specific fitness function. The function scores each system based on how well it fits with the desired outcome. It also suggests which systems would be best to act as 'parents' to new 'children' in the population.

   In our example, the fitness function was the total epidemic size over 100 days. Thus, the parameter values are inputted into the ODE system and solved. The 'score' that was assigned was the total number of infected individuals over the course of the epidemic. The start point for the solution for the ODEs is the disease free equilibrium with one infected individual introduced and a total population size of 1000. The final population size is then calculated as the number of individuals infected over that timespan using an extra compartment in the model, as in previous chapters.

3. Parent Selection

   Now the test systems have all been evaluated, the 'best' can be chosen to become parents. These are then averaged or elements of each are used to create new children in the population. The idea is that their suitability is carried on and increased in the children.

   We chose the 'best' four parameter sets i.e. those with lowest epidemic size.

4. Children through Recombination

   Once the parents are chosen they are recombined to produce children.

   In our example, the parameter values of the 1st and 4th and the 2nd and 3rd best systems are averaged in their children. The children are then added to the set of possible parameter sets.

5. Children through Mutation

   In order to stop the 'gene pool' stagnating with a narrowing range of values, children are also added by mutation. This could occur through a new random set of parameters being chosen or through permutation of an existing set.

   We introduced new, random parameter sets to create two new children.

6. Re-evaluation and Survival

   After the new children are added to the population the whole population is assessed again and the weakest chosen for deletion.

   The highest scoring elements were chosen and deleted. This means that the parameter sets that produced the most infected individuals over the course of the epidemic were deleted. At this point, the process repeats.

7. Desired Outcome

   The outcome after a number of iterations is hopefully a system or population with the required properties.

   We continued until there was a parameter set leading to an epidemic size of less than ten individuals. This is considered our optimal parameter set. The best parameter selection here was $\beta = 0.8602$, $\gamma = 0.6081$ and $\mu = 0.0014$. It took 23 iterations and 98 seconds to arrive at this conclusion. However, it will not always be the case as it depends on how close the starting set of systems is to the goal set.

The simplicity of the model illustrates the methods and begins to illustrate the issues. It takes 98 seconds to run this algorithm if only 23 iterations are needed. However, on another run, 73 iterations were required and this took five minutes. As the systems under test become more complicated, the time of each iteration will increase. Therefore reducing the number of iterations will become more important. We detailed a number of methods for targeting areas for improvement and speeding the process. Therefore, if we considered more complicated structures and possible changes, we could employ these techniques to get a head start on calculating the optimal system.

7.4 Comparison

There have been many methods that we used for our epidemiological model analysis that are also used in systems biology. We measured the sensitivity of our system in a variety of ways. We examined the relation between input and output at points across the parameter space with an elasticity analysis; an element in metabolic control analysis. The speed of this calculation was improved by approximating the derivative with a finite difference approximation. We examined the global sensitivity using three separate methods, all with their individual benefits. The PRCC gave us insight into the magnitude and direction of influence of an input on output. Whereas, the FAST allowed us to see correlation without the need for a monotonic input-output relationship. The MPSA

highlighted influential areas of the parameter space. We have also extensively used bifurcation analysis when examining the complicated dynamics introduced by a limited capacity for treatment. Therefore, we have already exploited some of the intersecting methodologies between epidemiology and systems biology.

We feel there is great opportunity for further use of systems biology techniques in epidemiological model analysis. The example of a simple SIR model has allowed us to examine these techniques in a familiar setting but there is more to be said. Firstly, the concept of abstraction hierarchies could be explored to a much greater extent. We may consider how a model such as this one could be abstracted into layers with a limited exchange of information. We start with the most basic layer, the DNA which forms all layers above. In a human population, the DNA could be considered the individuals themselves. Thus, on this layer we examine the individual transition through disease classes. Using the individual as our start point, there are a few places we could move next. We could examine households or neighbourhoods of individuals and their intersection. In essence, this is considered a metapopulation with each patch a sub-population of individuals. At this stage, we need not think about the individual transitions but rather the average dynamics over each sub-population. From here we could consider cities where each city is linked by a small transport link. The group of cities would form the system. Therefore there are three different modelling techniques that could be employed separately to different components in an epidemiological database. The idea of a database of standard epidemiological components and their interactions is an attractive one and could be used to form a composite picture of the epidemiological dynamics. This picture could then be used for simulation, sensitivity or pathway analysis.

There are number of sensitivity analyses that we used in our work. However, there are a few methods left unexplored such as the alternative control coefficients. We used the elasticity coefficients as a measure of the sensitivity throughout our work. The flux control coefficients and concentration control coefficients could be useful in their own right with the right definitions. We already drew a parallel between our variables S, I and R and the metabolites of the system, and the flux with the epidemic growth rate. Yet, we could also examine the effect of an 'enzyme' on the system. An enzyme works as a catalyst, facilitating a reaction without being altered by that reaction. We could consider the control measures such as treatment facilities as the 'enzymes' of our epidemiological system. Thus, the concentration control coefficients could denote how our variables were affected by the action of a treatment facility.

The local sensitivities we have used, such as the elasticity, could be used with WALS. We examined the range and mean of our elasticity values. However, the WALS could allow us to weight our individual values to arrive at one value relating input and output across the parameter space.

The big opportunities for advancing our understanding come from the metabolic and regulatory network analyses. A large, spatially structured population in an epidemiological model becomes increasingly difficult to deal with. Therefore, the concept of stoichiometry, examining each transition as a reaction and sidestepping the ODEs and non-linearity, is very appealing. In our simple SIR model, it is easy to see which pathways or transitions sustain steady state operation. However, if we considered a city network with many sub-populations, those pathways become less clear and elementary mode analysis could be very useful. This is particularly the case when is it used in conjunction with flux balance analysis. If we wished to examine how a control facility placement affects the network we could consider introducing a new flux constraint and examine how that constraint alters the results of the FBA and pathway distribution.

The final method of interest is one we have briefly examined in the latter part of this thesis. We examined optimal control facility distributions through simulation and

alternative indicators. Therefore, we defined a fitness function through the simulation of an epidemic and the indicators in Chapter Six. We used this fitness function to asses our control facility distributions until the 'best' was found. The format of an evolutionary algorithm could speed this process. In our work we either prioritised patches for control facility placement or found them by exhaustive search. However, with an evolutionary algorithm, we could start with a selection of arbitrary distributions and whittle them down. Therefore, the maximum time taken would be the same as the exhaustive search. The only problem is knowing an optimal distribution when you find it. We compared each distribution to each other through our fitness function but we could consider aiming to have a distribution that brings the total epidemic size below a certain threshold. This process could additionally be accelerated through using the prioritisation of patches in Chapter Six as the starting points for the evolutionary algorithm. This would mean we start closer to the 'answer'.

We have analysed our increasingly complex model with a variety of methods. There have been classical modelling techniques, methods used in both epidemiology and systems biology and those analyses borrowed from ecology. We have learnt a many things, the key parameters and their affects, the type of oscillations brought about by limited control and the ramifications of a natural disaster. However, there are a whole range of methods in systems biology that could help us evolve our system further. We could examine a multi-layered complex system through its stoichiometry to find the key nodes and reactions. We could use these as potential targets for control and evolve the system from these. This methodology could also be used as a template for a standardised database and analysis tool set.

7.5   Conclusion

We have viewed our spatially structured population with an epidemiological eye. Apart from brief forays into ecology and systems biology, we have only just begun to explore the possibilities for analysis. When we examine the bigger picture, we see the opportunity for an automated, multi-level model builder with extensive capabilities for analysis, simulation and evolution. We have started the work with the automation of our five patch model equations. The next step would be to break our model into its key components in order to recombine them in a range of complex, resilient and, above all, realistic systems.

Chapter 8

Conclusion

8.1 The epidemiological analysis so far

We started with a simple environmental transmission model with commuter movement in Chapter Two. This was initially in a homogeneous population which we then split into two coupled patches; the start of our metapopulation work. We examined the model through the basic reproductive number and its decomposition, the resilience and reactivity, all calculated at disease free equilibrium. We took a Latin Hypercube Sample of the parameter space and used this in two sensitivity analyses, the elasticity and partial rank correlation coefficient. The sensitivity analyses were used to find the important system parameters and the direction in which they affected the system outputs. Also, simulations starting at the disease free equilibrium allowed us to examine the transient system dynamics. The key parameters were the bacteria degradation rate, shed rate, recovery rate, population size, contact rate and half-saturation constant. When the population was split over two patches the coupling parameters determined the importance of the local parameters in each patch.

In Chapter Three, we extended our model to include treatment of infected individuals and a corresponding behavioural change. The aim was to find the effect of control on the dynamics of an environmentally transmitted disease present in a metapopulation. Treatment was available in one of the two patches. Therefore, the exposure weightings for infected individuals were revised as the individuals were assumed to seek treatment. The outputs of the model were then defined with some analyses to examine them. The analyses focused on the sensitivity of the outputs to the model parameters. We used the elasticity and PRCC once more to compare the results of the new model to those of the model in Chapter Two. Furthermore, we used the FAST and MPSA to examine the progress of uncertainty from input to output and highlight the areas of the parameter space which were particularly important. Finally, we examined the transition from disease free to endemic equilibrium using a bifurcation analysis.

In our four sensitivity analyses, we highlighted some key parameters, all of which were mentioned in Chapter Two. These parameters were the degradation rate, recovery rate, half-saturation constant and contact rate which are fundamental parts of the force of infection and duration of infection. However, we discovered additional information. The edge scaling towards the treatment facility is increased, raising the exposure of infected individuals to the environment of the patch containing the treatment facility. Therefore, the local parameters of the patch with the treatment facility were found to be more influential on average than those in the patch without a treatment facility. The edge scaling also led to a non-monotonic relationship between R_0 and the treatment rate. Increasing the treatment rate reduces R_0 for the majority of parameter sets. Yet,

when the shed rate in the patch without treatment is high, the edge scaling towards treatment is also high and the edge scaling away from treatment is low, increasing the treatment rate increases R_0. The increase is because the edge scaling leads to almost all infected individual exposure being experienced in the patch with a treatment facility. However, as soon as an infected individual becomes treated, their exposure returns to 'normal' and their contribution of bacteria in the patch with high shed rate increases. The raised contribution increases the number of infections. Therefore, the behavioural change of infected individuals in response to treatment can affect the disease dynamics in surprising ways. We also conducted a bifurcation analysis and found the endemic prevalence to be lower in the patch with a treatment facility. Thus, whilst the behaviour can affect the dynamics, the treatment of infected individuals is generally beneficial.

In the second part of Chapter Three we incorporated a limit on treatment capacity. This led to a reduction in the treatment rate as the number of infected individuals rose because the medical facility was overwhelmed with infected individuals. Only the dynamics away from disease free equilibrium were of interest; when there were no infected individuals, the treatment rate was at a constant maximum. As such, we examined the epidemic size for the epidemic initiated from disease free equilibrium and the endemic prevalence through a bifurcation analysis. The epidemic size when simulated from disease free equilibrium depended mainly on R_0, a property relevant when the system is disease free. Therefore, the epidemic size at this equilibrium is unaffected by a limited treatment capacity. Yet, the capacity influenced the dynamics away from disease free equilibrium. Using `MATCONT` and `MATLAB`, we found a transcritical bifurcation where the disease free equilibrium lost its stability. After this bifurcation, the endemic equilibrium was stable until a sub-critical Hopf bifurcation. The Hopf bifurcation led to unstable limit cycles appearing backward until a fold rendered the limit cycles stable. Therefore, there is an interval where both the endemic equilibrium and oscillations are stable. We further categorised these oscillations using a Poincaré section and found them to be doubly periodic. Therefore, there are two regimes when the rate of treatment is linked to medical capacity. The first holds when the number of infected individuals is low. In this situation, we remain in region one in figure 8.1 and the treatment rate stays near its maximum. However, if there is a large influx of infected individuals we move into region two of figure 8.1. In this case, the treatment rate drops dramatically allowing a large epidemic to deplete the susceptible population. Epidemics reoccur when the susceptible population is replenished and we have a cycle of large epidemics.
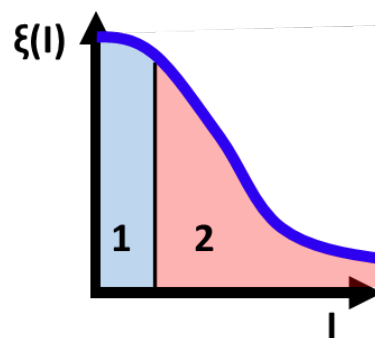

Figure 8.1: Regions, shown in blue and pink, of treatment rate for stable equilibrium and stable oscillatory behaviour. The treatment rate, $\xi(I)$ is a function of the number of infected individuals, shown with a blue line.

In Chapter Four we further segregated our population and looked at the influence of patch arrangement. We also investigated the consequences of a natural disaster on disease dynamics. Our model was reformulated and we defined our exposure weightings to account for different numbers of connected patches and treatment facilities. This allowed us to define a function in `MATLAB` to generate equations given a particular arrangement of patches, placement of treatment facilities and parameter set. The benefit of this automation was accuracy and it left us in a position to exploit our equations further in `MATLAB`. We examined R_0 and the epidemic size and made use of a concept more commonly applied in ecology, the impact. The impact quantifies the effect of a perturbation on each each system element. We defined our perturbation in terms of a flood, assuming it changed the shed and contact rates. Thus, we could examine which arrangements of patches were most resilient to a natural disaster.

There was no correlation between R_0 or epidemic size and the number of patches when the patches were in a cycle or complete arrangement. In these arrangements, as the number of patches increases, the local population size of each patch decreases; however, the local shed rate proportionally increases as the reservoir volume is reduced. Thus, the net effect of increasing the number of patches is almost zero. In contrast, when the patches are in a star arrangement, there is a correlation between R_0, epidemic size and number of patches. In this arrangement, there is always one central patch which the entire population can access. As such, the rise in local shed rate when the number of patches increases is not balanced by a reduction in the number of individuals accessing the central reservoir. It is as a result of this central reservoir that R_0 and the epidemic size are also generally higher when the patches are in a star arrangement.

In the latter part of Chapter Four, we examined the effects of a natural disaster through the impact analysis. The capacity for the infected class to react to a perturbation is partly dictated by the size of the susceptible population; if there are few susceptible individuals then there can not be many infections. As such, the response of the infected class to a perturbation is far greater at disease free equilibrium than at endemic equilibrium. This difference is particularly apparent when the patches are in a star arrangement. The central patch, with its high amount of human traffic facilitates the amplification of the perturbation. When the endemic equilibrium is stable, the situation is quite different. The susceptible population is far smaller, particularly when the patches are in the star arrangement. As such, the impact is smallest for infected individuals when patches are arranged in a star arrangement. Therefore, the structure of the patches is a vitally important influence on the disease dynamics.

In Chapter Five we based our patch arrangement on models of developing world city structures. Therefore, they formed a star arrangement. We included heterogeneities such as a variation in patch density and contact with the environmental reservoir. This was in order to model the variation in sanitation and population distribution you would expect to find in a real city. We found optimal intervention strategies in this spatially structured population using simulation. The environmentally transmitted disease was either introduced or endemic in the population and there was a perturbation in transmission caused by a flood. This perturbation instigated an epidemic and we noted the number of infections over the epidemic's course and its duration. We found the optimal control distributions through exhaustive search, assessing each possible arrangement of control facilities by the allowed epidemic size and duration. The arrangement with the smallest epidemic size or shortest duration was deemed optimal and each arrangement was either formed from treatment facilities, decontamination facilities or both. The decontamination facilities shortened the lifespan of the bacteria in the patch where they were positioned. Simulation steps can be found in figure 8.2.

The optimal distributions of treatment <u>or</u> decontamination facilities were good in-
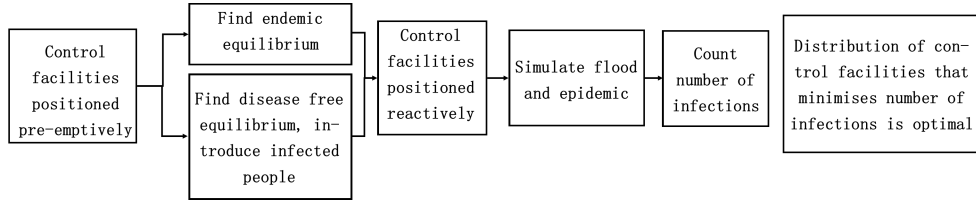
Figure 8.2: Flowchart depicting simulation steps.

dicators of the optimal distributions of facilities when both control types could be positioned. Generally, when the system was initially at disease free equilibrium, the centre and highest density/ contact rate peripheral patches were prioritised for decontamination and the centre and low density/ contact rate patches were prioritised for treatment facilities. This was also the case when facilities were placed reactively at endemic equilibrium. When the facilities were placed pre-emptively, the lowest density/ contact rate peripheral patches were prioritised for facility placement. These distributions allowed the susceptible population to deplete, leaving the population resilient to infection. The optimal distributions of treatment facilities were not always easy to describe with a simple rule. The edge scaling attached to the placement of a treatment facility meant that the optimal distributions of treatment facilities were a trade-off between accessibility and contamination of the environment. When a treatment facility was located in a patch, it encouraged infected individuals to be exposed and shed in that patch, therefore increasing the local bacterial population size. As such, we may choose to place treatment facilities in patches with a low force of infection or level of human traffic to encourage them away from vulnerable environments. We called this an *auto-quarantine* effect. Therefore, there were a few important considerations when determining optimal distributions of control facilities. The most vital consideration is the population response to the provision of a control measure. However, the number of facilities to be placed, placement time and state of the system prior to perturbation all affect the optimal distributions of control facilities as well. We assumed facilities were all placed at the same time, as such there were cases where the optimal distribution of n facilities was not featured in the optimal distribution of $n + 1$ facilities. The state of the system and placement time were both important factors; the optimal distributions at disease free equilibrium were drastically different to those placed pre-emptively at endemic equilibrium. Therefore, the optimal placement of control facilities is a complex problem affected by many characteristics of the structure and population.

In the Chapter Six, we set out to find alternative indicators of optimal control facility distributions. We used methods introduced throughout the thesis, as well as some new ones, to find optimal control facility distributions. We also used the indicators to prioritise patches for control measures based on their local values for each patch in the absence of treatment or decontamination. The indicators were divided by the characteristic of the epidemic to which they applied. For instance, for the state of the system prior to the flood, we examined the basic and effective reproduction numbers and their decompositions, the endemic prevalence and size of the susceptible population at endemic equilibrium. When we prioritised patches for decontamination facilities based on their local part reproduction numbers or endemic population composition, the order matched that for their placement to minimise epidemic size. This was not the case for treatment facilities. However, when we examined each control facility distribution by exhaustive search, those distributions of both control facility types that optimised these indicators, also minimised the epidemic size. The reproduction numbers and size of the susceptible population at endemic equilibrium were particularly effective

indicators here.

We also assessed indicators that describe the response of the system to a perturbation; these were the impact, influence and sensitivity. The influence and sensitivity can be seen as decompositions of the impact when there is a press perturbation. The impact was an effective indicator of the optimal control facility distributions. The influence, which highlights which system variables amplify the perturbation, was almost as effective as the impact as an indicator of optimal distributions. In contrast, the sensitivity may be more beneficial as a measure of which patches are most susceptible to the effects of a perturbation rather than the most effective positions for treatment or decontamination facilities. Lastly, we examined those indicators that describe the recovery of the system from perturbation, namely the resilience, the reactivity and their decompositions. The reactivity was a good indicator of the optimal reactively placed control facility distributions. However, the resilience may be better employed when examining the long-term dynamics rather than highlighting effective positions for control facilities. We established various methods to use as indicators of the optimal control facility distributions to minimise epidemic size. Yet, there was more information to be gained for these methods and in some cases they may be more beneficial when examining the long-term dynamics or structure rather than the relatively brief epidemic.

8.1.1 Summary

This thesis examined the dynamics and control of an environmentally transmitted disease in a perturbed system. We developed the model in stages to understand the dynamics and the reasons for certain behaviours. Therefore, we examined only the disease in a homogeneous population as our first step. Only after we understood this behaviour could we segregate the population and introduce control measures. The patch structure and control were introduced separately and we took pains to examine the effect of spatial segregation and patch arrangement independently of the response to treatment provision. We also examined the situation where infected individuals affect the control through a saturating treatment rate and found interesting oscillatory dynamics which may hold for more complicated systems. We then combined patch arrangement and control to begin answering the question: what is the optimal control strategy in a city given a natural disaster. To find this answer, we established a 'realistic' heterogeneous arrangement of patches as our city and simulated a flood as a perturbation in transmission. We used this to establish the optimal control facility distributions which we further calculated using a range of analysis methods. Thus, we arrived at a definitive answer for our specific model formulation through an arsenal of methods. However, the question we asked in Chapter Seven is whether there are methods from another field, namely systems biology, that could have helped us and be used in future for models of this type. We defined systems biology and some of its key methods before trying them out in an epidemiological context.

8.2 The future

There are two main directions that this work could take in future. The first builds on the analysis of the simple models shown. We discussed in the Introduction four main steps in the models of environmentally transmitted diseases. Namely, the inclusion of susceptible individuals, HI bacteria, asymptomatic infection and spatial structure. We have only included two of these aspects and arguably only half of spatial structure as, for various reasons, we have omitted bacterial transport. Therefore, there are a number of elements we could include in our model. The HI bacterial state may affect the optimal

deployments of facilities that we found in Chapter Five. This is because the HI state could make the freshly shed bacteria more influential rendering a patch experiencing fresh shedding disproportionately contaminated. However, this HI state only really becomes relevant when the bacteria may move between settlements. Therefore, if we were to include bacterial transport and HI bacteria it may be interesting to see if localised shedding preserves the optimal spatial arrangement of facilities even if those bacteria can move. Lastly, the asymptomatic infection may be included through varying the level of exposure of infected individuals i.e. assuming severe, symptomatic cases are only exposed to their own patch environment. This may also be tied to the dose of bacteria where an individual is more likely to be severely infected if they have a high dose of bacteria. The results of the asymptomatic/ severe infection may be that the contamination of the environment is even more of an issue, exacerbating the auto-quarantine effect.

The alternative direction is the extension to highly complex models parametrized by real data. We have examined fairly theoretical population structures despite our use of city structure models. Thus, could we use the framework developed throughout this thesis to model dynamics in a real city? Let us examine Port au Prince, for example. Port au Prince is the capital of Haiti and does not conform to the mono-centric city structure we examined in Chapter Five. However, it does have similar characteristics to the Latin American city model [69]. Figure 8.3 shows the different districts of Port au Prince with their corresponding population densities according to the 2003 census data. Using data such as this we could construct a 171 patch model as there are 171 districts. Then we could build and analyse the potential dynamics of an environmentally transmitted disease through this population. There may be issues
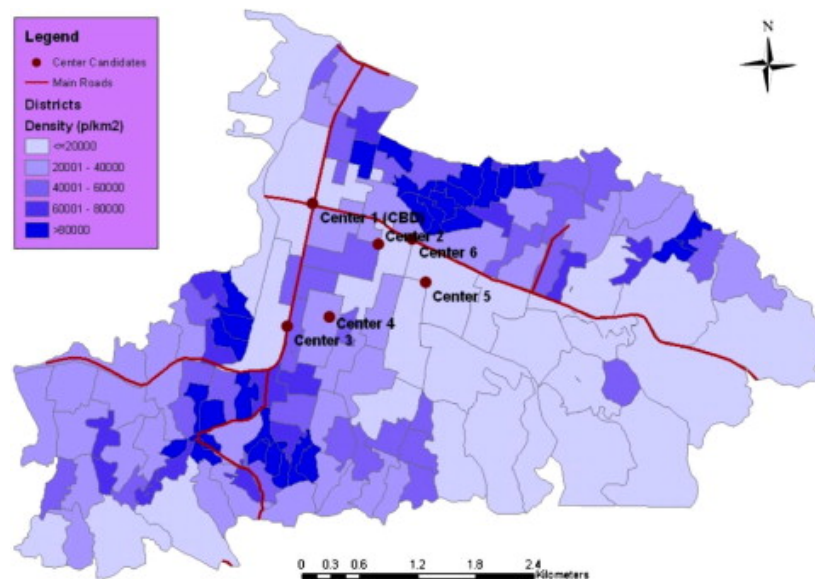
Figure 8.3: Density map of Port-au-Prince, Haiti [69].

with the parametrisation of such a model, the local parameters for each district may be difficult to obtain. Additionally we must consider the movement patterns of both humans and bacteria. These could be found through mobile phone data and mapping the river network but may be highly sensitive to changes in behaviour and man-made hydrological networks.

However, such a model could be developed within the framework of this thesis. Given the appropriate parametrization, we could automate the construction of the model equations. Once these are built, we can find reproductive numbers both locally

and for the entirety of Port au Prince. These, and other model outputs could be used to conduct sensitivity analyses and simulations. We could also abstract the model into a stoichiometric matrix in order to conduct pathway and flux analyses. These could show us bottlenecks and hotspots for disease transmission in the population. Lastly, we could employ a mixture of the above analyses in an evolutionary algorithm to find optimal control strategies in this particular city. Thus, if we compare our framework to that of Bertuzzo et al. [16], we have included more specific movement parameters for host individuals, on a city-wide rather than nationwide scale with a variety of methods for finding and constructing optimal control strategies.

Thus, once we have the structure and a parameter set, we can automate the construction of the equations for the system; stoichiometry; pathways; sensitivity; model outputs and simulations, see figure 8.4. We could construct some standardised software within `MATLAB` with all of these capabilities. This would be a step forward in epidemiological modelling and one that could be rolled out for a variety of transmission types.
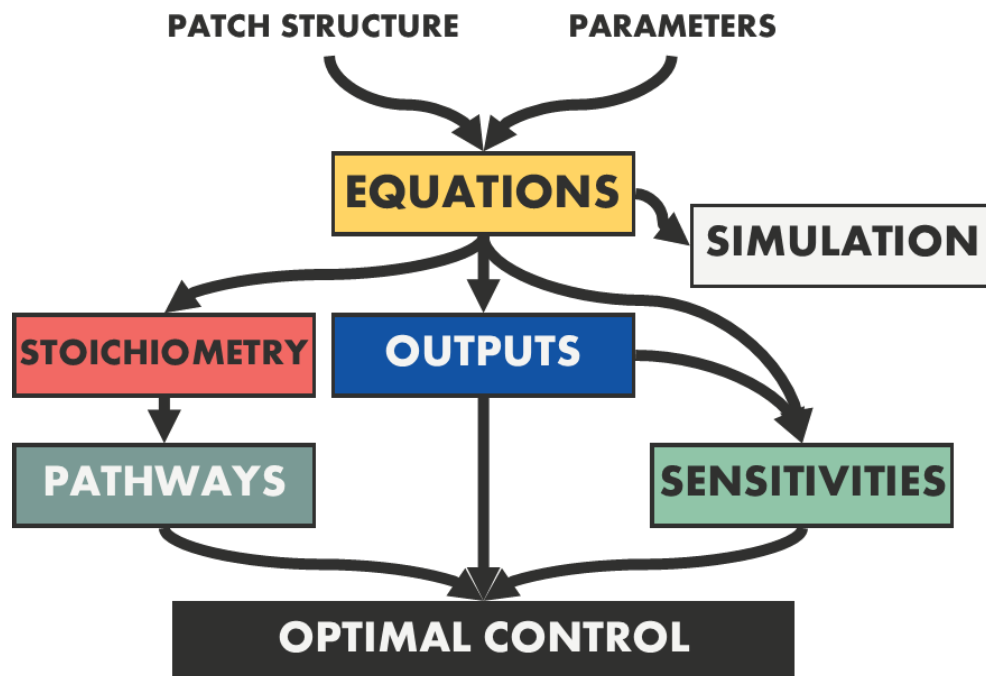
Figure 8.4: A framework for model development and analysis.

Appendix A

Parameter values

Parameter/ Variable	Meaning	Range	Units	Ref
X_{pq}	Susceptible population resident in patch p currently in patch q.	$[0, 10^7]$	Individuals	
Y_{pq}	Infected population resident in patch p currently in patch q.	$[0, 10^7]$	Individuals	
Z_{pq}	Recovered population resident in patch p currently in patch q.	$[0, 10^7]$	Individuals	
S_p	Susceptible population resident in patch p. $S_p = X_{pp} + X_{pq}$.	$[0, 10^7]$	Individuals	
I_p	Infected population resident in patch p. $I_p = Y_{pp} + Y_{pq}$.	$[0, 10^7]$	Individuals	
R_p	Recovered population resident in patch p. $R_p = Z_{pp} + Z_{pq}$.	$[0, 10^7]$	Individuals	
N_p	Population resident in patch p.	$[0, 10^7]$	Individuals	[30]
B_p	Concentration of bacteria in environment of patch p.	$[0, 10^8]$	Bacteria/ Volume	[30, 109]
μ	Birth/death rate.	$[0, 4.5 \times 10^{-5}]$	Days^{-1}	[51, 86]
ϕ_p	Leave rate from patch p.	$[0,1]$	Days^{-1}	
τ_p	Return rate to patch p.	$[0,1]$	Days^{-1}	
σ_p	Proportion of time an individual resident in patch p spends in resident patch.	$[0,1]$	Days	[28]
β_p	Contact rate with environment.	$[0,10]$	Days^{-1}	[51, 86, 91]
κ_p	Half-saturation constant for transmission in patch p.	$[0, 10^8]$	Bacteria/ Volume	[30, 109]
γ_p	Recovery rate in patch p.	$[0,0.5]$	Days^{-1}	[28, 30, 51, 86]
η_p	Bacterial shedding rate in patch p, scaled by reservoir volume	$[0,1]$	Bacteria/ Volume / Days	[30, 109]
θ_p	Natural bacterial degradation rate in patch p.	$[0,0.5]$	Days^{-1}	[28, 30]

Table A.1: Parameters used from Chapter Two onwards unless stated otherwise.

θ	η_i	γ	μ	N (one patch model)	N_i	β_i	κ	σ_i
0.25	0.25	0.2	4.5×10^{-5}	10^7	5×10^6	1	2×10^7	0.6

Table A.2: Parameters used in simulations in Chapter Two.

Parameter/Variable	Meaning	Range	Units	Notes
W_{pq}	Treated population resident in patch p currently in patch q.	$[0, 10^7]$	Individuals	
T_p	Treated population resident in patch p.	$[0, 10^7]$	Individuals	
μ	Birth/death rate, average lifespan 70 years	$[2.5 \times 10^{-5}, 6.8 \times 10^{-5}]$	Days^{-1}	
ϕ_p	Weighting on outward edge of patch p.	1		Fixed
τ_p	Weighting on inward edge of patch p	$[0,\infty]$		
χ_1	Weight scaling on outward edge of patch with treatment facility	$[0,1]$		
χ_2	Weight scaling on inward edge of patch with treatment facility	$[1,5]$		
σ	Proportion exposure to the environment an uninfected individual experiences at home.	$[0.5,1]$		
γ	Recovery rate	$[0,1]$	Days^{-1}	
α	Scaling for treated recovery rate.	$[1,5]$		
ξ	Treatment rate	$[0,1]$	Days^{-1}	Treatment only available in patch q

Table A.3: Parameters used from Chapter Three A onwards. These are amended from or additional to the values shown in table A.1.

θ	η_p	η_q	ξ^*	N_p	N_q	σ
0.8000	0.4989	0.3024	0.4988	10^7	10^7	0.8666
χ_1	χ_2	γ	α	κ	Υ	μ
0.6351	4.7882	0.2000	4.2816	10^7	10^4	6.27×10^{-5}

Table A.4: Parameters used in bifurcation analysis in Chapter Three part B.

Parameter	Meaning	Range	Units	Notes
Υ	Capacity of treatment facility	$[0,\infty]$	Individuals	
$\xi(I)$	Saturating treatment rate	$[0,1]$	Days^{-1}	Equation (3b.4)

Table A.5: Parameters used from Chapter Three B. These are amended from or additional to the values shown in table A.3.

Parameter	Meaning	Range	Notes
σ	Proportion of exposure a non-infected individual spends at from home.	[0,1]	
σ_{ij}^I	Proportion of exposure an infected individual from patch i experiences in patch j.	[0,1]	Defined in equations (4.3) and (4.4)
C^i	Number of connected patches to patch i.	$[0,\infty]$	
c^i	Proportion of patches connected to patch i *with* treatment facilities.	[0,1]	
ξ_i	Treatment rate in patch i.	[0,1]	$\xi_i = \begin{cases} \xi & \text{treatment facility in } i \\ 0 & \text{else} \end{cases}$
P_{ij}	Distributions of exposure of individuals from patch i, away from home, in patch j.	[0,1]	$P_{ij} = \begin{cases} \frac{1}{C^i} & \text{patches } i \text{ and } j \text{ connected} \\ 0 & \text{else} \end{cases}$
X_{ij}	Edge scaling from patch i to patch j.		$X_{ij} = \begin{cases} \chi_2 & \text{treatment facility in patch } j \\ \chi_1 & \text{treatment facility in patch } i \end{cases}$ $X_{ii} = \begin{cases} \chi_1 & \text{no treatment facility in patch } i \\ \chi_2 & \text{treatment facility in patch } i \end{cases}$

Table A.6: Parameters used from Chapter Four onwards. These are amended from or additional to the values shown in table A.3.

Parameter	Meaning	Range
η	Shed rate	[0,1]*M
N	Total population size	5×10^7

Table A.7: Parameter values used from Chapter Four. These are amended from or additional to the values shown in table A.3.

194

Parameter	Meaning	Value for endemic infection
N	see table A.3	5×10^7
N_j	see table A.3	$[1, 0.7124, 0.9203, 1.0797, 1.2876] \times 10^7$
μ	see table A.3	4×10^{-5}
ϕ	see table A.3	1
τ	see table A.3	2
σ	see table A.3	2/3
χ_1	see table A.3	0.2
χ_2	see table A.3	2
β_j	see table A.3	$1, 0.7124, 0.9203, 1.0797, 1.2876$
κ	see table A.3	2×10^7
ξ	see table A.3	0.5
γ	see table A.3	0.2
α	see table A.3	3
η	see table A.3	0.25
ζ	Decontamination rate of the bacteria in the environment	0.5
θ	see table A.3	0.25

Table A.8: Parameter values used from Chapter Five onwards. All rates are per day. These values lead to a stable equilibrium where infection is endemic. For analyses that require a stable disease-free equilibrium, The contact rate is changed to $\beta_j = 0.1$ on average i.e. there the rate of contact with the environment is reduced.

Appendix B

Optimal control facility distributions to minimise epidemic size and duration

Category	Assessments	Heterogeneity	Deployment time	Equilibria	Control
Type	Epidemic Size	Contact rate	Reactive	Disease free	Treatment
	Return time	Population Density	Pre-emptive	Endemic	Decontamination
		Both			Both

Table B.1: Table of possible assessment criteria, heterogeneity, placement time, equilibrium and control examined in this chapter.

Equilibrium	Cases	Number of control facilities available			
		1	2	3	4
Endemic Pre-emptive	Treatment (β, N, β&N)				
	Decontamination (β, N, β&N)	see above			
Endemic Reactive	Treatment (β, N,β&N)				
	Decontamination (N,β&N)				
	Decontamination (β)	see directly above		see directly above	
Disease free	Treatment (N)				
	Treatment (β)				
	Treatment (β&N)		see treatment (N)		
	Decontamination (β, N, β&N)				

Table B.2: Optimal distributions of between one and four control facilities in a city structured by a heterogeneity. Optimisation minimises the size of the epidemic associated with a flood in a system that is initially at endemic equilibrium (top row) or disease free equilibrium (bottom row). The heterogeneity may be in the contact rate, population density or both. Larger circles indicate higher contact rates/ densities. Control facilities may provide treatment or decontamination. Shaded circles denote control facility locations. The distributions shown are optimal for all combinations of heterogeneity, control measure and placement time mentioned in table B.1.

Equilibrium	Cases	Number of control facilities available			
		1	2	3	4
Endemic Pre-emptive	Treatment (β,N,β&N)				
	Decontamination (β,N,β&N)				
Endemic Reactive	Treatment (N)				
	Treatment (β,β&N)	see directly above		see directly above	see directly above
	Decontamination (β,N,β&N)				
Disease free	Treatment (N)				
	Treatment (β)				
	Treatment (β&N)				
	Decontamination (N,β)				
	Decontamination (β&N)				

Table B.3: Optimal distributions of between one and four control facilities in a city structured by a heterogeneity. Optimisation minimises the return time to equilibrium after an epidemic associated with a flood in a system that is initially at endemic equilibrium (top row) or disease free equilibrium (bottom row). The heterogeneity may be in the contact rate, population density or both. Larger circles indicate higher contact rates/ densities. Control facilities may provide treatment or decontamination. Shaded circles denote control facility locations. The distributions shown are optimal for all combinations of heterogeneity, control measure and placement time mentioned in table B.1.

Equilibrium	Cases	Number of control facilities available								
		1	2	3	4	5	6	7	8	9
Endemic Pre-emptive	N, β&N									
	β									
Endemic Reactive	β, β&N									
	N									
Disease free	N									
	β							see N		
	β&N									

Table B.4: Optimal distributions of between one and nine control facilities placed in a city structured by a heterogeneity. Optimisation minimises the epidemic size for an epidemic associated with a flood in a system that is initially at endemic or disease free equilibrium. Larger circles denote higher contact rates/densities. Shaded circles denote control facility locations with grey representing decontamination and black, treatment. The distributions shown are optimal for all combinations of heterogeneity mentioned in table B.1.

Equilibrium	Cases	Number of control facilities available								
		1	2	3	4	5	6	7	8	9
Endemic Pre-emptive	N,β,β&N									
	N									
Endemic Reactive	β									
	β&N									
Disease free	N									
	β									
	β&N									

Table B.5: Optimal distributions of between one and nine control facilities placed in a city structured by a heterogeneity. Optimisation minimises the return time following an epidemic associated with a flood in a system that is initially at endemic or disease free equilibrium. Larger circles denote higher contact rates / densities. Shaded circles denote control facility locations with blue representing decontamination and red, treatment. The distributions shown are optimal for all combinations of heterogeneity mentioned in table B.1.

Appendix C

Differences in optimal control facility distributions to minimise epidemic size and duration

Equilibrium	Disease free						Endemic
Number of facilities	2 Treatment		3 Treatment	4 Treatment	7	8	5
Heterogeneity	N	β&N	β&N	β&N	N	N	β
% difference between exception and alternative distribution	1.78	1.48	35.88	30.65	0.58	0.33	5.81
Maximum % difference	323.06	763.72	815.23	74.81	18814	5231	152.89

Table C.1: Proportional differences in epidemic size between different key treatment facility pre-emptively placed distributions. The exception optimal distribution is compared to the alternative optimal distribution and distribution that allows the largest epidemic size. Distributions minimise epidemic size.

Equilibrium	Disease free										
Number of facilities	2 decontamination	2 treatment		3 treatment		4 treatment	7		8		9
Heterogeneity	β&N	N	β&N	N	β&N	β&N	β	β&N	β	β&N	β&N
difference between exception and alternative distribution in days	23.7	1.2	0.9	1.0	0.7	3.6	0.1	0.3	0.1	0.0	0.2
Maximum difference in days	54.6	92.4	77.7	91.1	75.4	4.8	156.9	143.0	70.7	85.0	57.9

Table C.2: Proportional differences in return time between different key treatment facility pre-emptively placed distributions. The exception optimal distribution is compared to the alternative optimal distribution and distribution that allows the longest return time.

Equilibrium	Endemic		
Number of facilities	2 decontamination	7	8
Heterogeneity	β	N	N
% difference between exception and most commonly optimal distribution	0.88	0.25	0.15
Maximum %difference	24.54	9633	7020

Table C.3: Proportional differences in epidemic size between different key facility reactively placed distributions. The exception optimal distribution is compared to the most common optimal distribution and distribution that allows the largest epidemic size.

Equilibrium	Endemic			
Number of facilities	2 treatment facilities	7		8
Heterogeneity	N	N	β&N	N
difference between exception and alternative distribution in days	0.02	1.2	0.1	1.4
Maximum difference in days	6.14	289.6	353.8	199.4

Table C.4: Proportional differences in return time between different key facility reactively placed distributions. The exception optimal distribution is compared to the most common optimal distribution and distribution that allows the longest return time.

Appendix D

Optimal control facility distributions to minimise alternative indicators

Table D.1: Optimum distributions of one control facility type in a city structure by a heterogeneity. The optimisation minimises influence of the infected and bacterial classes. The parameters used are those found in table A.8 at DFE and EE. Larger circles denote higher contact rates/ densities. The shaded cells indicate those distributions also minimise epidemic size at disease free equilibrium (blue) and at endemic equilibrium when placed pre-emptively (yellow) or when placed reactively (green).

Table D.2: Optimum distributions of one control facility type in a city structure by a heterogeneity. The optimisation minimises sensitivity of the infected and bacterial classes. The parameters used are those found in table A.8 at DFE and EE. Larger circles denote higher contact rates/ densities. The shaded cells indicate those distributions also minimise epidemic size at disease free equilibrium (blue) and at endemic equilibrium when placed pre-emptively (yellow) or when placed reactively (green).

Table D.3: Optimum distributions of two control facility types in a city structure by a heterogeneity. The optimisation minimises the system reactivity. The parameters used are those found in table A.8 at DFE and EE. Larger circles denote higher contact rates/ densities. The shaded cells indicate those distributions also minimise epidemic size at disease free equilibrium (blue) and at endemic equilibrium when placed pre-emptively (yellow) or when placed reactively (green).

Table D.4: Optimum distributions of two control facility types in a city structure by a heterogeneity. The optimisation minimises the infectious class part reactivities. The parameters used are those found in table A.8 at DFE and EE. Larger circles denote higher contact rates/ densities. The shaded cells indicate those distributions also minimise epidemic size at disease free equilibrium (blue) and at endemic equilibrium when placed pre-emptively (yellow) or when placed reactively (green).

Table D.5: Optimum distributions of two control facility types in a city structure by a heterogeneity. The optimisation minimises the sum of the infected class part resiliences.The parameters used are those found in table A.8 at DFE and EE. Larger circles denote higher contact rates/ densities. The shaded cells indicate those distributions also minimise epidemic size at disease free equilibrium (blue) and at endemic equilibrium when placed pre-emptively (yellow) or when placed reactively (green).

Table D.6: Optimum distributions of two control facility types in a city structure by a heterogeneity. The optimisation minimises the system resilience. The parameters used are those found in table A.8 at DFE and EE. Larger circles denote higher contact rates/ densities. The shaded cells indicate those distributions also minimise epidemic size at disease free equilibrium (blue) and at endemic equilibrium when placed pre-emptively (yellow) or when placed reactively (green).

Bibliography

[1] 150 years of cholera epidemiology. *The Lancet*, 366(9490):957, 2005.

[2] Metatool 5.1 for GNU Octave and MATLAB. *http://pinguin.biologie.uni-jena.de/bioinformatik/networks/metatool/metatool5.1/metatool5.1.html*, 2008.

[3] R. Aebersold, L. Hood, and J. Watts. Equipping scientists for the new biology. *Nature Biotechnology*, 18:359, 2000.

[4] M. Ahern, R. S. Kovats, P. Wilkinson, R. Few, and F. Matthies. Global health impacts of floods: epidemiologic evidence. *Epidemiologic Reviews*, 27(1):36–46, 2005.

[5] A. S. Akanda, A. S. Jutla, D. M. Gute, T. Evans, and S. Islam. Reinforcing cholera intervention through prediction-aided prevention. *Bulletin of the World Health Organization*, 90(3):243–244, 2012.

[6] J. R. Andrews and S. Basu. Transmission dynamics and control of cholera in Haiti: an epidemic model. *The Lancet*, 377(9773):1248–1255, 2011.

[7] E. Andrianantoandro, S. Basu, D. K. Karig, and R. Weiss. Synthetic biology: new engineering rules for an emerging discipline. *Molecular Systems Biology*, 2(1), 2006.

[8] J. Arino and P. Van Den Driessche. The basic reproduction number in a multi-city compartmental epidemic model. In *Positive Systems*, pages 135–142. Springer, 2003.

[9] J. Arino and P. Van den Driessche. A multi-city epidemic model. *Mathematical Population Studies*, 10(3):175–193, 2003.

[10] J. Arino and P. van den Driessche. Disease spread in metapopulations. *Nonlinear Dynamics and Evolution Equations, Fields Inst. Commun*, 48:1–13, 2006.

[11] L. Arriola and H. eds. Sensitivity analysis for uncertainty quantification in mathematical models. In *Mathematical and Statistical Estimation Approaches in Epidemiology*, pages 195–247. Springer, 2009.

[12] H. Aufderheide, L. Rudolf, T. Gross, and K. D. Lafferty. How to predict community responses to perturbations in the face of imperfect knowledge and network complexity. *Proceedings of the Royal Society of London B: Biological Sciences*, 280(1773):20132355, 2013.

[13] G. Batt, B. Yordanov, R. Weiss, and C. Belta. Robustness analysis and tuning of synthetic gene networks. *Bioinformatics*, 23(18):2415–2422, 2007.

[14] A. Bertaud. The spatial organization of cities: deliberate outcome or unforeseen consequence? *Institute of Urban and Regional Development*, 2004.

[15] E. Bertuzzo, S. Azaele, A. Maritan, M. Gatto, I. Rodriguez-Iturbe, and A. Rinaldo. On the space-time evolution of a cholera epidemic. *Water Resources Research*, 44(1), 2008.

[16] E. Bertuzzo, R. Casagrandi, M. Gatto, I. Rodriguez-Iturbe, and A. Rinaldo. On spatially explicit models of cholera epidemics. *Journal of the Royal Society Interface*, 7(43):321–333, 2010.

[17] E. Bertuzzo, L. Mari, L. Righetto, M. Gatto, R. Casagrandi, M. Blokesch, I. Rodriguez-Iturbe, and A. Rinaldo. Prediction of the spatial evolution and effects of control measures for the unfolding Haiti cholera outbreak. *Geophysical Research Letters*, 38(6), 2011.

[18] L. Bianco and A. Castellini. Psim: a computational platform for metabolic P systems. In *Membrane Computing*, pages 1–20. Springer, 2007.

[19] L. Bianco, F. Fontana, G. Franco, and V. Manca. P systems for biological dynamics. In *Applications of Membrane Computing*, pages 83–128. Springer, 2006.

[20] D. Bjørner. Property-oriented and model-oriented abstraction. *Software Engineering 1: Abstraction and Modelling*, pages 231–262, 2006.

[21] S. Blower and H. Dowlatabadi. Sensitivity and uncertainty analysis of complex models of disease transmission: an HIV model, as an example. *International Statistical Review/Revue Internationale de Statistique*, pages 229–243, 1994.

[22] M. Bouzid, L. Hooper, and P. R. Hunter. The effectiveness of public health interventions to reduce the health impact of climate change: a systematic review of systematic reviews. *PloS One*, 8(4):e62041, 2013.

[23] R. J. Brennan. Rapid health assessment in Aceh Jaya district, indonesia, following the december 26 tsunami. *Emergency Medicine Australasia*, 17(4):341–350, 2005.

[24] N. F. Britton. *Essential Mathematical Biology*. Springer Science & Business Media, 2012.

[25] W. Bynum. In retrospect: On the mode of communication of cholera. *Nature*, 495(7440):169–170, 2013.

[26] V. Capasso and S. Paveri-Fontana. A mathematical model for the 1973 cholera epidemic in the European Mediterranean region. *Revue d'epidemiologie et de sante publique*, 27(2):121–132, 1979.

[27] H. Caswell. Perturbation analysis of nonlinear matrix population models. *Demographic Research*, 18(3):59–116, 2008.

[28] D. L. Chao, M. E. Halloran, and I. M. Longini Jr. Vaccination strategies for epidemic cholera in Haiti with implications for the developing world. *Proceedings of the National Academy of Sciences*, 108(17):7081–7085, 2011.

[29] K.-H. Cho, S.-Y. Shin, W. Kolch, and O. Wolkenhauer. Experimental design in systems biology, based on parameter sensitivity analysis using a monte carlo method: A case study for the tnfα-mediated nf-κ b signal transduction pathway. *Simulation*, 79(12):726–739, 2003.

[30] C. T. Codeço. Endemic and epidemic dynamics of cholera: the role of the aquatic reservoir. *BMC Infectious Diseases*, 1(1):1, 2001.

[31] W. J. Conover. *Practical Nonparametric Statistics*. John Wiley and Sons, 1998.

[32] J. Cui, X. Mu, and H. Wan. Saturation recovery leads to multiple endemic equilibria and backward bifurcation. *Journal of Theoretical Biology*, 254(2):275–283, 2008.

[33] K. A. Date, A. Vicari, T. B. Hyde, E. Mintz, M. C. Danovaro-Holliday, A. Henry, J. W. Tappero, T. H. Roels, J. Abrams, B. T. Burkholder, et al. Considerations for oral cholera vaccine use during outbreak after earthquake in Haiti, 2010- 2011. *Emerging Infectious Diseases*, 17(11):2105, 2011.

[34] H. De Kroon, J. Van Groenendael, and J. Ehrlén. Elasticities: a review of methods and model limitations. *Ecology*, 81(3):607–618, 2000.

[35] B. Deb, B. Sircar, P. Sengupta, S. De, S. Mondal, D. Gupta, N. Saha, S. Ghosh, U. Mitra, and S. Pal. Studies on interventions to prevent eltor cholera transmission in urban slums. *Bulletin of the World Health Organization*, 64(1):127, 1986.

[36] O. Diekmann, J. Heesterbeek, and M. Roberts. The construction of next-generation matrices for compartmental epidemic models. *Journal of the Royal Society Interface*, 7(47):873–885, 2010.

[37] O. Diekmann and J. A. P. Heesterbeek. *Mathematical Epidemiology of Infectious Diseases: Model Building, Analysis and Interpretation*, volume 5. Wiley, 2000.

[38] G. Ding, Y. Zhang, L. Gao, W. Ma, X. Li, J. Liu, Q. Liu, and B. Jiang. Quantitative analysis of burden of infectious diarrhea associated with floods in northwest of Anhui Province, China: A mixed method evaluation. *PLoS One*, 8(6):e65112, 06 2013.

[39] E. Drew. Foundations for engineering biology. *Nature*, 438:449–453, 2005.

[40] J. S. Edwards and B. Ø. Palson. Metabolic flux balance analysis and the in silico analysis of escherichia coli k-12 gene deletions. *BMC Bioinformatics*, 2000.

[41] M. C. Eisenberg, Z. Shuai, J. H. Tien, and P. van den Driessche. A cholera model in a patchy environment with water and human movement. *Mathematical Biosciences*, 246(1):105–112, 2013.

[42] P.-A. Ekström. Eikos: A simulation toolbox for sensitivity analysis. *Master's*, 2005.

[43] J. M. Epstein, J. Parker, D. Cummings, and R. A. Hammond. *Coupled contagion dynamics of fear and disease: mathematical and computational explorations*. Center on Social and Economic Dynamics, 2007.

[44] P. Farmer, C. P. Almazor, E. T. Bahnsen, D. Barry, J. Bazile, B. R. Bloom, N. Bose, T. Brewer, S. B. Calderwood, J. D. Clemens, et al. Meeting cholera's challenge to Haiti and the world: a joint statement on cholera prevention and care. *PLoS Neglected Tropical Diseases*, 5(5):e1145, 2011.

[45] N. Floret, J.-F. Viel, F. Mauny, B. Hoen, and R. Piarroux. Negligible risk for epidemics after geophysical disasters. *Emerging Infectious Diseases*, 12(4):543, 2006.

[46] P. Francois and V. Hakim. Design of genetic networks with specified functions by evolution in silico. *Proceedings of the National Academy of Sciences of the United States of America*, 101(2):580–585, 2004.

[47] I. C.-H. Fung, D. L. Fitter, R. H. Borse, M. I. Meltzer, and J. W. Tappero. Modeling the effect of water, sanitation, and hygiene and oral cholera vaccine implementation in Haiti. *The American Journal of Tropical Medicine and Hygiene*, 89(4):633–640, 2013.

[48] S. Funk, S. Bansal, C. T. Bauch, K. T. Eames, W. J. Edmunds, A. P. Galvani, and P. Klepac. Nine challenges in incorporating the dynamics of behaviour in infectious diseases models. *Epidemics*, 10:21–25, 2015.

[49] S. Funk, E. Gilad, and V. Jansen. Endemic disease, awareness, and local behavioural response. *Journal of Theoretical Biology*, 264(2):501–509, 2010.

[50] S. Funk, M. Salathé, and V. A. Jansen. Modelling the influence of human behaviour on the spread of infectious diseases: a review. *Journal of the Royal Society Interface*, 7(50):1247–1256, 2010.

[51] M. Gatto, L. Mari, E. Bertuzzo, R. Casagrandi, L. Righetto, I. Rodriguez-Iturbe, and A. Rinaldo. Generalized reproduction numbers and the prediction of patterns in waterborne disease. *Proceedings of the National Academy of Sciences*, 109(48):19703–19708, 2012.

[52] J. A. Goler. *BioJADE: a design and simulation tool for synthetic biological systems*. PhD thesis, Massachusetts Institute of Technology, 2004.

[53] B. Gomero. Latin hypercube sampling and partial rank correlation coefficient analysis applied to an optimal control problem, 2012.

[54] D. Gonze. Matlab demo programs.

[55] W. Govaerts, Y. A. Kuznetsov, and A. Dhooge. Numerical continuation of bifurcations of limit cycles in matlab. *SIAM Journal on Scientific Computing*, 27(1):231–252, 2005.

[56] R. Grünberg and L. Serrano. Strategies for protein synthetic biology. *Nucleic Acids Research*, 38(8):2663–2675, 2010.

[57] S. Gulati, V. Rouilly, X. Niu, J. Chappell, R. I. Kitney, J. B. Edel, P. S. Freemont, et al. Opportunities for microfluidic technologies in synthetic biology. *Journal of The Royal Society Interface*, 6(Suppl 4):S493–S506, 2009.

[58] D. Hamby. A review of techniques for parameter sensitivity analysis of environmental models. *Environmental Monitoring and Assessment*, 32(2):135–154, 1994.

[59] E. D. Harris. Biochemical facts behind the definition and properties of metabolites, 2008.

[60] D. M. Hartley, J. G. Morris, and D. L. Smith. Hyperinfectivity: a critical element in the ability of V. cholerae to cause epidemics? *PLoS Medicine*, 3(1):63, 2006.

[61] E. L. Haseltine and F. H. Arnold. Synthetic gene circuits: design with directed evolution. *Annu. Rev. Biophys. Biomol. Struct.*, 36:1–19, 2007.

[62] J. Heffernan, R. Smith, and L. Wahl. Perspectives on the basic reproductive ratio. *Journal of the Royal Society Interface*, 2(4):281–293, 2005.

[63] R. Heinrich and T. A. Rapoport. A linear steady-state treatment of enzymatic chains. *European Journal of Biochemistry*, 42(1):97–105, 1974.

[64] K. Hiroaki. Systems biology: A brief overview. *Science*, 295:1662–1664, 2002.

[65] iGen. Registry of standard biological parts. *http://parts.igem.org/Part_ Names*.

[66] R. L. Iman and W. J. Conover. The use of the rank transform in regression. *Technometrics*, 21(4):499–509, 1979.

[67] R. L. Iman and J. C. Helton. An investigation of uncertainty and sensitivity analysis techniques for computer models. *Risk Analysis*, 8(1):71–90, 1988.

[68] G. Jenkinson and J. Goutsias. Numerical integration of the master equation in some models of stochastic epidemiology. *PloS One*, 7(5):e36160, 2012.

[69] M. Joseph and F. Wang. Population density patterns in Port-au-Prince, Haiti: A model of Latin American city? *Cities*, 27(3):127–136, 2010.

[70] H. Kacser. The control of flux: 21 years on. *Biochemical Society Transactions*, 1995.

[71] T. Katsumata, D. Hosea, E. B. Wasito, S. Kohno, K. Hara, P. Soeparto, and I. G. Ranuh. Cryptosporidiosis in Indonesia: a hospital-based study and a community-based survey. *The American Journal of Tropical Medicine and Hygiene*, 59(4):628–632, 1998.

[72] M. Keeling, O. Bjørnstad, and B. Grenfell. Metapopulation dynamics of infectious diseases. *Ecology, Genetics, and Evolution of Metapopulations. Elsevier, Amsterdam*, pages 415–445, 2004.

[73] M. J. Keeling and P. Rohani. Estimating spatial coupling in epidemiological systems: a mechanistic approach. *Ecology Letters*, 5(1):20–29, 2002.

[74] M. J. Keeling and P. Rohani. *Modeling Infectious Diseases in Humans and Animals*. Princeton University Press, 2011.

[75] A. A. King, E. L. Ionides, M. Pascual, and M. J. Bouma. Inapparent infections and cholera dynamics. *Nature*, 454(7206):877–880, 2008.

[76] I. Z. Kiss, J. Cassell, M. Recker, and P. L. Simon. The impact of information transmission on epidemic outbreaks. *Mathematical Biosciences*, 225(1):1–10, 2010.

[77] K. Koelle, X. Rodó, M. Pascual, M. Yunus, and G. Mostafa. Refractory periods and climate forcing in cholera dynamics. *Nature*, 436(7051):696–700, 2005.

[78] S. Kotz, N. L. Johnson, and N. Balakrishnan. Continuous univariate distributions, vol. 1, 2000.

[79] E.-W. Lameijer, J. N. Kok, T. Bäck, and A. P. IJzerman. The molecule evoluator. an interactive evolutionary algorithm for the design of drug-like molecules. *Journal of Chemical Information and Modeling*, 46(2):545–552, 2006.

[80] S. K. Lee, H. Chou, T. S. Ham, T. S. Lee, and J. D. Keasling. Metabolic engineering of microorganisms for biofuels production: from bugs to synthetic biology to fuels. 2008.

[81] E. Leonard, D. Nielsen, K. Solomon, and K. J. Prather. Engineering microbes with synthetic biology frameworks. *Trends in Biotechnology*, 26(12):674–681, 2008.

[82] J. Li and N. Cui. Dynamic behavior for an sirs model with nonlinear incidence rate and treatment. *The Scientific World Journal*, 2013, 2013.

[83] L. Lloyd, A. Sensitivity of model-based epidemiological parameter estimation to model assumptions. *Mathematical and Statistical Estimation Approaches in Epidemiology*, pages 123–141, 2009.

[84] J. T. MacDonald, C. Barnes, R. I. Kitney, P. S. Freemont, and G.-B. V. Stan. Computational design approaches and tools for synthetic biology. *Integrative Biology*, 3(2):97–108, 2011.

[85] L. Mari, E. Bertuzzo, F. Finger, R. Casagrandi, M. Gatto, and A. Rinaldo. On the predictive ability of mechanistic models for the Haitian cholera epidemic. *Journal of The Royal Society Interface*, 12(104):20140840, 2015.

[86] L. Mari, E. Bertuzzo, L. Righetto, R. Casagrandi, M. Gatto, I. Rodriguez-Iturbe, and A. Rinaldo. Modelling cholera epidemics: the role of waterways, human mobility and sanitation. *Journal of The Royal Society Interface*, 9(67):376–388, 2012.

[87] S. Marino, I. B. Hogue, C. J. Ray, and D. E. Kirschner. A methodology for performing global uncertainty and sensitivity analysis in systems biology. *Journal of Theoretical Biology*, 254(1):178, 2008.

[88] A. Matser, N. Hartemink, H. Heesterbeek, A. Galvani, and S. Davis. Elasticity analysis in epidemiology: an application to tick-borne infections. *Ecology Letters*, 12(12):1298–1305, 2009.

[89] M. D. McKay, R. J. Beckman, and W. J. Conover. Comparison of three methods for selecting values of input variables in the analysis of output from a computer code. *Technometrics*, 21(2):239–245, 1979.

[90] K. S. McLeod. Our sense of snow: the myth of john snow in medical geography. *Social Science & Medicine*, 50(7):923–935, 2000.

[91] Z. Mukandavire, S. Liao, J. Wang, H. Gaff, D. Smith, and J. Morris. Estimating the reproductive numbers for the 2008–2009 cholera outbreaks in Zimbabwe. *Proceedings of the National Academy of Sciences*, 108(21):8767–8772, 2011.

[92] A. Mwasa and J. M. Tchuenche. Mathematical analysis of a cholera model with public health interventions. *Biosystems*, 105(3):190–200, 2011.

[93] R. L. M. Neilan, E. Schaefer, H. Gaff, K. R. Fister, and S. Lenhart. Modeling optimal intervention strategies for cholera. *Bulletin of Mathematical Biology*, 72(8):2004–2018, 2010.

[94] M. G. Neubert and H. Caswell. Alternatives to resilience for measuring the responses of ecological systems to perturbations. *Ecology*, 78(3):653–665, 1997.

[95] J. Njagarah and F. Nyabadza. A metapopulation model for cholera transmission dynamics between communities linked by migration. *Applied Mathematics and Computation*, 241:317–331, 2014.

[96] E. K. Noji. The public health consequences of disasters. *Prehospital and Disaster Medicine*, 15(04):21–31, 2000.

[97] E. K. Noji. Public health in the aftermath of disasters. *BMJ*, 330(7504):1379–1381, 2005.

[98] M. Novak, J. T. Wootton, D. F. Doak, M. Emmerson, J. A. Estes, and M. T. Tinker. Predicting community responses to perturbations in the face of imperfect knowledge and network complexity. *Ecology*, 92(4):836–846, 2011.

[99] J. M. Ochoche. A mathematical model for the transmission dynamics of cholera with control strategy. *International Journal of Science and Technology*, 2(11), 2013.

[100] W. Olaf. Systems biology: The reincarnation of systems theory applied in biology? *Briefings in Bioinformatics*, 2:258–270, 2001.

[101] J. D. Orth, I. Thiele, and B. Ø. Palson. What is flux balance analysis? *Nature Biotechnology*, 2010.

[102] D. A. Oyarzún and G.-B. V. Stan. Synthetic gene circuits for metabolic control: design trade-offs and constraints. *Journal of The Royal Society Interface*, 10(78), 2013.

[103] T. Parker and L. Chua. Practical numerical algorithms for chaotic systems, 1989. *Springer, New York, Found. Phys*, 32:267, 2002.

[104] E. Parkes. Mode of communication of cholera. by John Snow, md second edition–London, 1855, pp 162. *International Journal of Epidemiology*, 42(6):1543–1552, 2013.

[105] M. Pascual, L. Chaves, B. Cash, X. Rodó, and M. Yunus. Predicting endemic cholera: the role of climate variability and disease dynamics. *Climate Research*, 36(2):131, 2008.

[106] M. Pascual, X. Rodó, S. P. Ellner, R. Colwell, and M. J. Bouma. Cholera dynamics and El Nino-southern oscillation. *Science*, 289(5485):1766–1769, 2000.

[107] H.-H. Peng and C. Dong. Systemic analysis of tumor cell-induced endothelial calcium signaling and junction disassembly. *Cellular and Molecular Bioengineering*, 2(3):375–385, 2009.

[108] T. Pfeiffer, J. Nu, F. Montero, S. Schuster, et al. Metatool: for studying metabolic networks. *Bioinformatics*, 15(3):251–257, 1999.

[109] R. Piarroux, R. Barrais, B. Faucher, R. Haus, M. Piarroux, J. Gaudart, R. Magloire, D. Raoult, et al. Understanding the cholera epidemic, Haiti. *Emerging Infectious Diseases*, 17(7):1161, 2011.

[110] R. B. Potter and S. Lloyd-Evans. *The city in the developing world.* Longman Harlow, 1998.

[111] F. Qadri, A. I. Khan, A. Faruque, Y. A. Begum, F. Chowdhury, G. B. Nair, M. A. Salam, D. A. Sack, and A.-M. Svennerholm. Enterotoxigenic *escherichia coli* and *vibrio cholerae* diarrhea, bangladesh, 2004. *Emerg Infect Dis*, 11(7):1104–7, 2005.

[112] L. Righetto, E. Bertuzzo, R. Casagrandi, M. Gatto, I. Rodriguez-Iturbe, and A. Rinaldo. Modelling human movement in cholera spreading along fluvial systems. *Ecohydrology*, 4(1):49–55, 2011.

[113] A. Rinaldo, E. Bertuzzo, L. Mari, L. Righetto, M. Blokesch, M. Gatto, R. Casagrandi, M. Murray, S. M. Vesenbeckh, and I. Rodriguez-Iturbe. Reassessment of the 2010–2011 Haiti cholera outbreak and rainfall-driven multiseason projections. *Proceedings of the National Academy of Sciences*, 109(17):6602–6607, 2012.

[114] G. Rodrigo, J. Carrera, and A. Jaramillo. Genetdes: automatic design of transcriptional networks. *Bioinformatics*, 23(14):1857–1858, 2007.

[115] W. F. Röling, B. M. Van Breukelen, F. J. Bruggeman, and H. V. Westerhoff. Ecological control analysis: being in control of mass flux and metabolite concentrations in anaerobic degradation processes. *Environmental Microbiology*, 9(2):500–511, 2007.

[116] A. Saltelli, S. Tarantola, and K.-S. Chan. A quantitative model-independent method for global sensitivity analysis of model output. *Technometrics*, 41(1):39–56, 1999.

[117] M. A. Sanchez and S. M. Blower. Uncertainty and sensitivity analysis of the basic reproductive rate: tuberculosis as an example. *American Journal of Epidemiology*, 145(12):1127–1137, 1997.

[118] L. Sattenspiel and K. Dietz. A structured epidemic model incorporating geographic mobility among regions. *Mathematical Biosciences*, 128(1):71–91, 1995.

[119] C. H. Schilling, J. S. Edwards, D. Letscher, and B. Ø. Palson. Combining pathway analysis with flux balance analysis for the comprehensive study of metabolic systems. *Biotechnology and Bioengineering*, 2000.

[120] S. Scott and C. J. Duncan. *Biology of Plagues: Evidence from Historical Populations*. Cambridge University Press, 2001.

[121] Z. Shuai and P. v. d. Driessche. Modelling and control of cholera on networks with a common water source. *Journal of Biological Dynamics*, pages 1–14, 2014.

[122] Z. Shuai, J. H. Tien, and P. van den Driessche. Cholera dynamics on community networks (13rit168) BIRS Research in Teams Report. 2013.

[123] C. Sim. Control and intervention of cholera outbreaks in refugee camps. *Global Societies Journal*, 1(1), 2013.

[124] J. Snow. *On the mode of communication of cholera*. John Churchill, 1855.

[125] W. M. Spears, K. A. De Jong, T. Bäck, D. B. Fogel, and H. De Garis. An overview of evolutionary computation. In *Machine Learning: ECML-93*, pages 442–459. Springer, 1993.

[126] M. Tabor. *Chaos and Integrability in Nonlinear Dynamics: an Introduction*. Wiley New York, 1989.

[127] D. L. Taylor, T. M. Kahawita, S. Cairncross, and J. H. Ensink. The impact of water, sanitation and hygiene interventions to control cholera: A systematic review. *PloS One*, 10(8):e0135676, 2015.

[128] J. M. T. Thompson and H. B. Stewart. Nonlinear dynamics and chaos: Geometrical methods for engineers and scientists. *Chichester, England and New York, John Wiley and Sons,*, 1986.

[129] J. H. Tien and D. J. Earn. Multiple transmission pathways and disease dynamics in a waterborne pathogen model. *Bulletin of Mathematical Biology*, 72(6):1506–1533, 2010.

[130] C. T. Trinh, A. Wlaschin, and F. Srienc. Elementary mode analysis: a useful metabolic pathway analysis tool for characterizing cellular metabolism. *Applied Microbiology and Biotechnology*, 81(5):813–826, 2009.

[131] A. R. Tuite, J. Tien, M. Eisenberg, D. J. Earn, J. Ma, and D. N. Fisman. Cholera epidemic in Haiti, 2010: Using a transmission model to explain spatial spread of disease and identify optimal control interventions. *Annals of Internal Medicine*, 154(9):593–601, 2011.

[132] A. M. Vollaard, S. Ali, H. A. van Asten, S. Widjaja, L. G. Visser, C. Surjadi, and J. T. van Dissel. Risk factors for typhoid and paratyphoid fever in Jakarta, Indonesia. *JAMA*, 291(21):2607–2615, 2004.

[133] H. Wan and J.-a. Cui. Rich dynamics of an epidemic model with saturation recovery. *Journal of Applied Mathematics*, 2013, 2013.

[134] W. Wang. Backward bifurcation of an epidemic model with treatment. *Mathematical Biosciences*, 201(1):58–71, 2006.

[135] W. Wang and S. Ruan. Bifurcations in an epidemic model with constant removal rate of the infectives. *Journal of Mathematical Analysis and Applications*, 291(2):775–793, 2004.

[136] J. T. Watson, M. Gayer, and M. A. Connolly. Epidemics after natural disasters. *Emerging Infectious Diseases*, 13(1):1, 2007.

[137] WHO. Cholera vaccines: WHO position paper.

[138] WHO. Projections of mortality and causes of death, 2015 and 2030.

[139] WHO. Flooding and communicable diseases fact sheet: Risk assessment and preventive measures. *WHO: Geneva*, 2006.

[140] WHO. Cholera. *http://www.who.int/topics/cholera/en/, accessed August*, 2014.

[141] WHO. Diarrhoeal disease. *http://www.who.int/mediacentre/factsheets/fs330/en/, accessed March*, 2015.

[142] WHO. Cholera cases reported to who by year and by continent 1989-2013. *WHO Regional Office for the Eastern Mediterranean, available at: http://www.who.int/gho/epidemicdiseases/cholera/cases/en/, accessed May*, 15, 2016.

[143] C. Xu and G. Z. Gertner. Uncertainty analysis of transient population dynamics. *Ecological Modelling*, 220(3):283–293, 2009.

[144] X. Zhang and X. Liu. Backward bifurcation of an epidemic model with saturated treatment function. *Journal of Mathematical Analysis and Applications*, 348(1):433–443, 2008.

[145] Z. Zhang and Y. Suo. Qualitative analysis of a sir epidemic model with saturated treatment rate. *Journal of Applied Mathematics and Computing*, 34(1-2):177–194, 2010.

[146] Y. Zheng and A. Rundell. Comparative study of parameter sensitivity analyses of the TCR-activated Erk-MAPK signalling pathway. *IEE Proceedings-Systems Biology*, 153(4):201–211, 2006.

[147] Y. Zheng and G. Sriram. Mathematical modeling: bridging the gap between concept and realization in synthetic biology. *Journal of Biomedicine and Biotechnology*, 2010.

[148] Z. Zi. Sensitivity analysis approaches applied to systems biology models. *Systems Biology, IET*, 5(6):336–346, 2011.

[149] Z. Zi, K.-H. Cho, M.-H. Sung, X. Xia, J. Zheng, and Z. Sun. In silico identification of the key components and steps in ifn-γ induced jak-stat signaling pathway. *FEBS Letters*, 579(5):1101–1108, 2005.